Studies on the Preparation and Characterization of U_3Si_2 intermetallic and U-Mo alloys

By

VED PRAKASH SINHA

ENGG01200704008

BHABHA ATOMIC RESEARCH CENTRE

A thesis submitted to the
Board of Studies in Engineering Sciences
In partial fulfillment of requirements
for the Degree of

DOCTOR OF PHILOSOPHY

of

HOMI BHABHA NATIONAL INSTITUTE

April, 2012

Homi Bhabha National Institute

Recommendation of the Viva Voce Board

As members of the Viva Voce Board, we certify that we have read the dissertation prepared by Shri Ved Prakash Sinha entitled "Studies on the Preparation and Characterization of U_3Si_2 intermetallic and U-Mo alloys" and recommend that it may be accepted as fulfilling the dissertation requirement for the Degree of Doctor of Philosophy.

Srikumar Banerjee Date: May 02, 2014
Chairman - Prof. S. Banerjee

Date: May 02, 2014
Guide - Prof. G. J. Prasad

Date: May 02, 2014
External Examiner - Prof. Anish Upadhyaya

Gautam Kumar Dey Date: May 02, 2014
Co-Guide & Member-1 - Prof. G. K. Dey

Date: May 02, 2014
Member-2: Prof. S. B. Roy

Date: May 02, 2014
Member-3: Prof. N. K. Maheshwari

Final approval and acceptance of this dissertation is contingent upon the candidate's submission of the final copies of the dissertation to HBNI.

I hereby certify that I have read this dissertation prepared under my direction and recommend that it may be accepted as fulfilling the dissertation requirement.

Date: May 02, 2014

Gautam Kumar Dey

Place: Mumbai **Guide: Prof. G. J. Prasad** **Co-Guide: Prof. G. K. Dey**

STATEMENT BY AUTHOR

This dissertation has been submitted in partial fulfillment of requirements for an advanced degree at Homi Bhabha National Institute (HBNI) and is deposited in the Library to be made available to borrowers under rules of the HBNI.

Brief quotations from this dissertation are allowable without special permission, provided that accurate acknowledgement of source is made. Request for permission for extended quotation from or reproduction of this manuscript in whole or in part may be granted by the Competent Authority of HBNI when in his or her judgment the proposed use of the material is in the interests of scholarship. In all other instances, however, permission must be obtained from the author.

Place: Mumbai

Signature:

Date: May 02, 2014

Name: Ved Prakash Sinha

DECLARATION

I, hereby declare that the investigation presented in the thesis has been carried out by me. The work is original and has not been submitted earlier as a whole or in part for a degree/diploma at this or any other Institution/University.

Place: Mumbai **Signature:**

Date: May 02, 2014 **Name: Ved Prakash Sinha**

CERTIFICATE

This is to certify that the thesis titled, "Studies on the Preparation and Characterization of U_3Si_2 intermetallic and U-Mo alloys" submitted by Shri Ved Prakash Sinha to Homi Bhabha National Institute, Mumbai for the award of the degree of Doctor of Philosophy is a bona fide record of the research work carried out by him under my (our) supervision and guidance. The content of the thesis, in full or parts have not been submitted to any other Institute or University for the award of any other degree or diploma.

Place: Mumbai **Signature of guide:**

Date: May 02, 2014 **Name of guide: Prof. G. J. Prasad**

Place: Mumbai **Signature of co-guide:** Gautam Kumar Dey

Date: May 02, 2014 **Name of co-guide: Prof. G. K. Dey**

DEDICATIONS

My Dear Parents & Family

My Supervisors

To the Profession

It is hard to say what is difficult

For the dreams of yesterday, to hope of today and reality of tomorrow

ROBERT H. GERRARD

ACKNOWLEDGEMENTS

It is my pleasant duty to place a deep sense of indebtedness and gratitude to the authorities of Bhabha Atomic Research Centre, in particular to ***Mr. H.S. Kamath, Former Director, Nuclear Fuels Group and Mr. P.V. Hegde, Former Plant Superintendent, IF3 & Head, Fuel Development Section*** for their kind permission to carry out this research work and their strong support and encouragement towards the development of high density uranium system as potential fuel material for our next generation research and test reactor programme, which indeed is the main context of this dissertation imparting direct relevance for practical usage.

It is again with a pleasant sense of duty that I express my deep gratitude and thankfulness to my thesis supervisors ***Dr. G.J. Prasad, Director, Nuclear Fuels Group & Dr. G.K. Dey, Head, Materials Science Division*** for having guided me so ably in my Ph.D. programme. I fondly recall their strong support, friendly advice, help in taking up this project and valuable suggestions at various stages of the experimental investigation and discussions in the successful completion of this dissertation. Their constant inspiration throughout the work, even on temporary setback during the course of this work, has kept my spirits high and resurgent.

I thankfully acknowledge the generous support, motivation and help given by ***Mr. Arun Kumar, Head, Radiometallurgy Division and Mr. S.***

Anantharaman, Head, Post Irradiation Examination Division. It is also my pleasant sense of duty to thank ***Dr. Deep Prakash, ECMS & Mr. Rajeev Keswani, Plant Superintendent, A&PF3*** for their valuable comments, suggestions and help in writing the thesis.

I am indebted to many of my colleagues for supporting me during the course of study. I thankfully acknowledge the help and cooperation given by ***Messer S. Pal, G.P. Mishra, V.R. Nagvekar, M.R. Shaikh, S.S. Gotad, S.S. Prasad, R.K. Singh, A.B. Chowdhury, B.N. Pisal, R.M. Malagi and B.K. Mondal*** in synthesizing the material inside the glovebox. My special thanks are due to ***Dr. K.B. Khan, Head, PC&NS*** for offering me his valuable time in discussing the X-ray diffraction results.

I also extend my sincere thanks and acknowledge the generous help and support of ***Dr.(Mrs) S.B. Roy, Head, Uranium Extraction Division*** for facilitating the supply of uranium metal powder in desired quantity and specification to carry out the research work. I sincerely acknowledge ***Mr. R.S. Prasad, ED&DD*** for providing me the necessary help and support of workshop, if and when desired. I am also thankful to ***Shri Amit Sharma, AFD*** for providing natural uranium pellets in desired dimension and also in machining ingots of uranium molybdenum alloys for various experiments. I would also like to put my sincere thanks to ***Shri Arijit Laik, MSD*** for helping me in EPMA experiments. I would also extend my thanks to ***Dr. M.K. Saxena, RACD, RC&IG*** for providing chemical characterization results of different materials.

I owe a special distinction to my parents ***Mr. Uday Prakash Sinha & Mrs. Maya Sinha*** who have stood behind me during my most difficult times and always encouraged me to look forward. I am also infinitely thankful to my wife ***Mrs. Nutan Sinha*** for the unconditional love, advice, care and emotional support in the entire endeavor. My daughters ***Srishti & Soumya*** have always been a source of happiness and joy during the course of writing this dissertation. I take this opportunity to acknowledge the good wishes and support given by my brother ***Amit Prakash Sinha***, sister ***Deepti Srivastava***, brother in law ***Praveen Kumar Srivastava*** and all my other family members.

CONTENTS

Page No.

Synopsis ...*i*
List of Publications ...*xvii*
List of Figures ...*xviii*
List of Tables ...*xxv*
List of symbols ...*xxviii*

Chapter 1 *1.* *Introduction* ...*1*
1.1 *General* ...*1*
1.1.1 *History of self-sustaining chain reaction* ...*1*
1.1.2 *Nuclear energy for peaceful application* ...*2*
1.2 *Research Reactors* ...*4*
1.2.1 *Global scenario* ...*4*
1.2.2 *Research and test reactors in India* ...*8*
1.3 *Research reactor fuel and its development* ...*12*
Dispersion fuel ...*14*
1.4 *Aim of the present investigation* ...*17*
1.5 *Scope and objective of the present work* ...*19*
1.6 *Outline of the thesis* ...*22*

Chapter 2 *2.* *Literature Review* ...*25*
2.1 *Physical metallurgy of uranium* ...*25*
2.1.1 *Crystal structures of uranium* ...*25*
α-uranium ...*25*
β-uranium ...*26*
γ-uranium ...*26*
2.1.2 *Phase transformation in uranium* ...*26*
β→α transformations ...*27*
γ→β transformation ...*29*
γ→α transformation ...*29*

		2.1.3	*Phase transformation in uranium alloy systems*	*…30*
		2.1.4	*Effect of alloying on irradiation behaviour of uranium*	*…33*
	2.2	*Some nuclear properties of uranium*		*…36*
	2.3	*Dispersion fuel fabrication aspects*		*…38*
	2.4	*Uranium-Silicon alloy system*		*…41*
	2.5	*Uranium-Molybdenum alloy system*		*…44*
			Crystallography data of U-Mo system	*…49*
	2.6	*Summary of earlier studies & work carried on similar type of fuel and their reactor performance*		*…51*
	2.7	*Research approach and methodology*		*…55*
Chapter 3	3.	*Experimental Work & Technique*		*…58*
	3.1	*Experimental techniques*		*…58*
		3.1.1	*A brief account on alloy sample preparation*	*…58*
		3.1.2	*Crucible coating*	*…59*
	3.2	*Preparation of compound/alloy*		*…63*
		3.2.1	*Alloying of U_3Si_2 compound by powder metallurgy route*	*…63*
		3.2.2	*Powder metallurgy route for U-Mo alloys*	*…71*
		3.2.3	*Induction melting route for U-Mo alloys*	*…75*
	3.3	*Heat treatment*		*…79*
		3.3.1	*Hot rolling of as cast U-Mo alloy ingots*	*…81*
		3.3.2	*Quartz encapsulation and heat treatment of U-Mo alloy ingots*	*…84*
	3.4	*Characterization*		*…85*
		3.4.1	*Chemical analysis*	*…85*
		3.4.2	*X-ray diffraction (XRD) analysis*	*…85*
		3.4.3	*Metallography practice*	*…87*
		3.4.4	*Optical microscopy*	*…89*
			3.4.4.1 Phase analysis	*…90*

3.4.4.2 Grain size determination …91
3.5 Preparation of U-Mo diffusion couple & its characterization …93

Chapter 4 4. Results & Discussion …97
4.1 Characterization of U_3Si_2 compound prepared by powder metallurgy route …97
4.1.1 Phase analysis …97
4.1.2 Microstructural analysis …99
4.2 Characterization of U-Mo alloys prepared by powder metallurgy and melting casting routes …104
4.2.1 Phase analysis …104
4.2.2 Microstructural analysis …109
4.3 Characterization of U-Mo alloys for investigation on metastability in cubic γ-uranium …114
4.3.1 Phase analysis …114
4.3.2 Precise lattice parameter calculation …119
4.3.3 Microstructural analysis …122
4.3.4 Image analysis …132
4.4 Study on phase transformation of U-Mo alloys …134
4.4.1 Phase analysis …136
4.4.2 Precise lattice parameter calculation …144
4.4.3 Microstructural analysis …147
4.4.4 Study on end of life prediction for U-Mo alloys …157
4.5 Study on U-Mo diffusion couple …159

Chapter 5 5. Conclusions …166
5.1 Alloying of U_3Si_2 intermetallic by powder metallurgy route …166
5.2 Alloying of U-Mo by powder metallurgy & induction melting routes …168
5.3 Evaluation of cubic γ-phase metastability in U-Mo alloys …169
5.4 Phase transformation in U-Mo alloy …170
5.5 Experimentation on U-Mo diffusion couple …172

5.6 Scope for future studies ...173

Appendix-1 ...175
Appendix-2 ...178
Appendix-3 ...180
Appendix-4 ...183

Chapter 6 6. References ...185

SYNOPSIS

Synopsis of the Ph.D. thesis of Shri Ved Prakash Sinha submitted to the Homi Bhabha National Institute, Mumbai for the award of the degree of Doctor of Philosophy in Engineering Sciences.

Name of the candidate: Ved Prakash Sinha

Title of the thesis: Studies on the Preparation and Characterization of U_3Si_2 intermetallic and U-Mo alloys

Name of the Guide: Prof G. J. Prasad, Senior Professor, HBNI (Engineering Sciences)

Name of the co-Guide: Prof G. K. Dey, Senior Professor, HBNI (Engineering Sciences)

Place of Research: Metallic Fuels Division
Bhabha Atomic Research Centre, Trombay
Mumbai-400085

Enrollment particulars: ENGG01200704008

Synopsis on "Studies on the Preparation and Characterization of U_3Si_2 intermetallic and U-Mo alloys"

This thesis deals primarily with the development of process route/s for the preparation of high density uranium compound/alloys, to fulfill the requirement of upcoming and future Indian Nuclear Research and Test Reactors. It is of relevance to mention that due to the recent policy shift of Government of India which is also in trend with the present international practice, the development of LEU (Low Enriched Uranium) based fuel cycle programme for our existing and upcoming research and test reactors has become a major thrust area in the Department of Atomic Energy (DAE). In this context, nuclear fuels viz. uranium silicide (i.e. U_3Si_2) and U-Mo alloys are eminent candidate materials. Further, a processing method for their preparation needs to be developed keeping in view our special approach and specific requirements, where LEU is produced in metal powder form as well.

This study on the alloying of uranium silicide compound (i.e. U_3Si_2) by powder metallurgy route is perhaps the first reported attempt to systematically evaluate the effect of novel set of process parameters on the product characteristics. Further, the study on the preparation of U-Mo alloys with elemental powders as starting material has also been attempted for the first time. However, work on U-Mo alloy granule preparation by HDH (hydriding-dehydriding) process has been carried out and reported in Korea, Belgium, USA, France, Brazil etc. The process includes preparation of alloy by either induction or arc melting, followed by microstructure tailoring and grain spalling by HDH technique.

The U_3Si_2 compound and U-Mo alloys (three compositions) used in this study were prepared by powder processing route, using natural uranium and silicon powders in the first case and by using natural uranium and molybdenum metal powders in the second case. However, U-Mo alloys with seven different compositions were also prepared by conventional induction melting process where natural uranium and molybdenum metal pellets were used as starting materials.

Nuclear research and test reactors comprise a wide range of civil and commercial reactors that are not used for power generation purpose and their primary objective is to provide high emission rate (beam/irradiation position) neutron source [1]. Nuclear research reactors play a very crucial role in the peaceful use of nuclear energy such as production of radioisotopes, transmutation doping of silicon, testing of nuclear fuel and structural material, gem stone irradiation, nuclear physics and solid state physics studies involving neutron beam research and neutron radiography [2].

Fuel assemblies of these research reactors are made in various designs, typically plates, cylinders, convolutes etc. with uranium-aluminium alloy (U-Al) clad in nuclear grade commercially pure aluminium/alloy. HEU (U^{235}>85%) based fuels allow more compact cores, with high neutron fluxes and high burnup, therefore, reactors up to the 1970's have used this fuel technology. However, with time growing concerns related to fissile material diversion and proliferation gave rise to internationally accepted stipulation of 20% enrichment limit, thus emerging guidelines of LEU (Low Enriched Uranium) fuels. It was therefore required to develop high density fuel compound/alloys to successfully convert the existing reactor cores from HEU based fuels to LEU based fuels, without altering the basic reactor core design and other features [3].

Studies on various alloys systems to address the issues mentioned above gave rise to U-Si binary alloy system, which is still the most widely used option. Out of various line compounds existing in the U-Si system, U_3Si has the highest density. However, this phase is formed by peritectoid transformation at 925 °C. Also, U_3Si is tough and difficult to grind besides being prone to oxidation and has higher irradiation swelling. In contrast, the U_3Si_2, though has lower density as compared to U_3Si, is formed by congruent melting at 1665 °C, has better swelling characteristics on irradiation and is extremely friable, hence could be converted easily to powder form [4]. All these characteristics of U_3Si_2 have resulted in being the most favored/better compound for dispersion fuel application. In fact worldwide research reactor core conversions till date are based on U_3Si_2 compound dispersed in aluminium matrix and with Al alloy clad.

Aluminium base dispersion fuel with U_3Si_2 compound as fuel material was very useful to achieve heavy metal loading of up to 5 gm/cm^3 in the fuel meat. However, in order to achieve higher metal loading of 8 to 9 gm/cm^3 in the fuel meat with aluminium based dispersion fuel for ultra high flux research reactor, heavier compounds of uranium like U_6X (X: Mn, Fe, Ni) or Uranium alloys were attempted. It may be noted here that Uranium in the elemental form alone, cannot be used as dispersoid because of its poor chemical stability with the matrix at fuel fabrication and reactor operating conditions and also due to irradiation induced detrimental effects.

Uranium exists in three allotropic forms, α (Room Temperature to 668 °C orthorhombic crystal structure), β (668 to 775 °C, base centered tetragonal) and γ (775 °C to Melting Point, body centered cubic crystal structure). Out of these, γ-phase is the most stable under irradiation. This phase is thermodynamically not stable below 775 °C, however, there are some alloying elements which can metastabilize γ-uranium at room temperature [5].

Later, the use of U_6X compounds as fuel dispersoids was not found suitable because of their inherent break-away swelling characteristics. Hence the only choice left was to use uranium alloys as dispersoids for this purpose [6-7]. Most of these elements which form solid solution with uranium and stabilize γ-phase are transition metals, particularly from Group IVA to Group VIIIA of the periodic table. The stabilizing power of these elements to retain or metastabilize cubic γ-phase at room temperature increases with their atomic number, since more and more d-electrons participates in bonding due to hybridization with s- and p- orbital electrons. However, their solubility in uranium decreases because of the increase in atom size difference. Therefore, the choice of U-Mo system is identified as the best compromise between these two extreme ends [8].

The fuel compounds/alloys which have been discussed above are mostly prepared by induction or arc melting techniques. However, much of the literature on their preparation, characterization and basic metallurgy exists in classified work and only part of it is available in open literature [9]. It was also observed that the arc and induction melting technologies for preparing these compounds/alloys have their own difficulties and challenges. The major difficulties and challenges with induction melting technique while minimizing the segregation (mainly due to large density difference between the constituent elements in liquid phase) are impurity pickup due to crucible contamination, additional step for product homogenization and therefore leading to further product contamination and higher uranium losses because of higher processing temperatures, and are difficult to overcome. On the other hand, the compounds/alloys prepared by arc melting technique are with low impurity pickup but the product inhomogenity and the limitation for cost effective mass scale production had posed many challenges and involved repeated melting.

In this work, a systematic approach has been adopted for the preparation of U_3Si_2 compound and U-Mo alloys by powder metallurgy technique using elemental powders as starting material, so as to address the fuel fabrication requirements for modified core of APSARA and upcoming High Flux Research Reactors in India.

To fulfill the objectives of this study, the congruent melting U_3Si_2 compound was prepared with uranium metal powder and silicon powder as starting materials and processed at suitable temperature, so as to avoid any bulk liquid phase formation.

In a similar way, U-Mo alloys with three different compositions (i.e. 2, 5 & 10 wt% Mo) were also prepared by powder metallurgy technique with uranium and molybdenum metal powder as starting material. The chosen compositions were based upon the phase transformations expected from U-Mo phase diagram. The most dilute U-Mo alloy (2 wt% Mo) selected in the study, remains as γ-phase at high temperature and passes through β-phase field before transforming into equilibrium phase products, U_2Mo and α. The medium composition in the alloy was selected because γ-phase transforms directly to equilibrium phases and thus avoid transformation through β-phase field. The basis for selecting higher composition was to study the phase transformation in the alloy at near eutectoid composition. U-Mo alloys with above said compositions were also prepared by induction melting technique so as to compare the final product characteristics.

One of the objectives of the present study was to investigate the lowest possible concentration of molybdenum required to metastabilize cubic uranium phase at room temperature under the given furnace cooling conditions because molybdenum has higher parasitic capture cross section and hence its higher concentration in the alloy is undesired. For this purpose, seven different U-Mo alloys (i.e. 2, 5, 6, 7, 8, 9, 10 wt% Mo) were prepared by induction melting technique. It is also of importance that the fuel meat with stabilized γ-phase must also withstand the processing and reactor operating conditions for the life-time of the fuel plates. Therefore, another objective of the study was to investigate the effect of hot rolling of some select alloys samples followed by their heat treatment at 560 °C. The temperature chosen for the heat treatment is below the eutectoid phase transformation, albeit much higher than the reactor operating temperature (~250 °C) in this case.

As mentioned earlier, one of the motivations behind the present investigation has been to explore a processing route of dispersion fuels starting with Uranium metal powder. With this in view, select compositions from the U-Mo system were also attempted by P/M (Powder Metallurgy) route.

Having conducted a number of experiments to prepare and characterize the alloys and after accomplishing extensive literature survey, the thesis has been written and suitably divided into five chapters and further classified into sub-chapters and sections, as and when appropriate. The figures and tables are also listed as per their order of appearance and relevant context in the respective chapters. Chapter 1 is a brief introduction to the present research work and its objectives. This chapter starts with a general introduction on how the nuclear energy has evolved for peaceful applications, followed by a brief account on the global status of research reactors and also on different types of research and test reactors which were developed in India, their present status and the proposed ones in the near future. A brief discussion in the same chapter is also provided on the historic development of dispersion type fuels and its connection with RERTR programme.

Chapter 2 is a review on the existing literature relevant to the present work. This chapter starts with concept of basic uranium physical metallurgy, describing different types of allotropic forms, its crystal structure and also the temperature range over which they are stable. A brief discussion on the radioactivity of uranium is also explained in the subsequent section with appropriate details on the precautions adopted for safe handling of radioactive material and the concept of glove boxes. Next section is devoted to the different types of phase transformations in uranium and then sub-sections are written on the phase transformations in various uranium alloys and the effect of alloying upon the irradiation behaviour of uranium. The last sub-section is written mainly for non-nuclear readers not familiar with nuclear fuels to underscore neutron irradiation effects on fuels which has decisive role in establishing its usefulness (like low temperature tearing phenomenon observed in α-uranium (i.e. cavitation swelling), the concept of adjusted uranium and the swelling due to nucleation and growth of fission gas atoms followed by its coalescence). The next section is devoted to uranium-silicon and uranium-molybdenum system. The sub-section on uranium-silicon system explains that the compounds like U_3Si_2 and U_3Si_5 are formed congruently and therefore are more stable if compared with USi_2 and U_3Si which are formed by sluggish peritectoid reaction and with low decomposition temperature [10]. The sub-section on uranium-molybdenum system elucidates the effect of cooling rates on the phase transformation characteristics of dilute U-Mo alloys. In addition, the section also reasons about the suppression of β-phase field when the cooling rate is increased to 1000 °C/m for very dilute (8 at%Mo) alloys, hence allowing them to undergo phase transformation which is similar to that of pure uranium [10].

The experimental techniques employed in the present study and methodologies are described in Chapter 3. In the first two sections a brief account on alloy sample preparation and the crucible coating method is described. The next section is written on the preparation method for alloying of U_3Si_2 compound and U-Mo alloys by powder metallurgy technique. The process equipment employed in the preparation of compound/alloys are also shown there. The next sub-section is written on U-Mo alloy preparation by induction melting technique, followed by hot rolling and quartz encapsulation so as to perform the heat treatment studies. In the next section, different characterization techniques employed in this study are briefly described.

The results obtained in the present work are presented and analyzed in Chapter 4. This chapter is further classified into five sub-chapters: Characterization of U_3Si_2 compound synthesized by powder metallurgy route; Characterization of U-Mo alloys synthesized by powder metallurgy and melting casting route; Characterization of U-Mo alloys for investigation on metastability in cubic uranium; Phase transformation of U-Mo alloys; Study on U-Mo diffusion couple. Results show that U_3Si_2 compound synthesized by powder metallurgy process is a single phase compound and no other phases were observed in the detectable range of the XRD instrument. The subsequent analysis done by optical microstructure on the as synthesized U_3Si_2 compound has also revealed observations leading to the same conclusion. Synthesized compound density was found to be around 78 to 80% TD with succinct intragranular porosity, as can be observed in the microstructures [11]. Similarly the U-Mo alloys with compositions (2, 5, 10 wt% Mo) synthesized by powder metallurgy technique and induction melting technique have shown very similar phase content and microstructural characteristics. The only difference observed in the product characteristics prepared by both the processing techniques was density (78 to 80% TD for U-Mo alloys prepared by powder metallurgy technique) and the same can also be observed from the optical microstructures of U-Mo alloys prepared by powder processing technique (presence of intragranular porosity) [12]. The metastability of cubic uranium phase with different molybdenum compositions was also characterized and the results obtained from X-ray diffraction analysis and optical microstructures clearly indicated the complete metastability of cubic uranium phase with minimum addition of 8 wt%Mo. The phase transformation characteristics of U-Mo alloys were studied and the results showed that with increased molybdenum percentage the metastability of cubic uranium phase increased. It was also observed from the X-ray diffraction results that peak broadening of γ-phase in heat treated U-Mo alloys after long hours of heat treatment has reduced however, there was no marked difference on the peak characteristics of α-uranium [13]. The microstructural characterization of heat treated U-Mo alloys reveals the presence of eutectoid phase product. A diffusion couple between uranium and molybdenum was also prepared and the results clearly indicate that although molybdenum has diffused into uranium gradually but the reverse is not evident, as uranium concentration after the diffusion couple interface has dropped to near zero value.

The work in the present study was carried out with the objective of preparation and characterization of higher density fuel compound/alloys in context of immediate and future requirements in BARC (e.g. refueling of modified APSARA reactor core and to achieve high flux in the upcoming/proposed reactor core).

In view of this, a process for the preparation of congruent melting U_3Si_2 line compound phase was developed successfully by powder metallurgy technique with uranium metal powder and silicon powder as starting materials at much lower temperature reported so far. The uranium silicide compound thus synthesized was then heat treated well below the melting point of U_3Si_2 compound, reduced the chance of picking impurity by the product in the process to minimum. This was corroborated from the chemical characterization results, which showed that the total impurity content of the product and the starting materials did not differ much. The final soaking temperature of 1550 °C was selected keeping in view of eutectic and peritectic reaction temperatures in the system at 1540 °C and 1580 °C respectively. The U_3Si_2 line compound prepared by powder processing technique was found to be fairly homogeneous and no other silicide phases could be detected, thus ascertaining that the mixing of constituent elemental powder was carried out very effectively. Hence, the product prepared by this technique obviated additional homogenizing step as may be desired in other preparation techniques. The extent of porosity in the clinker suggested that even after crushing the clinkers to desired size fraction, a good amount of intragranular porosity was available in the fuel granules, which in turn would help in retaining fission products.

On the other hand, in case of U-Mo alloys (i.e. 2, 5 and 10 wt%Mo) prepared by powder processing route, the final soaking temperature was restricted to 1050 °C because of complete solid solubility in γ-phase. The final soaking temperature of all the three compositions of U-Mo alloys was kept same because their respective solidus does not change much [10]. The similar compositions of U-Mo alloys prepared by both powder processing and induction melting route did not show any major difference in phase and microstructural characterization, except the porosity, which was found in U-Mo alloys prepared by powder processing technique. As mentioned earlier, the presence of some porosity is a desirable microstructural feature in the nuclear fuels, as it helps in retention of fission products/gases. The compound/alloy prepared by powder processing technique was carried out very carefully by using process equipments installed inside glove box only and also under once-through flow of high purity argon gas atmosphere so that impurity pickup can be minimized. The non metallic impurities like carbon and nitrogen were also required to be controlled strictly so that undesired phases (like carbides and nitrides) in the product can be minimized or avoided because being actinide, uranium has more affinity towards these elements. It was observed that among the different combinations, U-2wt%Mo alloy prepared by only powder processing technique could be crushed in desired size fraction while all the other compositions prepared by either route were unsuitable for granulation by crushing. This is most likely because increased volume percentage of cubic phase being ductile rendered the product un-friable [13].

Based on the results obtained, it can be clearly concluded that a complete retention of cubic uranium phase under furnace cooling condition at room temperature was achieved with minimum 8wt%Mo addition in uranium. This implies that molybdenum percentage in uranium could be reduced to lower values in order to metastabilize the cubic uranium phase. This conclusion is significant from neutron economy view point so that alloying content in U-Mo should be reduced to as low as reasonably required.

The nuclear fuel, once loaded in the reactor, must withstand the operating temperature for the life-time of fuel elements. Keeping this in view, U-Mo alloy compositions which exhibited stability of γ-phase (>8 wt.% Mo) were hot-rolled followed by heat-treatment at 500°C up to 240 h. The heat-treated samples did exhibit decomposition of γ-phase into U_2Mo and α, however, the extent of transformation was found to decrease with increasing Mo-content in the alloys [14]. Further, though the amount of transformed phases were more in samples heat-treated for longer times, as expected, the total retained γ-phase quantity was found to be significant, as evidenced by XRD as well as microscopy. This finding is remarkable because it indicated sufficiently long life of U-Mo alloys (≥ 8wt% Mo) thus confirming them as potential candidate materials. These studies also provide basis for further investigation on the transformation kinetics under influence of neutron flux to establish these compositions as potential fuel for the next generation research reactors for the Indian Programme.

References

[1] International Atomic Energy Agency, Nuclear Research Reactor in the World, ***Reference data series 3, December 1994 Edition***.

[2] G. Kennedy and J. St. Pierre, LEU Fuelled SLOWPOKE-2 Research Reactor: Operational Experience and Utilization, ***Proceedings of the International Meeting on Reduced Enrichment for Research and Test Reactors, Bariloche (2002)***.

[3] G. L. Hofman, A Short note on High Density Dispersion Fuel, ***Argonne National Laboratory, 9700 South Cass Avenue, Argonne, IL 60439 USA, June 1996***.

[4] A.N. Holden, Physical Metallurgy of uranium, ***Addison-Wesley publishing Co. Inc., USA, (1958)***.

[5] H.S. Kalish et al., Uranium Alloys in Reactor Handbook, ***Vol. I, Materials, p. 174, C.R. Tipton Ed., Interscience Publishers, Inc., New York (1960)***.

[6] G.L. Hofman, R F. Domagala and G.L. Copel, Irradiation behavior of Low-Enriched U_6Fe-Al Dispersion Fuel Elements, ***J. Nucl. Mater. 150(1987)238***.

[7] M.K. Meyer, T.C. Wiencek, S.L. Hayes and G. L. Hofman, Irradiation Behavior of U_6Mn-Al Dispersion Fuel Elements, ***J. Nucl. Mater. 278(2000)358***.

[8] G.L. Hofman, M.K. Meyer and A.E. Ray, Design of High Density gamma-phase Uranium alloys for LEU Dispersion Fuel applications, ***Reduced Enrichment for Test Reactor Conference, Sao Paulo, Brazil, October 18-23, 1998***.

[9] N.L. Peterson, Diffusion in refractory metals, ***Wright air development division, United States air force, Wright-Patterson air force base, Ohio, 29-1102, May 1961***.

[10] ASM Handbook, ***Alloy Phase Diagram, Vol. 3, 2004***.

[11] V.P. Sinha, G.P. Mishra, S. Pal, K.B. Khan, P.V. Hegde, G.J. Prasad, Development of powder metallurgy technique for synthesis of U_3Si_2 dispersoid, ***J. Nucl. Mater. 383(2008)196***.

[12] V.P. Sinha, G.J. Prasad, P.V. Hegde, R. Keswani, C.B. Basak, S. Pal, G.P. Mishra, Development, Preparation and Characterization of uranium molybdenum alloys for dispersion fuel application, ***J. Alloys and Comp. 473(2009)238***.

[13] V.P. Sinha, G.J. Prasad, G.K. Dey and P.V. Hegde, Effect of molybdenum addition on metastability of cubic γ-uranium, ***J. Alloys and Comp. 491(2010)753***.

[14] V.P. Sinha, G.J. Prasad, G.K. Dey and P.V. Hegde, Phase transformation of metastable cubic γ-phase in U-Mo alloys, ***J. Alloys and Comp. 506(2010)253***.

As a consequence of this study and thesis work, the publications which were accomplished are listed in the next page.

LIST OF PUBLICATIONS

1. "Development of powder metallurgy technique for synthesis of U_3Si_2 dispersoid", V.P. Sinha, G.J. Prasad et.al. J. Nucl. Mater. 383(2008)196.

2. "Development of high density uranium compounds and alloys as dispersion fuel for the research and test reactors", V.P. Sinha, G.J. Prasad et.al. Trans. Indian Inst. Met. Vol. 61, No. 2(2008), 1-6.

3. "Development, Preparation and Characterization of uranium molybdenum alloys for dispersion fuel application", V.P. Sinha, G.J. Prasad et.al. J. Alloys and Comp. 473(2009)238.

4. "Development of high density uranium molybdenum alloys by powder metallurgy route for dispersion fuel application in research and test reactors", V. P. Sinha, G.J. Prasad et.al. 17th Plansee Seminar, 2009, vol 1, RM 78/1-16.

5. "Effect of molybdenum addition on metastability of cubic γ-uranium", V.P. Sinha, G.J. Prasad, G.K. Dey et.al. J. Alloys and Comp. 491(2010)753.

6. "Phase transformation of metastable cubic γ-phase in U-Mo alloys", V.P. Sinha, G.J. Prasad, G.K. Dey et.al. J. Alloys and Comp. 506(2010)253.

LIST OF FIGURES

Figure	*Description*	*Page No.*
1.1	**Graphical representation on the status of research reactor (numbers in developed and developing countries)**	**5**
1.2	**Status of operational research reactors in IAEA Member States (Total numbers of research reactor-273)**	**6**
1.3	**PIE chart showing the distribution of thermal powers of operating research reactors**	**7**
1.4	**Schematic of plate fuel fabrication by picture frame technique**	**9**
2.1	**Effect of alloy concentration on structure and hardness of quenched alloys**	**31**
2.2	**Transformation of γ-uranium alloys (solution heat treated at 900 ^{0}C)**	**34**
2.3	**Swelling rate of various γ-stabilized uranium alloys as a function of irradiation temperature**	**35**
2.4	**Uranium - silicon phase diagram**	**42**
2.5	**Magnified view of Uranium - silicon phase diagram**	**44**
2.6	**Uranium - Molybdenum phase diagram**	**46**
3.1	**Photograph of graphite crucibles (a) Top view of high density graphite crucible used for induction melting of U-Mo alloys, (b) Interior view of Na-CMC water solution based Y_2O_3 coated graphite crucible after curing**	**62**

Figure	*Description*	*Page No.*
3.2	**Photographs of starting materials (a) Uranium metal powder (b) Silicon chunks (c) Silicon powder**	**63**
3.3	**Facility for preparation of U_3Si_2 compound and U-Mo alloys by powder metallurgy route**	**66**
3.4	**Photographs of process equipment installed inside glove box (a) Blender, (b) Hydraulic Press, (c) Furnace, (d) Jaw Crusher, (e) Sieve Shaker**	**67**
3.5	**Flow-sheet for fabrication of U_3Si_2 fuel granules by powder metallurgy route**	**69**
3.6	**Photograph of U_3Si_2 pellets after synthesis**	**70**
3.7	**Photographs of starting materials (a) Uranium metal powder (b) Molybdenum metal powder**	**71**
3.8	**Photograph of U-Mo alloy pellets prepared by powder metallurgy route**	**74**
3.9	**Process flow sheet for preparation of U-Mo alloys by powder metallurgy route**	**75**
3.10	**Photograph of (a) Uranium metal pellets, (b) Molybdenum metal pieces**	**76**
3.11	**Photograph of as cast U-Mo alloy ingots**	**78**
3.12	**Photograph of copper jacketed as cast U-Mo alloy samples**	**81**
3.13	**Photograph of heat treatment furnace**	**82**
3.14	**Magnified view of U-Mo phase diagram and the basis for the selection of heat treatment**	**82**

Figure	*Description*	*Page No.*
3.15	**Photograph of rolled copper jacketed U-Mo alloy samples (a) U-8wt%Mo, (b) U-9wt%Mo and (c) U-10wt%Mo**	**83**
3.16	**Photograph of 2-high reversible hot rolling mill**	**83**
3.17	**Photograph of quartz encapsulated U-Mo alloy pieces**	**84**
3.18	**Photograph of θ-θ XRD machine**	**86**
3.19	**Photograph showing uranium and molybdenum pieces wrapped inside tantalum foil and loaded in inconel assembly**	**94**
3.20	**Photograph of quartz encapsulated diffusion couple**	**94**
3.21	**Photograph of uranium and molybdenum pieces taken out after diffusion couple experimentation**	**94**
3.22	**Schematic of uranium and molybdenum piece used in hot pressing**	**95**
3.23	**Photographs of U-Mo diffusion couple after vacuum hot pressing (a) Horizontal image, (b) Vertical image**	**96**
4.1	**XRD pattern of synthesized product (U_3Si_2) prepared by powder processing route**	**98**
4.2	**Optical microstructure of U_3Si_2 clinker**	**103**
4.3	**SEM photomicrographs of U_3Si_2 clinker (a) at 1500 magnification and (b) at 1200 magnification**	**104**
4.4	**X-ray diffraction patterns of U-2wt%Mo alloy prepared by (a) powder metallurgy route (b) induction melting route**	**106**

Figure	*Description*	*Page No.*
4.5	**X-ray diffraction patterns of U-5wt%Mo alloy prepared by (a) powder metallurgy route (b) induction melting route**	**107**
4.6	**X-ray diffraction patterns of U-10wt%Mo alloy prepared by (a) powder metallurgy route (b) induction melting route**	**108**
4.7	**Optical microstructures of U-2wt%Mo alloy prepared by (a) powder metallurgy route (b) induction melting route**	**110**
4.8	**Optical microstructures of U-5wt%Mo alloy prepared by (a) powder metallurgy route (b) induction melting route**	**111**
4.9	**Optical microstructures of U-10wt%Mo alloy prepared by (a) powder metallurgy route (b) induction melting route**	**112**
4.10	**X-ray diffraction patterns of as cast (a) U-2wt%Mo alloy, (b) U-5wt%Mo alloy, (c) U-6wt%Mo alloy, (d) U-7wt%Mo alloy, (e) U-8wt%Mo alloy, (f) U-9wt%Mo alloy and (g) U-10wt%Mo alloy**	**119**
4.11	**Plot showing change in precise lattice parameter of cubic γ-uranium with varying amount of molybdenum**	**121**
4.12	**Superimposed X-ray diffraction pattern of as cast U-Mo alloys with different molybdenum percentage (i.e. 2, 5, 6, 7, 8, 9, 10 wt% molybdenum)**	**123**
4.13	**Microstructures of as cast (a & b) U-2wt%Mo alloy**	**125**
4.14	**Microstructures of as cast (a & b) U-5wt%Mo alloy**	**126**

Figure	*Description*	*Page No.*
4.15	**Microstructures of as cast (a & b) U-6wt%Mo alloy**	**127**
4.16	**Microstructures of as cast (a & b) U-7wt%Mo alloy**	**128**
4.17	**Microstructures of as cast (a & b) U-8wt%Mo alloy**	**129**
4.18	**Microstructures of as cast (a & b) U-9wt%Mo alloy**	**130**
4.19	**Microstructures of as cast (a & b) U-10wt%Mo alloy**	**131**
4.20	**Quantitative analysis (in vol%) of cubic γ-phase for different molybdenum percentage in U-Mo alloys**	**133**
4.21	**X-ray diffraction patterns of as cast and hot rolled alloys (a) U-8wt%Mo, (b) U-9wt%Mo and (c) U-10wt%Mo**	**140**
4.22	**X-ray diffraction patterns of heat treated U-Mo alloy at 500^{0}C for 68 hrs (a) U-8wt%Mo, (b) U-9wt%Mo, (c) U-10wt%Mo**	**141**
4.23	**X-ray diffraction pattern of heat treated U-Mo alloy at 500^{0}C for 240 hrs (a) U-8wt%Mo, (b) U-9wt%Mo, (c) U-10wt%Mo**	**143**
4.24	**Bar chart showing volume percentage of retained γ-phase after different heat treatment for 8, 9 & 10wt% Mo alloys**	**144**
4.25	**Microstructures of hot rolled U-Mo alloy (a) U-8wt%Mo, (b) U-9wt%Mo, (c) U-10wt%Mo**	**150**

Figure	*Description*	*Page No.*
4.26	**Microstructures of heat treated U-Mo alloy at 500^{0}C for 68 hrs (a) & (b) U-8wt%Mo, (c) & (d) U-9wt%Mo, (e) & (f) U-10wt%Mo**	153
4.27	**Microstructures of heat treated U-Mo alloy at 500^{0}C for 240 hrs (a) & (b) U-8wt%Mo, (c) & (d) U-9wt%Mo, (e) & (f) U-10wt%Mo**	156
4.28	**Effect of soaking time on volume percentage of transformed phase at 500 °C**	158
4.29	**Optical microstructures of hot pressed U-Mo diffusion couple (a) at 500 X and (b) at 1000 X**	161
4.30	**BSE images of hot pressed U-Mo diffusion couple (a) at lower magnification and (b) at higher magnification**	162
4.31	**EPMA results (a) BSE image, (b) WDS scan on 2nd phase in uranium, (c) Intensity profile of U & Mo across the interface, (d) Intensity profile of 'Mo' on continuous line phase (e) Intensity profile of U & Mo across the interface with smaller region**	164
A-1	**Uranium - silicon phase diagram with desired composition and data points to evaluate different phase percentages**	175
A-2	**Plot between liquid and U_3Si_2 volume percentage for hyper composition and temperature**	177
A-3	**Schematic of heating profile followed in the alloying of U_3Si_2**	177
B-1	**Data plot of c_p as a function of temperature in the range 25 °C to 750 °C for U_3Si_2**	179

C-1 **Plot between transformed product and time** **182**

LIST OF TABLES

Table	*Description*	*Page No.*
1.1	Research reactors in India	11
1.2	Mechanical & Other relevant properties of unalloyed aluminium and its alloys	15
2.1	Details of α-decays of different uranium isotopes	37
2.2	Cross sections (in barn: 1 barn = 10^{-28} m^2) of different uranium isotopes for absorption and fission under high (fast) and low (slow) energy neutron fluence	38
2.3	Crystal structure data on uranium-silicon system	43
2.4	Crystal structure data on uranium-molybdenum system	50
3.1	Chemical analysis results of uranium metal powder	64
3.2	Chemical analysis results of silicon powder	65
3.3	Apparent and tap density of uranium metal powder	65
3.4	Pycnometer density and specific surface area of silicon powder	65
3.5	Chemical analysis results of as synthesized U_3Si_2 compound	70
3.6	Chemical analysis results of molybdenum metal powder	72
3.7	Pycnometer density and specific surface area of molybdenum metal powder	72

Table	*Description*	*Page No.*
3.8	Chemical analysis results of as synthesized U-Mo alloys by powder metallurgy route	74
3.9	Chemical analysis results of uranium metal pellet	77
3.10	Chemical analysis results of molybdenum metal piece	77
3.11	Weights of constituent elements and cast U-Mo alloys	79
3.12	Chemical analysis result of as cast U-Mo alloys	80
3.13	Description of etchants used for U_3Si_2 compound and U-Mo alloys in as cast, hot rolled and heat treated condition	89
4.1	ASTM grain size number for different compositions of U-Mo alloys with different preparation techniques (calculated as per ASTM 1382 intercept method)	114
4.2	Precise lattice parameter and lattice volume of orthorhombic α-uranium in U-Mo alloys	121
4.3	Precise lattice parameter and lattice volume of cubic γ-phase in U-Mo alloys	122
4.4	ASTM grain size number for different compositions of U-Mo alloys (calculated as per ASTM 1382 intercept method)	134
4.5	Volume percentage of phases in U-Mo alloys after different heat treatment history (calculated by POWDER CELL method)	143

Table	*Description*	*Page No.*
4.6	**Precise lattice parameter and lattice volume of cubic γ-uranium in hot rolled U-Mo alloys**	**145**
4.7	**Precise lattice parameter and lattice volume of orthorhombic α-uranium in heat treated U-Mo alloys**	**146**
4.8	**Image analysis result on heat treated U-Mo alloys**	**149**
A-1	**Phase volume percentage calculation of liquid phase for off-stoichiometry compositions (e.g. 92.5wt% U & 7.5wt% Si)**	**176**
C-1	**Transformation kinetics data**	**182**

LIST OF SYMBOLS

α-decay	*Alpha decay (Removal of helium nucleus from radioactive daughter product)*
β-decay	*Beta decay (Removal of an electron from the radioactive daughter product)*
γ-decay	*Gamma decay (Removal of electromagnetic radiation from radioactive daughter product)*
α-uranium	*Room temperature allotrope of uranium (Stability range (Room Temperature to 668 ^{0}C)*
β-uranium	*Allotrope of uranium (Stability range (668 ^{0}C to 775 ^{0}C)*
γ-uranium	*High temperature allotrope of uranium (Stability range 775 ^{0}C to 1132 ^{0}C)*
μm	*Micron (1 micron = 10^{-6} meter)*
Al	*Aluminium*
A	*Amperes*
BSE Image	*Back Scattered Electron Image*
BCC	*Body Centered Cubic Structure*
DU	*Depleted Uranium ($U^{235} < 0.7\%$)*
DC	*Direct Current Source*
EU	*Enriched Uranium ($U^{235} \geq 2\%$)*
EPMA	*Electron Probe Micro Analysis*
FCC	*Face Centered Cubic Structure*
HEU	*High Enriched Uranium ($U^{235} \geq 20\%$) for use in weapon grade $U^{235} \geq 85\%$)*

h	*Hours*
ID	*Inner Diameter*
I/M	*Induction Melting Route*
ID	*Internal Diameter*
KW	*Kilo Watt*
LEU	*Low Enriched Uranium* ($U^{235} < 20\%$)
MW(th)	*Mega Watt Thermal (Thermal Reactor Power)*
MW(e)	*Mega Watt Electrical (Electrical Reactor Power)*
MeV	*Million Electron Volt*
Mo	*Molybdenum*
OD	*Outer Diameter*
P/M	*Powder Metallurgy Route*
Pu	*Plutonium*
RERTR	*Reduced Enrichment in Research and Test Reactor Programme*
SEM	*Scanning Electron Microscopy*
SE Image	*Secondary Electron Image*
Si	*Silicon*
SEU	*Slightly Enriched Uranium* ($0.7\% < U^{23} < 2.5\%$)
SS	*Stainless Steel*
U	*Uranium*
V	*Volts*
XRD	*X-ray Diffraction*
Zr	*Zirconium*

1. Introduction

1.1 General

1.1.1 History of self-sustaining chain reaction

In the early part of 1930's, physicist *Enrico Fermi* and many other competing groups like *Otto Hahn, Strassman and Lise Meitner's team in Germany* had started independent experiments on splitting of heavy atoms into relatively lighter elements under neutron bombardment. Later, *Lise Meitner* migrated to *Denmark* due to the problems in *Nazi Germany*. Meanwhile *Fermi conducted* his experiments by bombarding uranium with neutrons. The results from these experiments were completely unexpected as the reaction product had different elements [1]. Independently, by the end of 1938, *Otto Hahn* and *Fritz Strassman* also conducted similar experiment, where neutrons from a source *(like radium and beryllium)* were bombarded into uranium. The results from the experiment were much to surprise, since they also found lighter elements such as barium in the left over material. During that time *Lise Meitner* in Copenhagen discovered the theory of mass difference between fission products and uranium [2-3]. After that she used *Einstein's* theory to explain the conversion of lost mass into energy. At that time this theory had opened a completely different arena of nuclear energy [4]. However, from the history it is clear that though *Lise Meitner* did not get her due for discovery of Nuclear Fission with *Otto Hahn*, her contributions were appreciated and accorded by many. In fact, *Enrico Fermi* was awarded Nobel Prize for discovery of Transuranic elements (which were actually fission products) and *Otto Hahn* for discovery of Nuclear Fission.

In 1939, *Bohr* came to America and shared the discovery of *Hahn-Strassman-Meitner* with *Einstein* and also met *Fermi* at an international conference on theoretical physics in Washington D.C. to discuss the possibility of self sustaining chain reaction. It was by this time, that scientists all around the world began to believe the possibility of self sustaining chain reaction with critical mass of uranium. In early 1942, a group of scientists led by *Fermi* gathered at the University of Chicago to test their theories and by November 1942, they were ready to begin the construction of world's first nuclear reactor which was later named as *Chicago Pile-1* [5]. The reactor was constructed on the floor of a squash court beneath the University of Chicago's athletic stadium. Uranium was used as fuel with graphite as moderator and cadmium metal rods were used to control chain reaction. On the morning of December 2, 1942 the scientists began demonstration of *Chicago Pile-1* and finally at 3:25 p.m., Chicago time, the nuclear reaction became self-sustaining and the world entered into the *Nuclear Age* [6].

1.1.2 Nuclear energy for peaceful application

Chicago Pile-1 was the beginning of civil nuclear programme since most of the earlier atomic research was focused on the development of effective weapon programme used in *World War II* and was done under the code name *'Manhattan Project'* [7-8]. It was only after the war, the United States Government encouraged the development of nuclear energy for peaceful civilian purposes, mainly because the economically recoverable resources of nuclear fuel materials (uranium and thorium) had the potential to provide energy that was several times larger than any other resource of fossil fuel. A single atom of uranium-235 isotope under fission would release around 200 MeV of energy which is well above the energy released by the combustion of a carbon atom (e.g. 4 eV). In addition to this, increase of oil price all around the world had also given an impetus on economical and commercial utilization of this large energy reservoir. It was also realized that the fertile isotopes such as uranium-238 in natural uranium and thorium-232 alone cannot sustain chain reaction. However, they can be converted into fissile isotopes of plutonium-239 and uranium-233 respectively by neutron absorption followed by beta decays. This had provided a great solution and opened up a completely different avenue to fulfill the increased global energy demand.

In 1946 the US congress had created the Atomic Energy Commission (AEC) to address this objective. The AEC authorized the construction of *Experimental Breeder Reactor-I* at a site in Idaho and the reactor had generated the first electricity from nuclear energy on *December 20, 1951* [9]. To achieve the major goal of peaceful application of nuclear energy for the production of electricity on commercial scale, the first commercial electricity-generating plant powered by nuclear energy was located in *Shippingport, Pennsylvania* and was operated at full design power in 1957 [10]. Although the main objective, for the peaceful application of nuclear energy programme around the world was to generate electric power, but there were many other areas, where it had helped enormously in the betterment of society. In this regard, nuclear research reactors have played a very crucial role, in the production of radioisotopes, transmutation doping of silicon, testing of nuclear fuel and structural material, gem stone irradiation, nuclear physics and solid state physics studies involving neutron beam research and neutron radiography [11-12].

1.2 Research Reactors

1.2.1 Global scenario

In the present days, the worldwide demand of research reactors for *nuclear science research, technology development, reactor services & for personnel education and training* does not require their large numbers, unlike in the 70's and 80's. Therefore, research reactors that stand out in the present generation were either with special attributes *(i.e. a high neutron flux, a cold source and in-core loops to simulate power reactor conditions)* or with diversified applications, to take advantage of commercial opportunities *(i.e. radioisotope production, gem coloring or silicon doping)*. In addition, research reactors also provide important training to the scientists/engineers and help in generating a pool of skilled human resource for future requirements.

For over 50 years, research reactors had made valuable contributions in the field of nuclear energy. As per IAEA database, there were 672 research reactors all over the world, 274 were operational in 56 countries

(85 in 39 developing countries), 214 were shutdown, 168 decommissioned and 16 others planned or under construction as in June 2004 [12-14].

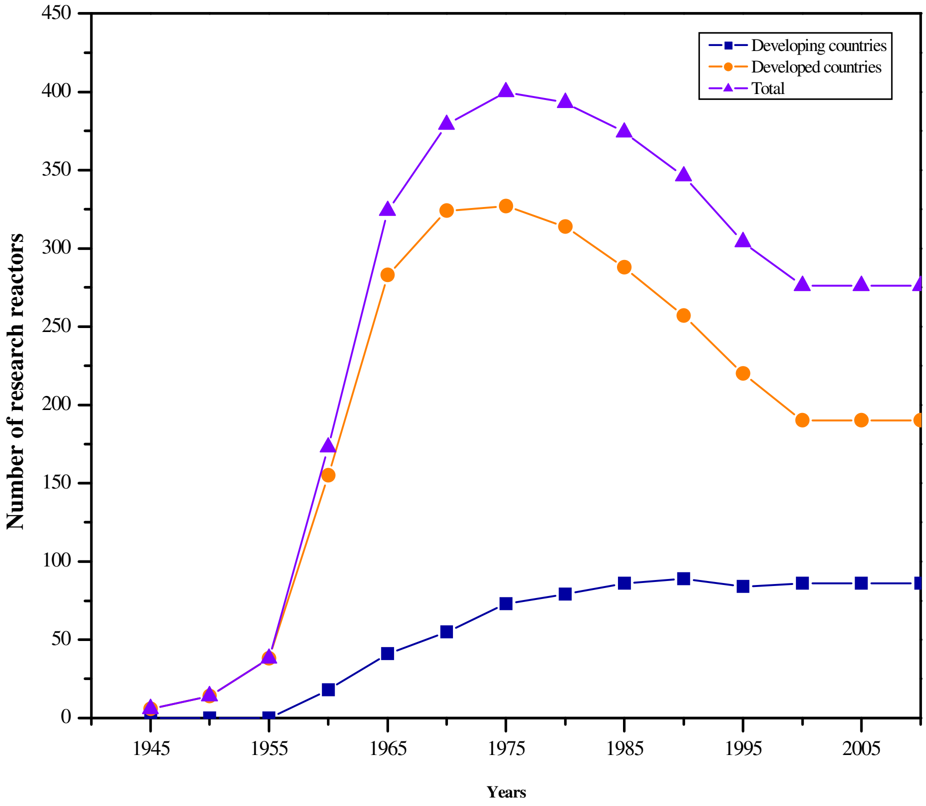

Fig. 1.1 Graphical representation on the status of research reactor (numbers in developed and developing countries) [12].

The number of countries with at least one research reactor had peaked to 60 in the mid-eighties. This had incidentally coincided to its peak of 41 numbers for developing countries in the same period *(as shown in Fig. 1.1)* [12]. However, the number of developed countries with at least one research reactor remained almost constant since 1965 and for developing countries since 1985 to the present. Only four developed countries and three developing countries that once had operational research reactor do not have any more now.

The worldwide distribution of research reactors among the member countries of IAEA, suggests that around 70% of them are located in the developed countries with *Russian Federation and USA* having the largest numbers *(as shown in Fig. 1.2)* [15]. It had also been observed that over the years there is a considerable decrease in the number of new research reactors being brought into operation and at the same time their shutdown numbers have also decreased. The present statistics accounts to the fact that nuclear energy in the present state has evolved from a relatively new science into an established technology.

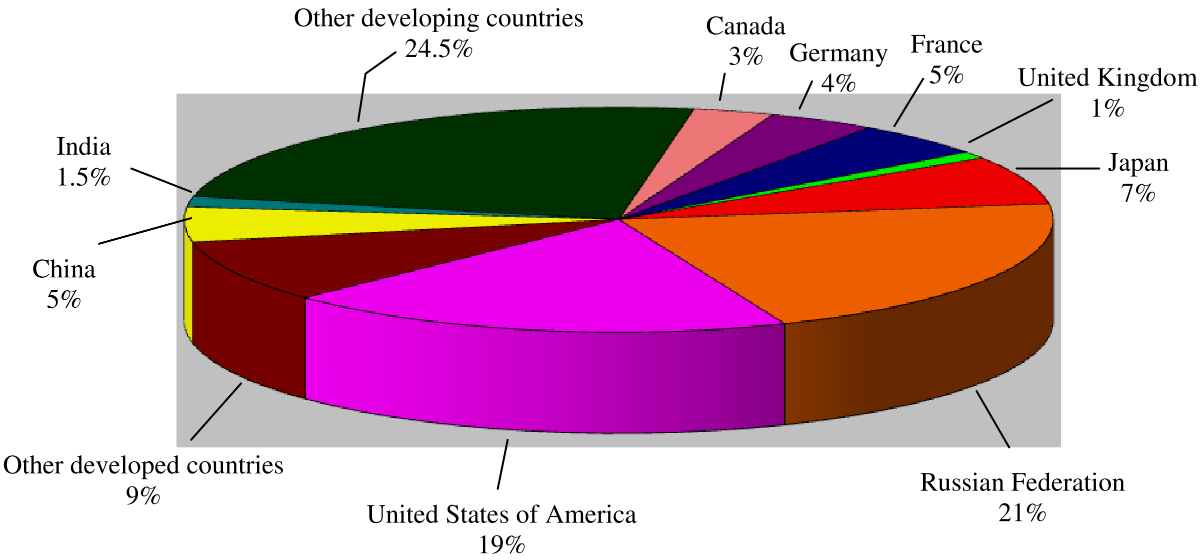

Fig. 1.2 Status of operational research reactors in IAEA Member States (Total numbers of research reactor-273) [15].

Most of these research reactors were operated with specific applications and under stringent safety norms so as to avoid any significant consequences in the worst case accidental scenario. Hence, almost 77% of the operational research reactors were commissioned with less than 5 MW power while 50% research reactors worldwide were operated at either 100 kW power or less. A pie chart shown in *Fig. 1.3* [15] gives an idea on the distribution of thermal powers of currently operating research reactors. The figure also confirms that the requirement of reactor core power density is not very high in many cases.

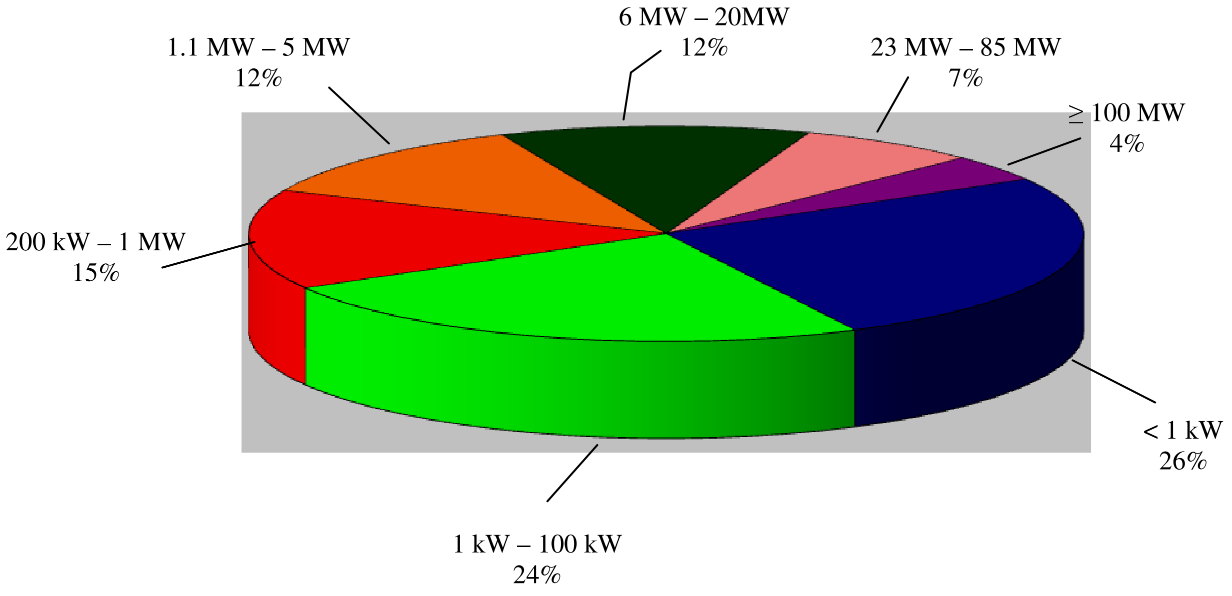

Fig. 1.3 PIE chart showing the distribution of thermal powers of operating research reactors [15].

1.2.2 Research and test reactors in India

One of the earliest milestones in India's nuclear programme was the commissioning of its first nuclear reactor at Trombay, in the year 1956, which was named *APSARA* by then *Prime Minister, Pandit Jawaharlal Nehru.* Incidentally, *APSARA* happened to be the first of its kind in Asia too. The basic design of the reactor was swimming pool type, and the fuel used was imported *Al clad Al-U (HEU)* alloy plate type fuels [16-17].

The success of *APSARA* has provided enough expertise as well as experience for DAE to come up with many other types of research reactors with different purposes and objectives. In this chain, a zero energy fast reactor *PURNIMA-I* was made critical on 18 May, 1972 at Trombay, by using PuO_2 pellets stacked inside stainless steel tube as fuel. Incidentally, this campaign was the first major plutonium based fuel fabrication activity in India. In the early 70's Al clad Al-Pu ($\leq$20% Pu; Al-10wt%Pu & 18wt%Pu) plate type fuel elements were fabricated at Trombay by "picture frame" technique *(as shown in Fig. 1.4)* followed by "roll bonding" for reactor physics experiments in *ZERLINA* critical assembly at Trombay [18]. It is also well established from the literature that aluminium has very poor solid solubility with uranium and plutonium. Therefore, in order to minimize the segregation between heavy metal and aluminium, a master alloy was prepared and then diluted to the desired composition [19]. The alloy was then picture framed and hot roll bonded to fabricate fuel plates of desired specification. Later, the knowhow was further developed and utilized for 30 kWth neutron source reactor, *KAMINI* at Kalpakkam. In total 9 fuel sub-assemblies were fabricated with Al clad Al-20%U^{233} and 3 sub-assemblies with Al clad Al-23%Pu for *KAMINI* [20-26]. A *Fast Breeder Test Reactor* is also in operation at Kalpakkam with mixed U-Pu carbide fuel and is mainly used for experiments related to fast reactor system. There are two more research reactors namely *CIRUS and DHRUVA* with 40MW and 100MW power respectively, and are located at Trombay. The fuel elements for these reactors are natural uranium rods clad in 1S aluminium. The *APSARA* research and test reactor is presently undergoing core conversion programme and will be upgraded to 2MW power with indigenous *LEU* based plate type fuel elements [16]. A brief description on the present status of Indian research reactors *(i.e. decommissioned, operational & planned in future)* is shown in *Table 1.1*.

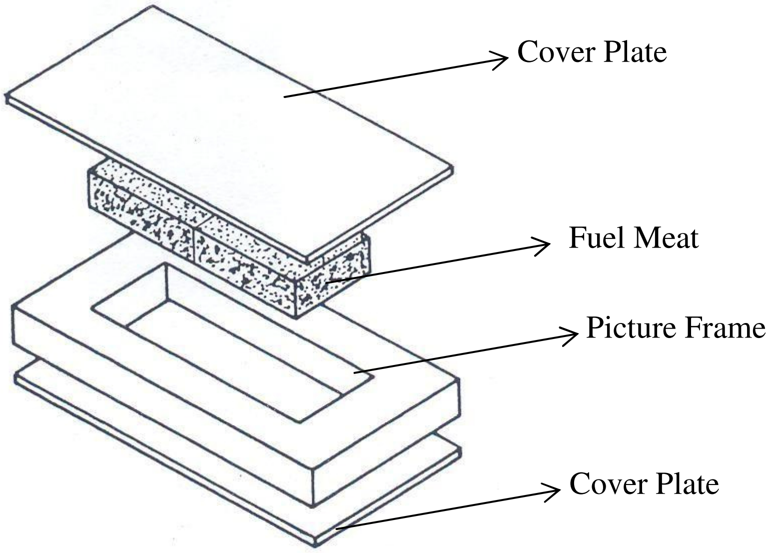

Fig. 1.4 Schematic of plate fuel fabrication by picture frame technique.

Name of the reactor	*Reactor Power*	*Date of criticality*	*Present status*	*Fuel employed*
APSARA	1 MW	August 4, 1956	Loading of 1st fuel charge was on July 30, 1956 & was removed from core in 1965	U-Al alloy with 46% enrichment *(Imported)*
			Loading of 2nd fuel charge was on May 4, 1965 & was removed from core in 1983	U-Al alloy with 80% enrichment *(Imported)*
			Loading of 3rd fuel charge was on August 1983 & was removed from core in 2010	U-Al alloy with 93% enrichment *(Imported)*
CIRUS	40 MW	July 10, 1960	Permanently shut down on December 31, 2010	Natural uranium rod with 1S Al-clad
ZERLINA	100 watt	January 14, 1961	Decommissioned in 1983	Natural uranium with imported heavy water
PURNIMA-I	1 watt	May 18, 1972	Decommissioned in 1974	21.6 kg of Pu^{239} in the form of PuO_2 pellets stacked in SS
PURNIMA-II	10 watt	May 10, 1984	Decommissioned in 1986	400 gram U^{233} in nitrate solution form

* Table continued in the next page

DHRUVA	100 MW	August 8, 1985	In service	Natural uranium rod with 1S Al-clad
PURNIMA-III	1 watt	November 9, 1990	Decommissioned in 1991	600 gm U^{233} in plate type fuel
KAMINI	30 kW	October 29, 1996	In service	9 SFA with U-20%U^{233} & 3 SFA with U-23%Pu^{239}
FBTR	40 MW	October 18, 1985	In service	Uranium and Plutonium mixed carbide fuel
Modified APSARA	2 MW	Expected in 2014	Construction stage	LEU based U_3Si_2 dispersed in Al-matrix and with Al-alloy clad
HFRR	30 MW	Expected in 2019	Plan project stage	LEU based U_3Si_2 dispersed in Al-matrix and with Al-alloy clad
DHRUVA-II	125 MW	Expected in 2020	Plan project stage	Mixed core of Natural and SEU metal rod in Al-clad

Table 1.1 Research reactors in India.

1.3 Research reactor fuel and its development

The fuel elements that have mainly been used in research reactors include; uranium metal, uranium alloys, dispersions in aluminium *(*UAl_x*,* U_3O_8*,* U_3Si_2*)*, dispersions in graphite and stainless steel *(*UO_2*)*, UZr-hydride, aqueous solutions (uranyl sulfate, nitrate or phosphate) [27-31] etc. A significant knowledge on experimental fuel and reactor concepts exists at the present moment however the majority of the fuel/reactor designs are based upon either *MTR* or *Triga* concept [32]. In the year 1952, the starting up of high-flux 45 MWth *Material Test Reactor (MTR) at Idaho*, gave origin to a wide group of similar types of research reactors with similar fuel concept and power installations to test materials in intense radiation field. In 1950s and 1960s, lower power research reactors were also built around the world using *MTR type* fuel elements containing low enriched uranium fuel; *LEU (*$U^{235} < 20$ *wt%).* However, in contrary, to low power research reactors based upon *MTR fuel design* which have utilized low enriched uranium for fuel, the high power research and test reactors have used high enriched uranium *HEU (*$U^{235} \cong 85$ *wt%).* The use of *HEU* has some benefits such as; it avoids the need of higher uranium concentration in the fuel, offers longer core resident time, higher specific reactivity and lower fuel costs. The above referred advantages with *HEU* based fuel, derived the designers to gradually convert the core from *LEU* to *HEU* even for the lower power reactors in the early years [33-34].

It was only when the concerns related to proliferation and diversion with *HEU* was raised in the *United States*, the commerce in *HEU* for research reactors fuel fabrication was discouraged. In general, to achieve the objective of complete elimination of *HEU* in the fuel cycle, the *United States* later introduced the *Reduced Enrichment for Research and Test Reactors (RERTR) programme* in 1978 [35-45]. A similar programme was also initiated in the former *Soviet Union* for their research and test reactors. In the later years both the programmes were merged together after *Russian Federation* became full partner to RERTR. It is also important to point out that three different types of fuels systems were in use with high enriched uranium *(HEU)* namely *UAl_x-Al dispersion fuel with uranium densities up to 1.7 g/cm^3, U_3O_8-Al dispersion fuel with uranium densities up to 1.3 g/cm^3, and $UZrH_x$ alloy fuel with uranium densities up to 0.5 g/cm^3 (8.5 wt% U)* prior to the inception of RERTR programme. UAl_x-Al (or aluminide) fuel was developed at the *Idaho National Engineering Laboratory* in the 1960s for use in the 250 MW ATR reactor. U_3O_8-Al (or oxide) fuel was developed at the *Oak Ridge National Laboratory* in the 1960s for use in the 100 MW HFIR reactor while $UZrH_x$ *(or TRIGA)* fuel was developed by *General Atomics* and used in TRIGA reactors with power levels up to 14 MW [46-58]. A major component of RERTR programme is the development and qualification of new, high-density, LEU fuels based on uranium silicon and later with uranium molybdenum alloys. The programme was focused with two major objectives, first to enable further conversions of reactors from *HEU to LEU* without effecting any major modification in the core and second to develop a substitute for *LEU silicides* which can be reprocessed more easily [59-62].

Dispersion fuel

Over the years plate fuel technology was established as the most proven and reliable method for the fabrication of fuels for research and test reactors all over the world. However, it was also reported that *Russia* had pursued their design of tube type fuel assembly and later converted to rod type design for their research reactors [34]. The advantage of tube/rod type fuel design over plate type geometry is its better geometrical stability *(i.e. hoop stress)*. However, plate type fuel geometry provides higher heat transfer rate because of its large surface area [63-65]. This attribute of plate fuel allows it to operate almost in cold condition leading to higher neutron flux in the reactor. In view of this, many materials *(like Mg, Graphite, Be, Zr and Al)* were initially considered for clad but aluminium and its alloys had found edge over others due to the ease in fabrication, high thermal conductivity, excellent irradiation stability, good corrosion resistance in water at reactor operating temperatures, adequate mechanical property and low parasitic capture cross section for thermal neutrons. The relevant properties of alloyed and unalloyed aluminium are shown in *Table 1.2* [18].

A thermal neutron flux of the order 10^{13} to 10^{14} n/cm^2/s could be achieved easily with the existing conventional fuel design and fuel fabrication technology. However, when the neutron flux was required to increase by an order or two then a new design philosophy was desired. The objective of increase in neutron flux could be achieved either by increasing fissile atom density or by changing the fuel geometry.

Alloy Number	***ALCOA (US)***		***1050***	***1100***	***5052***	***6061***
	IS (INDIA)		***19500***	***19000***	***52000***	***65032***
Composition (wt%)	*Aluminium*		*99.5*	*99*	*Balance*	*Balance*
	Magnesium		-	-	*2.5*	*1.2*
	Silicon		-	-	-	*0.8*
Temperatures (^{0}C)	*Liquidus*		*657*	*657*	*649*	*652*
	Solidus		*646*	*643*	*607*	*582*
	Annealing		*345*	*345*	*345*	-
	Solution Treatment		-	-	-	*530*
	Aging		-	-	-	*175*
Properties	*Tensile Strength*	*Ksi*	*11*	*13*	*28*	*18*
		MPa	*76*	*90*	*193*	*124*
	Yield Strength	*Ksi*	*4*	*5*	*16*	*8*
		MPa	*28*	*34*	*110*	*55*
	Shear Strength	*Ksi*	*9*	*9*	*18*	*12*
		MPa	*62*	*62*	*125*	*83*
	Total Elongation (%)		*39*	*35*	*30*	*25*
	Hardness (500 kg, 10mm ball)		*19*	*23*	*47*	*60*
	Specific Heat (J/Kg/K)		*900*	*904*	*895*	*896*
	Thermal Conductivity (W/m/K)		*231*	*222*	*218*	*180*

Table 1.2 Mechanical & Other relevant properties of unalloyed aluminium and its alloys [18].

An inevitable consequence of the requirement for these ultrahigh flux intensities in a reactor was a tenfold increase in core power density, which would put an enormous burden on burnup reactivity and core cycle length *(and consequently on fuel cycle cost)*. In the earlier days, of fuel design and technology development, enrichment of fissile atom was increased up to ~95wt%U^{235} to achieve this goal but due to issues related to proliferation and international policy of *LEU* usage in research reactor this technology had received a setback. Hence, alternate methods were explored and developed for the purpose [66-68]. In an alternate method the requirement to achieve ultrahigh thermal flux intensities in a large reflector volume surrounding the core lead to core designs that would reduce internal neutron moderation and enhance neutron leakage. Neutron leakage could be maximized for core configuration with following ways [69-70]:

i. A relatively hard neutron energy spectrum which would enhance the probability of fast neutron leakage into the reflector/moderator.

ii. High surface to volume ratio.

iii. Selection of different moderating materials (such as D_2O) with a longer neutron mean free path when compared to the dimensions of the fuel region.

High neutron flux intensity of the order 10^{15} to 10^{16} n/cm^2/s required high fission rate densities which in turn would require a small and compact core volume while keeping the total reactor power as low as possible. The required high core power density resulted in relatively high heat flux value which was a major challenge for effective core cooling. However the challenge could be encountered by number of ways [71]:

i. Thickness of fuel plates could be reduced so that a large fuel plate surface area per unit core volume was created.

ii. The coolant flow velocity would also been increased.

iii. Shortening flow path and efficient hydraulic geometries could have been introduced.

There were many high flux reactors which were designed as central flux trap machines for material irradiation and isotope production. In this design an annulus region was made by combining different numbers of curved shape fuel plates. The neutrons were under moderated in this location and then the leaked neutrons were moderated efficiently by the combination of reflector/moderator near specific irradiation locations [72].

1.4 Aim of the present investigation

The aim of the present work was primarily to study process route/s for the preparation of high density uranium compound/alloys. However, the basic knowhow of plate type fuel technology did exist in BARC. In the earlier developmental work *U-Al alloy* and *Pu-Al alloy* was employed as fuel meat and was sandwiched between aluminium plates for physics experiments and later in *KAMINI* reactor. The uranium used was in U^{233} isotopic form for *KAMINI* fuel plates. BARC also commissioned studies yielding significant amount of development and research work on the phase stability of UAl_3 compound. [26]. The work reported, in this thesis was successfully adapted for fuel fabrication activity to make nine fuel assemblies with U-20%U^{233} and three fuel assemblies with U-23% Pu^{239}. Thus part of the motivation for the present work was derived from the success story of fuel development activity carried out for *KAMINI* in the past.

It may be stated that due to our recent policy shift and also keeping in trend with the prevailing international practice, the development of LEU (Low Enriched Uranium) based fuels Research & Development activities for our existing and upcoming research and test reactors would become a major thrust area in BARC, in lieu of HEU (High Enriched Uranium). In fact, the motivation for the present work also came from the requirement and need to develop indigenous fuel for the modified core of *APSARA* reactor. *APSARA* reactor has so far utilized imported fuel from UK in all its three refueling cycles *(as can be seen from Table 1.1)*. It was only after 2010, the need for developing LEU based indigenous fuel for the modified core of *APSARA* was realized by the department. In this context, it was identified that nuclear fuels viz. uranium silicide *(i.e.* U_3Si_2*)* and *U-Mo alloys* are the potential candidate materials. Therefore, the aim of the present work was to develop a processing method for their alloying keeping in view our unique and specific requirements, where LEU is available in metal powder form. The aim of this present work was also to employ the economical and feasible methodology of fuel development work which could easily be converted to fuel production activity.

1.5 Scope and objective of the present work

It is well understood from the previous chapters that fuel assemblies of most of the research reactors employed in the past are typically plates or cylinders of HEU based uranium-aluminium alloy (U-Al) clad in nuclear grade commercially pure aluminium/alloy. However, as already explained in *section 1.3*, studies on various alloys systems were carried out all over the world to encourage the commerce in LEU without employing any major design implications on the basic reactor core design. The results obtained from these studies have indicated the distinct advantages of U-Si binary alloy system. In fact U-Si system is still one of the most popular choice amongst the furl designers, mainly because of higher heavy metal density in the compound and its stable in pile characteristics under specified and desired reactor operating conditions. However, it is also known that U-Si system has extremely poor solid solubility with large number of intermediate phases of fixed stoichiometry.

Out of the seven line compounds existing in U-Si system, U_3Si_2 has evolved as the most practical and better compound for dispersion fuel application because of better swelling characteristics after irradiation, ease in fabrication and high heavy metal density. In contrary, if the heavy metal loading in aluminium based fuel meat is required to increase to 8-9 gm/cm^3 then *uranium alloys* are the only choice for dispersoids. Out of the many uranium alloys considered for the purpose, *U-Mo* has achieved the most favored attention because of its best compromise between solid solubility and intermetallic phase formation.

The fuel compounds/alloys which have been discussed above are mostly prepared by induction or arc melting techniques. However, much of the literature on their preparation, characterization and general metallurgy existed in classified work and only part of it is available in open literature after declassification [73]. It was also observed that the arc and induction melting technologies for preparing these compounds/alloys have their own difficulties and challenges. The major difficulties and challenges with induction melting technique are segregation *(mainly due to large density difference between the constituent elements)*, impurity pickup due to crucible contamination, additional step for product homogenization and therefore leading to further product contamination and higher uranium losses because of higher processing temperature. On the other hand, the compounds/alloys prepared by arc melting technique are with lower impurity pickup but the product inhomogenity and the limitation for cost effective mass scale production had posed many challenges.

In this work, a systematic approach has been adopted for the preparation of U_3Si_2 *compound* and *U-Mo alloys* by powder metallurgy technique, so as to address the fuel fabrication requirements for modified core of *APSARA* and upcoming high flux research reactors in India. This study on the alloying of uranium silicide compound *(i.e.* U_3Si_2*)* and *U-Mo* alloys by powder metallurgy route is perhaps the first attempt to systematically evaluate the effect of process parameters on the final product characteristics. The U_3Si_2 compound and *U-Mo* alloys used in this study were synthesized by powder processing route, using natural uranium and silicon powders in first case and by using natural uranium and molybdenum metal powders in the second case so as to address our unique requirement, where LEU is present in metal powder form.

Therefore, the first objective of the present work was to develop a solid state alloying process for the preparation of homogeneous U_3Si_2 line compound phase. The final heat treatment temperature was also desired to be kept well below the *liquidus* of U_3Si_2. As mentioned earlier, one of the motivations behind the present investigation has been to scout for a processing route of dispersoid fuels starting with Uranium metal powder. With this in view, select compositions from the U-Mo system were also attempted by P/M (Powder Metallurgy) route. These compositions were carefully selected and were based upon the different phase transformations expected from *U-Mo* phase diagram. It was observed that the most dilute *U-Mo* alloy selected in the study undergo phase transformation from γ to β first before transforming into equilibrium phase products. The medium composition in the alloy was selected because γ-phase transforms directly to equilibrium phases and thus avoid transformation through β-phase field. The basis for selecting higher composition was to study the phase transformation in the alloy at near eutectoid composition. *U-Mo* alloys with above said compositions were also prepared by induction melting technique so as to compare the final product characteristics. The objective was also to achieve excellent product characteristics by powder processing route, with low impurity pickup, low crucible/tray contamination and with no additional homogenization step.

One of the objectives of the present study was also to investigate the minimum quantity of molybdenum required to metastabilize cubic uranium phase at room temperature under furnace cooling conditions because molybdenum has higher parasitic capture cross section. For this purpose, seven different *U-Mo* alloys *(i.e. 2, 5, 6, 7, 8, 9, 10wt%Mo)* were prepared by induction melting technique. The fuel meat with stabilized γ-phase must withstand the processing and reactor operating conditions for the life-time of the fuel plates. Therefore, another objective of the study was to investigate the effect of hot rolling of some select alloys samples followed by their heat treatment at 500 °C. The temperature chosen for the heat treatment is below the eutectoid phase transformation, albeit much higher than the reactor operating temperature (~250 °C) in this case.

1.6 Outline of the thesis

The thesis is organized in five chapters which are further classified into sub-chapters and sections, as and when appropriate. *Chapter 1* is a brief introduction on the present work and its objective. The chapter starts with history of self sustaining chain reaction and the evolution of nuclear energy for peaceful application. This is followed by a global perspective on the development of research reactor followed by a brief overview on the present status of Indian research and test reactor programme. In the next section a brief account on the development of dispersion fuel and the influence of

RERTR programme on *LEU* fuel development is mentioned. This is followed by a section on the scope and objective of the present research programme.

Chapter 2 is written on literature review relevant to the present work. The chapter starts with small discussion on physical metallurgy of uranium and a brief note on the issue related to handling and radioactivity of uranium. The section on uranium physical metallurgy is then divided in four sub-sections, describing crystal structures, phase transformations and the effect of alloying addition on the irradiation behavior of uranium. Next section describes the most common fuel fabrication technology developed and followed by many around the world. It is then followed by the sections, where a brief discussion on uranium-molybdenum alloy system and uranium-silicon has been presented. In the last section of this chapter, the research approach adopted in the present work to achieve the desired objective has been discussed.

The experimental techniques employed in the present study and methodologies are described in *Chapter 3*. In the first section a brief account on the preparation of *U-Mo alloy* by induction melting technique and the methodology adopted for the coating of graphite crucible is presented. The next section describes preparation of U_3Si_2 compound and *U-Mo alloys* by powder processing route. The following section mentions the hot rolling of uranium molybdenum alloys followed by quartz encapsulation and its heat treatment. The section is then followed by a brief description on various characterization techniques employed in the present work.

The results obtained in the present work are presented and analyzed in *Chapter 4*. This chapter is further classified into five sub-chapters, where results are shown one after another on: alloying of U_3Si_2 compound by powder metallurgy route; alloying of *U-Mo* alloys by powder metallurgy and melting casting route; metastability of *U-Mo* alloys; phase transformation of *U-Mo* alloys; study on *U-Mo* diffusion couple.

Results obtained from the experiments and their analyses, as described in *chapter 4* eventually lead to conclusions, as summarized in subsequent *chapter 5*. List of references, in the order of appearance, is given at the end of the thesis.

2. Literature Review

2.1 Physical metallurgy of uranium

In general uranium is used as major alloying element for dispersion fuels, however plutonium based alloys have also been tried in many places but their application is limited and were used in special cases only. Therefore, it is pertinent to give a brief account on the physical metallurgy of uranium, an actinide in the periodic table. It is also important to note that due to the electronic configuration its alloying behavior is very complex and it does not exhibit large solubility with most elements.

2.1.1 Crystal structures of uranium

Solid elemental uranium exhibit three polymorphic forms: bcc γ phase (>775 °C), tetragonal β phase (between 668 °C and 775 °C) and orthorhombic α phase (<668 °C).

α-uranium

The orthorhombic α-uranium phase is stable from room temperature to 668 °C. Jacob and Warren [74], in 1937, first described the crystal structure of α-uranium by powder diffraction technique. It is clearly seen from the structure that the (010) plane is corrugated and from experiments it has been established that during heating it's a and c axis get expanded where as b axis contracts. The space group of α-U is determined as Cmcm with 4 atoms per unit cell. The coordinate of the four atoms are given as (0, y, ¼), (0, -y, ¾), (½, y+½, ¼) and (½, ½-y, ¾); where y=0.1025.

β-uranium

The tetragonal β-uranium phase is stable from 668 °C to 775 °C. Tucker [75], in 1950 first described the crystal structure of β-U by high temperature powder diffraction technique. The space group of β-U is determined as $P4_2nm$ with 30 atoms per unit. The coordinate of the atoms are given as follows, using the Wyckoff notations: 2 atoms are in b position, 4 atoms in f position (x=0.1033), 8 atoms are in j position (x=0.3183, z=0.27), 8 atoms are in I position (x=0.3667, y=0.0383) and 8 atoms are in I position (x=0.5608, y=0.2354). The crystal structure is considered to be composed of two densely populated planes (B and C) with one less populated rumpled intermediate plane A. So the structure can be reproduced with AB AC AB AC stacking in [001].

γ-uranium

The body centered cubic phase (BCC) of γ-uranium phase (space group $Im\bar{3}m$) is stable between 775 °C and 1132 °C. Wilson and Rundle [76], in 1939, first described the crystal structure of γ-U by high temperature powder diffraction technique. At 800 °C temperature the lattice parameter of γ-U was found to be 3.538 Å.

2.1.2 Phase transformation in uranium

It has been shown by *Duwez* [77] that it is improbable that any rate of cooling from the gamma phase will prevent the formation of first beta and then the alpha phase in pure uranium. The range in temperature over which the beta uranium phase exists is in fact increases with increasing cooling rates and the DTA result supports the same fact. *Klepfer and Chiotti* [78] have studied the rate and amount of transformation as a function of isothermal holding time in regions near each equilibrium transformation temperature. Their study included the transformations γ→β, β→α and vice versa and the work was done with uranium containing less than 150 ppm of impurities. The percent of metal transformed near each equilibrium transformation temperature was evidently a function of the isothermal temperature [79]. Under isothermal conditions, the rate of transformation proceeded rapidly at first and then slowed down to zero as an apparent end of transformation was reached and further change in isothermal temperature would cause additional transformation. These effects are similar to classical martensitic behavior and therefore all the transformations in pure uranium were defined as coherently nucleated martensite like transformation.

β→α transformations

For pure uranium TTT curve shows two 'C' shaped curves [80]. The curve near equilibrium temperature corresponds to diffusion controlled transformation whereas the lower 'C' curve stands for martensitic transformation. For pure uranium the lower 'C' curve is most predominant but with increasing alloying addition it has been seen that the diffusion controlled mechanism is prevalent. The salient features of β to α formation by martensitic transformation are as follows [81]:

i. The transformation occurred by the growth of plates of alpha on preferred habit planes in the beta matrix. These habit planes have been identified as principally the {321} plane.

ii. The plates grow by a mechanism that involves shear of the uranium metal within the beta plate. Hence straight surface scrathes in the beta matrix are observed to be sheared by the formation of the alpha plates.

iii. The rate of growth of the plates of alpha under isothermal condition is slow, yet much too rapid to the diffusion controlled even at room temperature. The rates of growth of these plates have been observed as few millimeters an hour.

iv. The plates of martensite are profusely twinned, a process that seems to be required to relieve the stress.

v. The transformation seems to go to completion isothermally even at room temperature. Plates already formed catalyze the formation of others in the regions between existing plates.

The principal {321} habit plane is crystallographically unimportant because of less population of atoms. It seems that the relief of shear stresses using martensitic transformation, is easier across poorly matched, crystallographically unimportant interfaces. Two different important crystallographic relationships were established; $\{001\}_\alpha \parallel \{101\}_\beta$ and $\{001\}_\alpha \parallel \{212\}_\beta$ and for both the cases it was observed that $\langle 021\rangle_\alpha \parallel \langle 410\rangle_\beta$. The twinning within the alpha plates seems to be exclusively {130}. These {130} are not far from the habit plane of the alpha plates and thus they relieve the shear stress readily as the plate grows. Most likely there is no matching of atoms between the two structures across the habit plane, which results in forked or flamelike ends of the growing alpha plates [82].

γ→β transformation

Based on metallography, the gamma to beta transformation in pure uranium appears to be a normal nucleation and growth type mechanism. However, *Klepfer's* [83] data indicates that at least coherent nucleation may be involved. Quantitative model proposed by *Kitchingman* [84] postulates that the main layers of beta uranium are produced by a shifting together of the A, B and C atom layers that lie normal to a given $[111]_\gamma$ direction in the A2 arrangement. Lattice relationships are predicted to be $(11\bar{1})_\gamma \parallel (001)_\beta$ and $[1\bar{1}0]_\gamma \parallel [\bar{1}\bar{4}0]_\beta$. However, no experimental verification of these relationships has been established.

γ→α transformation

As stated earlier in pure uranium, alpha phase does not form directly from gamma phase. However, it is possible to have retained gamma phase in many of the uranium alloys; like U-Mo, U-Zr, U-V and U-Nb. The quantity of the alloying elements and cooling rate required to accomplish the gamma phase retention varies greatly with each element. The retained gamma can be transformed to alpha either by diffusion controlled mechanism during continuous cooling or by martensitic mechanism with applied deformation [85].

One curious fact stands out in the information on phase transformations is that the beta to alpha martensites seems to grow slowly, whereas gamma to alpha martensite in many instances seems to grow very rapidly upon quenching. Although inadequate data and an interesting speculation is that martensite formed in the gamma-alpha transformation grows very rapidly, like the martensite in steel because the matrix is a ductile bcc metal. Thus the instantaneous growth of alpha martensite plates, in gamma matrix, is possible because matrix shear strains are easily accommodated, while beta-alpha martensite is slow because matrix shear strains are difficult and the martensite plates must twin, as previously discussed [86].

2.1.3 Phase transformation in uranium alloy systems

Uranium is frequently alloyed to improve its corrosion resistance and/or to modify its mechanical properties. These alloys are mostly fabricated by vacuum induction or arc melting technique. Solubility of various alloying elements is different in different phases. In most cases α-phase cannot dissolve any element in more than 0.3%, however extent of dissolution varies from element to element and also with temperature. β-phase can dissolve alloying elements to the tune of 1%. Alloying elements, like Mo, Nb, Ti, Zr can form a solid solution with γ-phase with a concentration ranging from 20% or higher, whereas Au, Pd, Pt, Re, Rh, Ru and V are soluble to γ-phase with 2% to 10% concentration [87]. In U-Zr system, for example γ-U can dissolve 100 at% Zr but β phase can dissolve maximum 1 at% Zr at 965K and that alpha phase can dissolve only about 0.6 at% Zr maximum at 935K. By and large slow cooling permits the γ-phase to decompose to two-phase structures morphologically similar to pearlite in steel. Rapid quenching suppresses these diffusional decomposition modes, resulting in various metastable phases. The microstructure and hardness produced by quenching are summarized in *Fig. 2.1* [88].

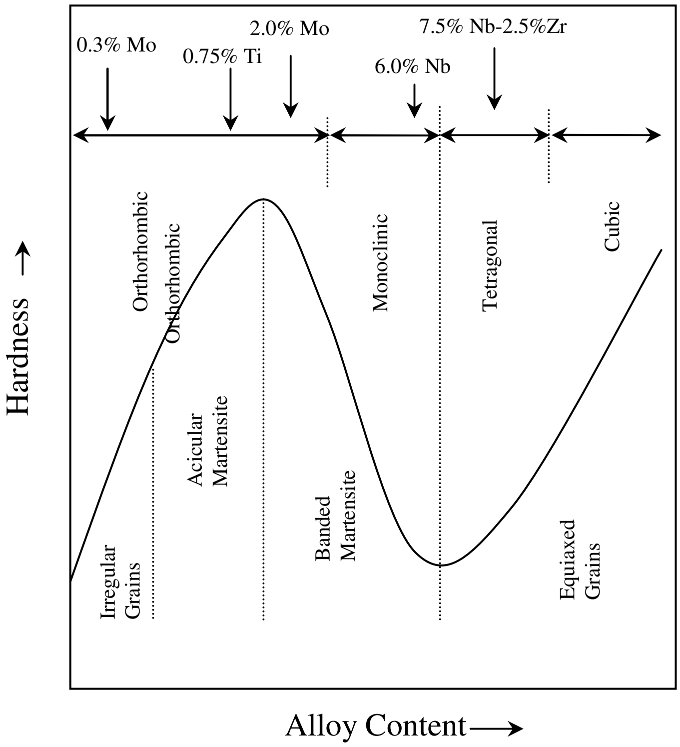

Fig. 2.1 Effect of alloy concentration on structure and hardness of quenched alloys [88].

Very dilute alloys exhibit supersaturated α-phase with irregular grain morphology similar to that of unalloyed uranium. Slightly more concentrated alloys exhibit acicular martensite microstructures. Both of these micro constituent are orthorhombic variants of α-uranium. Their hardness and yield strength increase with increasing alloy content due to solid solution effect. Further increase in alloy content cause a transition to a thermoelastic, or banded, martensite. The hardness and yield strength of the thermoelastic martensite decreases with increasing alloy content which is apparently due to increasing mobility of the boundaries of the many fine twins produced during the transformation. Midway in the thermoelastic martensite composition range, the crystal structure changes to monoclinic, as one lattice angle departs gradually from 90^0. This change in crystal structure has little apparent effect on mechanical behavior. These martensitic variants of α-uranium are frequently termed as a'_a, a'_b and a''_b where the subscripts a and b denote the acicular and banded morphology respectively and the prime and double prime subscript denotes the orthorhombic and monoclinic crystal structure respectively. Additional increase in alloy content produces a transition to γ^0, an ordered tetragonal variant of high temperature γ-phase. Further alloy addition cause retention of the cubic γ-phase. These variants of the γ-phase can be distinguished by X-ray diffraction but not by metallography [89].

From the previous discussion it can be concluded that with increasing concentration of alloying elements, the quenched specimen of uranium alloys from the γ-phase field, exhibit a sequence of structures at room temperature. The general sequence progress from $\alpha \rightarrow \beta \rightarrow a'_a \rightarrow a'_b \rightarrow a''_b \rightarrow \gamma^0 \rightarrow \gamma^s \rightarrow \gamma$ [90], here γ^s is variant of bcc γ with small distortions. However, all the phases in the sequence are not observed in every system and some systems may exhibit other metastable states such as omega phase that occurs in Ti and Zr alloys. Moreover, quenched structure is quite sensitive to gammatizing temperature and cooling rate, implying that stresses due to quenching, ordering and/or retained vacancy concentration are important.

2.1.4 Effect of alloying on irradiation behaviour of uranium

A great deal of effort had gone into attempts to reduce swelling of uranium by means of alloying. By and large this method was very successful in delaying the onset of high swelling rates to higher burnup levels so as to yield satisfactory fuel performance in thermal reactors. This had led to the development of adjusted uranium where uranium was alloyed with small amounts of Al, Fe or Si. These alloying elements form small precipitate phases which control the point defect behavior by pinning the defects, thereby reducing the low burnup tearing phenomenon [91-94]. Low burnup tearing phenomenon can again be explained as cavitation swelling mechanism. In this case even when the fission atom gas density is lower the swelling is observed due to the anisotropy of material; which in turn assist the irradiation growth. In addition, development work on high density uranium alloys was focused on a group of elements that form extensive solid solutions with uranium in high temperature cubic γ-phase. These elements lower the temperature of cubic γ-phase boundary, allowing more of the fuel to operate in the isotropic γ-phase [95-101].

The swelling behaviour of these alloys at low burnup was mainly driven by the relative stability of the γ-phase at low temperatures *(as shown in Fig 2.2)* [88]. The cooling curve shown in *Fig 2.2* explains the effect of cooling rate on the phase transformation product. As can be observed from *Fig 2.2* that if the nose of the curve could be avoided by increasing the rate of cooling to that of critical cooling rate then the cubic γ-uranium will not break into equilibrium phase products at room temperature and will metastabilize.

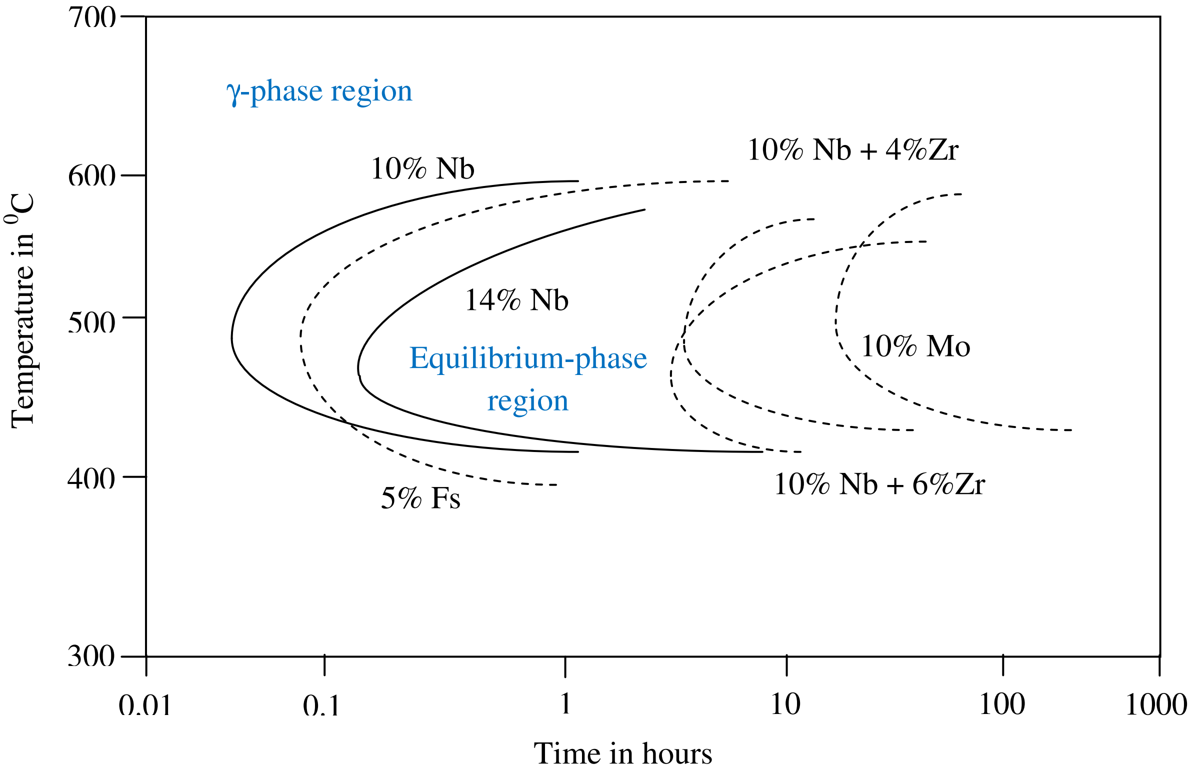

Fig. 2.2 Transformation of γ-uranium alloys (solution heat treated at 900 ^{0}C) [88].

The equilibrium phase products in different uranium alloy systems was explained and determined from their respective equilibrium phase diagrams. For example the cubic phase of U-Nb alloys decomposes very quickly into two phases *(predominantly to orthorhombic α-phase)* even at moderate temperatures. In turn, the swelling in these alloys was characterized by the rapid cavitation in α-phase, which in turn is similar to that of α-U in the temperature range of 300 to 400 °C. The cavitation swelling in uranium could also be suppressed with the addition of Zr and could further be decreased with the addition of Mo as shown in *Fig 2.3* [88]. On the other hand swelling, in γ-phase was due to the formation of fission gas atom followed by its coalescence. Hence, if the operational temperature of fuel is reduced then at very high fission rates, γ-phase will remain stable and cavitation swelling under those conditions could be suppressed [98].

A two stage swelling behavior was observed in UO_2 and U_3Si_2 compounds. Hence, their swelling behavior increases abruptly after certain fission density. The reason for increased swelling was the formation of sub grains, which in turn give shorter path for the migration of fission gas atoms [99].

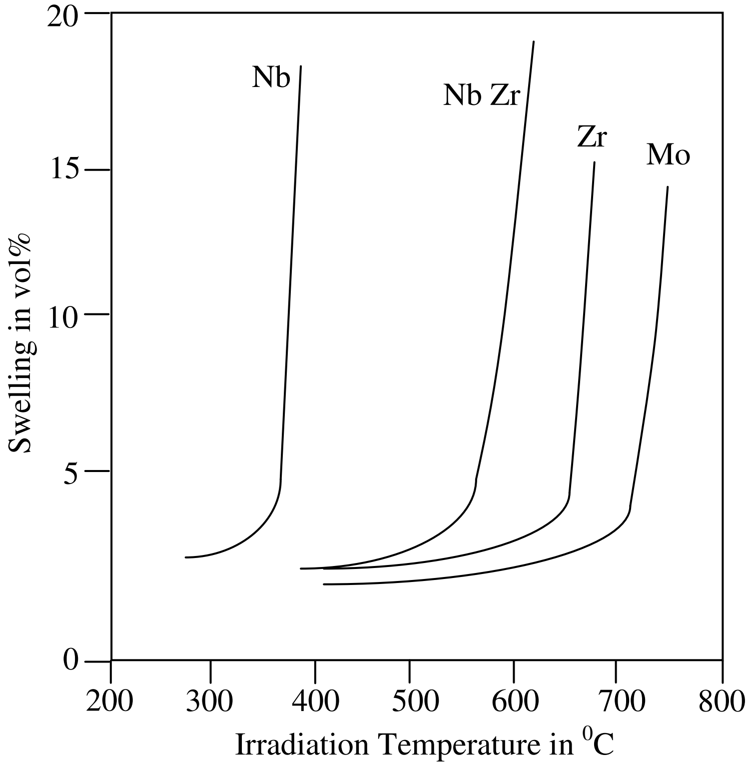

Fig. 2.3 Swelling rate of various γ-stabilized uranium alloys as a function of irradiation temperature [88].

2.2 Some nuclear properties of uranium

Natural uranium consists of three isotopes: U^{234} (0.006%), U^{235} (0.72%) and U^{238} (99.274%); however from strategic point of view U^{235} is of more importance. Depending upon the isotopic content of U^{235} there are two grades of metallic uranium. Enriched uranium *(EU)*, sometimes called "oralloy" consists of more than 0.7% U^{235}; whereas depleted uranium *(DU)*, sometimes termed "tuballoy" or D-38 contains only about 0.2% of U^{235} [102]. Density of natural uranium is 19.1 g/cc and is around 68% greater than lead.

There are also other isotopes of uranium that are produced by mutation reaction from the other nuclides. Most of the uranium isotopes are having α-decays and the relevant data is tabulated in *Table 2.1* [103].

Other than the α-decays, U^{235} undergoes γ-decays, U^{237} undergoes both γ and β decays only. On the other hand when neutronic reactions (fission, absorption etc.) are concerned only three isotopes of uranium are of importance and is tabulated in *Table 2.2* [104]. The data presented in *Table 2.2* clearly indicates that though the specific activity of natural uranium is very low, the specific activity of enriched uranium increases proportionately with enrichment. However, the biological half life of uranium is very low *(145 days)*, therefore handling and fuel processing difficulties are not so stringent as in case of actinides with higher atomic number and fission fragments.

Nonetheless, the safe working limits for handling uranium or LEU are again derived from the guidelines given by either *ICRP* or *AERB*. Therefore, the annual dose limit for occupational worker is 50 mSv and is restricted to 100 mSv for five year plan.

Isotope	***Specific Activity (Ci/gm)***	***Energy of α (MeV) and Yield (%)***	***Average Half Life (years)***
U^{230}	*9.99 X 10^{14}*	*5.815 (32%), 5.889 (67.4%)*	---
U^{232}	*7.77 X 10^{11}*	*5.320 (68.6%), 5.264 (31.7%)*	*72*
U^{233}	*3.52 X 10^{8}*	*4.783 (14.9%), 4.824 (82.7%)*	*1.59 X 10^{5}*
U^{234}	*2.29 X 10^{8}*	*4.775 (72.5%), 4.724 (28.4%)*	*2.44 X 10^{5}*
U^{235}	*7.77 X 10^{4}*	*4.556 (4.2%), 4.40 (55%), 4.365 (17%), 4.218 (5.7%), 4.599 (5%), 4.445 (26%)*	*7.03 X 10^{8}*
U^{236}	*2.33 X 10^{6}*	*4.494 (74%)*	*2.37 X 10^{7}*
U^{238}	*1.22 X 10^{4}*	*4.147 (23%), 4.196 (77%)*	*4.47 X 10^{9}*
Nat. U	*2.63 X 104*	*From appropriate isotopes*	---

Table 2.1 Details of α-decays of different uranium isotopes [103].

In addition, the powder form of uranium is highly pyrophoric and if handled without adequate care then it may cause fire and also enter the body by means of inhalation. Once the uranium is entered by inhalation then it would give internal dose until removed completely from the body by means of urine and faeces. The internal exposure in this case is measured in terms of *ALI (Annual Limit of Intake)*, which is cumulative for both internal and external exposures [105]. Hence, extreme care and precautions were taken in alloy & sample preparation and characterization. Therefore, the uranium powder was handled inside special designed glove boxes maintain under negative pressure and under once through flow of argon cover gas. These glove boxes are adequately kept in the amber zone of radioactive laboratory. The laboratories in radioactive area are classified in different zones and their classification depends completely upon the amount of activity handled, pressure gradients and dose levels. The other advantage of handling uranium metal powder inside glove box was careful material accounting.

Isotope	***Fast Neutron***		***Slow Neutron***	
	Absorption	***Fission***	***Absorption***	***Fission***
U^{233}	---	---	*47*	*531*
U^{235}	*0*	*1.3*	*98*	*580*
U^{238}	*2*	*0.5*	*2.8*	*0.0005*

Table 2.2 Cross sections (in barn: 1 barn = 10^{-28} m^2) of different uranium isotopes for absorption and fission under high (fast) and low (slow) energy neutron fluence [104].

2.3 Dispersion fuel fabrication aspects

Fuel cycle based on *LEU* either requires increase of fuel volume loading in the meat or high density uranium compounds/alloys to compensate lower fissile enrichment. The two most common fuel fabrication techniques employed globally for LEU fuel preparation were roll bonding process for plate geometry and extrusion process for rod or tube geometry [63, 106-108]. Roll bonding process was suitable for the loading of fuel particle up to around 55 vol% and extrusion method was likely to have a lower maximum fuel particle volume limit [54].

However, the development of high uranium density fuel compounds/alloys was imperative to fulfill the objective of increasing heavy metal loading up to 8-9 g/cm^3 so as to render the demand for high thermal neutron flux density to perform superior quality experiments. It was also observed that high uranium density compounds like *U_3Si and U_6Me (where Me can be Fe, Ni, Mn, Co or Ge)* was not formed suitable because of their inherent break-away swelling characteristics even at relatively lower burnup [91-92, 109-118].

It may also be noted that uranium in the elemental form alone, cannot be used as dispersoid for the purpose because of its poor chemical stability with the matrix at fuel fabrication and reactor operating conditions and also due to irradiation induced detrimental effects. Uranium exists in three allotropic forms, α *(Room Temperature to 668 °C orthorhombic crystal structure)*, β *(668 to 775 °C, base centered tetragonal)* and γ *(775 to Melting Point, body centered cubic crystal structure)*. Out of these, γ-phase is the most stable under irradiation as compared with α-uranium because swelling takes place mainly due to fission gas nucleation and growth mechanism as against by cavitation in α-uranium. This phase is thermodynamically not stable below

775 °C, however, there are some alloying elements which can metastabilize γ-uranium at room temperature [119]. Several transition metals, particularly from Group IVA to Group VIIIA of periodic table form solid solution with *γ-uranium* to metastabilize γ-phase at room temperature upon cooling. The stabilizing power of these elements to retain or metastabilize cubic γ-phase at room temperature increases with their atomic number, since more and more d-electrons participates in bonding due to hybridization with s- and p- orbital electrons. However, their solubility in uranium decreases because of the increase in atom size difference.

In addition, the increase in atom size difference between transition element and uranium favor intermetallic compound formation instead of a solid solution. The uranium alloys which have a tendency to form stable cubic phase at room temperature are *U-Zr, U-Mo, U-Nb, U-Re, U-Ru, U-Ti etc*. The first two transition elements of 4d series *(i.e. Zr & Nb)* forms complete solid solution with *γ-uranium* but complete retention of cubic *γ-phase* at room temperature, require their large concentration in uranium [120-122]. On the other extreme, *Pd and Pt* are very strong stabilizers of cubic *γ-uranium* at room temperature under furnace cooling condition but their limited solid solubility in uranium *(only ~2 at%)* leads to various intermetallic compounds. Therefore, the choice of *U-Mo* system is identified as the best compromise between these two extreme ends [123-127].

2.4 Uranium-Silicon alloy system

The solid solubility of silicon in all the three allotropes of uranium is negligible. Similarly the solid solubility of α-uranium in silicon is only 0.025 at% at room temperature and does not change much with the increase of temperature. In total there are seven intermediate phases in U-Si system and are stoichiometric line compounds *(as shown in Fig. 2.4).* Amongst them, U_3Si_2 and U_3Si_5 are formed congruently at 1665 °C and 1770 °C respectively. Therefore these compounds were formed directly from the liquid melt and they do not undergo any phase transformation until melting. $USi_{1.88}$ and USi_3 are formed by peritectic reactions at 1710 °C and 1510 °C respectively, $(L + U_3Si_5 \leftrightarrow USi_{1.88}$ *and* $L + USi_{1.88} \leftrightarrow USi_3)$ respectively. The compounds like USi_2 and U_3Si are formed by sluggish peritectoid reaction at 450 °C and 930 °C respectively, $(USi_3 + USi_{1.88} \leftrightarrow USi_2$ *and* $U_3Si_2 + U \leftrightarrow U_3Si)$. There is also a eutectic temperature of 1315 °C at 58 wt% U in the system [128-133]. Detail information of uranium silicon system has been compiled and is shown in *Table 2.3.* A further, magnified view of *U-Si* phase diagram with region of interest in the present study is also shown in *Fig. 2.5*

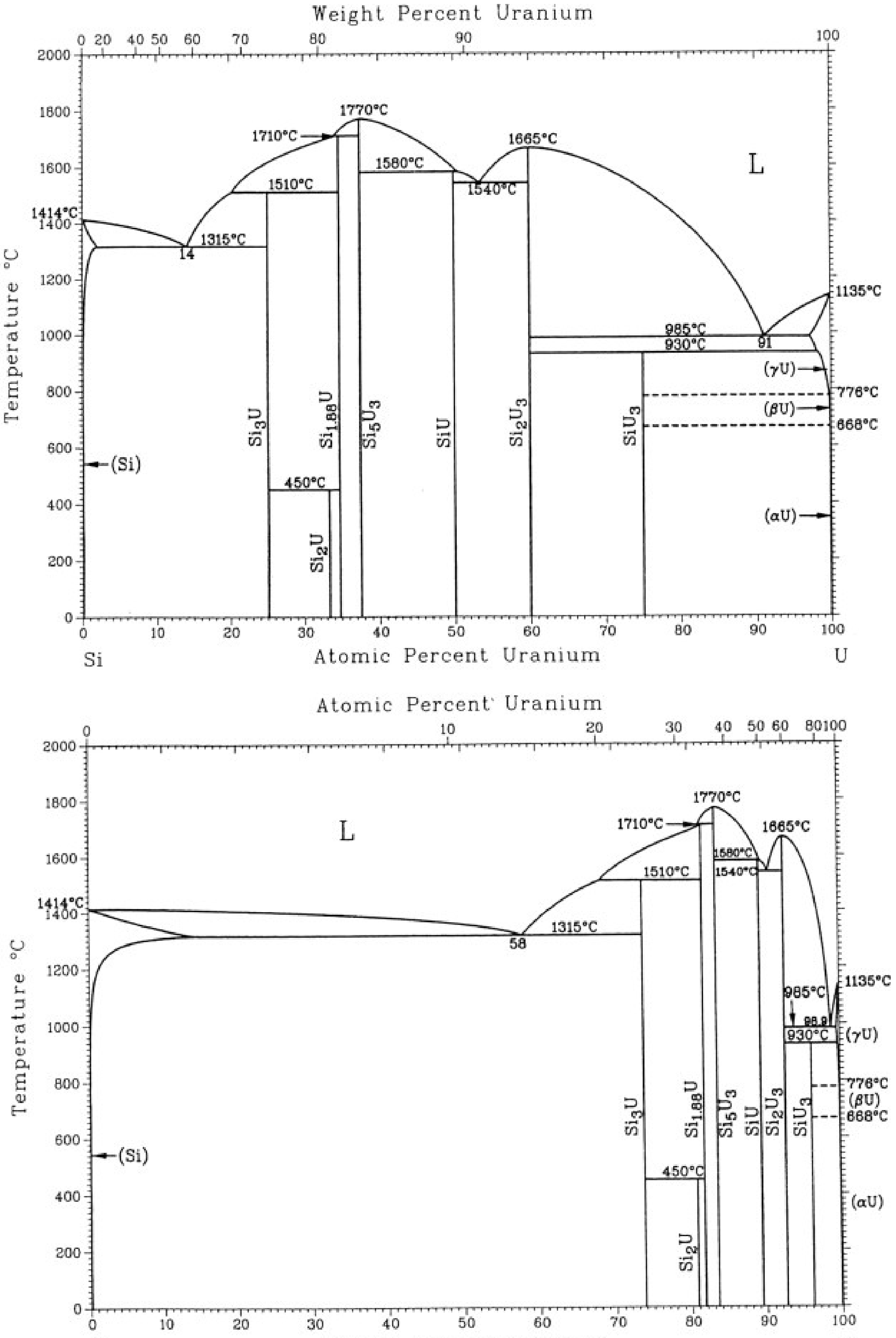

Fig. 2.4 Uranium - silicon phase diagram [113].

Phase	Composition (at% U)	Composition (wt% U)	Formation reaction	Formation temperature (℃)	Pearson symbol	Space group	Prototype
Si	0	0	-	-	cF8	Fd-3m	C (diamond)
Si_3U	25	74	Peritectic	1510	cP4	Pm-3m	$AuCu_3$
Si_2U	33.3	80.9	Peritectoid	450	hP3	P6/mmm	$A1B_2$
$Si_{1.88}U$	34.7	81.8	Peritectic	1710	tI12	$I4_1/amd$	$ThSi_2$
Si_5U_3	37.5	83.6	Congruent	1770	hP3	P6/mmm	$A1B_2$
SiU	50	89.4	Peritectic	1580	oP8	Pnma	FeB
Si_2U_3	60	93	Congruent	1665	tP19	P4/mbm	Si_2U_3
SiU_3	75	96	Peritectoid	930	cP4	Pm-3m	$AuCu_3$
γ-U	100	100	-	668	cI2	Im-3m	W
β-U	100	100	-	775	tP30	$P4_2/mnm$	β-U
α-U	100	100	-	1132	oC4	Cmcm	α-U

Table 2.3 Crystal structure data on uranium-silicon system.

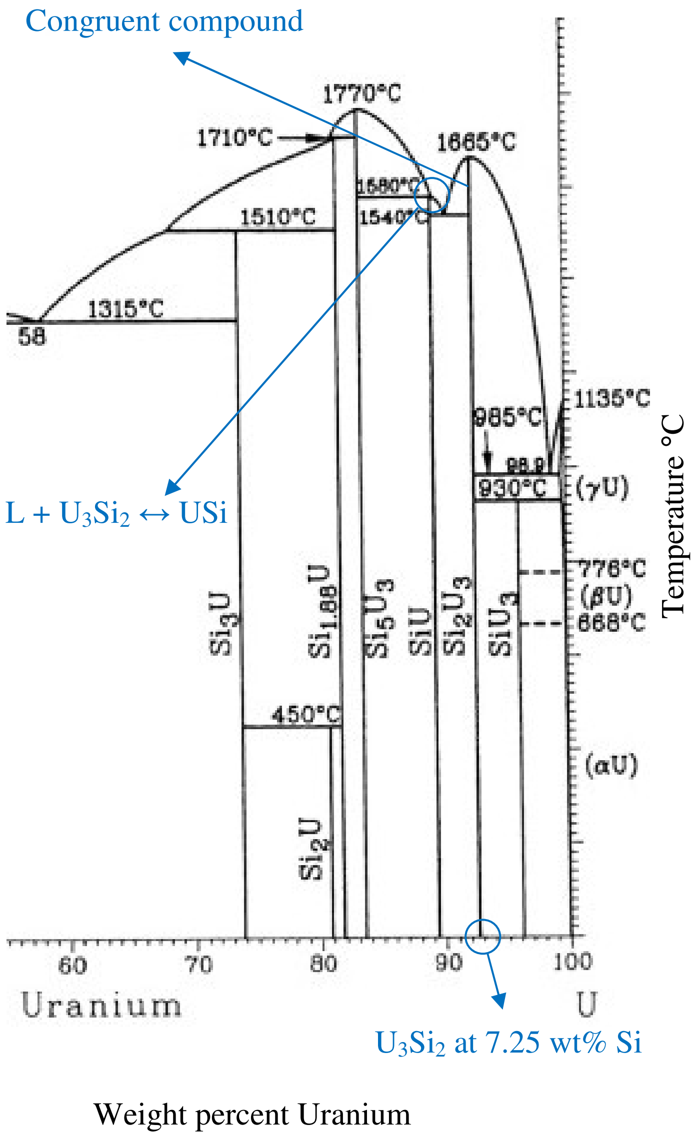

Fig. 2.5 Magnified view of Uranium - silicon phase diagram [113].

2.5 Uranium-Molybdenum alloy system

In uranium molybdenum system, below 560 °C, *γ-phase* exist only in a metastable state because under equilibrium cooling condition, below 560 °C the cubic *γ-phase* with the space group $Im\overline{3}m$ will transform into *orthorhombic α-phase* of space group Cmcm and body centered *tetragonal γ′-phase* (*U_2Mo*) of space group I4/mmm *(as shown in Fig 2.6)*. Therefore, the prospect of using *U-Mo alloy* as reactor fuel was closely connected with the possibility of retaining metastable *γ-phase* at temperature below 560^0C under fabrication and reactor operating conditions. The metastable cubic *γ-phase* could be retained below 560 °C either by rapid cooling from *γ-phase* field or by adding sufficient quantities of molybdenum as alloying element in uranium under normal furnace cooling condition. It was reported in the literature that uranium molybdenum alloy with maximum *11 at% Mo* under water quenching condition will transform into metastable α′ and α″ phases, which are slight variant of the orthorhombic lattice of *α-uranium*. On the other hand alloys containing 11.39-12.73 at% Mo, under water quenching condition will undergo an ordered *γ°-phase* with an ordered tetragonal structure [50-54]. This structure is derived from the high temperature bcc cell by doubling 'a' and 'b' axis and contracting the original 'c' axis. Hence water quenched uranium alloys containing up to about 11 at% Mo are termed as "alpha phase" alloys and with more than 11 at% Mo as "gamma phase" alloys. It has also been reported that under critical cooling condition the high temperature cubic *γ-phase* can be retained in metastable condition and by shear mechanism it will transform to distorted alpha which is termed as α′.

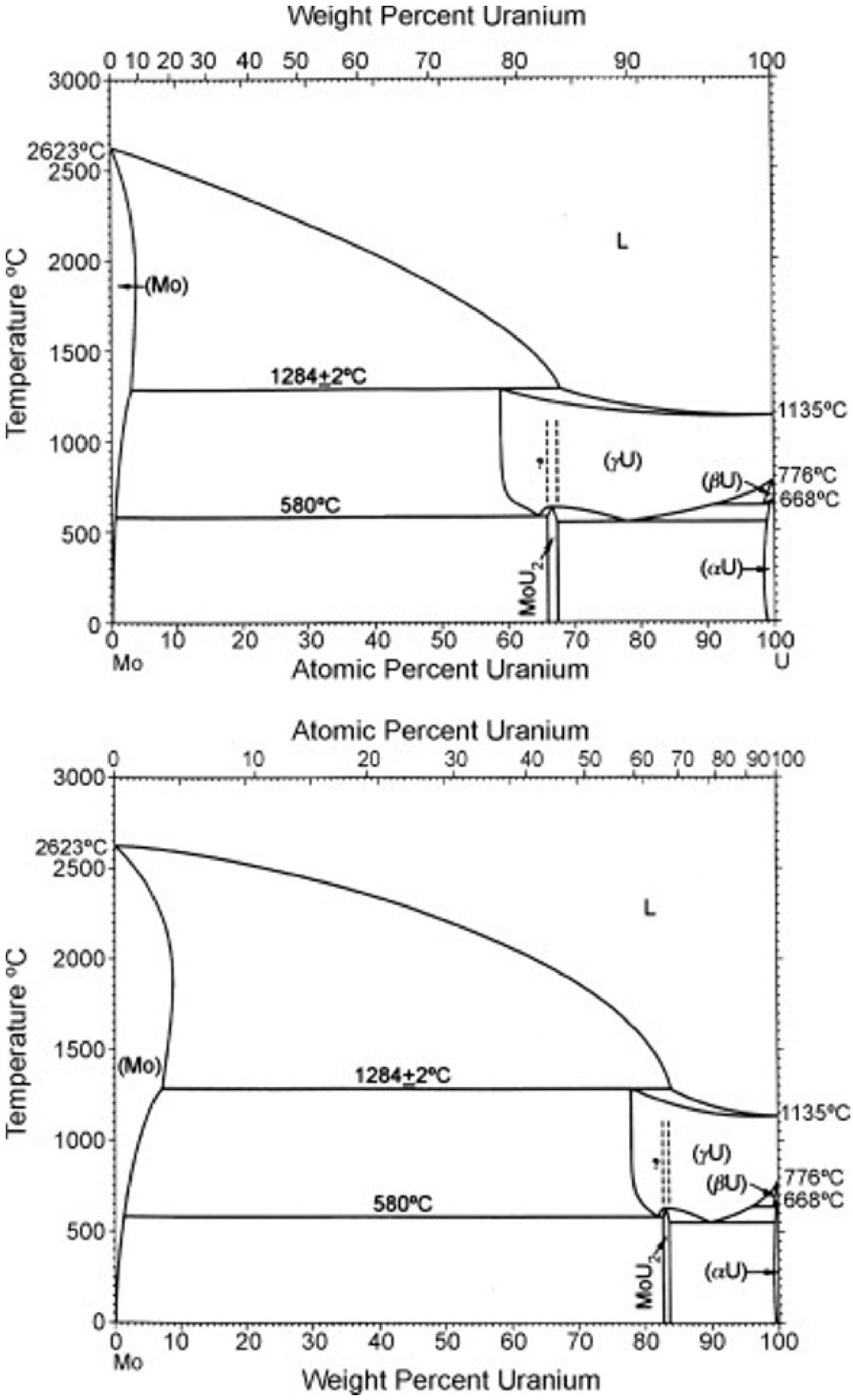

Fig. 2.6 Uranium - Molybdenum phase diagram [113].

The literature also confirms that X-ray diffraction pattern of α′ phase shows lattice contraction in 'a' and 'b' direction of the normal orthorhombic alpha cell. A monoclinic structure called α″ has also been reported in the as quenched alloys containing 4.6 to 9.4 at% Mo [134].

It was later shown by *Duwez* that cooling rates of 10000 °C/sec do not prevent the formation of beta and alpha phase in pure uranium and in case of U-Mo system, the β and (β+γ) phase fields extend up to about 2 and 8 at% Molybdenum respectively. Hence it was of interest to know if the formation of intermediate β phase is suppressed during the formation of α′ or α″ phase when uranium alloys containing up to 8 at% Mo were water quenched from the γ phase and was later shown that by water quenching the formation of intermediate β phase in these alloys was strongly dependent upon the molybdenum addition. So the γ phase in U-Mo alloys containing up to 0.69 at% Mo transform to α′ via phase β by a mechanism similar to that of pure uranium and in alloys with 2.9 at% Mo or more the bcc γ phase transforms directly to α′ phase without going through the intermediate β phase. The metastable phase *(i.e. cubic γ-uranium)* was important to characterize for fuel storage point of view in U-Mo alloy system. The study had also shown that γ-phase of U-2wt%Mo alloy transform to α-uranium and γ′-U_2Mo phase after annealing it for 100 hrs at 400 °C but the γ-phase of U-10wt%Mo alloy remains as it is under similar annealing conditions [135-138].

The transformation reaction of γ-phase in U-2wt%Mo alloy tends to be more thermodynamically favored with lamellar structures of α-uranium and

γ'-U_2Mo phase in the heat treated product. However it was also confirmed that the above said reaction was nucleated primarily at prior γ-uranium grain boundary which was followed by transformation of γ-uranium grains into α-uranium and γ-uranium (with higher molybdenum content) rather than γ' directly. Thereafter, the matrix will transform again by so called low temperature mechanism in which transformation was initiated by the formation of ordered γ'-U_2Mo. Consequently transformation occurs continuously involving the formation of an ordered intermediate γ' with α-uranium presumably formed from the solute depleted matrix around grain boundary. In case with U-10wt%Mo alloy the γ-phase remains untransformed under the condition stated above because large substitution of molybdenum atoms within the uranium lattice causes uranium atoms to become immobile due to the lower diffusivity of molybdenum [139].

The potential usage of *U-Mo alloys* is to substitute research reactor cores of very high enriched uranium to achieve high neutron flux. This also confirms their tremendous potential for use in dispersion fuels, where heavy metal loading requirement is high enough. However, latest investigation had also shown that *U-Mo alloy* fuel granules reacts with aluminium metal matrix at fuel fabrication temperature and will lead to undesired swelling [140-141].

In fact, the interaction product between U-Mo alloy granule and aluminium metal matrix has lower density with interconnected and isolated porosity, which in turn would increase the fuel plate swelling. The interaction of alloy fuel granule with aluminium matrix could be retarded either by putting barrier layer in the form of fuel granule coating or by developing ternary alloy system with lower chemical interaction potential [142-143]. It was also analyzed that coating of a barrier layer on dispersoids is not cost effective. Hence, a complete different approach was employed and adopted to solve the problem. In this case a monolithic layer of *U-Mo alloy* was introduced in between aluminium alloy cladding; therefore surface area for fuel matrix interaction was lowered. In addition, to avoid further interaction between fuel meat and cladding, a barrier layer of zirconium was placed in between the meat and cladding [144].

Crystallography data of U-Mo system

In contrast, to uranium-silicon system the uranium-molybdenum system exhibits excellent solid solubility of molybdenum in uranium with only one intermetallic compound U_2Mo. It was also observed that cubic γ-uranium will undergo eutectoid decomposition to form α-U and U_2Mo compound below 560 °C. Detail information of uranium molybdenum system are shown in *Table 2.4*

Phase	***Composition (at% U)***	***Composition (wt% U)***	***Formation reaction***	***Formation temperature (℃)***	***Pearson symbol***	***Space group***	***Prototype***
Mo	*0*	*0 to 9*	-	-	*cI2*	*Im-3m*	*W*
MoU_2	*66.7*	*83.2*	*Eutectoid*	*560*	*tI6*	*I4/mmm*	$MoSi_2$
γ-U	*100*	*98 to 100*	*Solid Solution*	*668*	*cI2*	*Im-3m*	*W*
β-U	*100*	*99 to 100*	*Solid Solution*	*775*	*tP30*	$P4_2/mnm$	*β-U*
α-U	*100*	*99 to 100*	*Solid Solution*	*1132*	*oC4*	*Cmcm*	*α-U*

Table 2.4 Crystal structure data on uranium-molybdenum system.

2.6 Summary of earlier studies & work carried on similar type of fuel and their reactor performance

Most of the earlier work, carried out in the development of *'LEU'* based fuel around the world for research and test reactor application was done under RERTR programme. Therefore, the earlier development work focused on the development of different types of dispersion fuel systems, including their fabrication, out of pile and in pile characterization was centered in USA, Russia, Korea, UK and France mostly. However, the major thrust on its development came from military application point of view *(i.e. rocket propulsion programme, advance fuel for submarine programme etc.)* [32]. Therefore, many of the experimental results on dispersion fuel derived for military application are classified and not available in open literature. It may also be noted that during earlier times and even now also for specific applications, the most proven dispersoid as fuel for research reactor application is UAl_x in aluminium matrix. Dispersoids of uranium aluminide had shown excellent resistance to swelling characteristics even at a burn up of 50 to 60 at% [145-150]. In most cases, UAl_x intermetallic is prepared by induction melting technique where master alloy is first prepared and then diluted to desired chemical composition. However, there are instances where UAl_x compound is prepared by powder metallurgy route but their details are not available in the open literature. The major problem of using UAl_x type dispersoid as fuel is its chemical interaction with either excess aluminium in the compound or from the matrix during fabrication and reactor operation condition, to form lower density compound UAl_4. The formation of UAl_4, would cause swelling because its density is lower if compared with UAl_3 *(density of UAl_3 and UAl_4 are 6.8 g/cm^3 and 5.7 g/cm^3 respectively)*.. Hence, in order to reduce the chemical interaction of fuel phase with matrix aluminium, it is highly desired to either operate the reactor at lower temperature or to stabilize the fuel phase with third element. The issue becomes more complicated when the desired burnup of the fuel and its operating temperature are both higher *(i.e. of the order of 60 to 70 at% and 500 °C respectively)*.

There are instances when *UO_2 and UC* have also been tried as fuel dispersoids and their reactor performance is documented elaborately in the literature [151]. Report on the use of *UO_2* dispersoid in stainless steel matrix are also available in brief because the main application was for military submarine programme in USA, hence classified. However, stainless steel alone is never recommended for matrix material because during irradiation it may lead to irradiation embrittlement and also due to overlapping of fission induced recoil zones the matrix ligament will crumble under applied stress and cause fuel failure. One more type of dispersion fuel design is under discussion for many a time. The design has been realized with potential to succeed for dispersion type fuel in the upcoming reactors desired to operate at higher temperatures. In this design the enriched UO_2 dispersoid will be dispersed in aluminium. During reactor operating conditions, the aluminium will cause partial reduction of uranium oxide, to form aluminium oxide *(with variable stoichiometry)* at the fuel matrix interface. The formation of aluminium oxide at fuel matrix interface would lower the fuel matrix thermal conductivity but at the same time would allow the operator to increase the fuel temperature *(melting point of Al_2O_3 is higher than aluminium).* This would eventually allow the reactor to operate at higher power and hence would increase the neutron flux.

Another type of dispersion fuel design was employed and was named *Triga* fuel. Here, UZr_2 was dispersed in $ZrH_{1.6}$ matrix and curved plates were used in the reactor. [152]. This design has attracted the attention of many fuel designers because the typical combination of fuel dispersoid and matrix result in the self controlling of nuclear chain reaction by expansion and contraction of $ZrH_{1.6}$ lattice under temperature. However, it must also be realized that the fabrication of UZr_2 intermetallic itself is a challenge because the formation is by peritectoid reaction. Therefore, it can be prepared either by powder metallurgy route or by soaking U-Zr alloy for prolonged duration. It is also important to note that the handling and processing of zirconium metal powder itself is a big challenge because oxygen and nitrogen stabilizes zirconium room temperature allotrope and exhibit further chemical interaction with constituent elemental powder.

The most proven and widely accepted fuel compound for LEU fuel application till date is dispersion of U_3Si_2 in aluminium matrix. In general, all over world almost 90% of the research reactor core conversion from HEU based fuel to LEU based fuel has been accomplished by using U_3Si_2 compound as dispersoid. The reason is mainly attributed to the fact that the interaction of U_3Si_2 with matrix aluminium is less if the reactor is operated at lower temperatures [153-156]. The work carried out by *Yeon Soo Kim and his co-workers* in determining the swelling characteristics of U_3Si_2 dispersoids under high temperature and fluence has further given the insight on its application at lower reactor operating temperatures [157].

In view of the limitations imposed on U_3Si_2-*Al* dispersion type fuel and also because of the fact that core conversion of ultra high enriched research reactor cannot be accomplished using uranium silicide dispersoid in aluminium matrix, a new set of compounds/alloys were considered for the purpose. In this connection, *U-Mo* alloys and other higher density uranium compounds *(like* U_6X*: X = Fe, Ni, Mn etc)* were tried and developed. It is also important to note that the major challenge imposed by *U-Mo alloy* usage as dispersoid is its increased chemical interaction with aluminium matrix which increases further under the fluence of neutron [158]. The efforts are put by many fuel designers/fabricators to address the issue either by selection of particular alloy composition/microstructure or by addition of third element in the fuel/matrix phase. Since molybdenum offers a very good solid solubility in uranium a complete set of trials with different Mo concentration in uranium is underway throughout the world [159]. In addition one more type of design where U-Mo alloy in monolithic form and sandwich between aluminium alloy is also being considered for the purpose [160].

In this regard metallurgical investigations presented in the current dissertation for different compositions of U-Mo alloys may provide valuable input in solving some core issues.

2.7 Research approach and methodology

In order to accomplish the objective *(as described in Section 1.5)* in the present work, the research approach adopted was as follows:

It was identified from the literature that most of the work reported was focused on fuel performance. However, much of the literature on their preparation, characterization and basic metallurgy existed in classified work and some part of it is available in open literature. Further, reported processing methods for preparation of dispersoids included either induction or arc melting techniques. In some instances, inert gas atomization (argon gas) was also used to prepare the dispersoids, though it involves processing the compound/alloy in liquid form. It was also noted that the arc and induction melting technologies have their own difficulties and challenges, such as segregation and impurity pickup. In view of preparing fuel compound/alloy with good homogeneity, minimum impurity pickup and also to incorporate desired porosity, a new technique was explored *(by Powder Metallurgy technique)* to prepare the fuel dispersoids. The powder processing method was also taken up keeping in view our unique and specific requirements, where LEU is available in metal powder form. Two completely different alloy systems were selected *(i.e. U-Si and U-Mo)* for the purpose. Though most of this work has a direct relevance to *LEU* based fuel, studies on uranium alloys were carried out using *natural uranium* only, because isotopic concentration would not affect chemical characteristics of material.

As stated earlier, the study on the alloying of uranium silicide compound *(i.e.* U_3Si_2*)* by powder metallurgy route is perhaps the first reported attempt to systematically evaluate the effect of process parameters on the final product characteristics. Therefore, it becomes imperative to study, optimize and standardize all the process variables to evolve a process flow-sheet that can be scaled up for larger batch production.

On the other hand, the study on the alloying of *U-Mo alloys* with elemental powders as starting materials has also been attempted indigenously for the first time, though literature suggests *U-Mo alloy* granule preparation by *HDH (hydriding-dehydriding)* process. Based on the phase-diagram of U-Mo system, select compositions from the U-Mo system *(i.e. 2, 5 and 10 wt% Mo)* were also attempted by P/M (Powder Metallurgy) route. *U-Mo alloys* were also prepared by induction melting technique, so that the final product characteristics could be compared.

The U-Mo alloy should have cubic structure, for it to be resistant to irradiation during application as a nuclear fuel. Since the equilibrium phases in these alloys are undesirable alpha-U and U_2Mo compounds, it becomes important to study the metastability of cubic γ-phase in these alloys with Mo-content. With this background, various alloys with varying Mo-compositions (2-10wt%Mo) were prepared. A detailed study of these alloys under furnace cooling conditions, such as microstructural examination and phase-analysis would provide crucial understanding about this alloy system.

Further, the fuel fabrication and reactor operation steps involve high temperature exposure to fuel dispersoids, during which the metastabilized γ-phase may undergo transformation into irradiation-incompatible equilibrium phases. Therefore, a study of decomposition of cubic phase was planned. It may be noted that the actual temperature the nuclear fuel dispersoids encounter during reactor operation may be quite low (~200 °C), an accelerated test at higher temperature would be significant to assess the suitability of the alloy as potential nuclear metallic fuel. The alloy samples for this purpose subjected to heat treatment at different time and the evolved phase content need to be evaluated.

3. Experimental Work & Technique

3.1 Experimental techniques

In the present work alloy samples of U_3Si_2 compound and *U-Mo alloys* with *(2, 5 and 10 wt% Mo*) compositions were prepared by powder processing technique while U-Mo alloy samples of seven different compositions *(i.e. 2, 5, 6, 7, 8, 9 and 10 wt% Mo*) were prepared by induction melting technique. The details of their preparation and characterization process are further described below.

3.1.1 A brief account on alloy sample preparation

Alloying of uranium based compounds/alloys by powder metallurgy route in general poses difficulty owing to the fact that uranium in small particulate size has strong affinity for impurities like moisture, oxygen, nitrogen etc. In addition it is highly pyrophoric and therefore requires very careful handling inside glove box under proper ventilation under once through flow of high purity argon gas atmosphere. In the same way, silicon and molybdenum powders also require careful handling and processing.

Similarly, melting of uranium alloy sample also poses difficulties but they are less prone to impurity pick up if compared with alloy preparation by powder processing route *(surface area of uranium metal button is less when compared with uranium metal powder).* It is thus favorable to melt lab scale *U-Mo alloys* in a chamber pressurized with argon/helium instead of using high vacuum system *(10^{-3} mbar or less).* Arc melting practice was definitely superior in that respect but there were some obvious limitations in the process *(as described in section 1.5)*. In order to assure good chemical homogeneity the standard practice was to re-melt the alloy several times by turning the alloy button/finger. However, in lab scale arc melting route one cannot melt the entire sample at once, unless sample size is quite small. So, the second problem of arc melting route was the limitation in the size of the sample. Therefore, the arc melting route offers a tradeoff between the alloy homogeneity and the size of the alloy sample. On the other hand induction melting does not pose such problems. Owing to the magnetic churning effect in the melt a good homogeneity was assured and the shape and size of crucible defined the sample size. The only problem with induction melting was the impurity pickup since at high temperature melt could react with the crucible. It was also important to state that in this case the crucible was not water cooled (unless one goes for skull melting practice) unlike arc-melting. Comparing all the advantages and disadvantages between the arc melting and induction melting routes, the later was found more suitable keeping in mind the amount of the alloy sample required in the successive experiments.

3.1.2 Crucible coating

In induction melting practice, crucible coating was an important parameter that would affect the impurity pickup of the alloy from the graphite crucible other than the contamination from the chamber environment. This effect becomes more of concern for alloy preparation of uranium and other reactive metals. Graphite crucible of 60mm height, 30mm OD and 13mm ID was used throughout in the present study. This graphite crucible acts as a susceptor as well as the mould, where the liquid melt gets solidified upon cooling. The coating materials for the graphite crucible must have the following parameters-

i. Structural stability at high temperature.

ii. It shall not react with either graphite or with alloying constituents.

iii. It shall not outgas at high vacuum level or high temperature during melting.

iv. Coating must be adherent and exhibit no cracking during application, drying and curing.

Alcohol based Al_2O_3 or Y_2O_3 slurry can be used as coating material on graphite crucible. However, it has been found that such thin coating of Al_2O_3 or Y_2O_3 is not stable in contact with graphite at temperature above 1000 °C. On the other hand it is also not possible to apply a thick coating of alcohol based slurry onto the graphite surface because it develops cracks after drying. In fact, graphite being a lubricating material is a tough candidate to make any coating adhere to it. Hence the first attempt was to find some means by which one can apply a relatively thick coating of Al_2O_3 or Y_2O_3. This means that a good binder is essential that ensures excellent binding of the coating to the graphite surface with relatively higher coating thickness. Also at higher temperature the binder must go out either by decomposition or by simple evaporation leaving a monolithic mass of Al_2O_3 or Y_2O_3 inside the crucible. Another important aspect is that during the decomposition or evaporation of the binder it should not create any crack or blister on the coating.

In order to make the coating composition useful it is necessary that the Y_2O_3 particles must be in suspension in an aqueous Na-CMC *(chemical formula:* $[C_6H_7O_2(OH)_2OCH_2COONa]_n$*)* solution. An operable range of Na-CMC concentration is about 1.5 to 4% by weight with respect to water volume. Below about 1.5% of Na-CMC, Y_2O_3 particles settles too rapidly and greater than about 4% provides an excessively viscous solution which is not easy to work with. It is also reported in the literature that a 3% aqueous CMC solution is the preferred concentration for suspending Y_2O_3 particles. It is also important to note that since Na-CMC is not easy to disperse in water and the moment it is added into water it coagulates which is difficult to disperse. Therefore it was identified that around 70 °C to 90 °C the rate of dispersion is optimum with continuous stirring with an electric hand mixer. For the present purpose two coating compositions with different Y_2O_3 concentrations were selected. Firstly, the Na-CMC solution was prepared by adding 3 gm of standard refined industrial grade CMC per 100 ml of water. The first coating composition was prepared by dispersing 50 gm of Y_2O_3 powder (99% pure) per 100 ml of aqueous Na-CMC solution. The second coating composition was prepared in a like manner by dispersing 100 gm of Y_2O_3 powder per 100 ml of the CMC solution.

Prior to the application of the coating the high density graphite crucible was de-dusted by ultrasonic cleaning in hot water. After the crucible was allowed to cool and dried with a hair drier. The first coating composition, containing 50gm yttria powder, was applied with a piece of sponge tightly held by a pair of tweezers. After the first coating composition was applied the crucible was allowed to dry under forced hot air for almost 30 minutes and then kept inside the furnace at 120 °C. After that the crucible was taken out of the furnace and then allowed to cool in air. Once the crucible attains room temperature the second coating is applied that contains 100 gm yttria powder. In this process the coating solution was poured inside the crucible and after filling it completely the solution was poured out, therefore a layer was established inside the crucible. Proper drying of the coating gives a milky white and smooth monolithic finish *(as shown in Fig. 3.1)*. The crucible is then loaded into induction furnace chamber without any charge material and was heated upto 300 °C under vacuum of 10^{-2} mbar. After this curing there was no visible crack on the coating or release of yttria powder was observed.

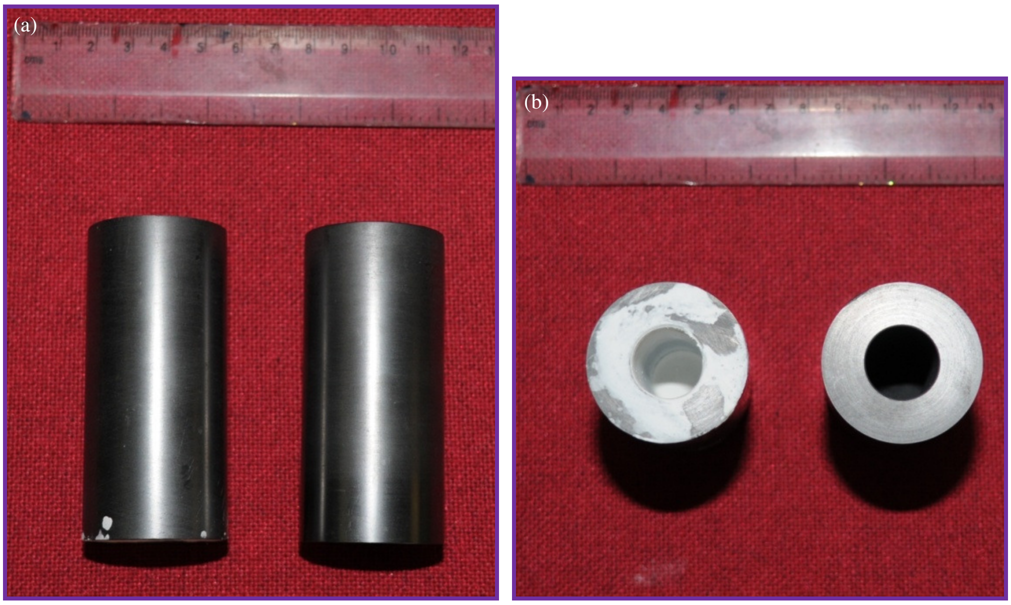

Fig. 3.1 Photograph of graphite crucibles (a) Top view of high density graphite crucible used for induction melting of U-Mo alloys, (b) Interior view of Na-CMC water solution based Y_2O_3 coated graphite crucible after curing.

3.2 Preparation of compound/alloy

3.2.1 Alloying of U_3Si_2 compound by powder metallurgy route

The starting material for the alloying reaction of U_3Si_2 compound was uranium metal powder *(as shown in Fig. 3.2 (a))* with average particle size of around 25 µm and silicon powder. These were received from *Uranium Extraction Division (UED, BARC)* and *M/s Alpha Azer, USA* respectively. Alternately, silicon chunks *(as shown in Fig. 3.2 (b))* were also crushed and sieved to get silicon powder *(as shown in Fig. 3.2 (c))* with average particle size of around 20 µm. The purity of *uranium* and *silicon* powders used for this study was 99.6 and 98.5 wt % respectively.

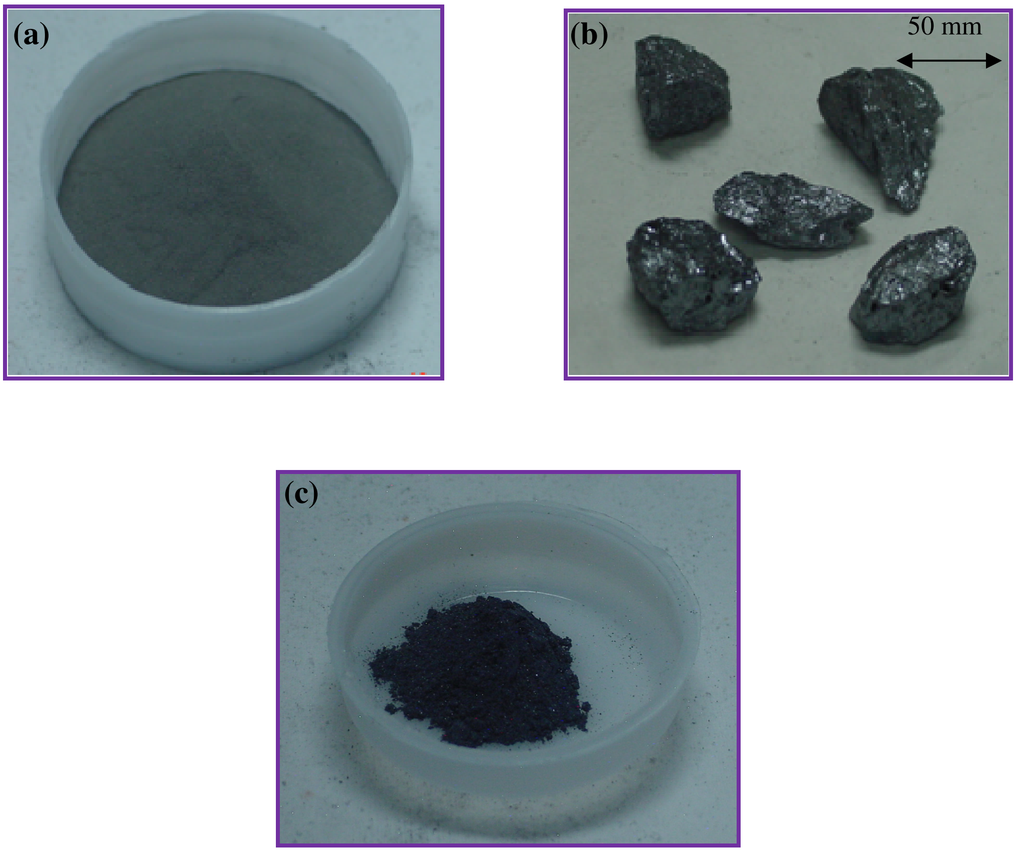

Fig. 3.2 Photographs of starting materials (a) Uranium metal powder (b) Silicon chunks (c) Silicon powder.

Chemical characterization of uranium metal powder and silicon powder used in this study is shown in *Table 3.1 and Table 3.2* respectively. The chemical analysis of as synthesized U_3Si_2 compound was done by an in-house classified procedure where chemical titration, inert gas fusion method and mass spectroscopy were used to determine different elemental content. Apparent density and tap density of uranium metal powder used in the study was calculated and is shown in *Table 3.3.* In addition the pycnometer density and surface area of silicon powder was also calculated by *ATC Helium gas pycnometer and BET respectively,* which are listed in *Table 3.4.*

Element	***Concentration (wt%)***
U	*99.6±0.1*
C	*0.063*
N	*0.050*
O	*0.150*
Fe	*0.300*
Ni	*0.020*
B	*0.0001*

Table 3.1 Chemical analysis results of uranium metal powder.

Element	*Concentration (wt%)*
Si	*98.5±0.1*
C	*0.240*
N	*0.140*
O	*0.950*
B	*0.0002*

Table 3.2 Chemical analysis results of silicon powder.

Element	*Apparent Density (gm/cc)*	*Tap Density (gm/cc)*
U	*10.2*	*11.5*

Table 3.3 Apparent and tap density of uranium metal powder.

Element	*Pycnometer Density (gm/cc)*	*Specific Surface Area (cm^2/gm)*
Si	*2.2834*	*1.8*

Table 3.4 Pycnometer density and specific surface area of silicon powder.

The entire powder handling process was carried out inside glove box and extreme care was taken to avoid any impurity pick up. The glove boxes were flushed with once through high purity argon gas with oxygen and moisture content limited to 10 ppm and 5 ppm respectively. The alloying was carried out initially with a batch size of 200 gm which was later increased to one kilogram level. The oxygen pickup of uranium during heating was avoided by continuously purging the furnace glovebox housing with high purity argon gas. The process instruments used inside glovebox train for the alloying of compound/alloy are shown in *Fig. 3.3 and Fig. 3.4*.

Fig. 3.3 Facility for preparation of U_3Si_2 compound and U-Mo alloys by powder metallurgy route.

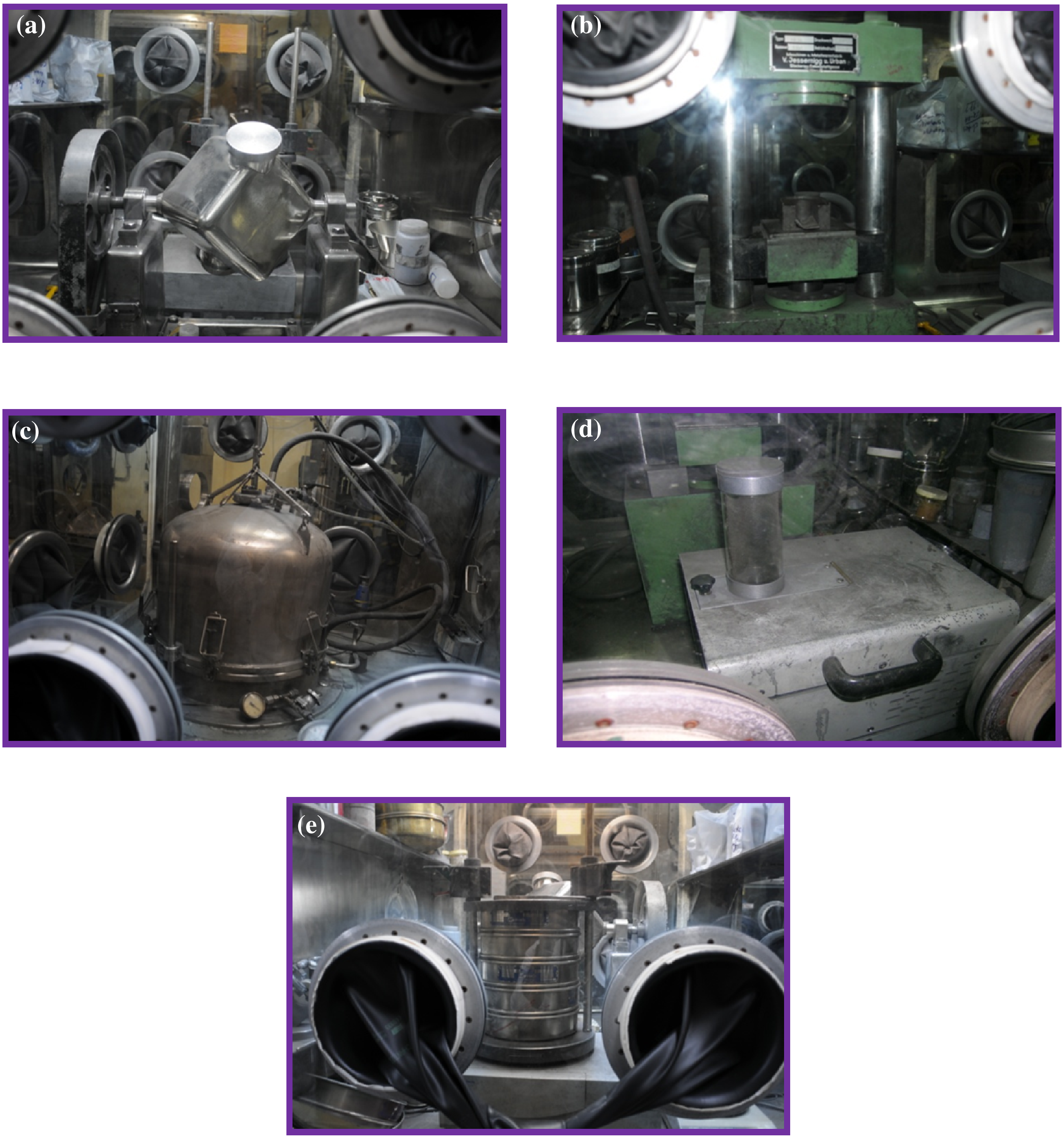

Fig. 3.4 Photographs of process equipment installed inside glove box

(a) Blender, (b) Hydraulic Press, (c) Furnace, (d) Jaw Crusher,

(e) Sieve Shaker.

A process flow-sheet has also been developed for the fabrication of U_3Si_2 fuel granules and is shown in *Fig. 3.5*. The uranium metal powder and silicon powder were first weighed in required proportion/stoichiometry and later mixed in a cubical blender for 4 hours. The powders were mixed thoroughly because this stage has large influence on the product homogeneity. The mixture was then compacted in a hydraulic press in the form of cylindrical pellets. During mixing, no admixed binder/lubricant was added to the mixture and only die-wall lubrication was used in the compaction. The pellets were compacted at 40 TSi pressure in a 20 mm diameter die and L/D ratio was kept at around 0.5 to 0.75. The green pellets were then loaded in molybdenum trays coated with plasma sprayed yttria. The charge carrier was then loaded in a 10 kW resistance heating furnace with graphite as heating element and alloying was carried out under vacuum of 10^{-2} mbar at 1550±10 °C for 4 hours. During the heating cycle, intermittent soaking was also carried out at 1000 °C and 1400 °C for one hour each.

The alloying temperature was kept well below the melting point of U_3Si_2 compound and was selected very carefully because the other silicide phase present nearby U_3Si_2 *compound* had a peritectic reaction temperature of 1580^0C and at no stage liquid phase was desired in the process. Hence liquid formation was avoided in the process which had eventually made the product more clean *(i.e. low impurity pick up)* as compared to the one synthesized by the conventional route of melting and casting. Once the furnace was cooled to room temperature, the synthesized U_3Si_2 clinkers were taken out. Pellets of U_3Si_2 compound synthesized by this method are shown in *Fig. 3.6.* The chemical analysis (characterization) is carried out by an in-house classified procedure (RCIG, BARC).

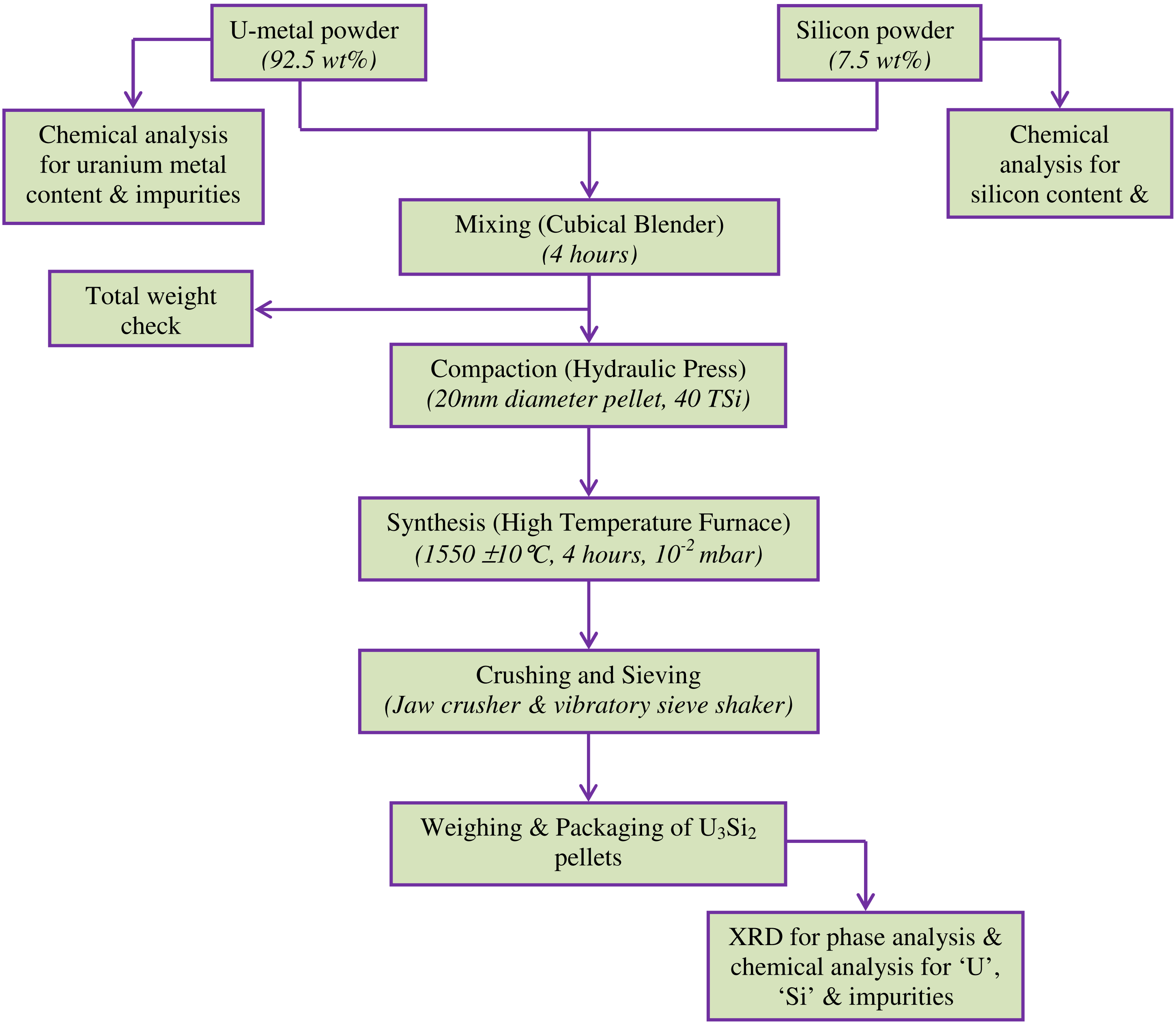

Fig. 3.5 Flow-sheet for fabrication of U_3Si_2 fuel granules by powder metallurgy route.

In brief, the methodology adopted for uranium was chemical titration and the impurities were measured by inert gas fusion technique and mass spectroscopy. The results for as synthesized U_3Si_2 compound are shown in *Table 3.5*.

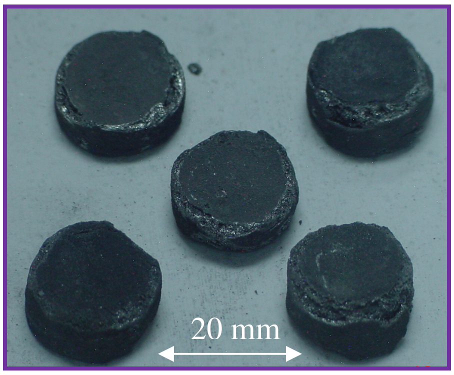

Fig. 3.6 Photograph of U_3Si_2 pellets after synthesis.

Element	***Concentration (wt%)***
U	*92.4±0.1*
Si	*7.3±0.1*
C	*0.075*
N	*0.050*
O	*0.200*
B	*0.0001*

Table 3.5 Chemical analysis results of as synthesized U_3Si_2 compound.

3.2.2 Powder metallurgy route for U-Mo alloys

Three different compositions of U-Mo alloys were also prepared by powder metallurgy route and the starting materials for the purpose was uranium metal powder with average particle size of around 25 µm *(shown in Fig 3.7(a))* and molybdenum metal powder with average particle size of around 20 µm *(shown in Fig 3.7(b))*. These were received from *Uranium Extraction Division (UED, BARC)* and *M/s Metal Works, PLANSEE* respectively. Uranium metal powder was having 99.6 wt% 'U' metal content and molybdenum metal powder was having 99.9 wt% 'Mo' metal content. The chemical analysis of uranium metal powder and molybdenum metal powder batch used in this study is shown in *Table 3.1 and Table 3.6* respectively. The chemical analysis was carried out by chemical titration, inert gas fussion method and mass spectroscopy for different elemental content. The pycnometer density and specific surface area of molybdenum metal powder determined by *ATC Helium Gas Pycnometer and BET* are *shown in Table 3.7.*

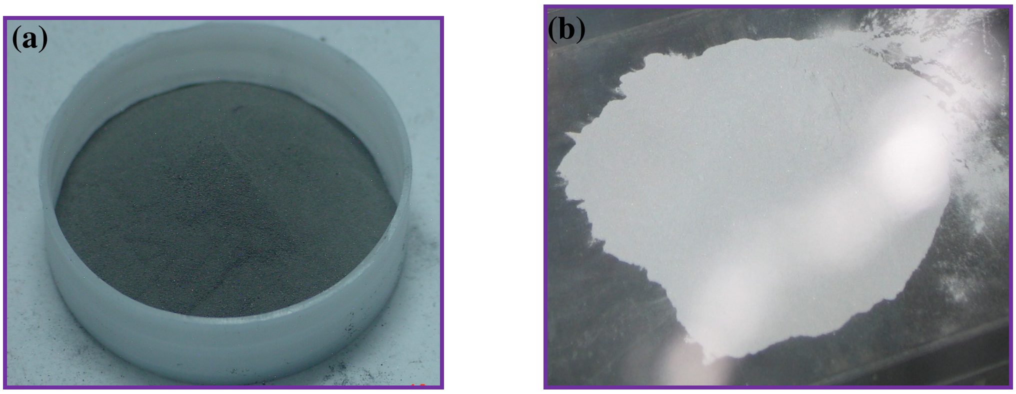

Fig. 3.7 Photographs of starting materials (a) Uranium metal powder (b) Molybdenum metal powder.

Element	*Concentration (wt%)*
Mo	*99.8±0.1*
C	*0.050*
N	*0.010*
O	*0.020*
B	*0.0001*

Table 3.6 Chemical analysis results of molybdenum metal powder.

Element	*Pycnometer Density (gm/cc)*	*Specific Surface Area (cm^2/gm)*
Mo	*10.0667*	*3.2*

Table 3.7 Pycnometer density and specific surface area of molybdenum metal powder.

Uranium metal powder was highly prone to oxidation hence extreme care was taken during the powder handling stage. Specially designed glove boxes with very good leak tightness were used for the purpose. These glove boxes were circulated with once through high purity argon gas. The uranium and molybdenum metal powders were thoroughly mixed in required proportion for all the three compositions. The mixing was carried out in a small blender for 4 hours to get good homogeneous mixture. Here also during mixing no admixed binder was added. The mixture was then compacted at 40 TSi pressure in a 20 mm die into cylindrical pellets. Die wall lubrication (mixture of 90vol% ethyl alcohol and 10vol% glycerol) was used during compaction to reduce die wall friction. The L/D ratio of compacted pellets was kept around 0.5. The green pellets were then loaded on molybdenum trays coated with plasma sprayed yttria. The charge carrier was then loaded inside the 10 kW resistance heated furnace and the compacts were heated at 1050±10 °C for 6 hours under vacuum of 10^{-2} mbar. The temperature was kept just below the *solidous* for all the three alloy compositions, hence liquid formation was avoided which enables the product cleaner (e.g. low impurity pick up) as compared to the conventional alloying route of melting and casting. The impurity pick up during high temperature alloying reaction was avoided by purging the furnace housing inside the glove box with once through high purity argon gas. The furnace was allowed to cool under vacuum and the product i.e. U-Mo alloy pellets were taken out *(shown in Fig 3.8).* The chemical analysis of as synthesized *U-Mo alloys* was done by an in-house procedure where chemical titration, inert gas fusion method and mass spectroscopy were used to determine different elemental content. The results of the chemical analysis are shown in *Table 3.8.* The process flow sheet used for *U-Mo alloy* preparation is shown in *Fig 3.9.*

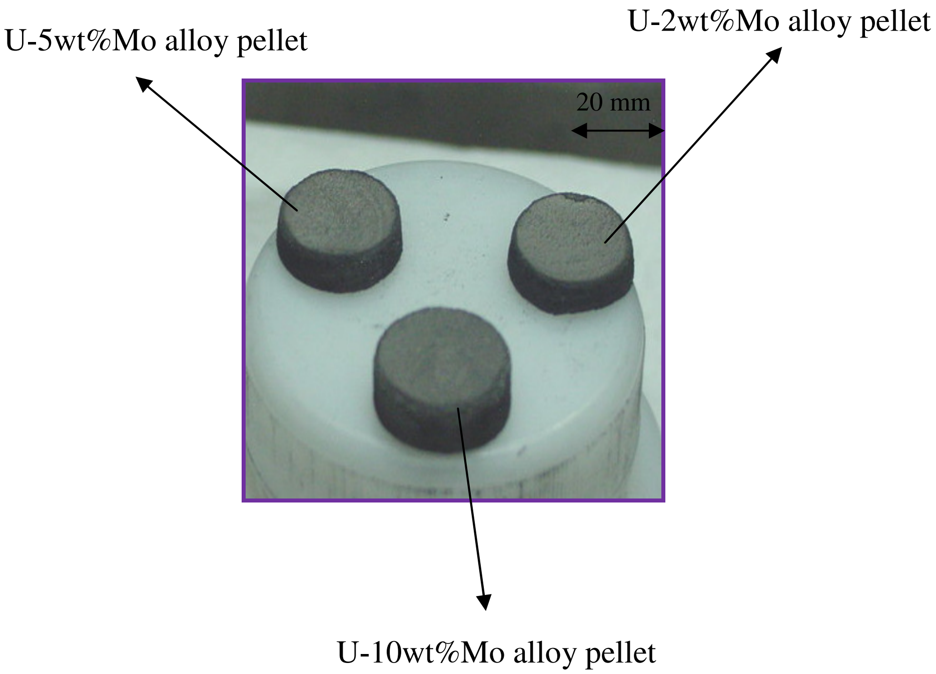

Fig. 3.8 Photograph of U-Mo alloy pellets prepared by powder metallurgy route.

Element	***U-2wt%Mo Concentration (wt%)***	***U-5wt%Mo Concentration (wt%)***	***U-10wt%Mo Concentration (wt%)***
U	*97.8±0.1*	*94.8±0.1*	*89.9±0.1*
Mo	*1.9±0.1*	*4.85±0.1*	*9.8±0.1*
C	*0.160*	*0.174*	*0.090*
N	*0.080*	*0.105*	*0.075*
O	*0.150*	*0.135*	*0.120*
B	*0.0001*	*0.0001*	*0.0001*

Table 3.8 Chemical analysis results of as synthesized U-Mo alloys by powder metallurgy route.

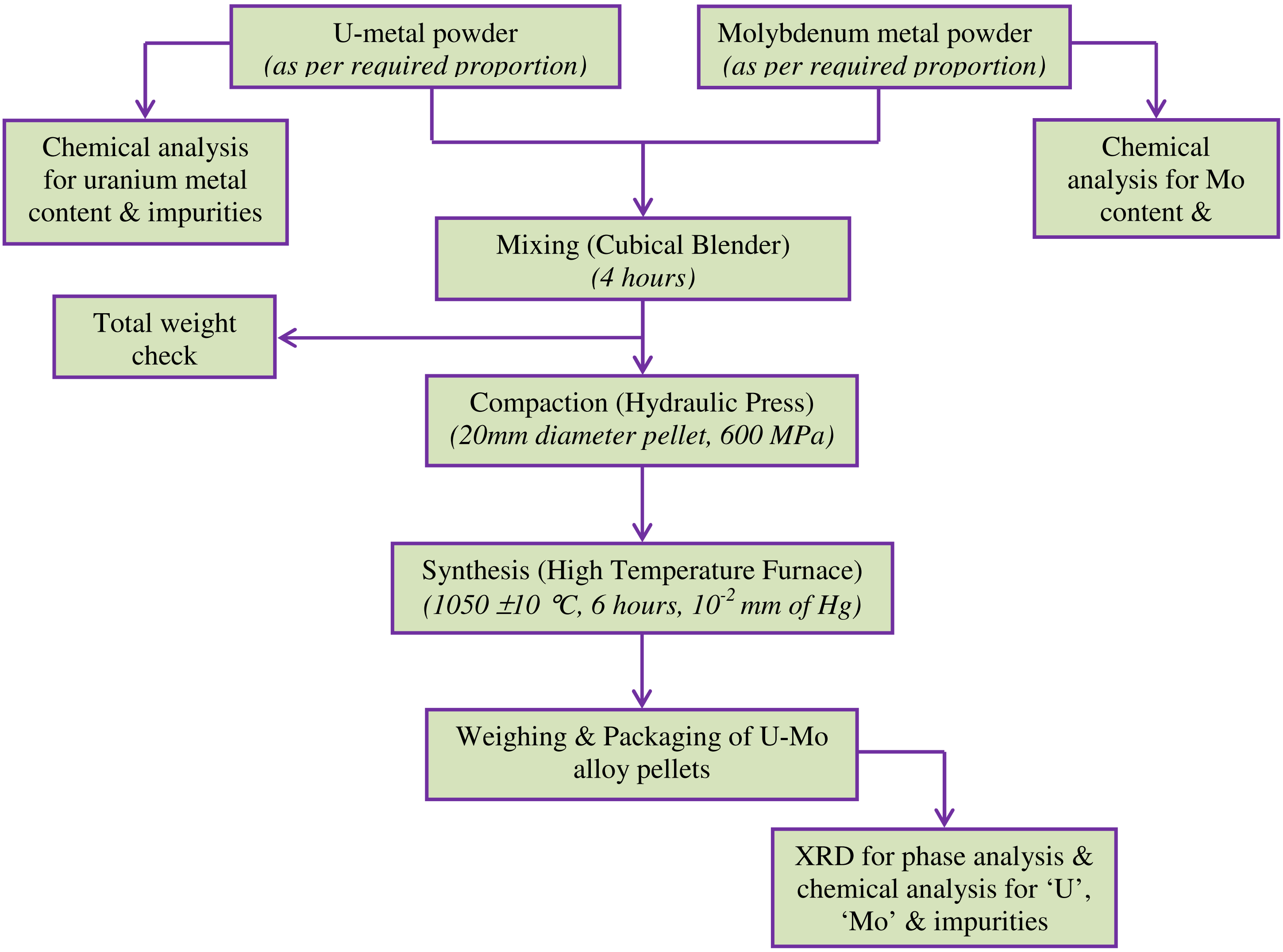

Fig. 3.9 Process flow sheet for preparation of U-Mo alloys by powder metallurgy route.

3.2.3 Induction melting route for U-Mo alloys

The starting materials for the purpose were cylindrical uranium metal pellets *(shown in Fig 3.10(a))* and molybdenum metal pieces *(shown in Fig 3.10(b))*. In the present study uranium metal pieces were having 99.9 wt%

‘U-content’ and molybdenum metal pieces were having 99.8 wt% ‘Mo-content’. The uranium metal pellets used in the study were received from *Atomic Fuels Division (AFD, BARC)* in approximately 12 mm diameter and around 10 mm length, while molybdenum metal pieces were received from *(M/s Metal Works, PLANSEE)*, which were then cut in small disks of around 3.5 mm diameter and 2 mm height. Uranium metal pieces were then electropolished using orthophosphoric acid to remove any surface oxide layer. The electropolished uranium metal pieces and molybdenum metal disks were then ultrasonically cleaned. The chemical analysis of uranium metal pellets and molybdenum metal pieces used in the present study is shown in *Table 3.9* and *Table 3.10* respectively. The chemical analysis was carried out by chemical titration, inert gas fusion technique and mass spectroscopy for different element content.

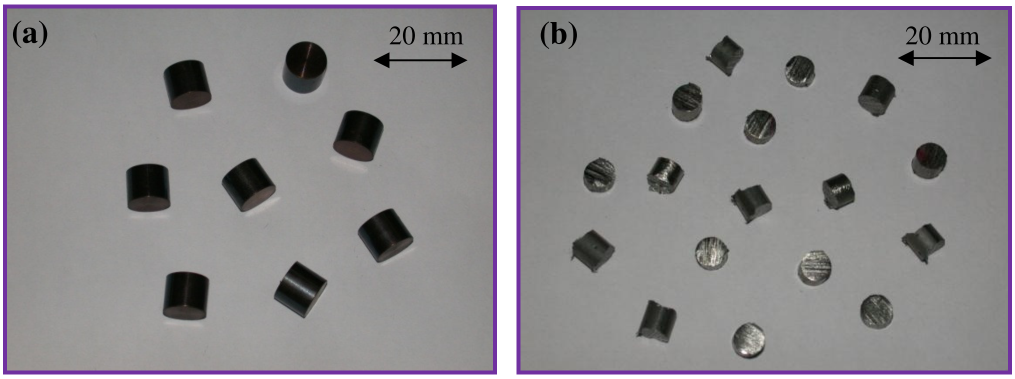

Fig. 3.10 Photograph of (a) Uranium metal pellets, (b) Molybdenum metal pieces.

Uranium metal pellets were then charged in yttria coated graphite crucible along *(as shown in Fig 3.1)* with molybdenum metal pieces in required quantity, to perform melting. The crucible was then loaded in an induction heating furnace and melting was carried out at 1500±10 °C for 30 minutes under vacuum of 10^{-5} mbar.

Element	*Concentration (wt%)*
U	*99.9±0.1*
C	*0.040*
N	*0.005*
O	*0.010*
B	*0.0001*

Table 3.9 Chemical analysis results of uranium metal pellet.

Element	*Concentration (wt%)*
Mo	*99.9±0.1*
C	*0.040*
N	*0.009*
O	*0.010*
B	*0.0001*

Table 3.10 Chemical analysis results of molybdenum metal piece.

The induction furnace was flushed thrice with high purity argon gas to remove any oxygen trace before heating. Melting was done consistently at 1500 °C for all *U-Mo alloy* compositions, since the *solidus* temperature for all the different compositions of *U-Mo alloys* discussed in the present study were around 1140±20 °C. Once the melting completed, the furnace was cooled under vacuum and *U-Mo alloy* ingots were taken out. The ingots were ultrasonically cleaned and weight was taken in a micro balance. *U-Mo alloys* with seven different compositions *(i.e. U-2wt%Mo, U-5wt%Mo, U-6wt%Mo, U-7wt%Mo, U-8wt%Mo, U-9wt%Mo & U-10wt%Mo)* were prepared to study the effect of molybdenum addition on uranium and to study the metastability of cubic γ-uranium. The *U-Mo alloy* ingots prepared by induction melting technique were having typical dimension of around 15mm diameter and 40mm length *(as shown in Fig. 3.11)*. The final weight of all alloy ingots was recorded and is shown in *Table 3.11.* A typical chemical characterization result carried out by chemical titration, inert gas fusion and mass spectroscopy for as synthesized *U-Mo alloys* is shown in *Table 3.12.*

Fig. 3.11 Photograph of as cast U-Mo alloy ingots.

Composition of U-Mo alloy	*Uranium weight (gm)*	*Molybdenum weight (gm)*	*U-Mo alloy weight (gm)*
U-2wt%Mo	*88.40*	*1.8*	*90.30*
U-5wt%Mo	*61.20*	*3.22*	*64.44*
U-6wt%Mo	*63.94*	*4.14*	*68.07*
U-7wt%Mo	*64.89*	*4.90*	*69.78*
U-8wt%Mo	*63.4*	*5.46*	*68.87*
U-9wt%Mo	*64.79*	*6.41*	*71.24*
U-10wt%Mo	*67.11*	*7.40*	*74.53*

Table 3.11 Weights of constituent elements and cast U-Mo alloys.

3.3 Heat treatment

In order to break the as cast structure of *U-Mo alloys* before actually performing any heat treatment operation, *U-Mo alloy* slugs were first cut into 50 mm long piece. The rest of the alloy slug was kept separately for the characterization and property evaluation of as cast ingot. The 50 mm long slug was then ultrasonically cleaned in water and nitric acid mixture (1:1 v/v) to remove all the oxide scale from the surface and then washed with water. It was then followed by ultrasonic cleaning in acetone. The samples for chemical analysis were also provided from the slugs only. These slugs were further processed to facilitate heat treatment by the method described in the following section.

Element (wt%)	*U-2wt%Mo alloy*	*U-5wt%Mo alloy*	*U-6wt%Mo alloy*	*U-7wt%Mo alloy*	*U-8wt%Mo alloy*	*U-9wt%Mo alloy*	*U-10wt%Mo alloy*
U	*97.8±0.1*	*94.8±0.1*	*93.8±0.1*	*92.8±0.1*	*91.8±0.1*	*90.8±0.1*	*89.9±0.1*
Mo	*1.9±0.1*	*4.9±0.1*	*5.8±0.1*	*6.8±0.1*	*7.8±0.1*	*8.8±0.1*	*9.8±0.02*
C	*0.050*	*0.058*	*0.064*	*0.045*	*0.048*	*0.072*	*0.056*
N	*0.035*	*0.042*	*0.054*	*0.041*	*0.035*	*0.049*	*0.038*
O	*0.120*	*0.135*	*0.128*	*0.090*	*0.128*	*0.139*	*0.100*
B	*0.0001*	*0.0001*	*0.0001*	*0.0001*	*0.0001*	*0.0001*	*0.0001*

Table 3.12 Chemical analysis result of as cast U-Mo alloys.

3.3.1 Hot rolling of as cast U-Mo alloy ingots

The cast *U-Mo alloy* ingot samples were first hot rolled to break their as-cast structure. In the process, ingots were first jacketed in copper casing with typical wall thickness of around 500 µm *(as shown in Fig. 3.12).* The copper jacketed alloy ingots were heated in a resistance heating furnace at 900 °C (γ-phase region in U-Mo phase diagram) *(as shown in Fig. 3.13).* Selection of heat treatment temperature for different U-Mo alloys is shown in *Fig. 3.14*. The copper jacketed pieces were then hot rolled to reduce the ingot cross section by more than 50% which is further shown in *Fig 3.15*. These hot rolled U-Mo alloy ingots were then dejacketed from copper casing and were cleaned in an ultrasonic cleaner. A 2-high reversible hot rolling machine used for the hot rolling of alloy samples is shown in *Fig. 3.16.*

Fig. 3.12 Photograph of copper jacketed as cast U-Mo alloy samples.

Fig. 3.13 Photograph of heat treatment furnace.

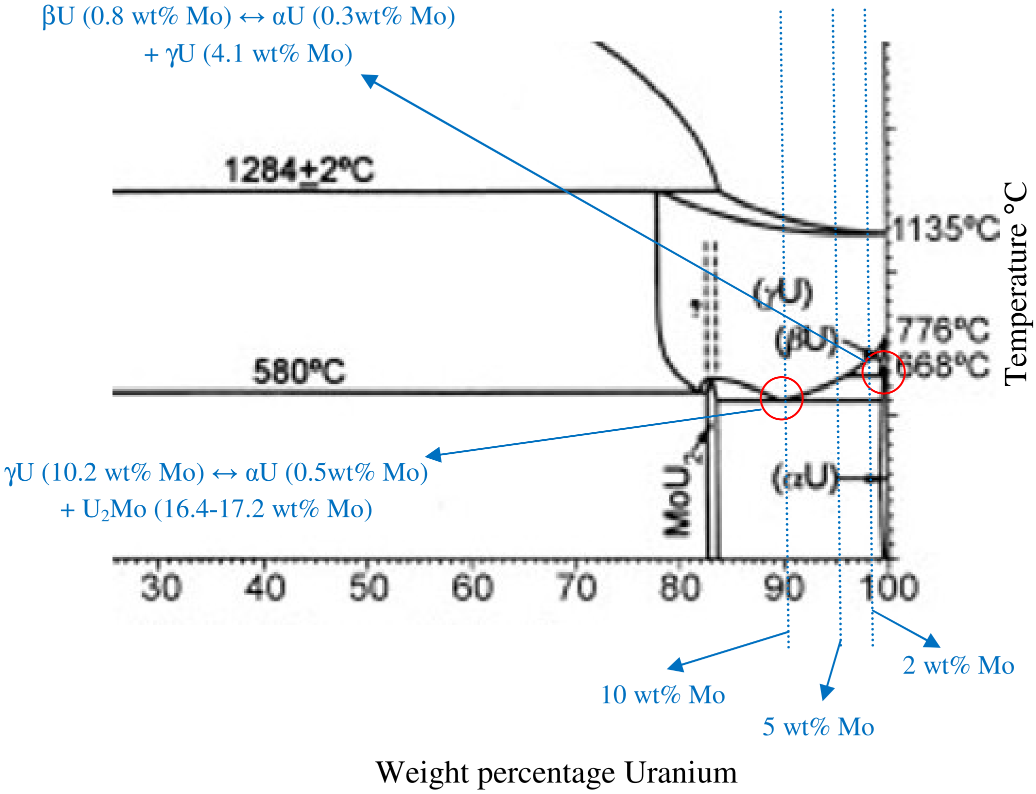

Fig. 3.14 Magnified view of U-Mo phase diagram and the basis for the selection of heat treatment [113].

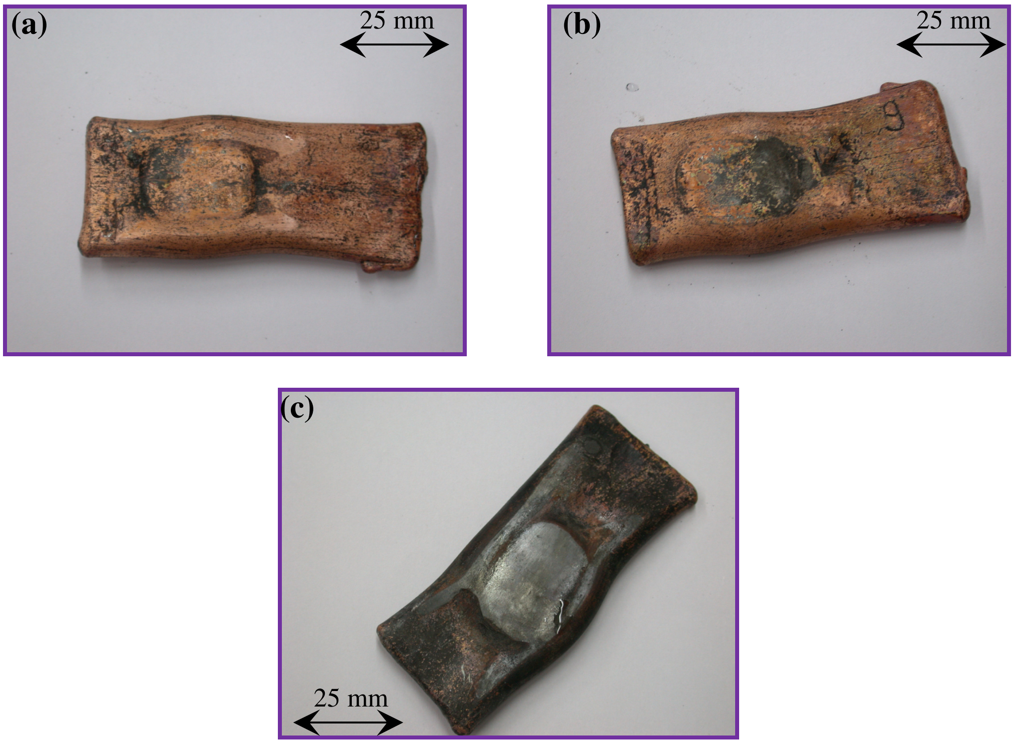

Fig. 3.15 Photograph of rolled copper jacketed U-Mo alloy samples (a) U-8wt%Mo, (b) U-9wt%Mo and (c) U-10wt%Mo.

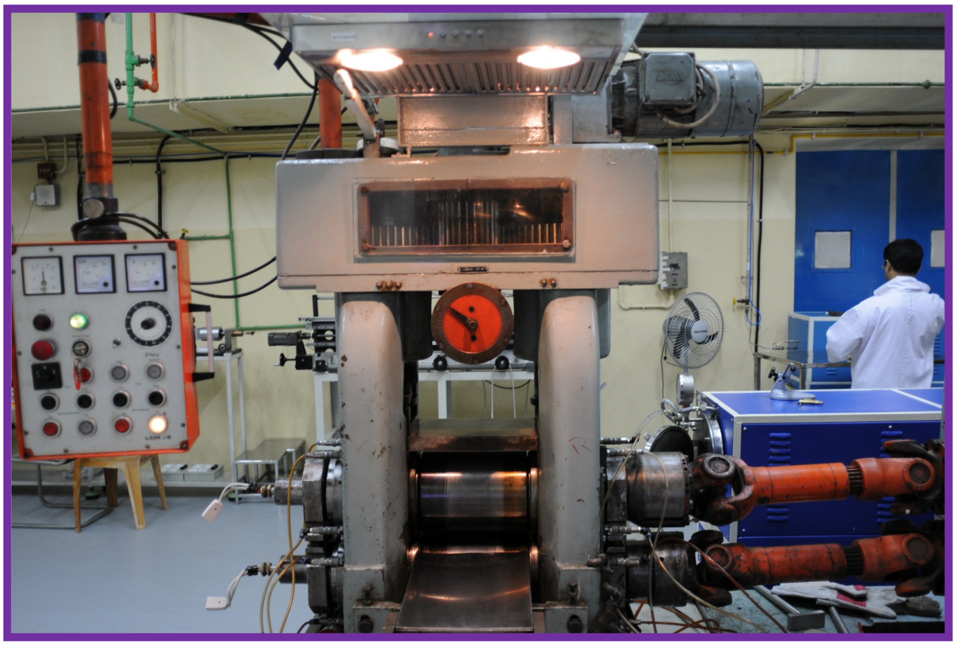

Fig. 3.16 Photograph of 2-high reversible hot rolling mill.

3.3.2 Quartz encapsulation and heat treatment of U-Mo alloy ingots

The hot rolled *U-Mo alloy* ingots were then encapsulated in a quartz tube under the partial pressure of helium at 10^{-1} mbar *(as shown in Fig 3.17)*. The *U-Mo alloy* ingots were then heat treated in a resistance heating furnace at 500 °C for 68 hrs and 240 hrs, so that metastable cubic γ-phase can transform to equilibrium phases of α-uranium and U_2Mo intermetallic compound. Two sets of *U-Mo alloy* samples with quartz encapsulation were prepared, so as to perform two different heat treatments cycles. The heat treated alloy pieces were then taken out of quartz tube by breaking them at room temperature.

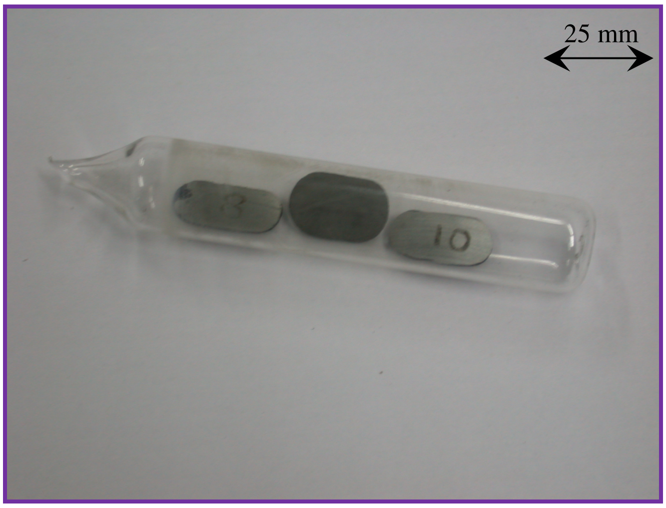

Fig. 3.17 Photograph of quartz encapsulated U-Mo alloy pieces.

3.4 Characterization

The *U_3Si_2* compound and *U-Mo alloys* with different molybdenum percentage were characterized chemically to determine the elemental content and also by XRD for phases. In addition, optical microstructure of the compound and alloys were also developed. Similarly, to study the effect of molybdenum addition on uranium lattice and out of pile characterization on metastable cubic γ-uranium, the X-ray diffraction analysis was carried out for phase & lattice parameter determination and optical microstructures were developed.

3.4.1 Chemical analysis

Chemical analysis for the metallic content of *U_3Si_2* compound and *U-Mo alloys* were carried out using standard analytical chemistry methodology and the results are presented from *Table 3.1* to *Table 3.10* and in *Table 3.12*. However, the analysis for non-metallic impurities *(i.e. Carbon, Oxygen and Nitrogen)* was carried out using standard CNO analyzer.

3.4.2 X-ray diffraction (XRD) analysis

Samples were prepared to carry out phase analysis of *U_3Si_2* compound, where synthesized *U_3Si_2* powders were compacted in 20 mm diameter tablet. The XRD pattern was generated in standard θ-θ equipment *(as shown in Fig. 3.18)* with the scan rate of 1 °/min. Tube voltage and current was kept at 40kV and 30 mA respectively. The X-Ray diffraction patterns of the pellets were obtained by using CuK_α radiation and monochromatized with curved graphite monochromator.

Fig. 3.18 Photograph of θ-θ XRD machine.

The three different compositions of *U-Mo alloys* prepared by both the powder metallurgy and induction melting route were characterized by XRD for phase determination, where scan rate was kept at 0.5°/minute. Standard θ-θ machine was used for the purpose. The source was Cu Kα and the tube voltage and current was 35.0 KV and 28.4 mA respectively. The tablets of uranium molybdenum alloys prepared by powder metallurgy route were directly used as sample for the analysis. The XRD samples for induction melted alloys were prepared by cutting the cast ingots in the form of small disk using silicon carbide wheel. These disks were then grinded in 600 µm emery paper, followed by polishing with 2 µm diamond paste to achieve good surface finish.

3.4.3 Metallography practice

The standard metallography practice adopted for uranium compounds/alloys in the present study was followed as per the guidelines mentioned in *ASM Metal's Handbook* [161]. Samples for U_3Si_2 pellet were prepared by first cold mounting them in 25 mm diameter mold followed by grinding in standard metallography equipment. The sample was then polished mechanically using 2µm diamond paste and finally etched with freshly prepared etchant (very dilute phosphoric acid).

Slow speed SiC cut-off wheels *(M/s Struers, DENMARK)* was used to cut *U-Mo alloy* samples under constant flow of water. Cold mounting resin was used to mount the sample in 25.4 mm ID Teflon mold. It is also important to state that only cold setting resins were used because edge retention was not important in preparing the sample for present course of study. After the mount was solidified *(usually within 20 minutes)* a hole was made on the opposite side of the mount to facilitate an electric contact for consecutive electro polishing/etching. However the electro polishing/etching methodology was not used in as cast and hot rolled *U-Mo alloys*, therefore in these samples drilling on the mold was not required while in rest it was done categorically. Grinding of the samples were carried out in water resistant SiC abrasive paper of different grit size as desired, while maintaining a constant water flow over the sample. Wet grinding with constant water flow was essential to avoid unwanted heat generation in the samples and more importantly to avoid fire hazard due to fines generated from *U-Mo alloys*. Final metallography grinding was done using 600 grit SiC paper and polishing was carried out using 2µm diamond slurry in alcohol based lubricating media. It was also found that the samples of U_3Si_2 compound and *U-Mo alloys* synthesized by powder metallurgy route are extremely difficult to polish, because during polishing the particulates in the samples tend to sprawl out. However, the use of low speed of polishing wheel *(around 50 to 100 rpm)* had yielded satisfactory results. On the other hand it was also found out that in *U-Mo alloys* with higher molybdenum content it was extremely difficult to remove the scratches by 600 grit paper grinding only and additionally prolonged polishing had given unwanted edge rounding and polishing artifacts in the sample.

Electro polishing and electro etching were employed for heat treated *U-Mo alloy* samples and for *U-Mo alloys* with low molybdenum content. However, it was also observed that electro polishing itself in many instances had revealed the microstructure of the sample under optical microscope. Selectable constant potential and constant current source were locally procured (*(M/s Sairush, INDIA)* for electro polishing and electro etching. The etchant details for different compounds and alloys which were used in the present study are shown in *Table 3.13*. In all the cases of electro polishing and electro etching pot made of SS 304 was used as cathode. During electro polishing a constant 25V DC potential was applied whereas, in electro etching the potential was dropped to 5V DC. Both electro polishing and electro etching was limited to 2 to 5 seconds initially and only after making due observations further application of potential was decided.

Composition of alloy	***Etchant composition and process details***
U_3Si_2 compound	*Dilute phosphoric acid (2 part acid and 100 part water)*
As cast and hot rolled U-8wt%Mo, U-9wt%Mo and U-10wt%Mo	*1 part orthophosphoric acid, 2 part H_2SO_4 and 2 part H_2O. Used as chemical etchant, freshly polished sample is attacked with few drops.*
Heat treated U-8wt%Mo, U-9wt%Mo and U-10wt%Mo and U-Mo alloys with composition 2wt%Mo, 5wt%Mo, 6wt%Mo, 7wt%Mo	*5 part orthophosphoric acid and 100 part H_2O. 2-2.5 V open circuit, stainless steel cathode is used for electrolytic etching.*

Table 3.13 Description of etchants used for U_3Si_2 compound and U-Mo alloys in as cast, hot rolled and heat treated condition.

3.4.4 Optical microscopy

Microstructures in U_3Si_2 compound and *U-Mo alloys* were developed using inverted optical microscope, *(i.e. DMI 5000M from M/s*

Leica, GERMANY). The inverted optical microscope contains selectable green light and day light filters for bright field and polarized light illumination respectively with 100W light source. A mono CCD chip with 8 mega pixel resolution camera of *M/s Lieca, Germany* was used to capture the microphotographs.

3.4.4.1 Phase analysis

Statistical determination of the volume phases and constituents from the respective microstructures was calculated by using *Leica Metallography Work Station Software*. The test method used by the purpose was based upon *ASTM E562* standard. This test method describes a systematic point count procedure for statistical estimation of volume fraction from an identifiable constituent or phase from a section through the microstructure using a point grid. The method is based on the principal that when an array of points is systematically placed over a two dimensional section of a microstructure, the proportion of points that fall within a randomly distributed second phase is equal to the area fraction and volume fraction of the second phase in the microstructure. This mathematical relationship is shown in equation 3.1.

$$V_V = \frac{V_\alpha}{V} = \frac{A_\alpha}{A} = \frac{P_\alpha}{P} \tag{3.1}$$

Here V_V is the volume fraction of the alpha phase. V_α is the volume of the ‘α’ phase in the sample. V is the total volume of the three dimensional sample. A_α is the area of the ‘α’ phase in a random planar section. A is the total area of the random planar section. P_α is the number of points falling in the ‘α’ phase in a random planar section. P is the total number of points laid down in the random planar section [162-163].

It is also important that the sample selected for the purpose shall be the representative of microstructure. Therefore all the image analysis was carried out on four sets of microstructures for each alloy composition, with different preparation and heat treatment history.

3.4.4.2 Grain size determination

The grain size of different optical microstructures was calculated using *Leica Metallography Work Station Software*. The analysis method used to determine average grain size is based upon *ASTM 1382 intercept* using automatic image analysis. This standard defines test methods for determining ASTM grain size using the following methods: Measurement of grain intercept lengths, intercept counts, intersection counts, grain boundary length and grain areas. However, this method has the limitation and is applicable provided that the grain boundaries can be segregated. Hence, this is strongly dependant on the composition of the sample and the preparation, which requires good polishing to remove scratches and etching methodology to expose the grain boundaries for a better view. It is also important to note that the accuracy of grain size measurements is highly dependent on the delineation of the grain boundaries on the specimen, since this has a direct effect on the ability of the automated image analysis system to segregate grain boundaries.

The simplest procedure for determining grain size is to detect the grain boundaries using grey level threshold. The boundaries that intersect with the image boundaries are not removed. The total length of the boundaries in the field is measured, which is then divided by the length of field area to obtain the grain boundary length per unit area in mm/mm^2 L_{iA}. The value of L_{iA} is then divided by $\pi/2$ to obtain P_{Li}, which is the number of grain boundary intersections per unit length of test line for each field and then is applied to calculate the mean linear intercept length for all measured fields. The standard deviation should also be calculated. The formula shown in *equation 3.2* represents the grain boundary intersections per unit length [164-167].

$$P_{Li} = \frac{L_{Ai}}{\pi / 2} \tag{3.2}$$

In addition mean intercept length is also calculated which is the reciprocal of the number of intersections per unit length.

$$l = \frac{1}{P_l} \tag{3.3}$$

The results were calculated on average five microphotographs of each alloy composition with particular history and then the average value has been reported to minimize error in calculation/analysis.

A general correlation between the grain sizes and the *ASTM grain size number* is shown in *equation 3.4.*

$$n = 2^{G-1} \tag{3.4}$$

Here, ‘n’ is the number of grains per square inch at 100X magnification and ‘G’ is the ASTM grain size number.

3.5 Preparation of U-Mo diffusion couple & its characterization

A diffusion couple between uranium and molybdenum was prepared to study the diffusion of elements in each other. The diffusion couple was prepared by two different techniques. In the first method, uranium and molybdenum pieces in desired dimension was cut using *SiC cut off wheel* and then wrapped inside tantalum foil *(as shown in Fig. 3.19)*. It was then loaded in special designed inconel assembly and the top lid was screw tightened. The entire assembly was encapsulated in quartz tube under partial pressure of helium (i.e. 10^{-1} mbar) and was heat treated at 900 °C for 24 hours in a resistance heated furnace *(as shown in Fig. 3.20)*. The heat treated diffusion couple was then retrieved by first breaking the quartz tube and then unscrewing the top. The discs of uranium and molybdenum received after this experimentation is shown in *Fig. 3.21*.

In another case the diffusion couple was prepared in hot press under vacuum of 10^{-5} mbar. In this case the pieces of uranium and molybdenum were first cut in the desired dimension and then polished to get scratch free surface. These pieces were then stacked in the sequence shown in *Fig. 3.22*.

Fig. 3.19 Photograph showing uranium and molybdenum pieces wrapped inside tantalum foil and loaded in inconel assembly.

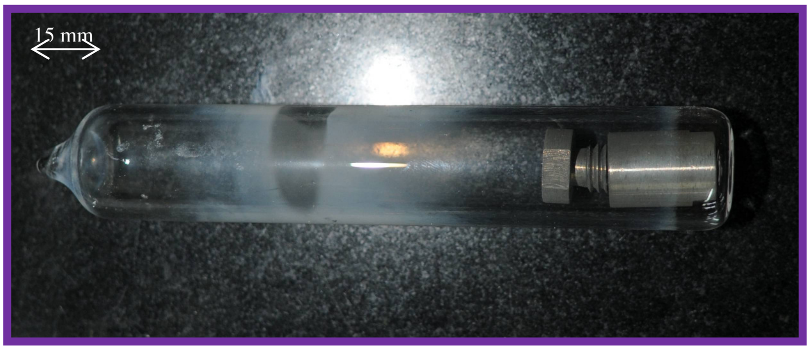

Fig. 3.20 Photograph of quartz encapsulated diffusion couple.

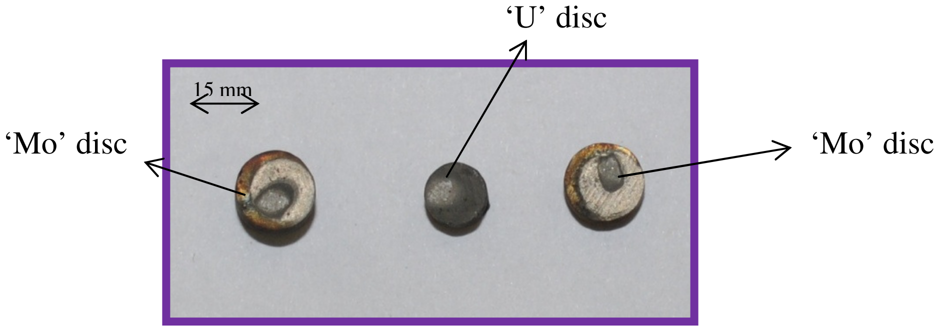

Fig. 3.21 Photograph of uranium and molybdenum pieces taken out after diffusion couple experimentation.

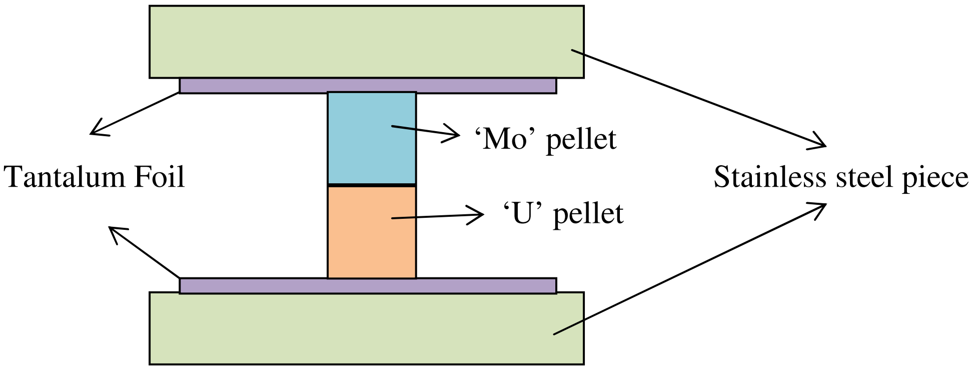

Fig. 3.22 Schematic of uranium and molybdenum piece used in hot pressing.

The sample *(as shown in Fig. 3.22)* was then loaded in a vacuum hot press. The hot press chamber was first evacuated to 10^{-5} mbar pressure and heating was started. Once the set temperature (i.e. 900 °C) was achieved then a load of 13.5 MPa was applied on the sample for 3 hours. The furnace was then allowed to cool under vacuum and the sample was removed from the hot press. The photograph shown in *Fig. 3.23* represents uranium molybdenum diffusion couple after vacuum hot pressing at above described parameters.

The diffusion couple prepared between uranium and molybdenum by above referred technique was then cut in longitudinal section and mounted for metallographic examinations using cold setting resin. The sample was then evaluated in optical and SEM microscopy to develop microstructures. The sample was also examined using EPMA and chemical compositions of molybdenum and uranium across the diffusion zone was determined.

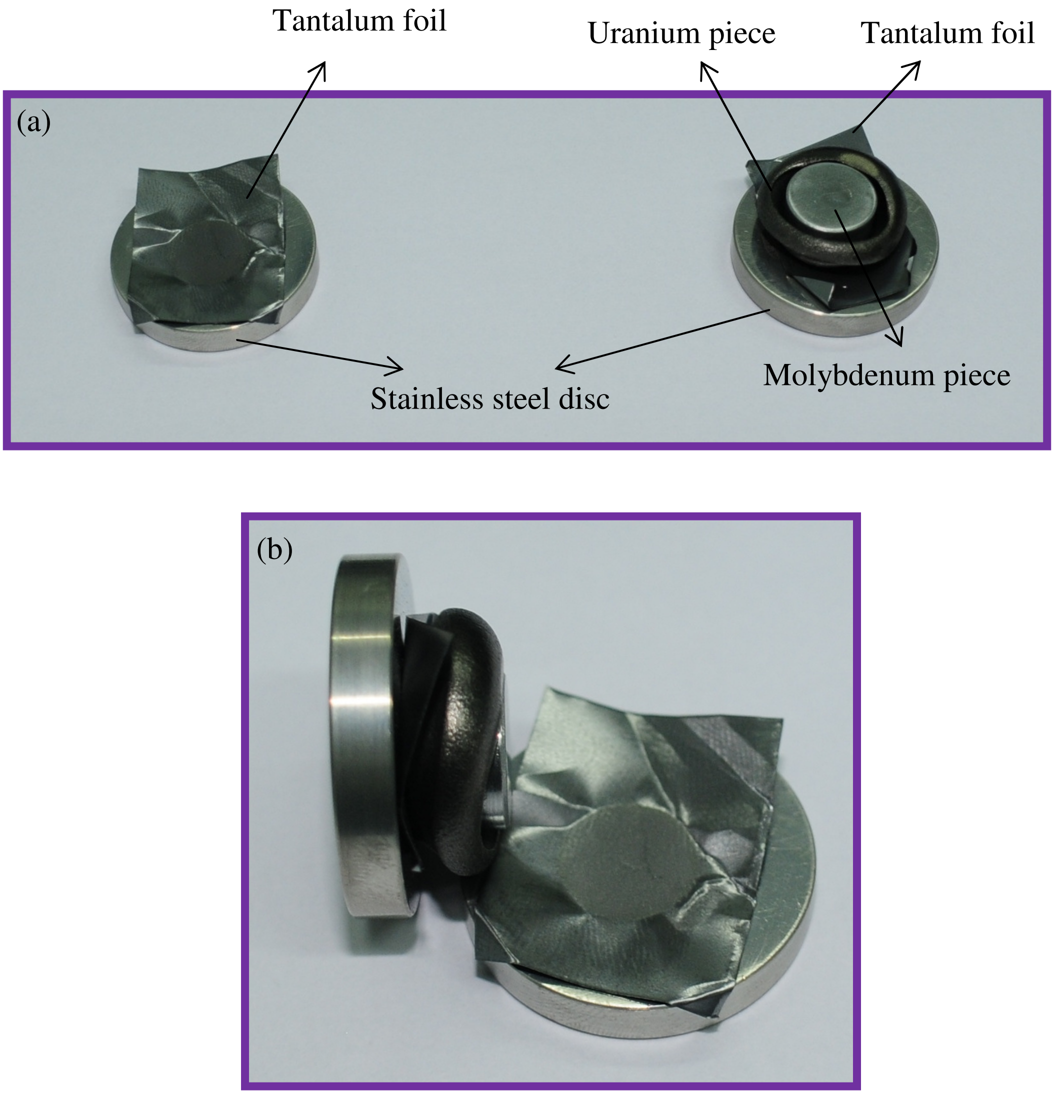

Fig. 3.23 Photographs of U-Mo diffusion couple after vacuum hot pressing (a) Horizontal image, (b) Vertical image.

4. Results & Discussion

4.1 Characterization of U_3Si_2 compound prepared by powder metallurgy route

4.1.1 Phase analysis

As stated earlier in *chapter-3*, the alloying of U_3Si_2 compound was accomplished in a single-step process. The uranium and silicon elemental powders were mixed in a cubical blender, followed by a heating profile with controlled dwell time and heating rates. The U_3Si_2 pellets thus obtained exhibited good pellet integrity without cracks, as shown in *Fig.3.6*. The chemical analyses of elemental powders as well as that of U_3Si_2 compound shown in *Tables 3.1, 3.2 and 3.5* respectively, confirms no impurity pickup during processing. This reflects the adequate care and precautions taken during powder processing stage. *Fig. 4.1* shows the XRD pattern of as synthesized compound. All the major peaks in the XRD pattern could be indexed to the U_3Si_2 phase and no other silicide or impurity phase/s could be observed within the detectable limit. It may be noted that the *U-Si* phase diagram contains several intermediate phases, therefore starting with elemental powders could result in the presence of one or more of them, due to local variations in relative concentrations. Further, the density difference between uranium and silicon is significant, i.e. density of uranium is 19.7 g/cm^3 and that of silicon is 2.33 g/cm^3. It is well known that mixing of dry powders with large differences in their densities may result in segregation of the constituents. Various mechanisms viz. agglomeration, floating, percolation or trajectory separation, generally utilized as a tool for mineral beneficiation, pose difficulties in obtaining a homogenous mixture of heavy and light constituent powders [168]. Therefore, it becomes imperative to select blender or mixer which may minimize the segregation of powders. Keeping this in view, a cubical blender was used to mix the metal powders in this study. Further, the mixture of powders requires intimate mixing of constituents for effective alloying reaction to take place. Therefore, the mixed powders were compacted at 600 MPa, to ensure plastic flow of constituent powder particles.

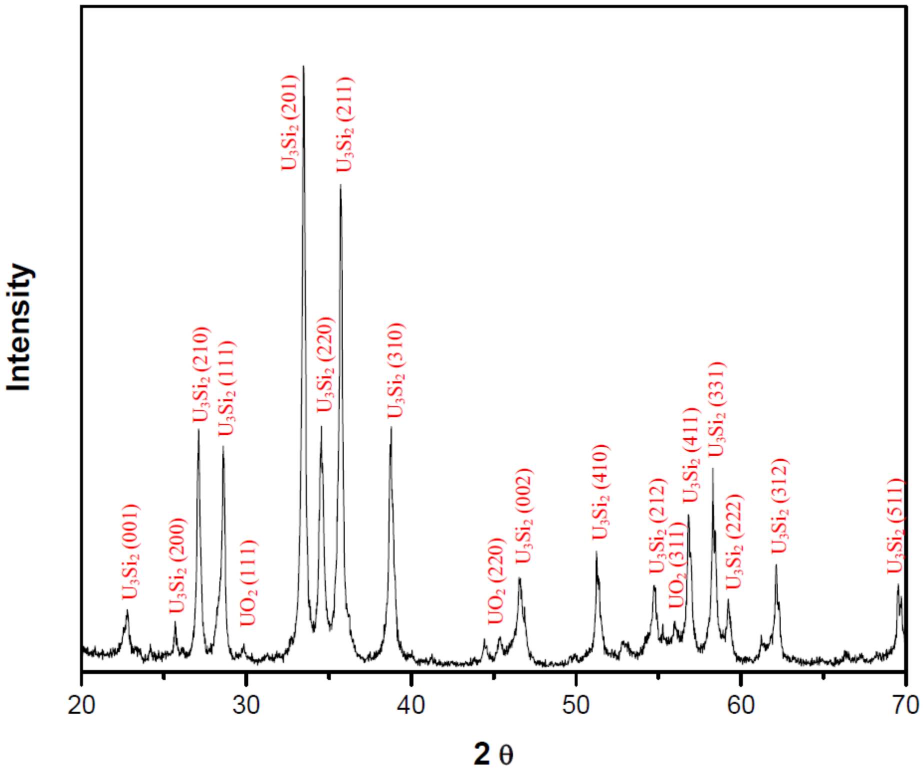

Fig. 4.1 XRD pattern of synthesized product (U_3Si_2) prepared by powder processing route.

In addition, as stated earlier, uranium being radioactive *(mainly alpha emitter)*, special precautions for handling and safety are needed while processing *(under glove boxes with once through argon ventilation).* Therefore, the choice of equipment becomes a constraint. Hence, in order to overcome any perceived variations in the local composition, soaking steps at 950 °C *(1 hour)*, 1400 °C *(30 minutes)* and 1550 °C *(4 hours)* were introduced. Therefore, it may be surmised that the combination of mixing procedure in the cubical blender and intermittent soaking steps in the heating schedule achieved the desired single-phase product as mentioned above. The XRD pattern also shows some minor peaks which were attributed to UO_2. Since the oxygen content of starting uranium as well as silicon powders was 1500 and 9500 ppm respectively, it lead to formation of UO_2. The oxygen content *(i.e. 2000 ppm)* found in the synthesized compound may, therefore be in the form of UO_2 phase formed. UO_2 being stable compound for irradiation points of view, the presence in these quantities may not be harmful. Therefore, the presence of oxygen which originates in the processing of uranium as well silicon powders, may be accepted as tolerable impurity in the intended U_3Si_2 to be used as dispersion fuel.

4.1.2 Microstructural analysis

Fig. 4.2 show bright field optical micrograph of as synthesized U_3Si_2 clinker after polishing and etching. The microstructure show equiaxed grains of single phase material, besides some pull-outs and etch pits. The density of the clinker was found to be between 75-80% TD, as measured by immersion technique using alcohol medium *(Archimedes principle)*. This low density is expected in the pellets, because the pellets were synthesized from elemental powders and were heated in stages. The first soaking was carried out at 950 °C for 1 hour to accomplish the alloying reaction between uranium and silicon. Subsequently the temperature was raised and heating was carried out at 1400 °C for 30 minutes.

These two intermediate soaking steps were employed to ensure that neither uranium nor silicon remains in elemental form, when the temperature was raised above their melting points, thereby eliminate the possibility of bulk melting. Soaking at 950 °C was critical because any free uranium after this stage would lead to local melting and hereby disturbing the stoichiometry *(uranium metal volume fraction is more if compared with silicon)*. The selection of temperature was on the basis of eutectic point at 985 °C. The duration for every step of soaking was optimized after repeated experimentation. It could further be illustrated that after first stage of soaking the temperature inside the furnace was raised slowly (~3°C/minute) until the next stage (1400 °C). The step was extremely critical in the formation of U_3Si_2 single phase compound because any stoichiometric deviation at localized micro scale would lead to hypo or hyper composition. In the first case if the localized micro scale composition goes hyper then further increase in temperature beyond 950 °C would result in small liquid phase generation. The formation of liquid phase at localized region would facilitate elemental diffusivity and result in homogeneous U_3Si_2 product phase by peritectic reaction. The results obtained in Appendix-1 also indicate that the relative phase volume percentage of U_3Si_2 and liquid phase will vary opposite to each other with the change in temperature. In fact the liquid phase volume percentage increases with temperature, therefore result in better homogeneous product phase (U_3Si_2). The microstructure also confirms that any bulk melting in the process was avoided however formation of small liquid phase during alloying was possible (as grain boundary does not show sharp edges).

Similarly the results derived in Appendix-1 also shows that any hypo composition during alloying at localized micro scale does not result in liquid phase formation until the temperature is raised beyond 1540 °C. Therefore, in order to homogenize the product phase even better by facilitating diffusion of elements at higher temperature the final soaking was accomplished at 1550 °C for 4 hours in a pressure less mode. The final soaking temperature of 1550 °C was selected on the basis of eutectic and peritectic reaction temperatures in the system at 1540 °C and 1580 °C respectively. Therefore, soaking at 1550 °C would help in improving the local alloying reaction kinetics because any small change in stoichiometry at the temperature may allow the product to enter into mushy zone *(liquid plus solid)* and favor U_3Si_2 formation (as shown in Appendix-1). The same was confirmed from the optical microstructure where no evidence of bulk liquid phase formation was observed. This could well be explained from U-Si phase diagram. It could be observed that small addition of silicon in the phase, near congruent compound composition increases the liquidus sharply, thereby eliminating any small possibility of bulk liquid phase formation.

It is also well known that the reaction between uranium and silicon is exothermic with heat of reaction -46.8KJ/mol [169]. This may lead to highly agglomerated product, full of porosity. Generally, compound formed in such process is crushed to break agglomerates followed by sintering to impart high densities [170]. In contrast to this, U_3Si_2 was heated directly, without employing any pre-compaction stage because, porosity in the synthesized compound is considered beneficial for the intended application and grinding of alloy product was considered futile due to men-rem considerations. The presence of porosity in the grains of U_3Si_2 can also be seen clearly in *Fig. 4.3* showing SEM micrograph of the fracture surface of pellets. On the other hand, optical microscopy did not reveal the porosity, (Fig. 4.2). This may be attributed to highly friable nature of the pellets and re-entering of polished particles in the microstructure during polishing [171]. Nonetheless, optical microscopy exhibited a single-phase U_3Si_2 compound, which matches with XRD data. The ASTM grain size of U_3Si_2 clinker was found to be 1.2 *(equivalent to 234 μm).*

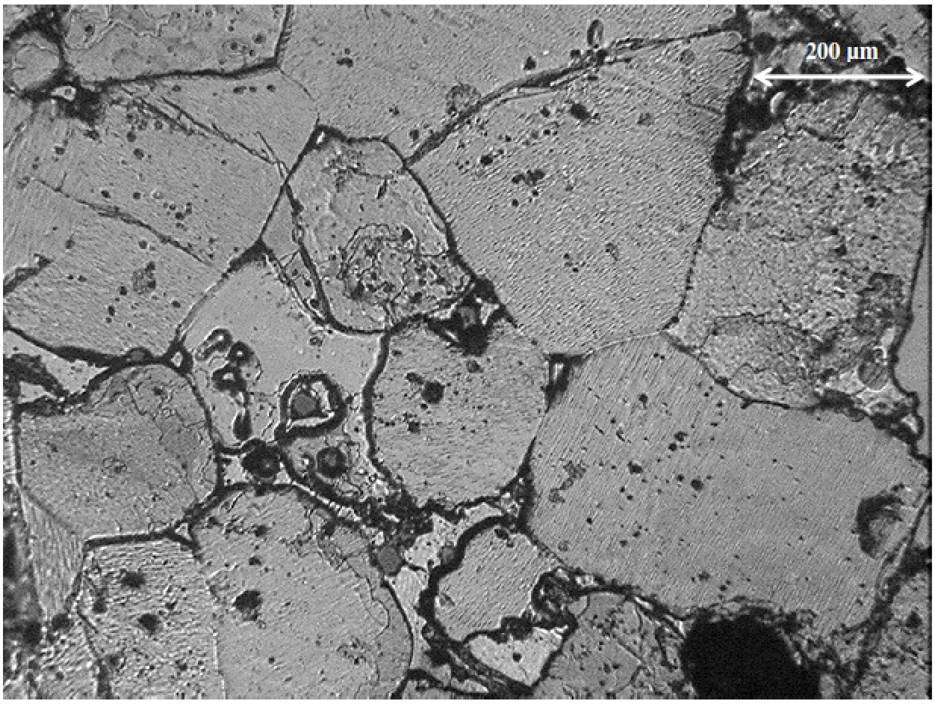

Fig. 4.2 Optical microstructure of U_3Si_2 clinker.

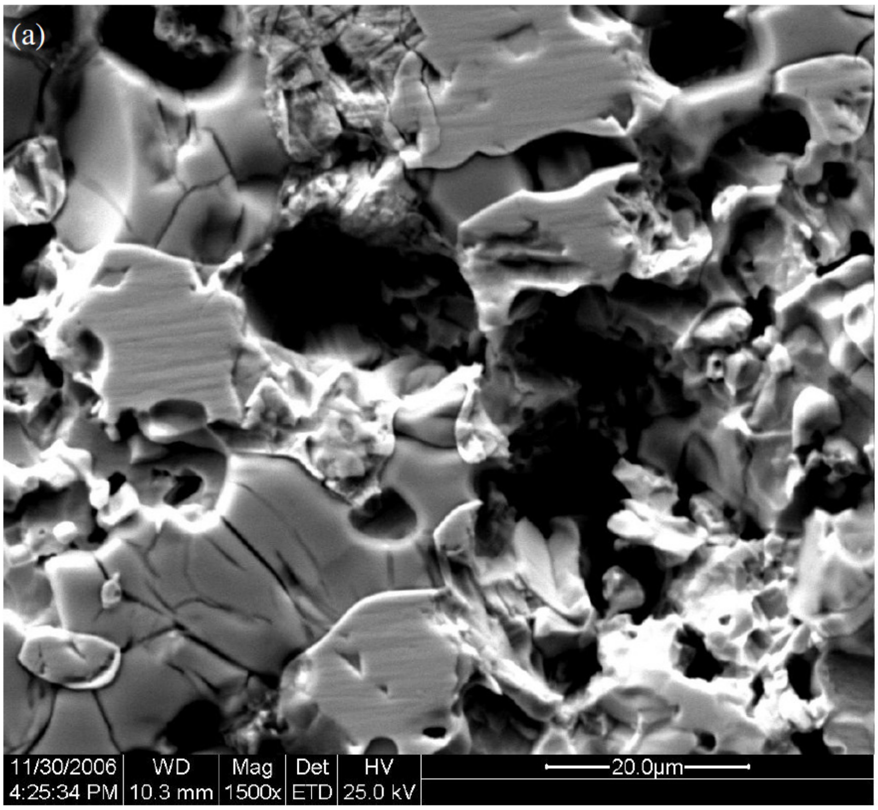

Fig. 4.3 (a).

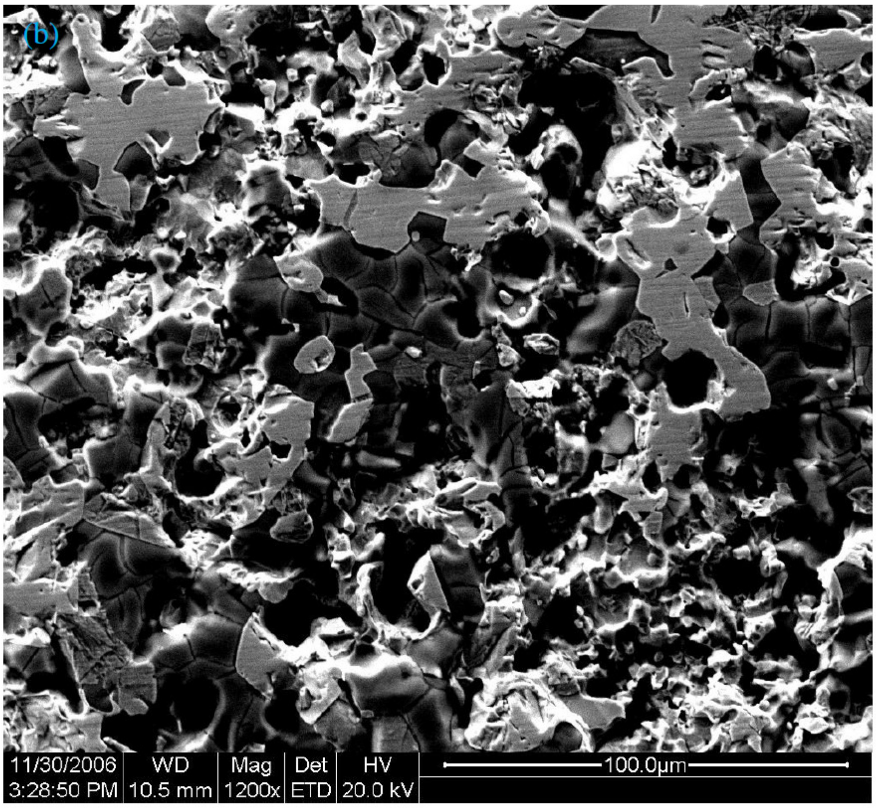

Fig. 4.3 SEM photomicrographs of U_3Si_2 clinker (a) at 1500 magnification and (b) at 1200 magnification.

4.2 Characterization of U-Mo alloys prepared by powder metallurgy and melting casting routes

4.2.1 Phase analysis

The XRD patterns for *U-Mo* alloys prepared by powder metallurgy as well as induction melting routes are shown in *Fig. 4.4 to 4.6*. *U-2wt%Mo* and *U-5wt%Mo* alloys show that the major phase in these alloy compositions was α-uranium with minor phases γ-uranium and U_2Mo intermetallic. The amount of γ-phase was more in *5wt%Mo* alloy as compared to those with

2wt%Mo. In alloys with 10wt%Mo, only gamma phase could be detected, thus indicating metastabiity of same with increased Mo content. Also, the XRD patterns for alloys with same compositions were found similar, irrespective of their processing method [172]. The increase in the quantity of gamma phase with increase in Mo concentration, and its eventual metastability is related to shifting of nose of TTT diagram, *(Fig. 2.2)* towards the right. This is in agreement with the related phase stability as depicted by the phase diagram. The alloying temperature, for the preparation of *U-Mo alloys* by powder metallurgy route was kept at 1050 °C, well below the melting point of constituent elements. Hence, the metallurgical reaction was only solid state reaction and the two-phase field (L+γ) was not encountered.

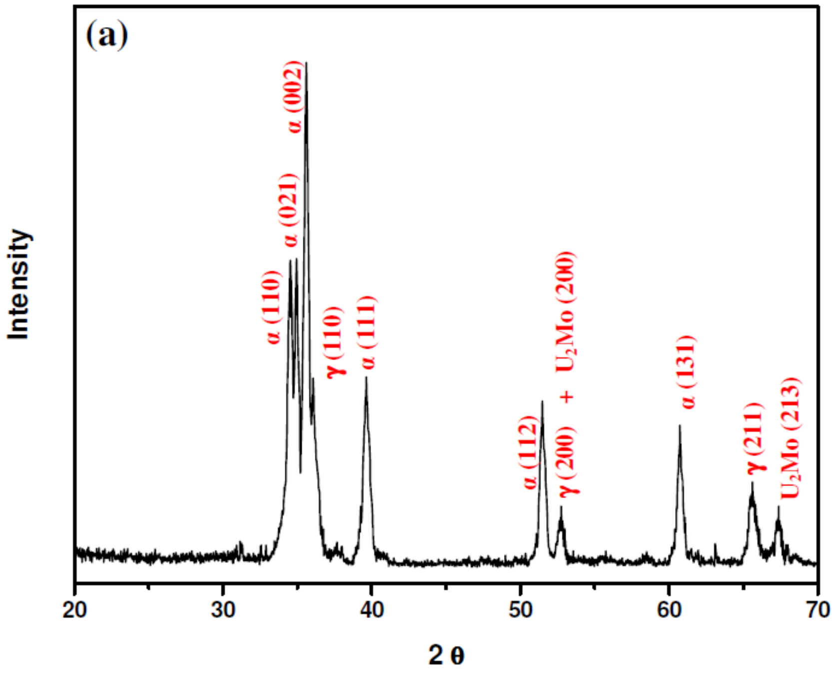

Fig. 4.4 (a).

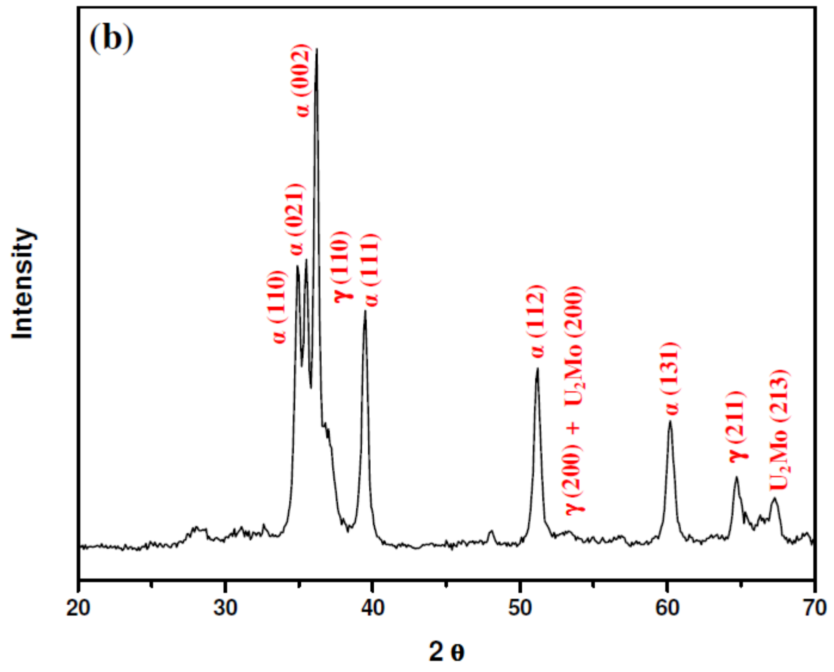

Fig. 4.4 X-ray diffraction patterns of U-2wt%Mo alloy prepared by (a) powder metallurgy route (b) induction melting route.

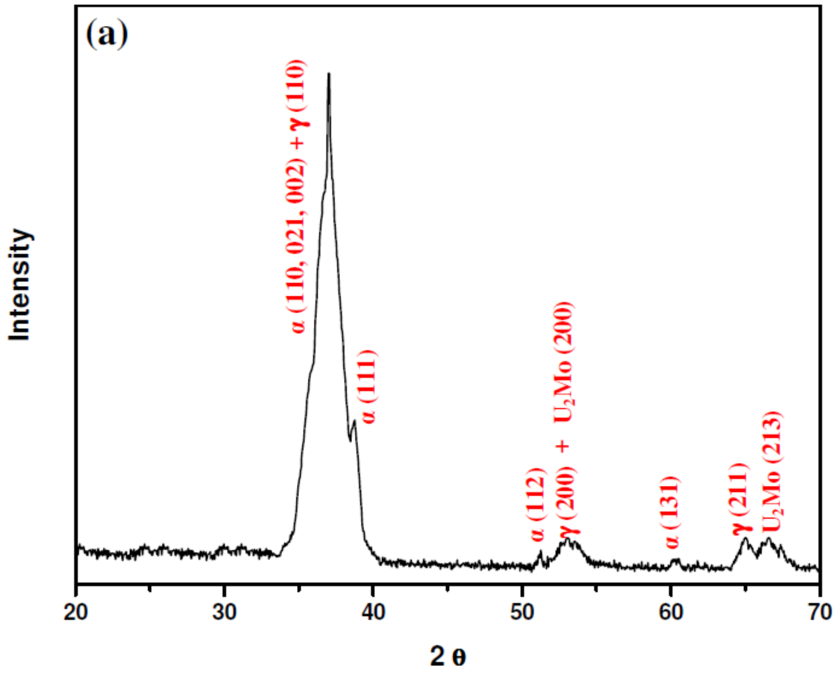

Fig. 4.5 (a).

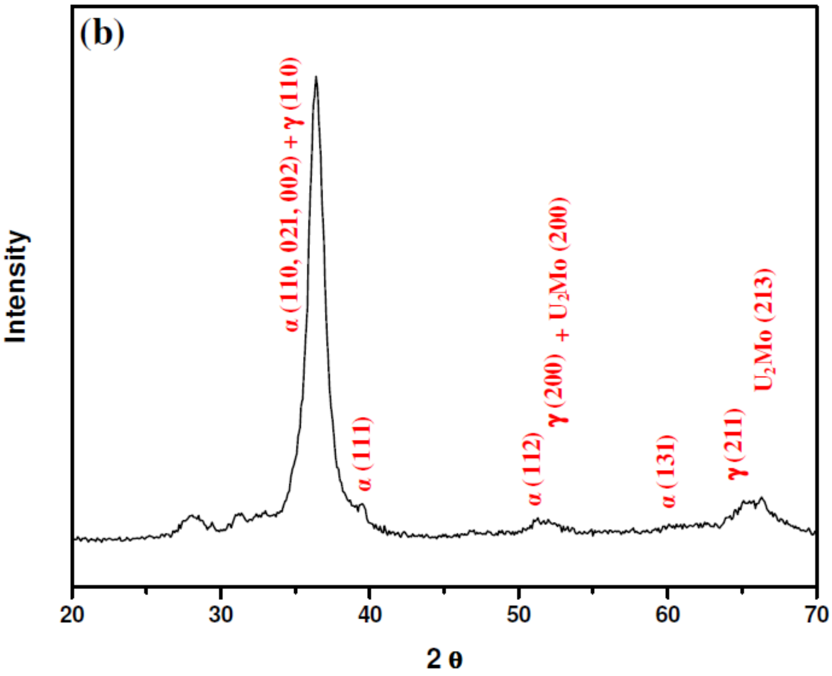

Fig. 4.5 X-ray diffraction patterns of U-5wt%Mo alloy prepared by (a) powder metallurgy route (b) induction melting route.

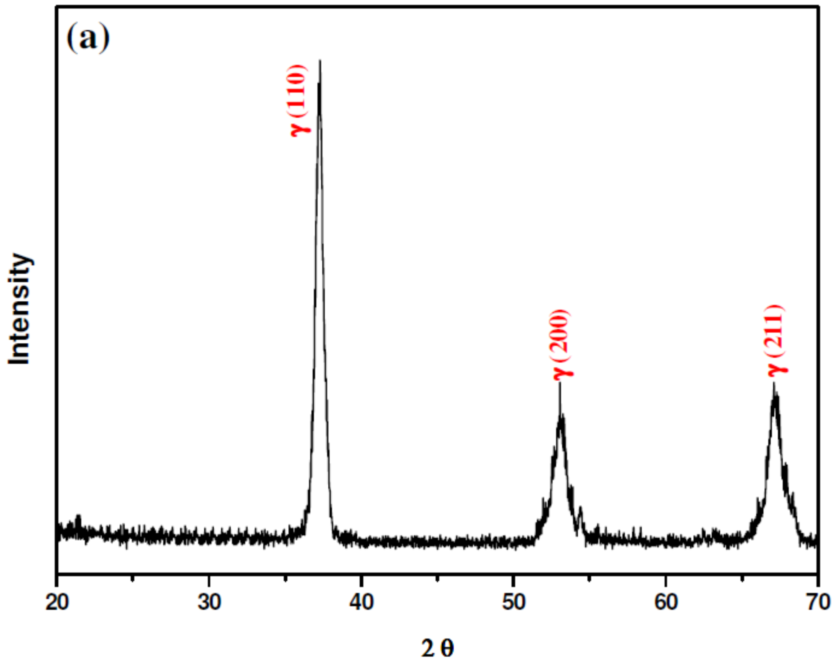

Fig. 4.6(a).

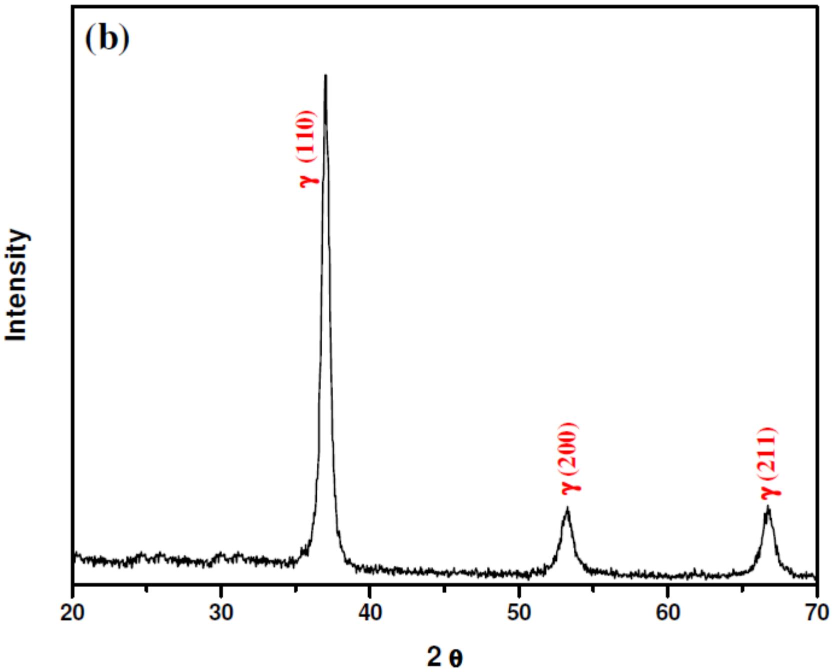

Fig. 4.6 X-ray diffraction patterns of U-10wt%Mo alloy prepared by (a) powder metallurgy route (b) induction melting route.

Due to this reason, the *U-Mo alloys* prepared by P/M route did not require any re-sintering or additional homogenization step. It may be recalled here that sufficient care was taken during mixing of elemental metal powders and also the compaction pressures (600 MPa) were beyond the flow-stress for constituent metals, the resultant product homogeneity was due to uniform and intimate particle to particle contacts. As for *U-Si* compound, the entire operation was carried out in glove box with once through flow of high purity argon gas to avoid any significant impurity pickup, which is also evident from its chemical analysis. A detailed chemical analysis of *U-Mo* alloys prepared by powder metallurgy route and by induction melting route is shown in *Table 3.8* and *Table 3.12* respectively. The chemical characterization result in *Table 3.8* also confirms that during *U-Mo alloy* preparation by induction melting technique, the oxygen pick up was completely eliminated, by putting oxygen getters in the form of zirconium over the crucible lid.

4.2.2 Microstructural analysis

The microstructure of *U-2wt%Mo* alloy prepared by powder metallurgy route is shown in *Fig. 4.7(a)*, whereas the microstructure of as cast *U-2wt%Mo* alloy is shown in *Fig. 4.7 (b).* Grey value difference in the microstructure may be related to the orientation difference between the grains. The microstructure of U_3Si_2 clinker prepared by powder metallurgy route *(as shown in Fig. 4.7(a)*) clearly reveals prior particle boundaries. The microstructure also exhibits typical widmanstatten pattern which indicates the phase transformation in *U-2wt%Mo alloy* and also the lamellar decomposition can be observed at some regions. The presence of widmanstatten pattern and lamellar decomposition suggests that the cooling rates along the pellet and ingot were not identical and the preferable nucleation site for the alloy prepared by both the routes is grain boundary. The microstructure of *U-5wt%Mo alloy* prepared by both powder metallurgy route *(as shown in Fig 4.8(a))* and by induction melting route *(as shown in Fig 4.8(b))* shows the presence of two phase region where larger grains are of γ-uranium and some grain refinement has taken place for α-uranium.

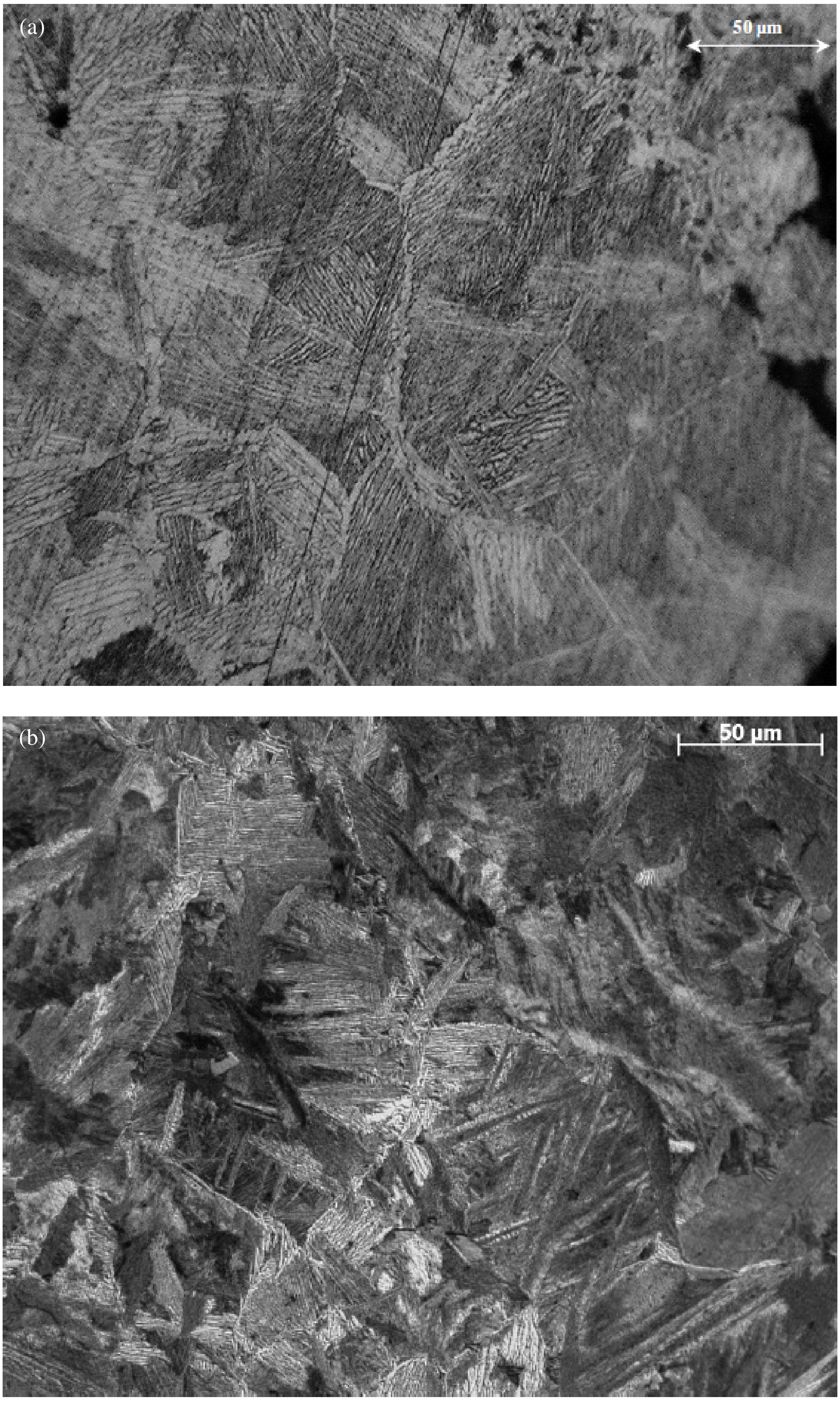

Fig. 4.7 Optical microstructures of U-2wt%Mo alloy prepared by (a) powder metallurgy route (b) induction melting route.

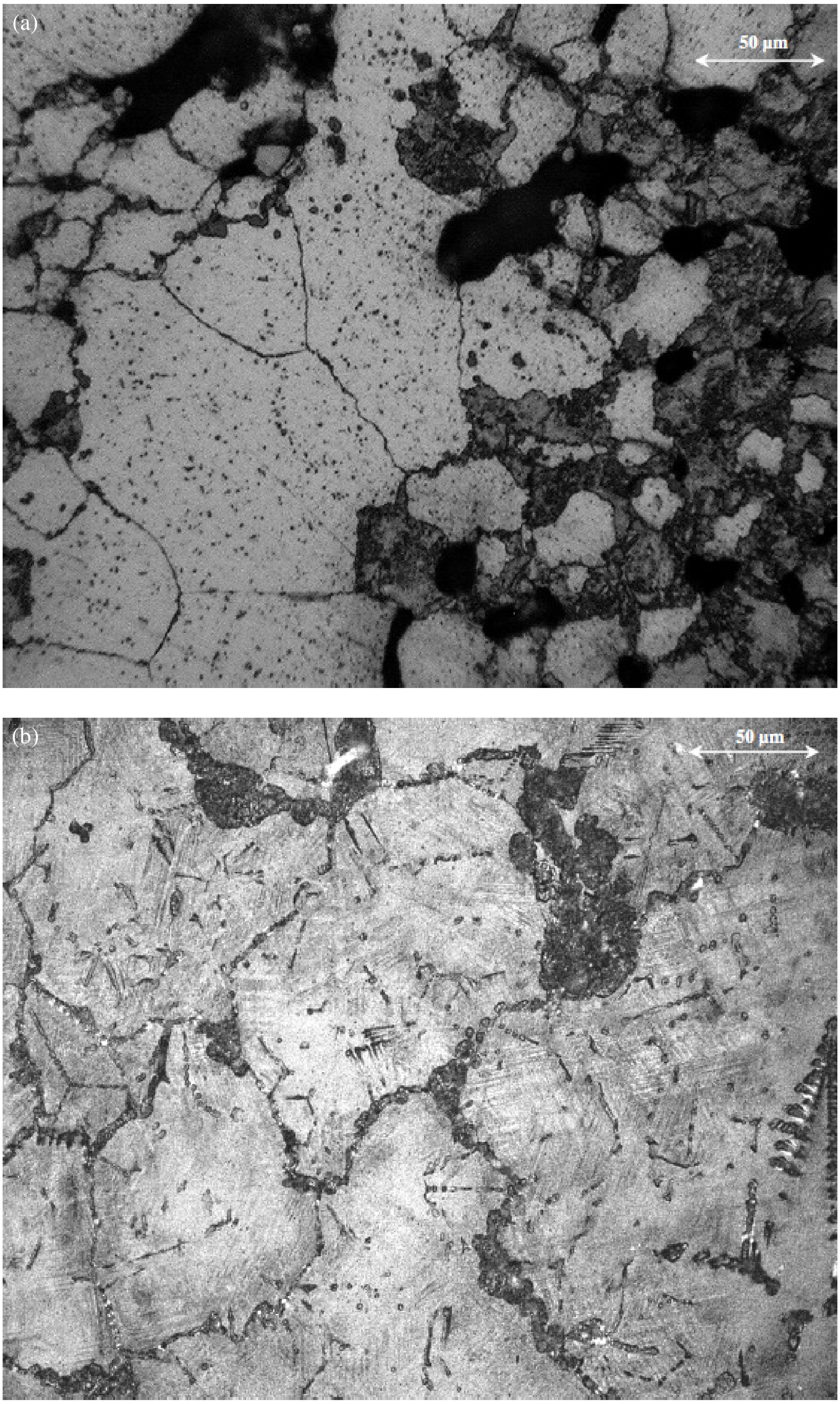

Fig. 4.8 Optical microstructures of U-5wt%Mo alloy prepared by (a) powder metallurgy route (b) induction melting route.

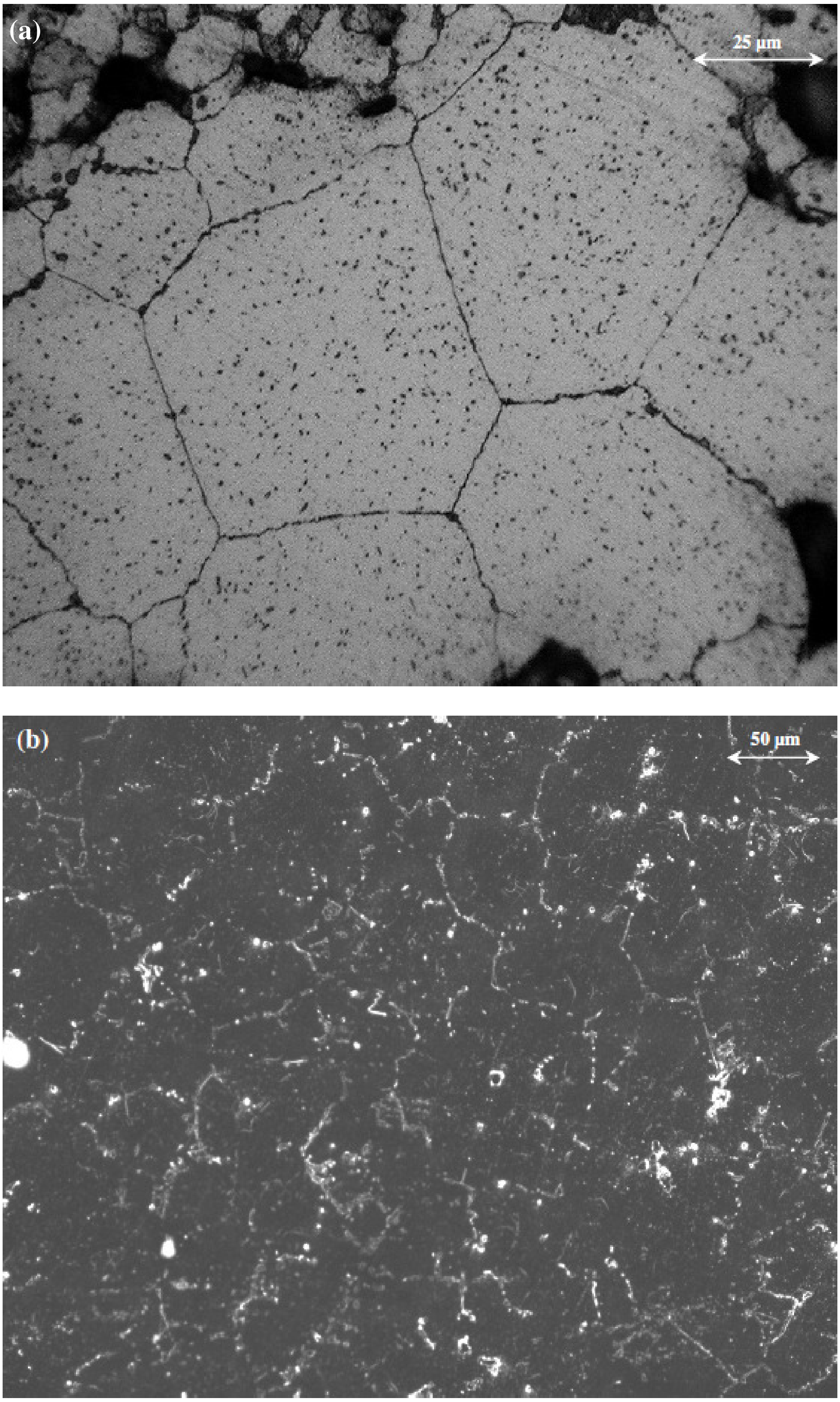

Fig. 4.9 Optical microstructures of U-10wt%Mo alloy prepared by (a) powder metallurgy route (b) induction melting route.

The microstructure of *U-10wt%Mo* alloy prepared by powder metallurgy route *(as sown in Fig 4.9(a))* and by induction melting route *(as shown in Fig 4.9(b))* shows single phase grains of only γ-uranium. The microstructures are therefore in agreement with the findings of XRD results Further, the microstructure of *U-Mo alloys* prepared by powder metallurgy route also show some dark regions. These dark regions could be identified as pores, typical of the P/M route, and conform to the density measurements. As stated earlier, these pores may be useful for the accommodation of fission gases and fission products during the irradiation. The grain size measurements of *U-Mo alloys* with two different preparation routes are shown in *Table 4.1.* The measurement of grain size was carried out as per the procedure described in *Section 3.4.4.2.*

It is evident from the data shown in *Table 4.1* that the grain sizes of alloys prepared by powder metallurgy technique are larger as compared to those of induction melting route. This may be related to the different time and temperature regimes followed in both the techniques. The induction melting, though carried out at 1300 °C, holds the alloys for 15 minutes, followed by quick cooling, however, P/M route involves soaking temperature of 1050 °C for 6 hours, followed by long time (~12 hours) for furnace cooling.

Composition of alloy	*Grain Size (μm)*	
	Alloy prepared by induction melting route	*Alloy prepared by powder metallurgy route*
U-2wt%Mo	160	203
U-5wt%Mo	155	198
U-10wt%Mo	153	194

Table 4.1 ASTM grain size number for different compositions of U-Mo alloys with different preparation techniques (calculated as per ASTM 1382 intercept method).

4.3 Characterization of U-Mo alloys for investigation on metastability in cubic γ-uranium

4.3.1 Phase analysis

The XRD pattern of *U-2wt%Mo alloy (Fig 4.10(a))* shows that the major phase for this alloy was α-uranium with small amount of γ-uranium and U_2Mo intermetallic compound. The XRD pattern of *U-5wt%Mo alloy (Fig 4.10(b))* shows presence of γ-uranium as major phase with very small amounts of α-uranium and U_2Mo intermetallic compound. The XRD patterns U-6wt%Mo alloy *(Fig. 4.10(c))*, U-7wt%Mo alloy *(Fig 4.10(d)),* U-8wt%Mo alloy *(Fig 4.10(e)),* U-9wt%Mo alloy *(Fig 4.10(f))* and U-10wt%Mo alloy *(Fig 4.10(g))* show the presence of cubic γ-uranium phase only. There were no oxide and carbide peaks observed in any of the XRD patterns which confirm that neither oxygen nor carbon in appreciable quantity was picked up during alloy preparation. This was verified by their chemical characterization as shown in *Table 3.12.* The XRD patterns suggest only gamma-phase without residual equilibrium phases, for alloys with Mo content of 6wt% and above. There could be two possibilities: either minor phases are in very small quantity and well below the detection limits of the analytical equipment, or, complete cubic γ-uranium has been retained at room temperature. It has been well documented that in U-Mo alloys, transformation of γ-phase into the equilibrium phases depends strongly on the cooling rate. This feature in U-Mo alloys is very similar to eutectoid decomposition in low carbon steels [173]. In dilute Mo alloys, the retention of gamma phase has been observed under fast cooling conditions [50-54]. Therefore, it is expected that addition of Mo may give rise to retention of gamma phase for furnace cooled alloys in this study. However, the minimum quantity of Mo, as described above, needs to be ascertained further. In this context, microstructural investigation of alloys samples was attempted, which is described later.

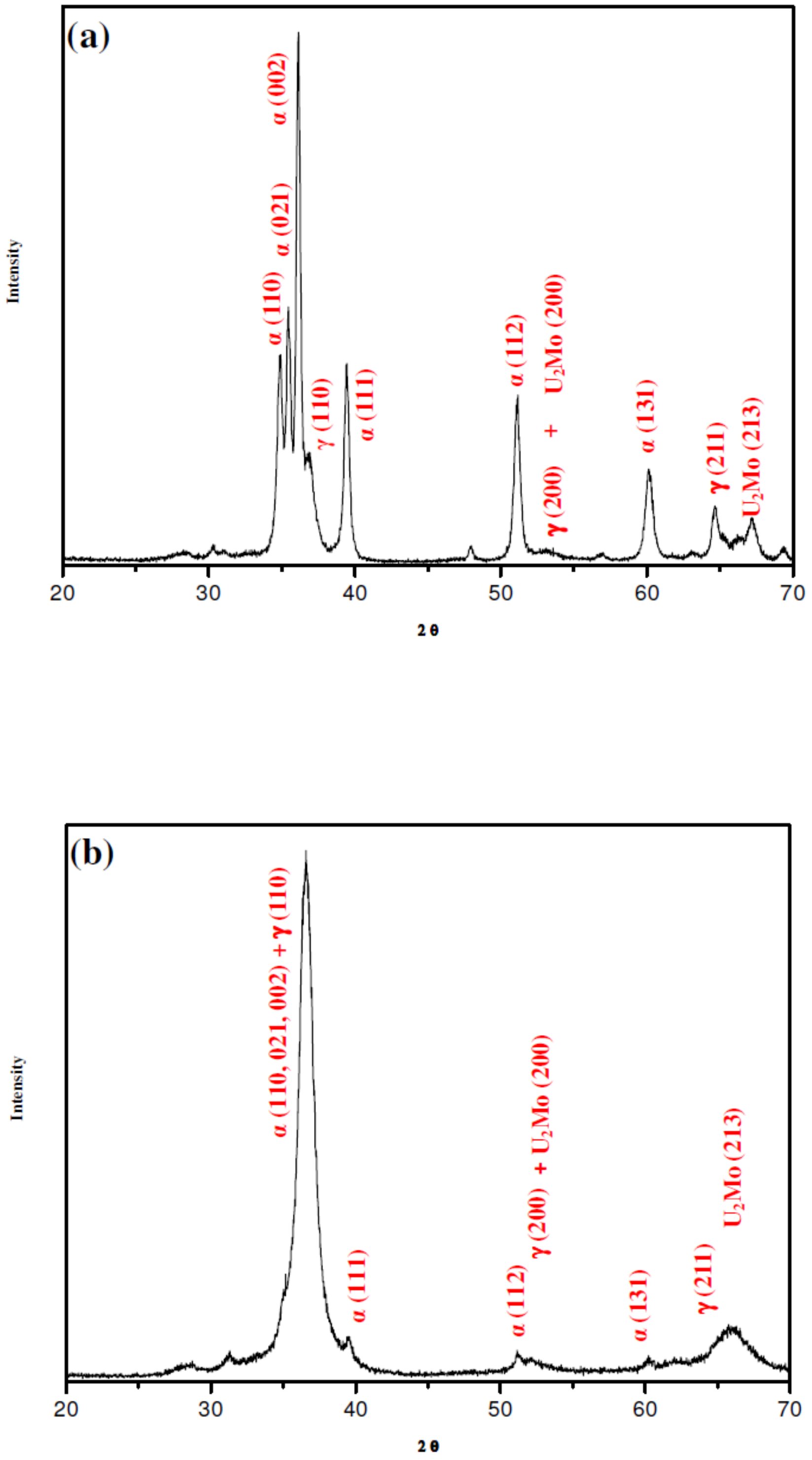
(a)
Intensity
α (002)
α (021)
α (110)
γ (110)
α (111)
α (112)
γ (200) + U₂Mo (200)
α (131)
γ (211)
U₂Mo (213)
20
30
40
50
60
70
2θ
(b)
Intensity
α (110, 021, 002) + γ (110)
α (111)
α (112)
γ (200) + U₂Mo (200)
α (131)
γ (211)
U₂Mo (213)
20
30
40
50
60
70
2θ

Fig. 4.10 (a) & (b).

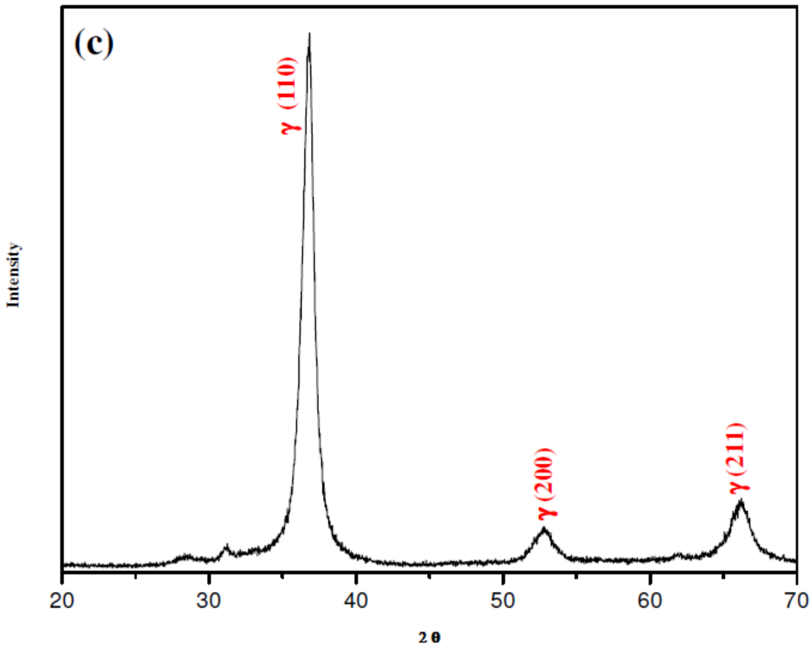
(c)
γ (110)
γ (200)
γ (211)
Intensity
20
30
40
50
60
70
2θ

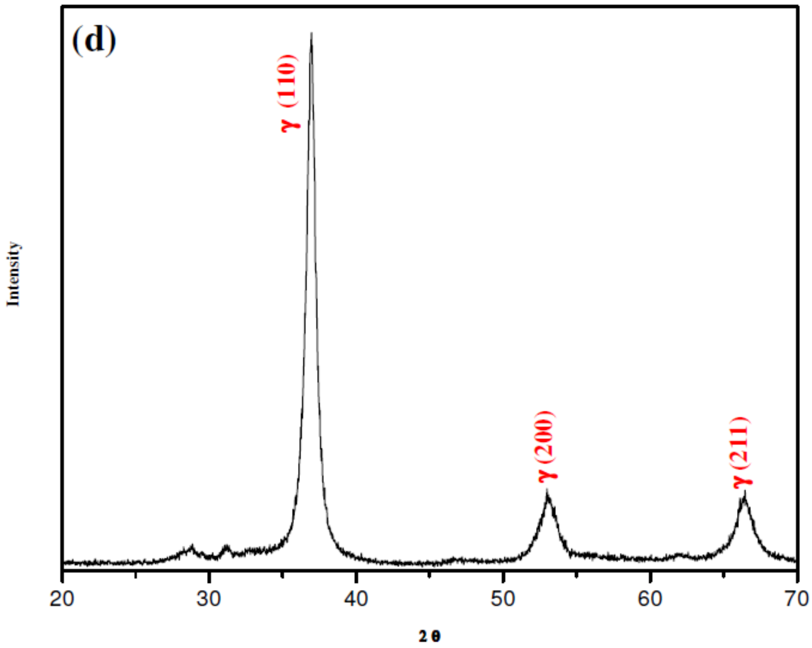
(d)
γ (110)
γ (200)
γ (211)
Intensity
20
30
40
50
60
70
2θ

Fig. 4.10 (c) & (d).

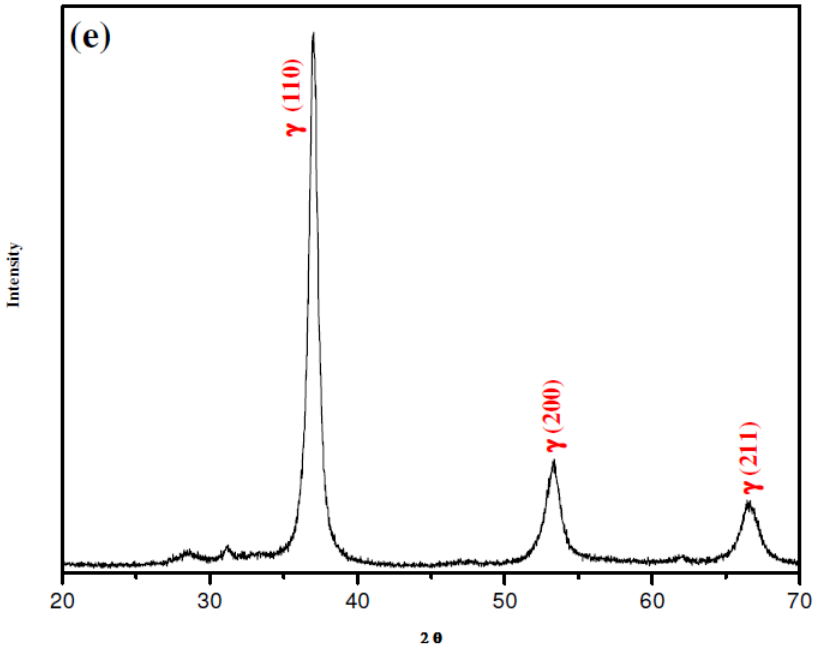
(e)
γ (110)
γ (200)
γ (211)
Intensity
20
30
40
50
60
70
2θ

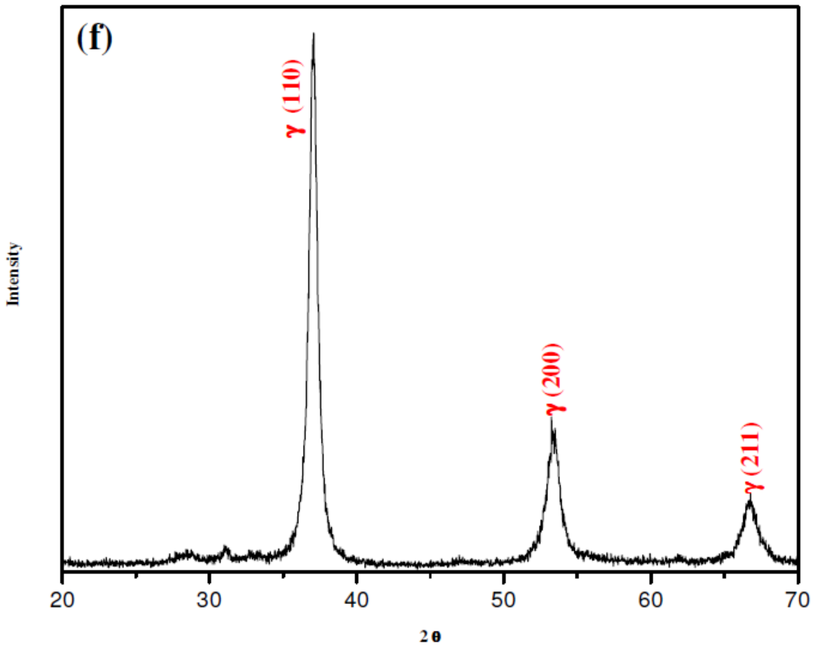
(f)
γ (110)
γ (200)
γ (211)
Intensity
20
30
40
50
60
70
2θ

Fig. 4.10 (e) & (f).

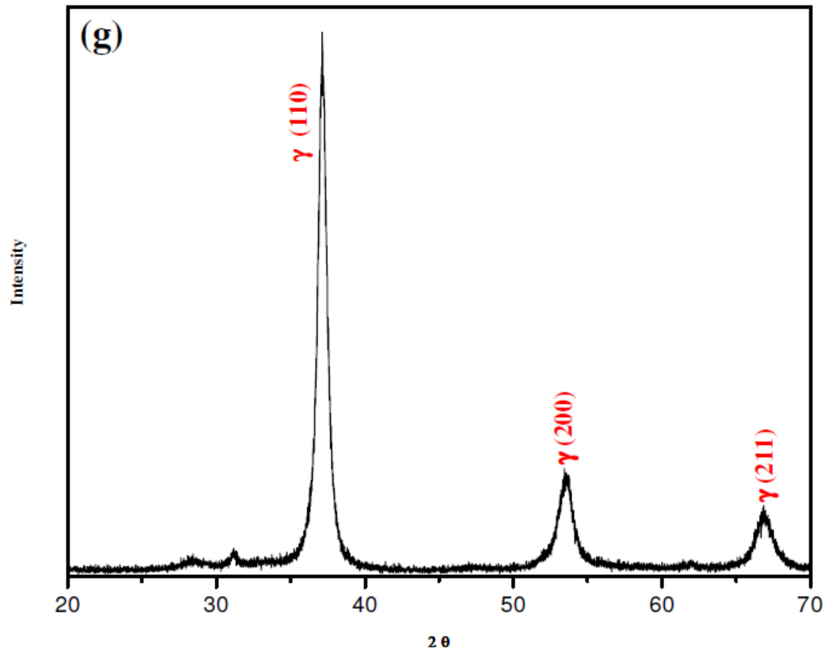

Fig. 4.10 X-ray diffraction patterns of as cast (a) U-2wt%Mo alloy, (b) U-5wt%Mo alloy, (c) U-6wt%Mo alloy, (d) U-7wt%Mo alloy, (e) U-8wt%Mo alloy, (f) U-9wt%Mo alloy and (g) U-10wt%Mo alloy.

4.3.2 Precise lattice parameter calculation

XRD patterns as shown in the previous section, showed different phases present in alloys samples. The intended γ-phase is a substitutional solid solution of Mo in bcc-Uranium. Also, there is small, limited solid solubility of Mo in α-phase. Therefore, in order to ascertain solubility of Mo in the alloys, lattice parameters of both the solid solutions were calculated using the XRD patterns. For this purpose, a computer program 'CELREF' was used to calculate precise lattice parameter of cubic γ-uranium unit cell for different *U-Mo alloys*. The program code uses method of least squares to determine the cell parameters [174]. The points were fitted using sigmoidal curve with the assumption that the curve may be described quantitatively by the three parameter sigmoid function (eq. 4.1), here $X_{1/2}$ is the point of inflection and k is a slope factor *(i.e. the change in X corresponding to the most significant change in Y values).*

$$Y = 10 + 8/(1 + \exp^{\frac{(1+e^{(X-\sqrt{X})})}{k}}) \tag{4.1}$$

The precise lattice parameters thus calculated using this programme, were plotted against molybdenum weight percent for different *U-Mo alloys (Fig 4.11).* The lattice parameters of orthorhombic α-uranium were also calculated for *U-2wt%Mo* and *U-5wt%Mo alloys (as shown in Table 4.2).* The same could not be calculated for higher Mo-compositions because the (hkl) values of α-uranium peaks were not distinctly visible. The lattice parameter of α-uranium in both *U-2wt%Mo* and *U-5wt%Mo alloys* did not show any appreciable change. This is perhaps due to the fact that the maximum solid solubility of molybdenum in uranium is very small, ~1 at% at room temperature under equilibrium conditions. On the other hand, shift in lattice parameter of cubic γ-uranium was quite appreciable as shown in *Fig. 4.12* and tabulated in *Table 4.3*. The decrease in lattice parameter of γ-phase with increasing Mo content is attributed to the differences in the atomic radii of Mo (145 pm) and U (175pm) [175].

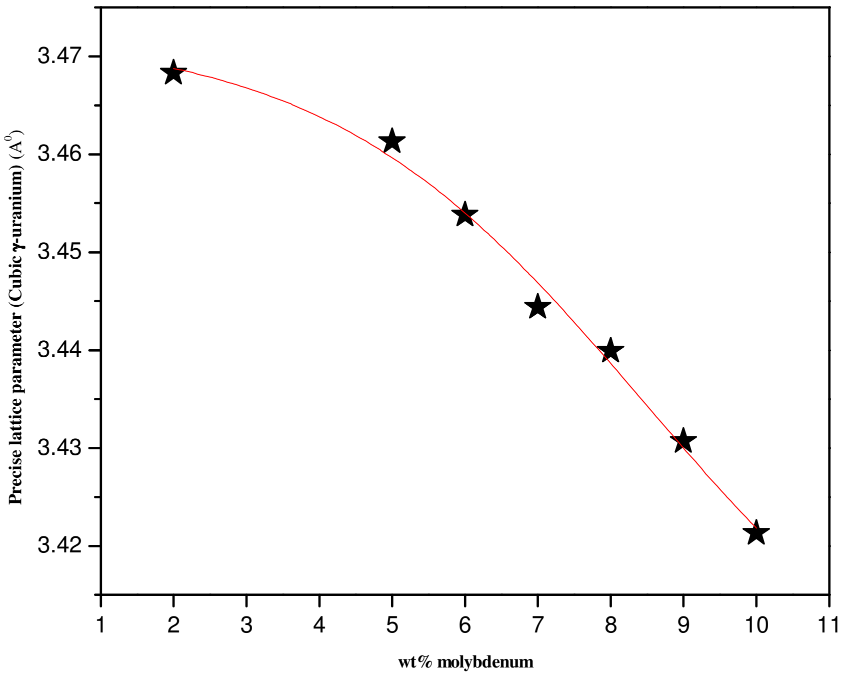

Fig. 4.11 Plot showing change in precise lattice parameter of cubic γ-uranium with varying amount of molybdenum.

Composition of alloy	***Precise lattice parameter of α-phase (A°)***			***Lattice volume (A^3)***
	a	*b*	*c*	
Unalloyed α-uranium at RT	2.8540	5.8700	4.9550	83.0110
U-2wt% Mo	2.8603	5.8729	4.9560	83.2434
U-5wt% Mo	2.8632	5.8741	4.9582	83.3906

Table 4.2 Precise lattice parameter and lattice volume of orthorhombic α-uranium in U-Mo alloys.

Composition of alloy	Precise lattice parameter of γ-uranium (A°)	Lattice volume (A^3)
Unalloyed γ-uranium at RT	3.4740	41.93
U-2wt% Mo	3.4683	41.72
U-5wt% Mo	3.4613	41.74
U-6wt% Mo	3.4538	41.20
U-7wt% Mo	3.4444	40.86
U-8wt% Mo	3.4399	40.70
U-9wt% Mo	3.4307	40.38
U-10wt% Mo	3.4213	40.05

Table 4.3 Precise lattice parameter and lattice volume of cubic γ-phase in U-Mo alloys.

4.3.3 Microstructural analysis

The microstructures of as cast *U-2wt%Mo alloy, as shown in Fig 4.13(a & b)* shows cellular decomposition and widmanstatten pattern all along the prior gamma grain boundary. During alloy cooling a part of γ-uranium had undergone eutectoid decomposition to form α-uranium and U_2Mo intermetallic which is clearly visible as the lamellar region in the microstructure while some regions in the microstructure, where diffusion has not taken place efficiently can be visualize as woven basket region *(i.e. widmanstatten pattern)*. In *U-5wt%Mo alloy* the microstructure *(as shown in Fig 4.14(a & b))* shows bright region as equiaxed γ-grains with dark gray patches as second phase, which is identified as a mixture of α-uranium and U_2Mo intermetallic. During cooling, a part of γ-phase was found to be retained while the rest had undergone eutectoid decomposition to form α-uranium and U_2Mo intermetallic phases.

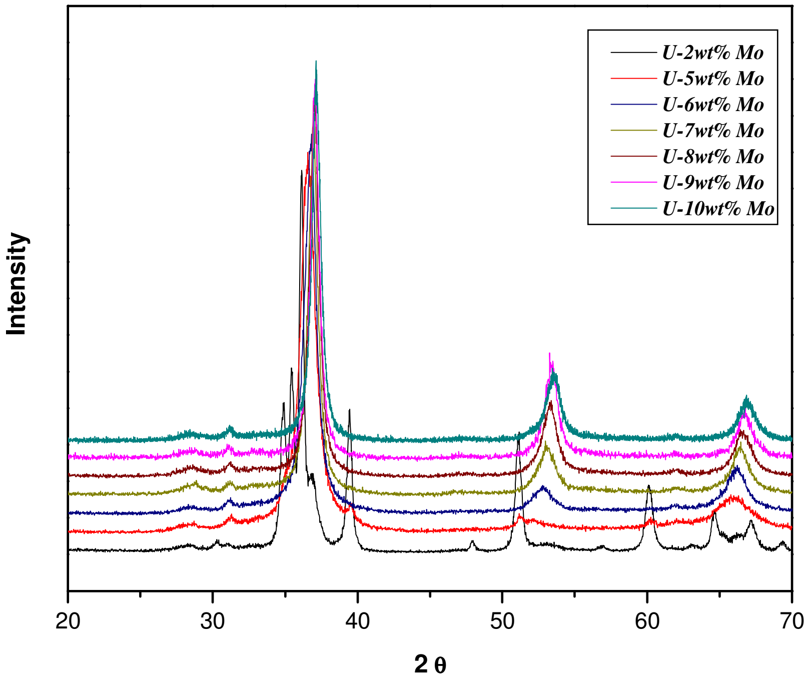

Fig. 4.12 Superimposed X-ray diffraction pattern of as cast U-Mo alloys with different molybdenum percentage (i.e. 2, 5, 6, 7, 8, 9, 10 wt% molybdenum).

Increasing Mo-content shows increase in retained fraction of γ-phase, as seen in the microstructure of U-6wt%Mo *(as shown in Fig. 4.15)* and U-7wt%Mo alloys *(as shown in Fig 4.16)*. It is interesting to note that though the XRD patterns of the alloy compositions where Mo-content was higher than 6wt% did not reveal presence of equilibrium phases, as discussion in section 4.3.1, optical microscopy provided evidence of their presence in the furnace cooled microstructures. It is also observed from the microstructures that the second phase occurs along the grain-boundaries of retained γ-phase. In the light of established fact that grain boundaries of the parent phase provide preferential sites for the transformation of phases, microstructural examination indicates fairly strong metastability, which may be due to small values of difference in their free energies, or sluggish kinetics of eutectoid decomposition or both. This observation also opens up another possibility that, if, grain boundaries of γ-phase of U-Mo could be engineered, so as to make them energetically less favorable for precipitation of equilibrium phases, lesser amount of Mo may be required to metastabilize the γ-phase. Unlike lower Mo-alloys as discussed above, microstructures of U-8wt%Mo, U-9wt%Mo and U-10wt%Mo alloys, as shown in *Fig. 4.17, Fig. 4.18* and *Fig. 4.19*, respectively have shown only equiaxed grains of γ-phase without any other phase. It is also important to point out that the features appear at the grain boundary and also inside the grains in the microstructures *(Fig. 4.17 to Fig. 4.19)* as second phase are the artifacts created during sample preparation. It may be noted that the corrosion resistance of alloys increase with increase in the Mo-content, which is beneficial from the applications point of view. However, the same attribute becomes difficult to reveal microstructures, because usual etchants lose their potency to reveal grain boundaries. Therefore, the alloys with Mo-content ≥8wt% were etched by electro-etching to reveal microstructures, which also resulted in some artifacts.

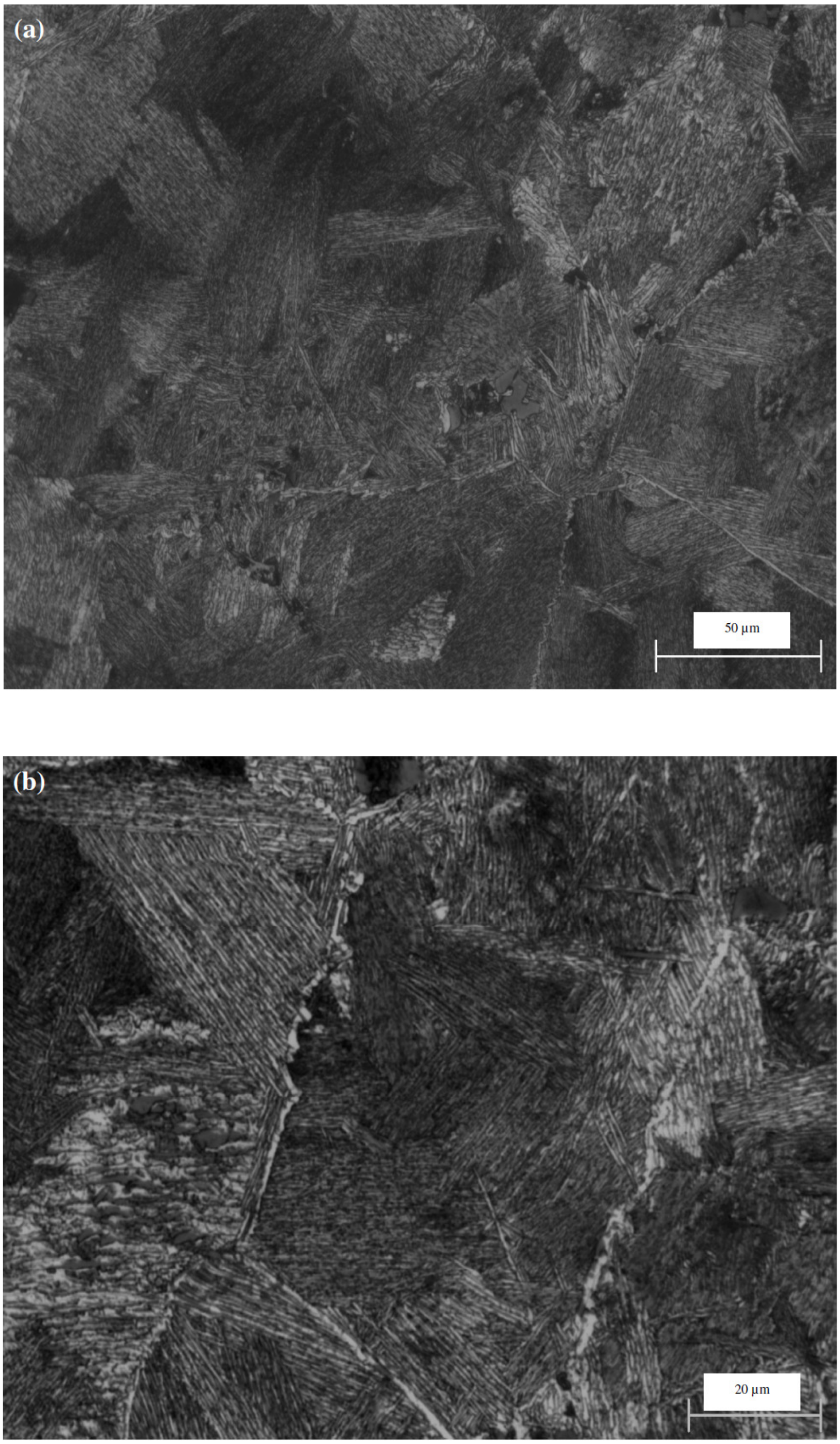

Fig. 4.13 Microstructures of as cast (a & b) U-2wt%Mo alloy.

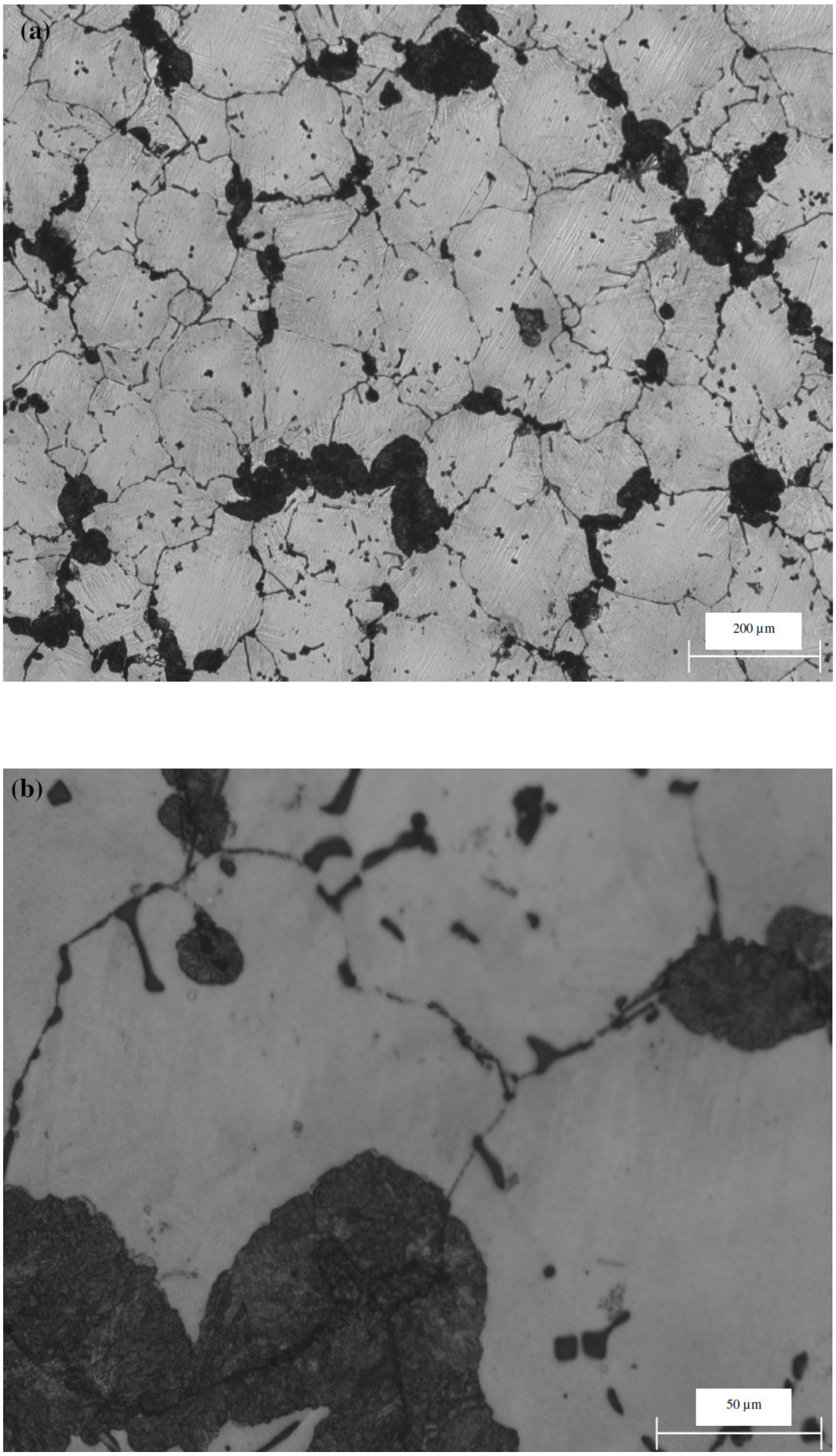

Fig. 4.14 Microstructures of as cast (a & b) U-5wt%Mo alloy.

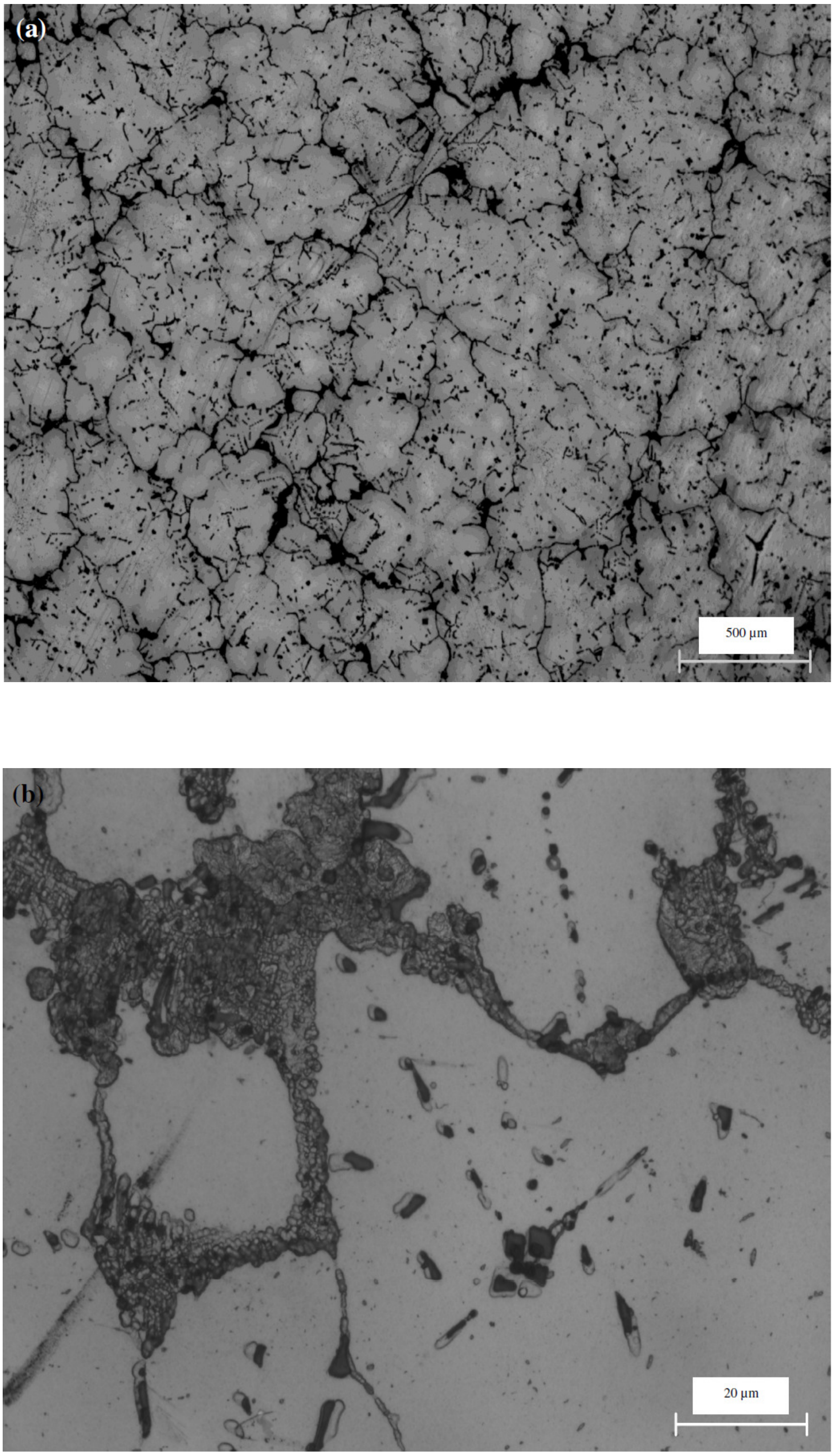

Fig. 4.15 Microstructures of as cast (a & b) U-6wt%Mo alloy.

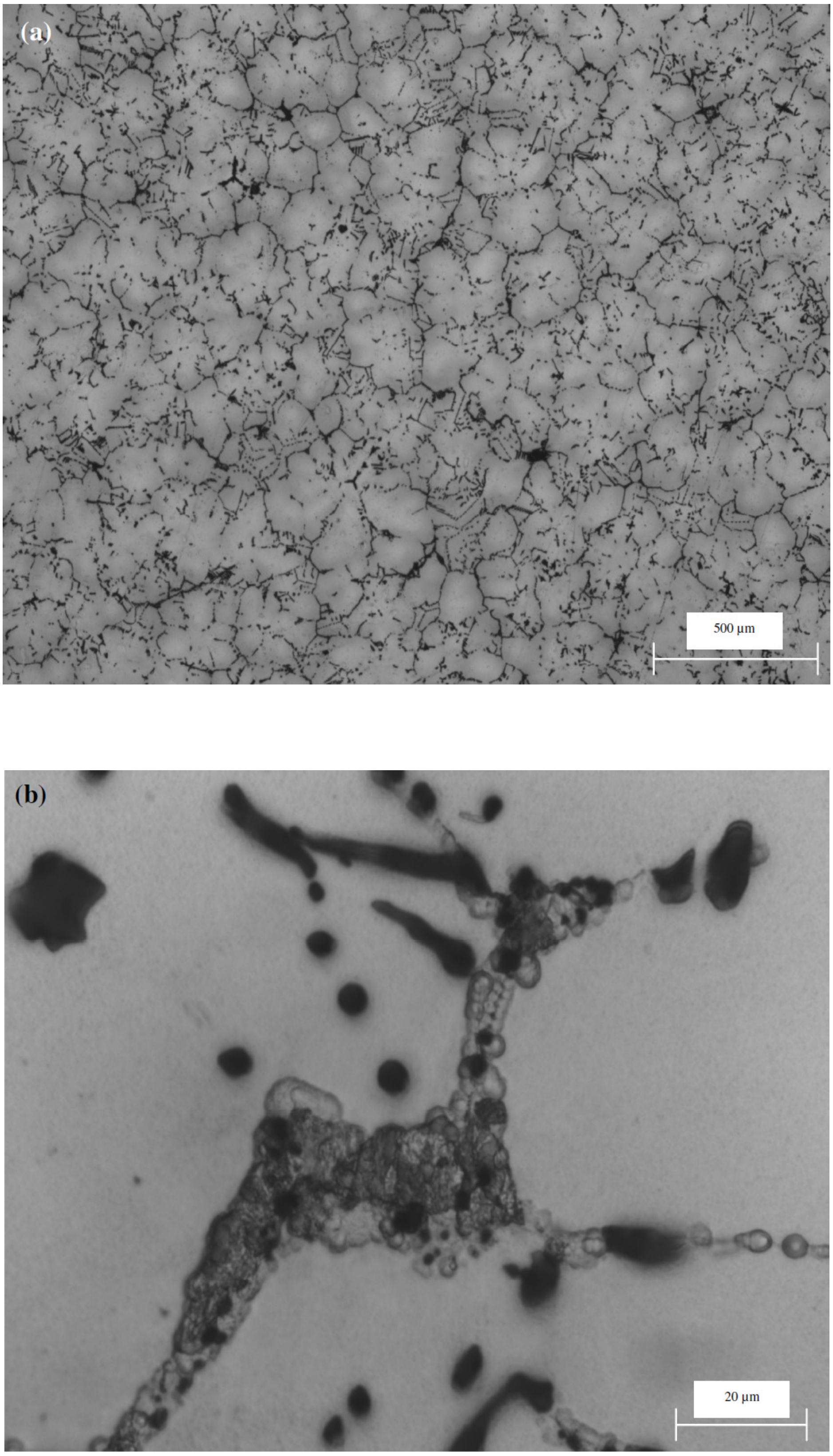

Fig. 4.16 Microstructures of as cast (a & b) U-7wt%Mo alloy.

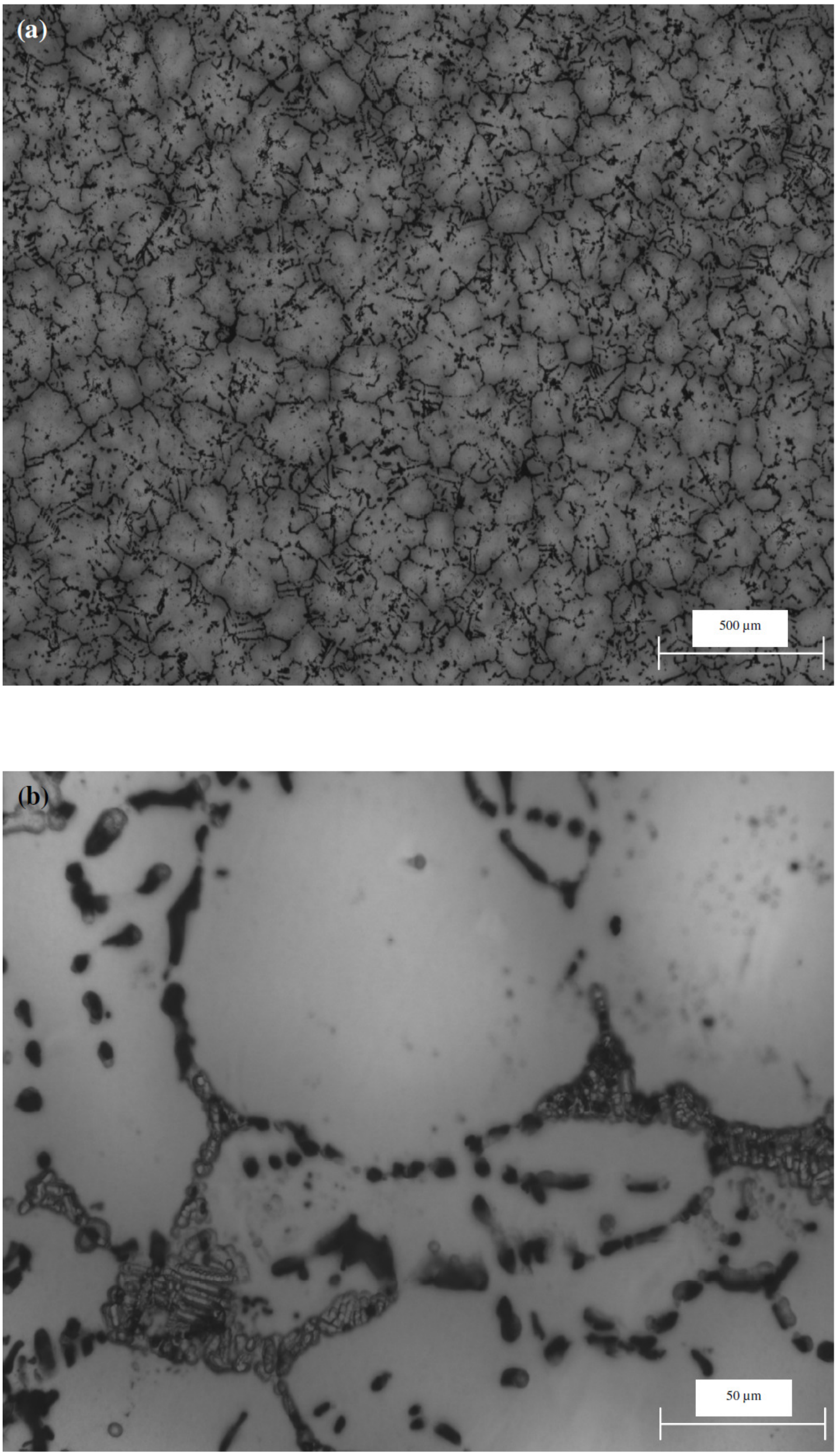

Fig. 4.17 Microstructures of as cast (a & b) U-8wt%Mo alloy.

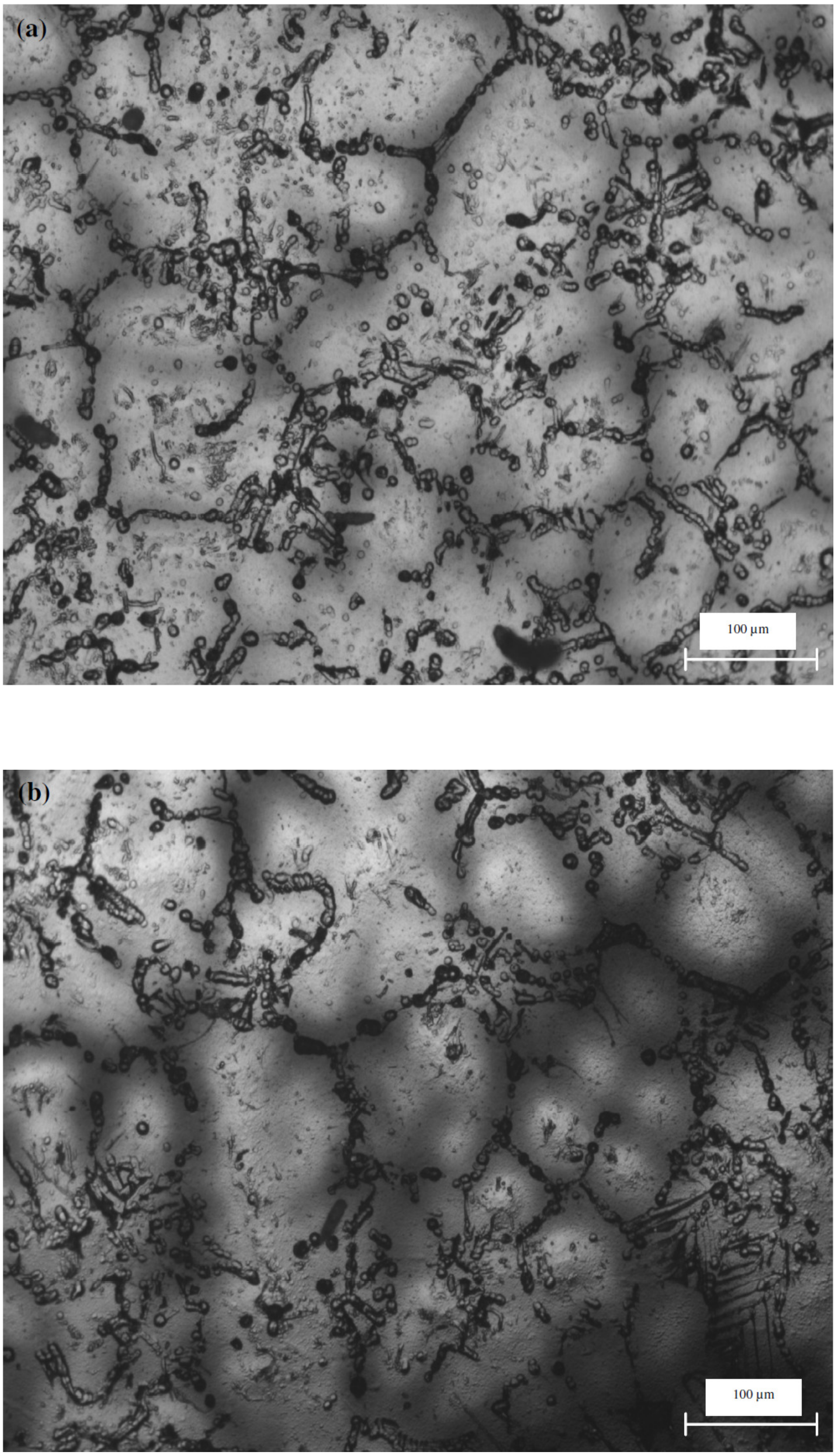

Fig. 4.18 Microstructures of as cast (a & b) U-9wt%Mo alloy.

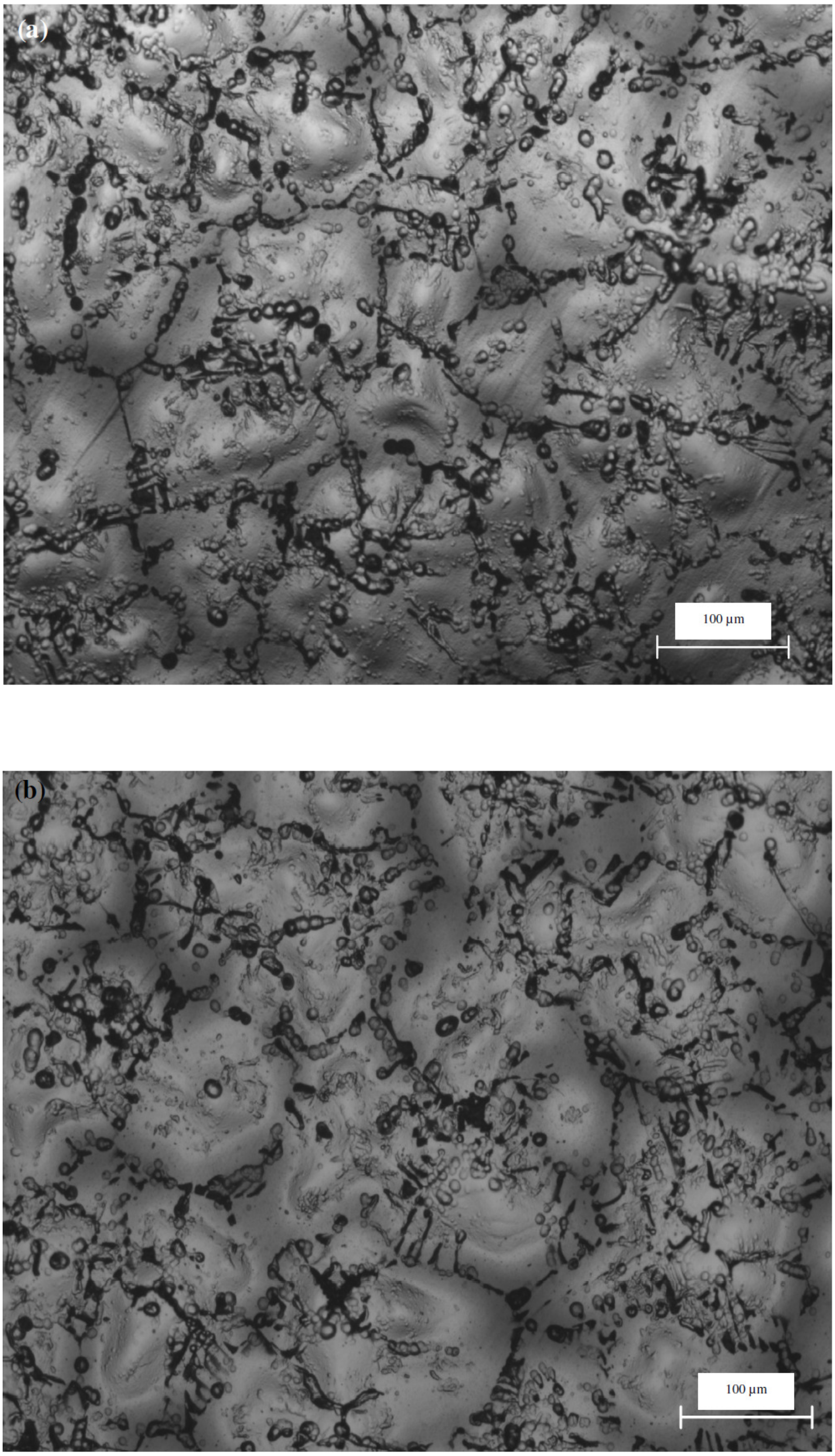

Fig. 4.19 Microstructures of as cast (a & b) U-10wt%Mo alloy.

Based on the basis of the microstructural examination it may be safely concluded that γ-phase can be completely retained at room temperature during furnace cooling, with the minimum 8wt% molybdenum addition in uranium [176]. A quantitative image-analysis of the microstructures discussed in this section is described in the proceeding section.

4.3.4 Image analysis

The quantitative image analysis was carried out using Metal work station programme *(as described under the section 3.4.4.1 in this dissertation)* to determine the quantity of different phases in *U-Mo alloy* ingot samples. The metal work station programme is based on the method described as per ASTM E562 standard for quantitative phase analysis. In the image analysis, the α-uranium and U_2Mo intermetallic phase mixture was considered as one phase (since α-uranium and U_2Mo intermetallic was formed due to the eutectoid reaction and they are present in the microstructure as either lamellar decomposed product or widmanstatten pattern) and γ-uranium as second phase. Image analysis was carried out by averaging fifteen results at different sections of microstructures for each *U-Mo alloy* compositions. The phase analysis result of γ-uranium was then plotted against molybdenum weight percentage for different *U-Mo alloy* compositions and is shown in *Fig 4.20.* The results clearly indicate that with minimum 8wt% molybdenum addition in uranium complete cubic γ-phase can be retained at room temperature under normal furnace cooling condition. Sigmoidal model was used to fit the points with the assumption that the curve may be described quantitatively by the three parameter sigmoid function (4.2), here $X_{1/2}$ is the point of inflection and k is a slope factor (i.e. the change in X corresponding to the most significant change in Y values).

$$Y = 10 + 8/(1 + \exp^{\frac{(1+e^{(X-\sqrt{X})})}{k}}) \tag{4.2}$$

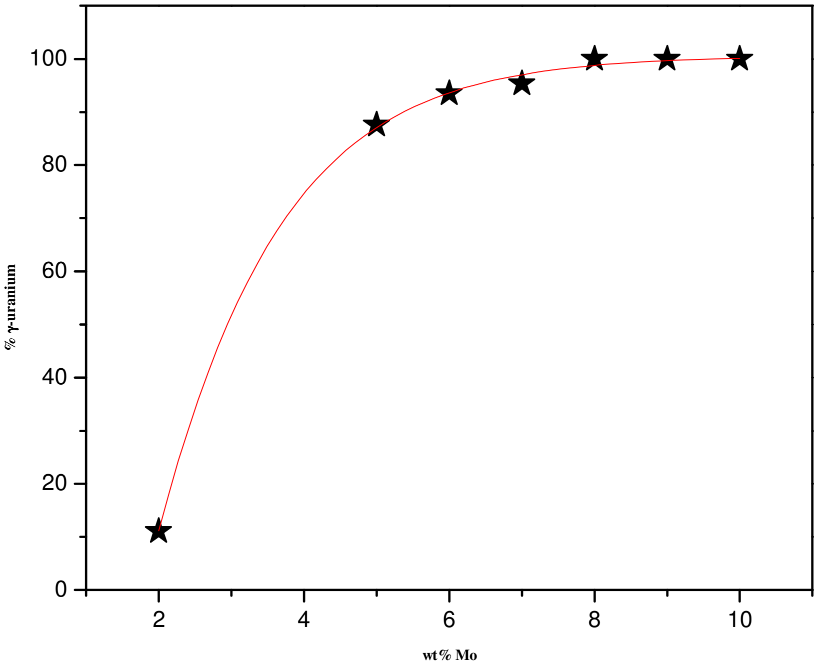

Fig. 4.20 Quantitative analysis (in vol%) of cubic γ-phase for different molybdenum percentage in U-Mo alloys.

In addition, the microstructures of *U-Mo alloy* with different molybdenum concentration in as cast and as rolled conditions were also characterized to determine the grain size by using *Lieca Metallographic Work Station* as described in *Section 3.4.4.2*. The results are shown in *Table 4.4.* The grain-sizes of different alloys are within a narrow range (std. deviation <10%), and do not follow any particular trend. Since the alloys are subjected to similar temperature regimes during processing, occurrence of nearly similar grain structure is not unexpected. Further, rolling of alloys at 900° C was not found to significantly affect the grain sizes.

Composition of alloy	***Grain Size (μm) in as cast and as rolled condition***	
	As cast alloy	***As rolled alloy***
U-2wt%Mo	186.7	-
U-5wt%Mo	194.2	-
U-6wt%Mo	204.4	-
U-7wt%Mo	193.0	-
U-8wt%Mo	196.2	135.2
U-9wt%Mo	188.0	128.8
U-10wt%Mo	194.5	136.1

Table 4.4 Grain size for different compositions of U-Mo alloys (calculated as per ASTM 1382 intercept method).

4.4 Study on phase transformation of U-Mo alloys

It was observed from the previous section *(i.e. section 4.3.4)* that in case of uranium molybdenum alloys, retention of cubic γ-phase is possible at room temperature with minimum 8 wt% molybdenum addition into uranium under furnace cooling conditions. However, it is extremely important to examine the metastability of this retained cubic phase at higher temperatures to establish out of pile fuel performance characteristics. U-Mo phase diagram *(Fig. 2.5)* shows that the cubic phase is stable above 560 °C but as the temperature falls below, it will be transformed into equilibrium phases, i.e. orthorhombic α-phase and body centered tetragonal intermetallic compound U_2Mo. The study of *U-Mo alloys,* particularly the eutectoid decomposition becomes more important because, as mentioned earlier in chapter-2, orthorhombic α-phase of uranium has very little solid solubility for molybdenum and it doesn't have good irradiation property. During operation of the nuclear reactor, more the amount of transformed α-phase in the fuel, more will be the probability of failure. Therefore, retention of cubic phase in U-Mo alloys was investigated in this study. In this context, *U-Mo alloys* with 8, 9 and 10 wt% Mo composition were selected. The reason for selecting these three compositions can be answered from the results of previous section, where it was concluded that minimum 8 wt% molybdenum addition into uranium under furnace cooling conditions would metastabilize cubic phase at room temperature. Hence, the heat treated *U-Mo alloys* (8, 9 and 10 wt% Mo composition) were studied for phase identification by XRD, lattice parameter calculation and microstructural investigation. The results obtained from each investigation are discussed one after another in the proceeding sections.

4.4.1 Phase analysis

The alloys samples employed for phase transformation study were prepared by induction melting technique as described in *section 3.2.3*. These as cast samples were first hot rolled at 900 °C, to eliminate cast structure. The hot rolling regime for these alloy samples was scheduled carefully and was kept well above the α and β phase field of *U-Mo alloy* phase diagram, so as to avoid cracking and operation difficulty during hot working. It is well understood that α phase of uranium is very brittle and the thermal stability of β phase is extremely narrow [71]. However, the γ-phase has good thermal stability and ductility for the working [47], therefore, the alloys were hot rolled in γ-phase region. The alloy samples were carefully jacketed in copper tube and the rolling conditions/cycles were controlled to eliminate any possibility of crack in the jacket. Therefore, hot rolling was done taking necessary precautions as mentioned in chapter-3, so that oxidation of uranium could be avoided completely. It is to be noted that uranium has high affinity for oxygen and at 900 °C it may oxidize completely and may lead to metal fire [177].

Therefore, the hot rolled alloy samples were characterized for phase by XRD to evaluate if any other minor second phase formation took place in the process. The XRD pattern of as cast and hot rolled *U-Mo alloys* with 8, 9 and 10 wt% Mo compositions are shown in *Fig. 4.21*. All the peaks in the XRD pattern shown in *Fig. 4.21* could be indexed to the γ-phase, and no significant change of hot-rolled xrd patterns was observed with those of as-cast patterns. It may therefore be surmised that the hot rolling process did not give rise to any other second phase viz. oxide and/or equilibrium phase product within the detectable range of instrument. It also suggests no oxygen pickup in the process. The hot rolled alloy samples of 8, 9 and 10wt% Mo compositions were sealed in quartz tube under partial pressure of helium as described in section 3.3.2. The sealing of *U-Mo alloy* samples in quartz tube was carried out under inert atmosphere. These samples were heat treated at 500 °C, to ensure eutectoid decomposition. It can be observed from *U-Mo phase* diagram that for 8, 9 and 10wt% Mo compositions, the eutectoid transition temperature is 560 °C. Therefore, to favor the kinetics of reaction and also to ensure transformation the temperature was selected at 500 °C. The heating duration of 68 hours and 240 hours were selected purely to facilitate operational convenience. The XRD patterns of 8, 9 and 10wt% Mo alloys after 68 hours and 240 hours of heat treatment are shown in *Fig. 4.22* and *Fig. 4.23* respectively.

The XRD patterns shown in *Fig. 4.22* and *Fig. 4.23* clearly indicate mixture of phases in the heat treated alloy samples. These phases could be identified and indexed as retained cubic γ-phase and equilibrium phase mixture of α and U_2Mo intermetallic. The presence of α-phase and U_2Mo intermetallic in heat treated *U-Mo alloys* is in agreement with the phase diagram. However, presence of γ-phase in the heat treated alloys indicate that phase transformation *(i.e.* $\gamma \leftrightarrow \alpha + U_2Mo$*)* has not accomplished completely even after relatively long heating duration (240 hours). This result is important to predict the end of life for fuel on completely thermal point of view, which invariably means the fuel performance in zero reactor power and at 500 °C fuel operating temperature. A detail discussion on this aspect is presented in section 4.4.4.

The XRD profile on *Fig. 4.22* and *Fig. 4.23* also indicate that the amount of retained cubic γ-phase is strongly dependent upon duration and molybdenum concentration in uranium. A further quantitative investigation on retained γ-phase and transformed equilibrium phases (α and U_2Mo) was done using the computer program 'POWDER CELL'. The program uses integrated intensity method to evaluate relative phase percentage of α, γ and U_2Mo phase. In this method, the program generates the theoretical profile of expected phases based upon their lattice details, space groups and Wyckoff notations. The theoretical profiles of different expected phases are then matched with the powder diffraction patterns of alloys, to evaluate their relative phase percentages. The volume percentage of all the three phases, calculated by the method described above is tabulated in *Table 4.5*. It can be observed from *Table 4.5* that U_2Mo phase percentage increases slowly if compared with α-phase for long heat treatment duration. This may be attributed to the lower intrinsic diffusion coefficient of molybdenum if compared with uranium [73]. A similar effect is shown by bar chart for retained γ-phase *(Fig. 4.24).* It is well understood that α-phase has very limited solid solubility for molybdenum therefore, longer duration for transforming higher volume percentage of α-phase is understandable.

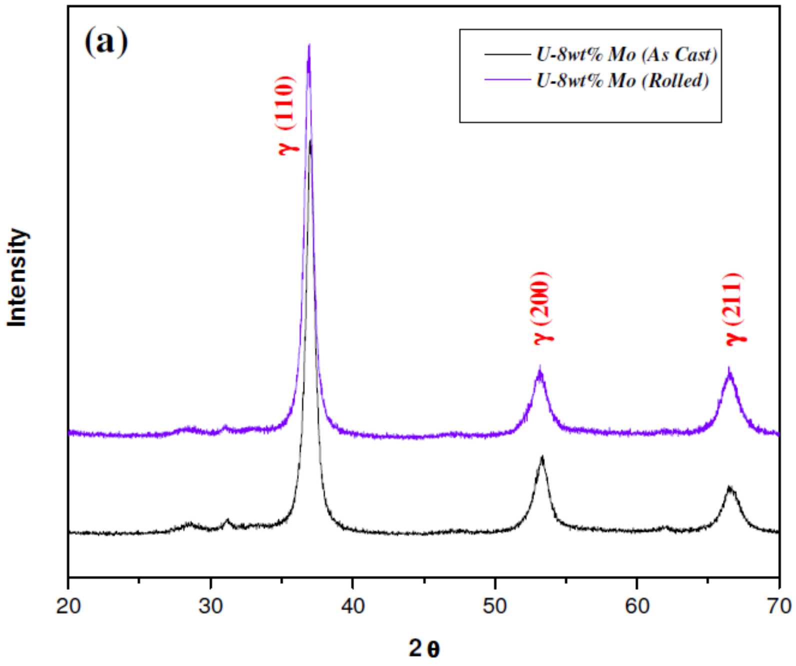
(a)
U-8wt% Mo (As Cast)
U-8wt% Mo (Rolled)
γ (110)
γ (200)
γ (211)
Intensity
20
30
40
50
60
70
2 θ

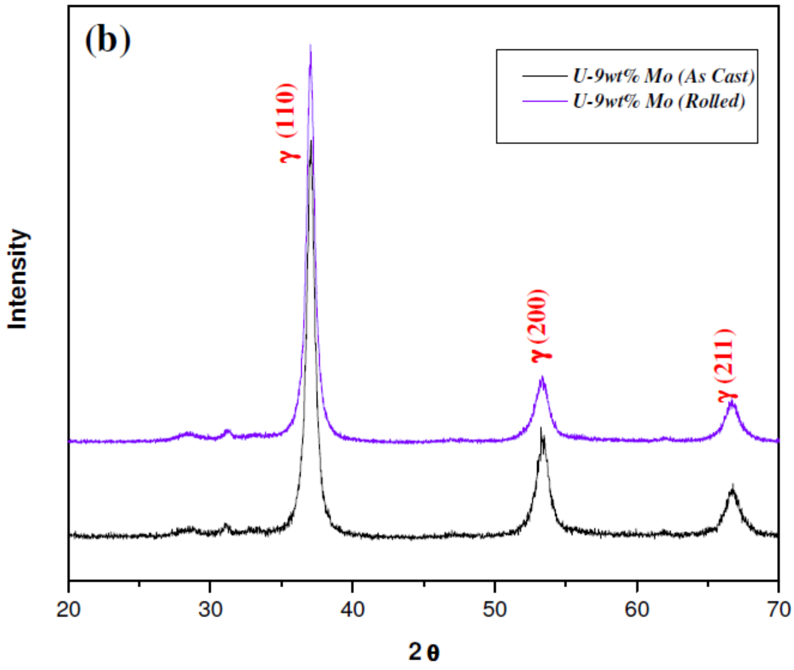
(b)
U-9wt% Mo (As Cast)
U-9wt% Mo (Rolled)
γ (110)
γ (200)
γ (211)
Intensity
20
30
40
50
60
70
2 θ

Fig. 4.21 (a) & (b).

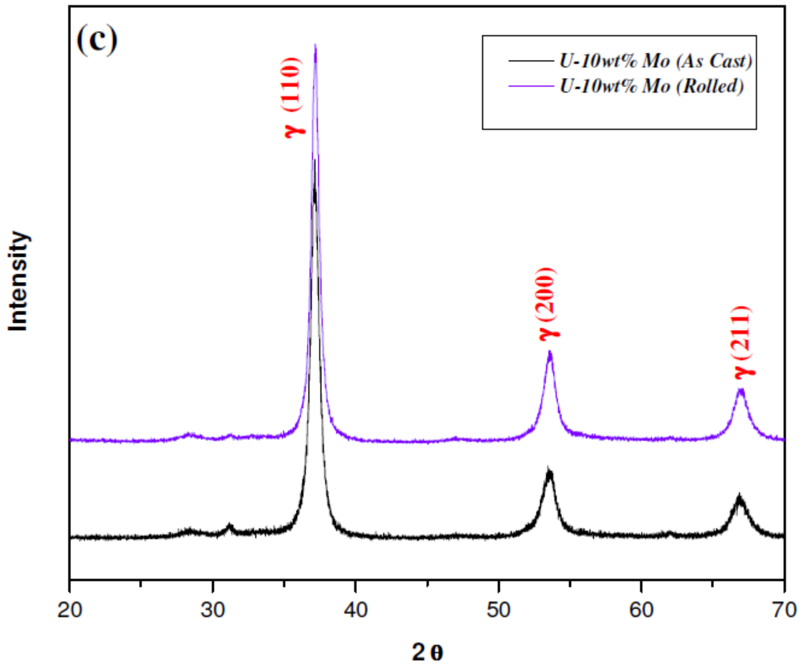

Fig. 4.21 X-ray diffraction patterns of as cast and hot rolled alloys (a) U-8wt%Mo, (b) U-9wt%Mo and (c) U-10wt%Mo.

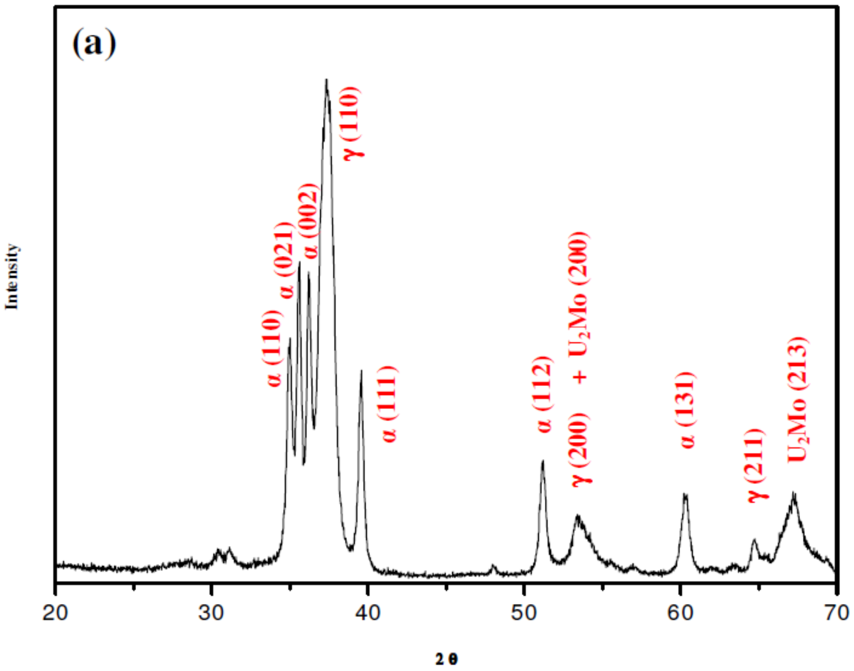

Fig. 4.22 (a).

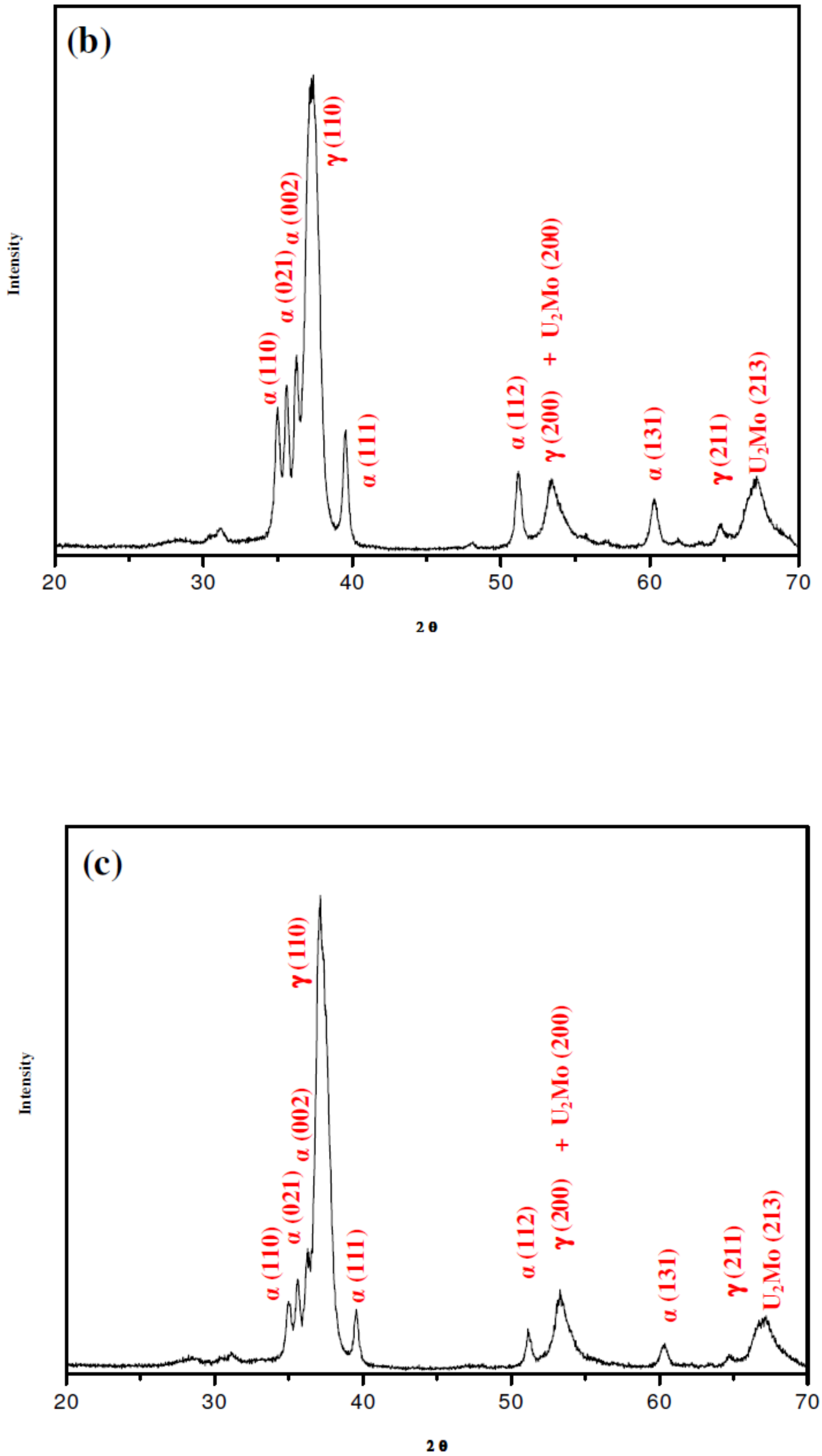

Fig. 4.22 X-ray diffraction patterns of heat treated U-Mo alloy at 500^{0}C for 68 hrs (a) U-8wt%Mo, (b) U-9wt%Mo, (c) U-10wt%Mo.

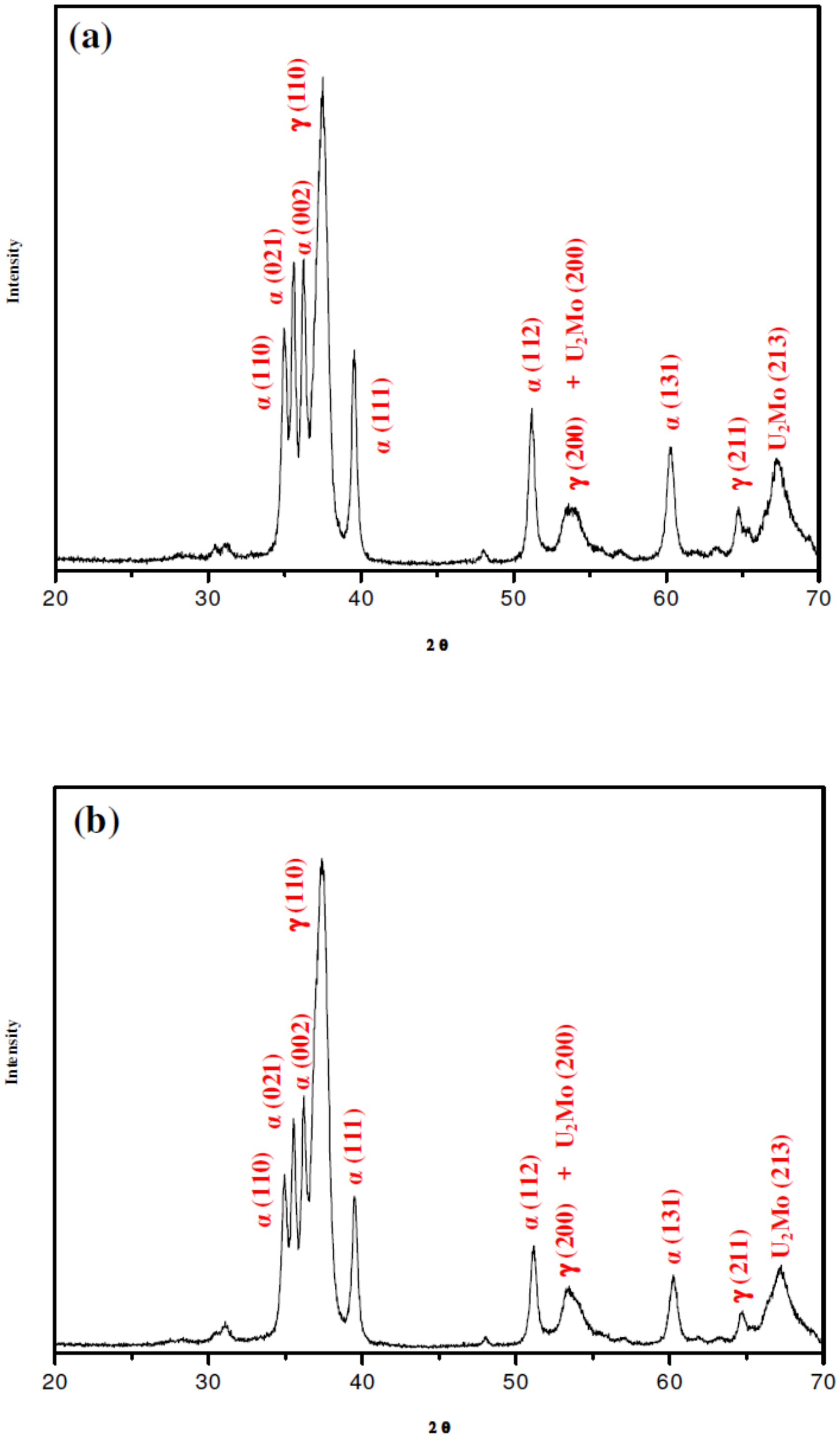
(a)
Intensity
α (110)
α (021)
α (002)
γ (110)
α (111)
α (112)
γ (200) + U₂Mo (200)
α (131)
γ (211)
U₂Mo (213)
20
30
40
50
60
70
2θ
(b)
Intensity
α (110)
α (021)
α (002)
γ (110)
α (111)
α (112)
γ (200) + U₂Mo (200)
α (131)
γ (211)
U₂Mo (213)
20
30
40
50
60
70
2θ

Fig. 4.23 (a) & (b).

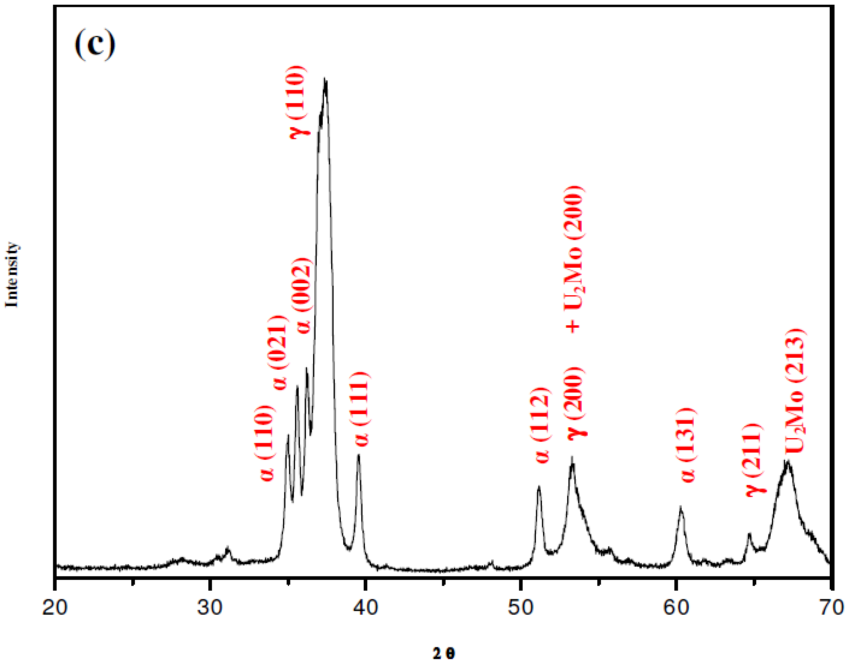

Fig. 4.23 X-ray diffractions pattern of heat treated U-Mo alloy at 500^{0}C for 240 hrs (a) U-8wt%Mo, (b) U-9wt%Mo, (c) U-10wt%Mo.

Alloy Composition	*Volume percent phase after 68 hours of heat treatment*			*Volume percent phase after 240 hours of heat treatment*		
	α	*U_2Mo*	*γ*	*α*	*U_2Mo*	*γ*
U-8wt% Mo	24.26	47.13	28.61	33.35	50.17	16.48
U-9wt% Mo	16.06	48.65	35.29	24.90	54.74	20.36
U-10wt% Mo	3.72	51.88	44.41	15.17	59.72	25.11

Table 4.5 Volume percentage of phases in U-Mo alloys after different heat treatment history (calculated by POWDER CELL method).

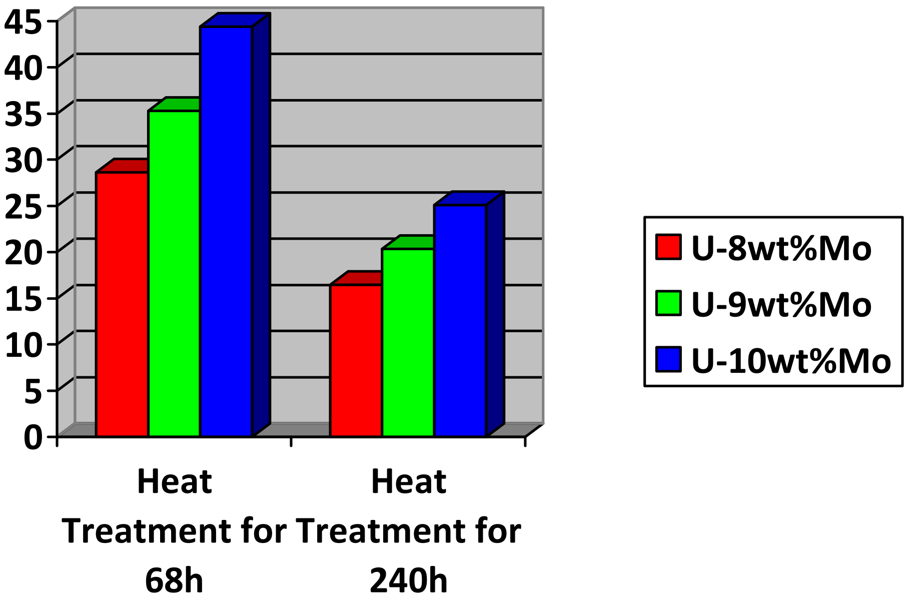

Fig. 4.24 Bar chart showing volume percentage of retained γ-phase after different heat treatment for 8, 9 & 10wt% Mo alloys.

4.4.2 Precise lattice parameter calculation

Precise lattice parameter was calculated at every stage during phase transformation study to corroborate the discussion in section 4.4.1. As stated earlier in section 4.3.2, a computer program 'CELREF' was used to calculate precise lattice parameters of both hot rolled and heat treated *U-Mo alloys.* Therefore, the lattice parameters of alloy samples (8, 9 and 10wt% Mo) after hot working were calculated and shown in *Table 4.6.* It could be ascertained after comparing the data from *Table 4.6* and *Table 4.3*, that precise lattice parameter of γ-phase for *U-Mo alloys* after hot rolling does not show any appreciable difference with the as-cast alloys. This reiterates that hot working of *U-Mo* alloys was accomplished effectively without any residual strain and precipitation of second phases.

Alloy Composition	*Precise lattice parameter of γ-uranium (A°)*	*Lattice volume (A^3)*
Unalloyed γ-uranium	3.4740	41.9266
Rolled U-8wt%Mo	3.4432	40.8213
Rolled U-9wt%Mo	3.4308	40.3818
Rolled U-10wt%Mo	3.4141	39.7950

Table 4.6 Precise lattice parameter and lattice volume of cubic γ-uranium in hot rolled U-Mo alloys.

Similarly the lattice parameters for α-phase of heat treated *U-Mo alloys* (8, 9 and 10wt% Mo) compositions were calculated and shown in *Table 4.7.* It can be observed from the table that α-phase lattice does not undergo any change even after heat treatment, which is understood from the fact that α-phase has very restricted solid solubility for molybdenum ~1at%. These results could also be used to explain the increase in α-phase volume percent after long heat treatment duration and higher molybdenum concentration as shown in *Table 4.5.* The lattice parameter of cubic phase in heat treated alloys could not be calculated with accuracy because the solid solution of γ-phase in these alloy samples was expected to be inhomogeneous and therefore selection of 2θ for γ-phase (hkl) was difficult. However, an assumption for average 2θ value in the calculation did not show any major difference in the lattice parameter of γ-phase. Similarly, the lattice parameter of U_2Mo was not attempted because being an intermetallic compound, its stoichiometry is fixed and therefore not much change in its lattice parameter is expected.

Composition of alloy	***Precise lattice parameter of α-uranium (A°)***			***Lattice volume (A^3)***
	a	*b*	*c*	
Unalloyed α-uranium at RT	2.8540	5.8700	4.9550	83.0110
U-8wt%Mo after heat treatment for 68 hrs at 500^0C	2.8533	5.8595	4.9549	82.8405
U-8wt%Mo after heat treatment for 240 hrs at 500^0C	2.8528	5.8628	4.9560	82.8911
U-9wt%Mo after heat treatment for 68 hrs at 500^0C	2.8528	5.8607	4.9565	82.8696
U-9wt%Mo after heat treatment for 240 hrs at 500^0C	2.8563	5.8658	4.9541	83.0034
U-10wt%Mo after heat treatment for 68 hrs at 500^0C	2.8519	5.8638	4.9546	82.8556
U-10wt%Mo after heat treatment for 240 hrs at 500^0C	2.8542	5.8606	4.9601	82.9692

Table 4.7 Precise lattice parameter and lattice volume of orthorhombic α-uranium in heat treated U-Mo alloys.

4.4.3 Microstructural analysis

The microstructure of hot rolled alloy samples of *U-8wt%Mo*, *U-9wt%Mo* and *U-10wt%Mo (as shown in Fig 4.25)* show single phase equiaxed grains without any evidence of second phase [178]. It is also important to mention that the features appear at the grain boundary and also inside the grains in the microstructures *(as shown in Fig 4.25)* as second phase are the artifacts created during sample preparation. These microstructures does not show any preferred grain orientation and dendrite, thus indicate equiaxed cubic γ-phase all along the grain. The grain sizes of hot rolled *U-Mo alloy* and the as cast samples are also in close agreement with each other. This indicates that alloys were not exposed at high temperature for very long duration and hence did not result in grain coarsening *(as shown in Table 4.4).*

The microstructures of *U-Mo alloy* samples after 68 and 240 hours of heat treatment are shown in *Fig. 4.26* and *Fig. 4.27* respectively. The microstructure of each heat treated alloy show two distinct grey colors. The bright region in the microstructure is retained γ-phase because the feature remain un-etched during sample preparation. This effect is understandable because increase of molybdenum percentage in uranium increases its resistance to chemical interaction and the same could be observed distinctly in the microstructures shown in *Fig. 4.26* and *Fig. 4.27.* It is understood that solid solubility of Mo in α-phase is extremely limited when compared with γ-phase. Therefore, the etching response of both the phases is contrasting to each other. The microstructures clearly show prior gamma grain boundaries to indicate that recrystallization was not a predominant feature in the heat treated alloys. It confirms that though hot working was performed at higher temperatures and recrystallization could be evident however, during heat treatment the temperature regime has not favored the effect. It can also be observed from the microstructures that prior γ-grain boundaries act as preferential nucleation site for eutectoid reaction. It is more evident from the heat treated microstructures of *U-9wt%* and *U-10wt% Mo alloys* where retained γ-phase is present in islands surrounded by equilibrium phase products of α-phase and U_2Mo. It is also evident from these microstructures that the volume of island (γ-phase) increases for higher Mo compositions alloys. The presence of lamella could be treated as strong evidence suggesting the phase transformation reaction as eutectoid.

The microstructures were further examined by image analysis to quantify the phases and the values are shown in *Table 4.8.* Image analysis was carried out for two phase system therefore, α and U_2Mo phases were assumed as one phase system. The approximation was made because both α and U_2Mo are eutectoid transformed product. The image analysis was not performed for heat treated *U-8wt% Mo alloy* because γ-phase and eutectoid transformed products could not be identified without error. Therefore, phase analysis was carried out for *9* and *10wt% Mo alloys.*

It can clearly be seen from *Table 4.8* and *Table 4.5* that quantitative phase analysis results by two independent methods *(i.e. POWDER CELL & Image analysis)* are in close agreement with each other.

Alloy Composition	Heat treatment at 500 ℃ for 68 hours		Heat treatment at 500 ℃ for 240 hours	
	Retained γ-phase (in vol %)	Eutectoid transformed product (in vol %)	Retained γ-phase (in vol %)	Eutectoid transformed product (in vol %)
U-8wt% Mo	29.42	70.58	18.84	81.16
U-9wt% Mo	36.63	63.37	21.48	78.52
U-10wt% Mo	45.78	54.22	27.36	72.64

Table 4.8 Image analysis result on heat treated U-Mo alloys.

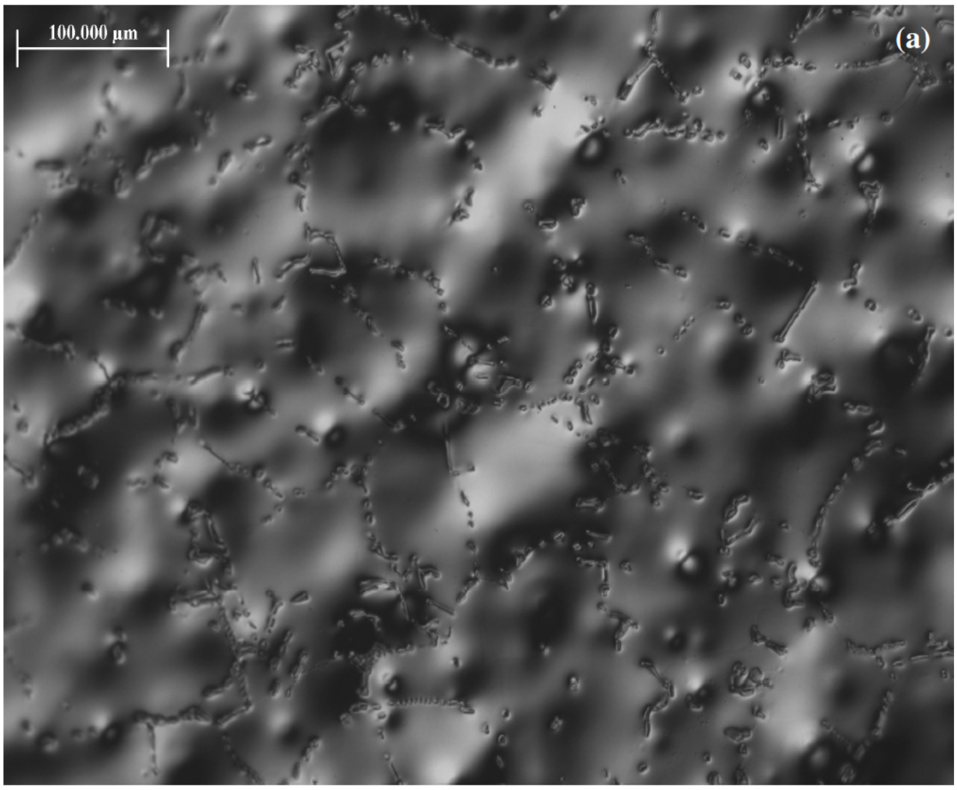

Fig. 4.25 (a).

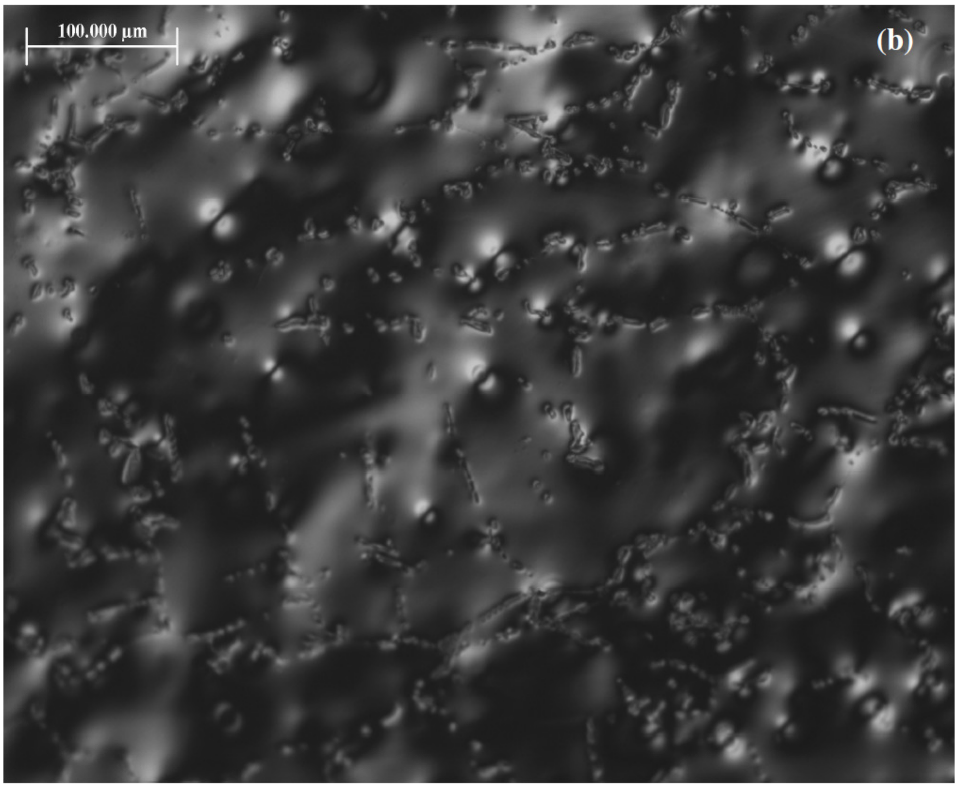

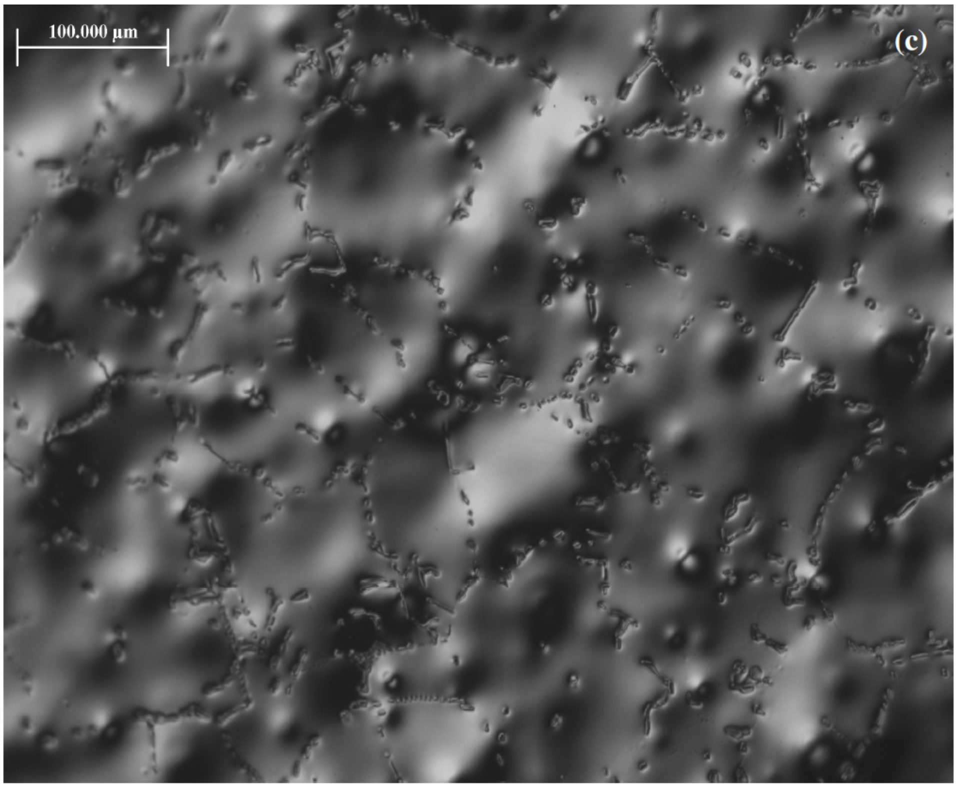

Fig. 4.25 Microstructures of hot rolled U-Mo alloy (a) U-8wt%Mo, (b) U-9wt%Mo, (c) U-10wt%Mo.

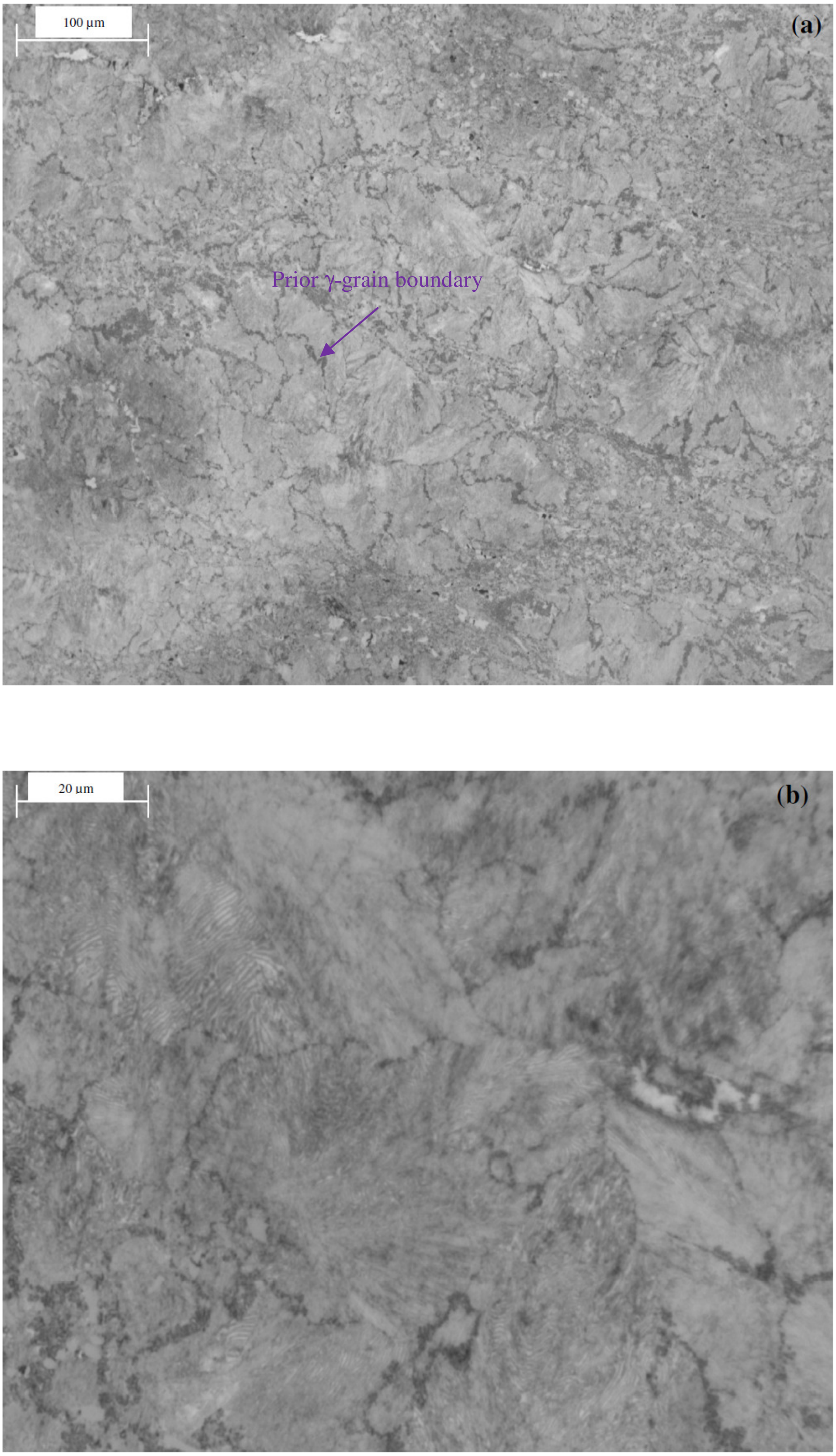

Fig. 4.26 (a) & (b).

Fig. 4.26 (c) & (d).

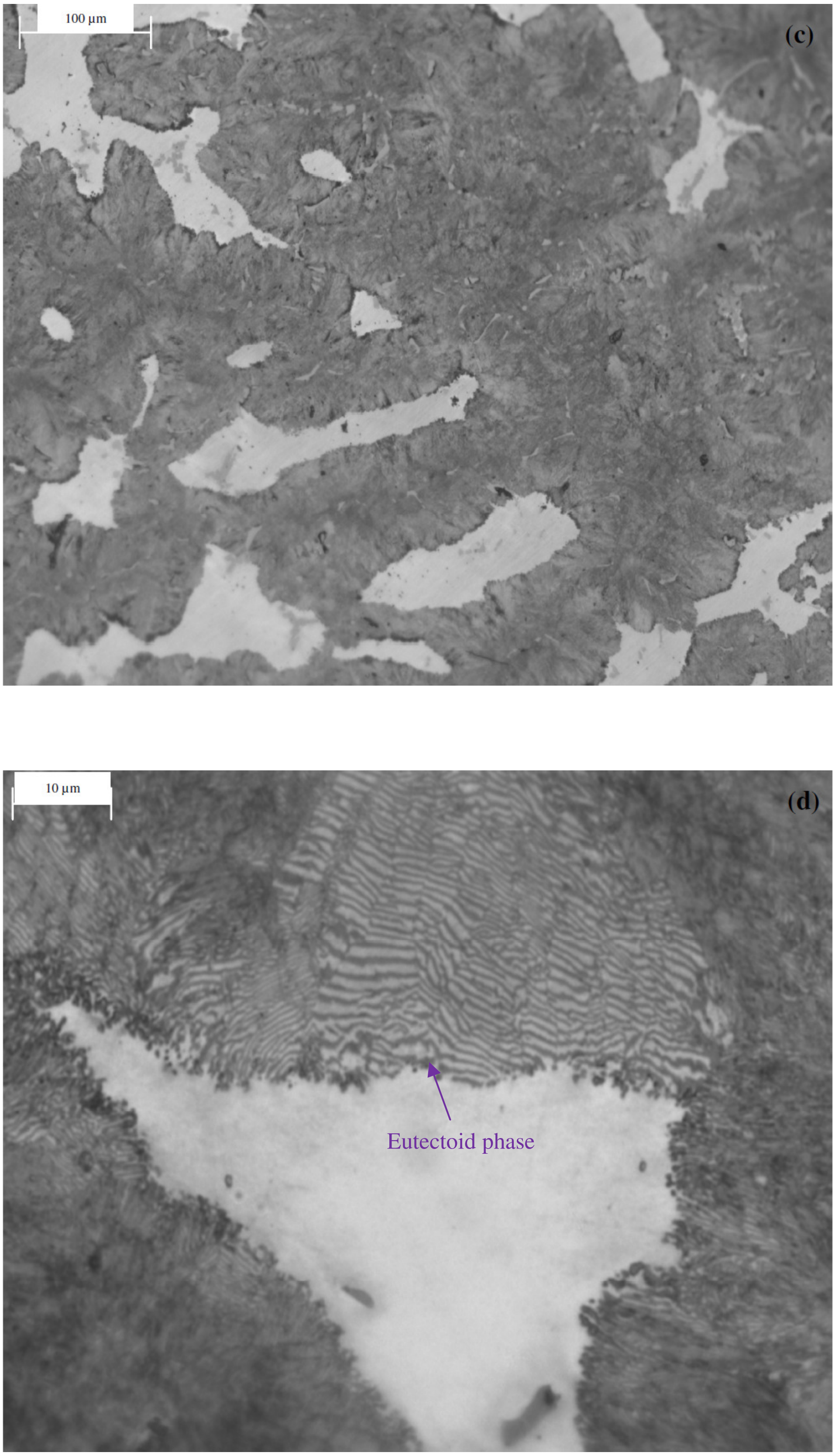

Fig. 4.26 (c) & (d).

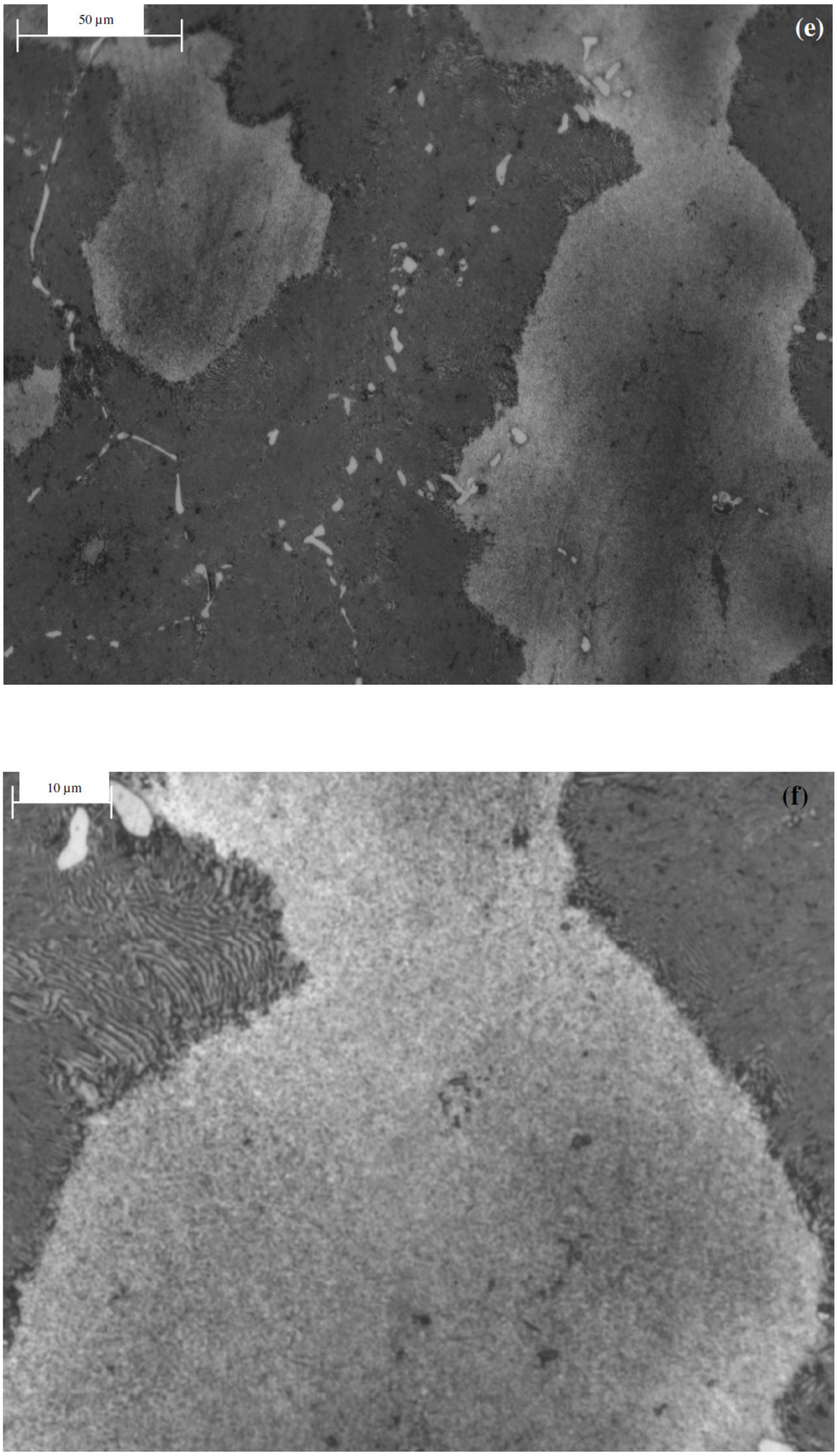

Fig. 4.26 Microstructures of heat treated U-Mo alloy at 500^0C for 68 hrs (a) & (b) U-8wt%Mo, (c) & (d) U-9wt%Mo, (e) & (f) U-10wt%Mo.

Fig. 4.27 (a) & (b).

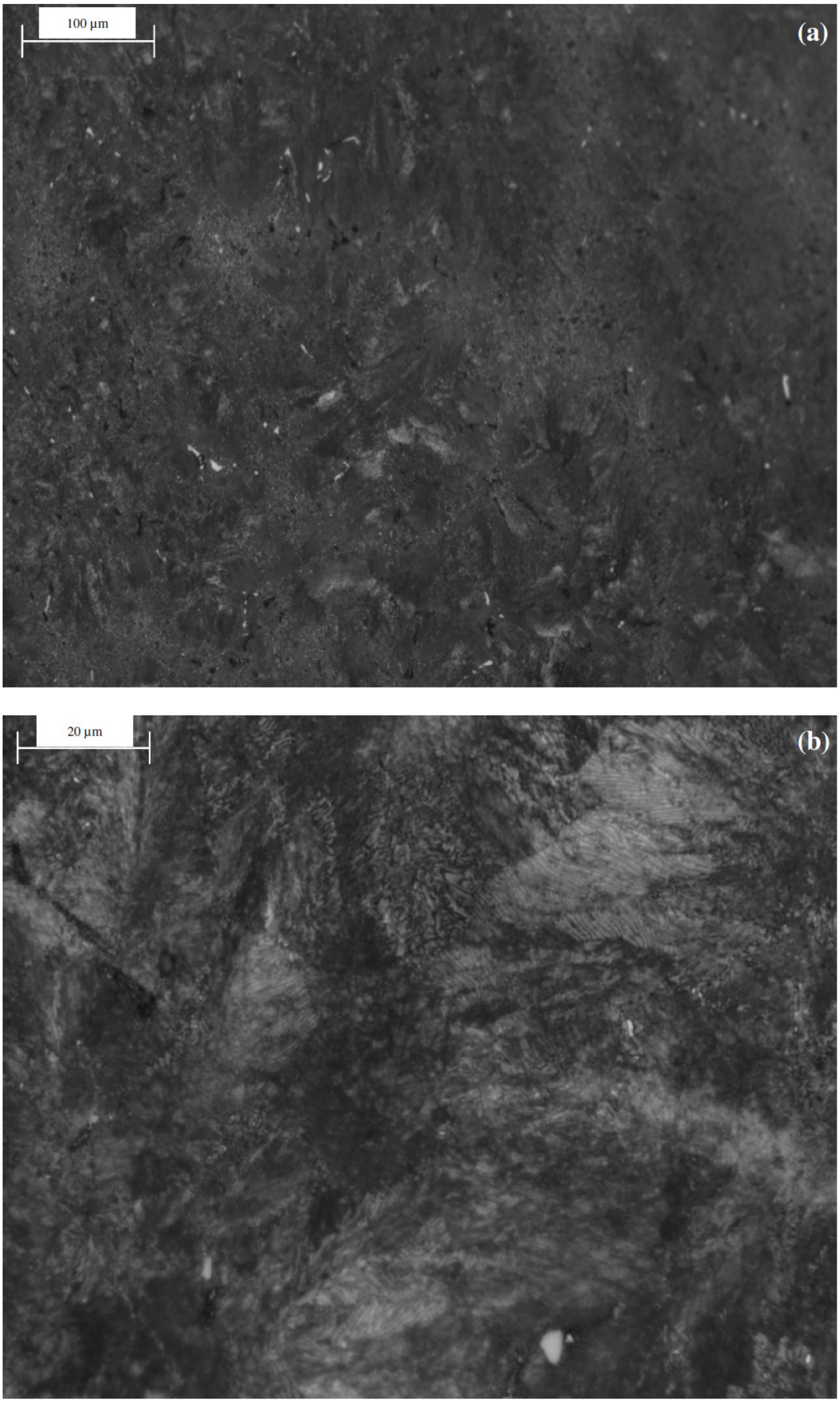

Fig. 4.27 (a) & (b).

Fig. 4.27 (c) & (d).

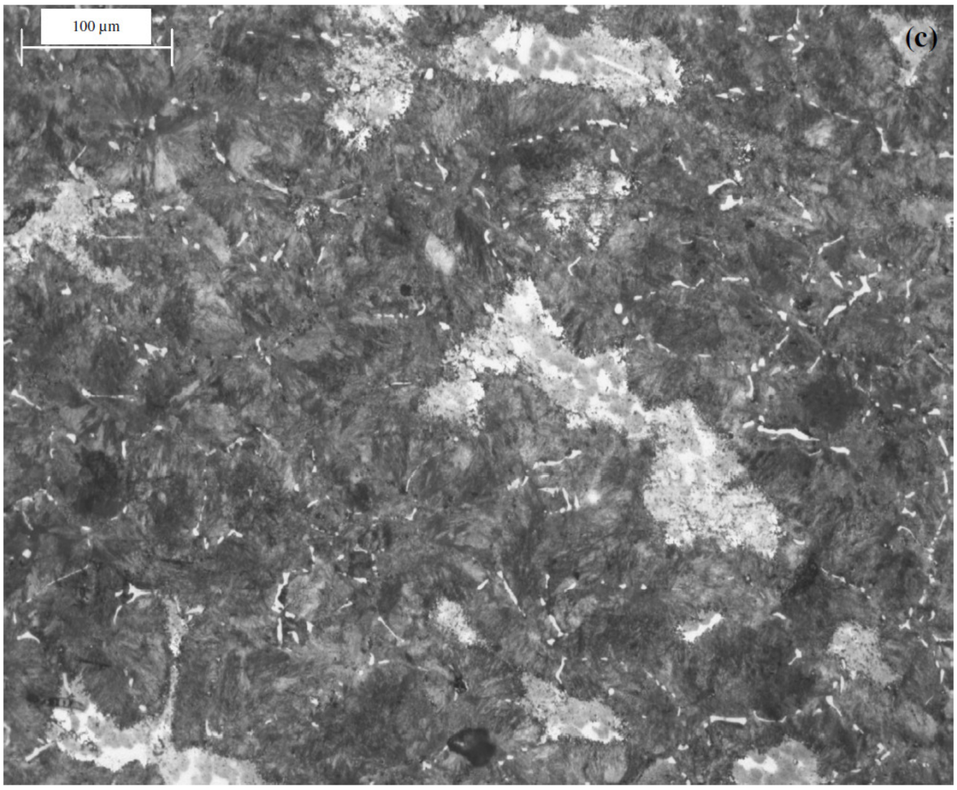

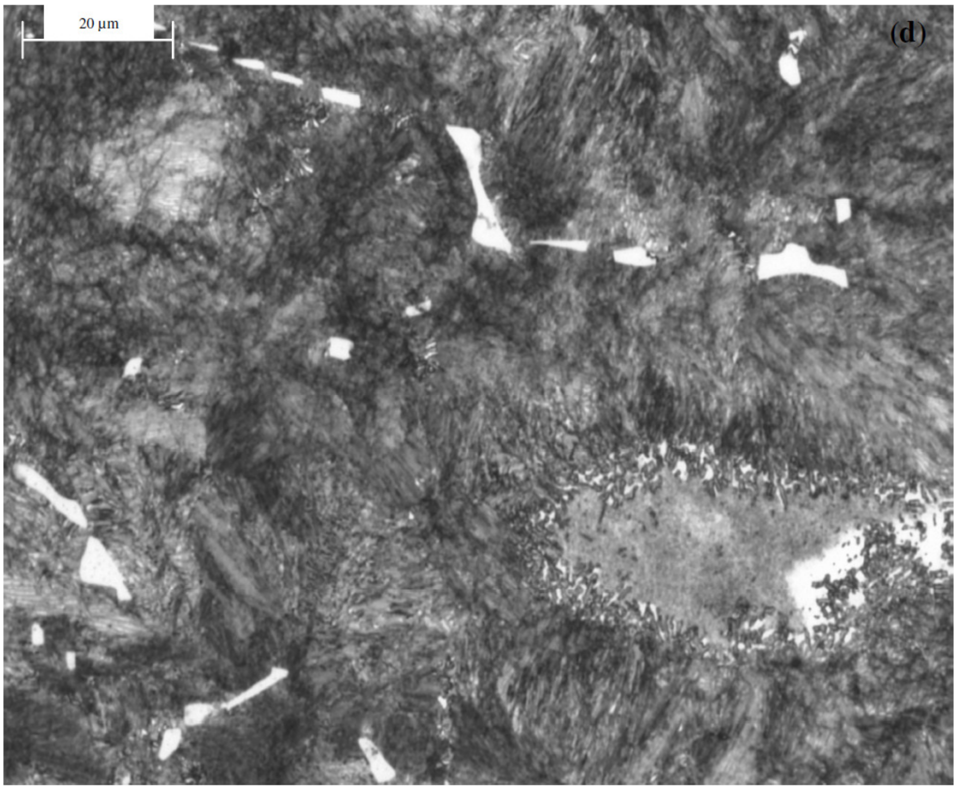

Fig. 4.27 (c) & (d).

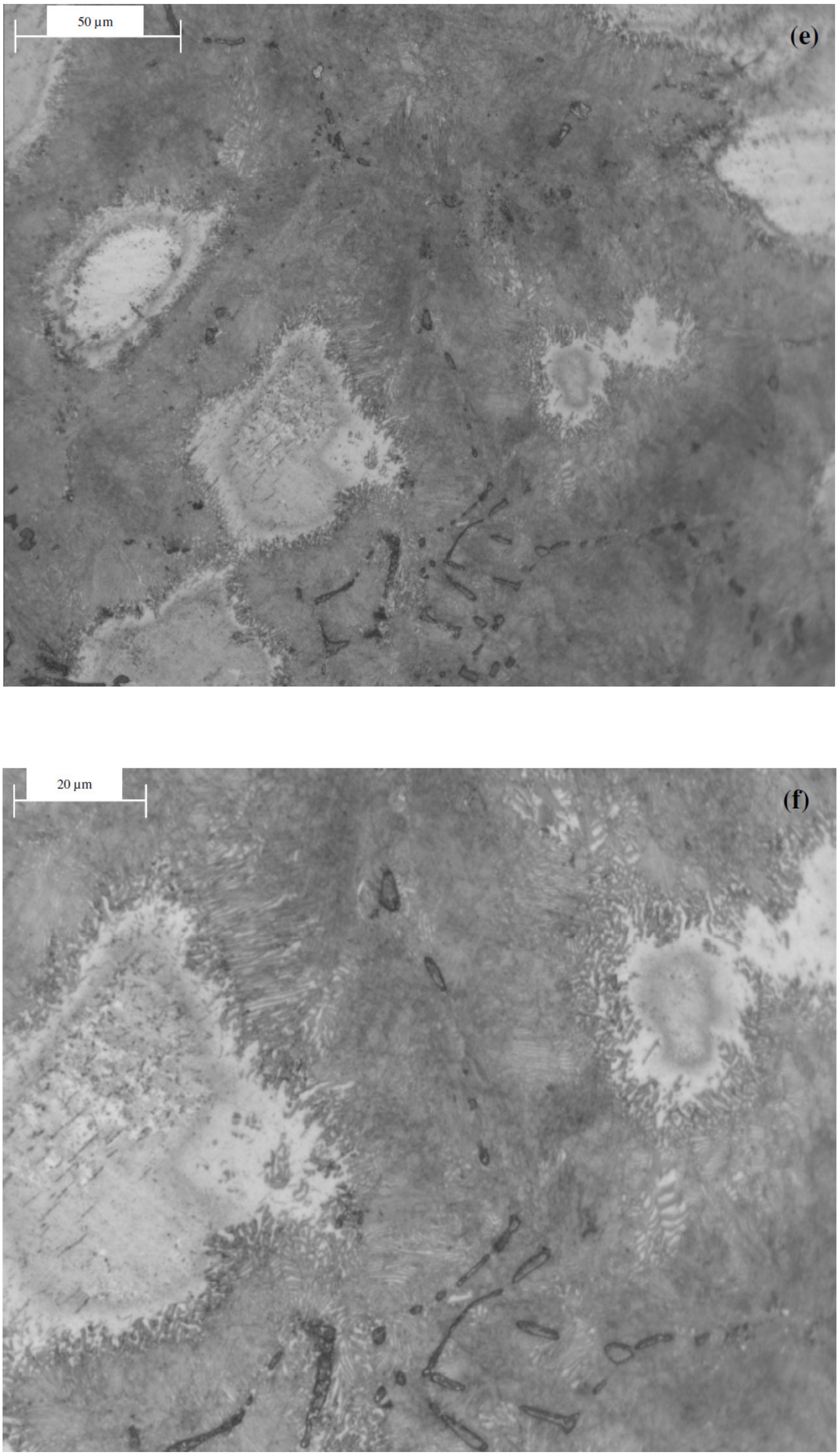

Fig. 4.27 Microstructures of heat treated U-Mo alloy at 500^{0}C for 240 hrs (a) & (b) U-8wt%Mo, (c) & (d) U-9wt%Mo, (e) & (f) U-10wt%Mo.

4.4.4 Study on end of life prediction for U-Mo alloys

The phase transformation study on *U-Mo alloys* was further extended to evaluate the end of life prediction. This invariably means the time required to estimate complete phase transformation of γ-phase to equilibrium phase products viz. α-phase and U_2Mo at 500 °C. The analysis, as shown in Appendix-3 was performed using *"Kolmogorov-Johnson-Mehl-Avrami equation"* [173]. The analysis was done with the approximation that α and U_2Mo phases are considered as single entity. This approximation is considered because both the phases result due to eutectoid phase transformation of γ-phase. The *KJMA* equation used in the study is shown as follows

$$f = 1 - e^{-kt^{n}} \tag{4.3}$$

Equation 4.3, correlates fraction of transformed phase with time. Here, f indicates fraction of transformed product, k is the value contains all the temperature dependent terms because thermal activation affects the growth strongly through boundary/interface mobility, and because the nucleation density depends very strongly on driving force. Therefore, k in the present study is assumed constant because the history of different alloy preparation and their heat treatment regime was identical. Here, n in the equation is related to the geometry of the transformation.

The data shown in *Table C-1* and *Fig. C-1* from *Appendix-3* was used to evaluate the relative time required by γ-phase to transform into equilibrium phases at 500°C for different compositions of *U-Mo alloys* and is shown in *Fig. 4.28*.

The plot shown in *Fig. 4.28* correlates transformation of equilibrium phases in *U-Mo alloys* upon soaking time, which increases monotonically and exponentially. The retained γ-phase fraction would then be found decreasing. It can be observed that time required for initial phase transformation for all the three compositions are almost same. However, the time required for transformation of higher quantity is more dependent upon composition and therefore, *U-10wt%Mo alloy* exhibit highest resistance for the eutectoid decomposition of γ-phase in equilibrium phase products of α and U_2Mo.

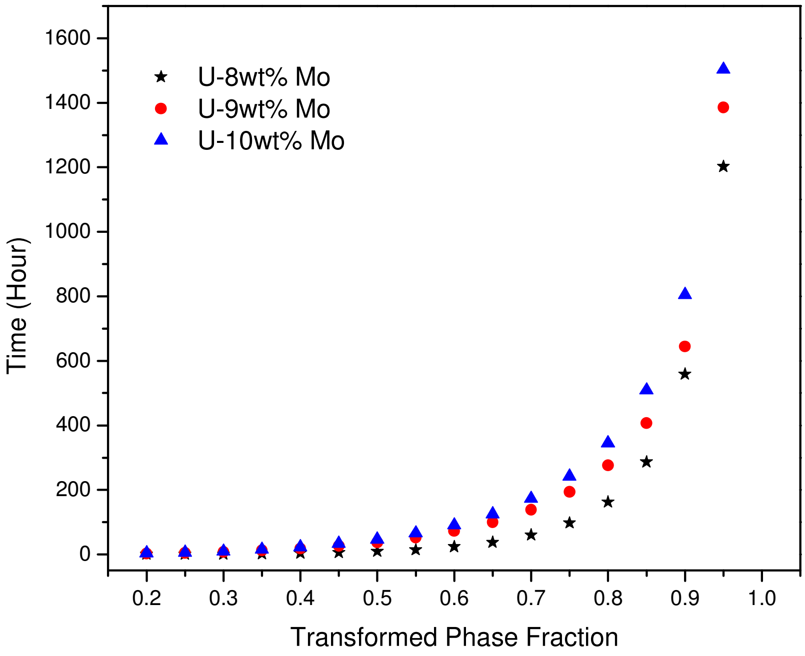

Fig. 4.28 Effect of soaking time on volume percentage of transformed phase at 500 °C.

The above calculation may lead to very important life-expectancy of dispersions in the fuel plates. The fuels in the nuclear reactor once loaded, in the form of fuel plates, would be expected to undergo fission without undergoing transformation or irradiation related defects such as growth or swelling. Any such physical change in the fuel may lead to its failure much earlier than the expected residence time. The above plot shows that it takes more than 50 days for 8 wt.%Mo and 60 days for 10 wt.%Mo to transform 95% of the retained cubic phase. It is important to note here that these data has been collected at 500°C, which is much higher than the actual temperature encountered during reactor operation. Therefore, this analysis may well serve as an indicator of actual time taken for transformation, hence may be termed as accelerated test under out-of-pile condition. Since this decomposition is basically diffusion controlled reactions, the fraction transformed is expected to be much lesser at lower temperatures, indicating very low possibility of deterioration of fuels in research reactors. Further, it may be added that additional studies are needed to evaluate the effect of neutron flux on the transformation kinetic of cubic phase.

4.5 Study on U-Mo diffusion couple

Study on *U-Mo* diffusion couple was carried out to examine if molybdenum diffuses completely in uranium at desired process temperature. The study is useful especially, to evaluate the kinetics of *U-Mo alloy* preparation by powder processing route. A detailed calculation to determine Mo diffusion length in uranium using *U-Mo* diffusion couple is shown in

Appendix-4. The result obtained from the calculation is discussed later in this section.

The microstructure of *U-Mo* diffusion couple prepared by hot pressing was evaluated in detail by optical microscope and by SEM. The microstructure shown in *Fig. 4.29* clearly indicates an interaction layer between uranium and molybdenum interface. It can also be observed from the microstructure that uranium rich region shows phase transformations up till certain distance from the interaction layer. This indicates that molybdenum has entered into uranium and depending upon its concentration the lamella and other phase transformation product viz. widmanstatten are observed. Similar observations could also be established from the BSE images as shown in *Fig. 4.30.* The diffusion couple sample was polished using 1µm diamond paste and was left open in atmosphere for natural etching before being examined under microscopy.

The diffusion couple sample was then examined under micro probe to evaluate molybdenum diffusivity in uranium and vice versa. The results of micro probe analyses are shown in *Fig. 4.31.*

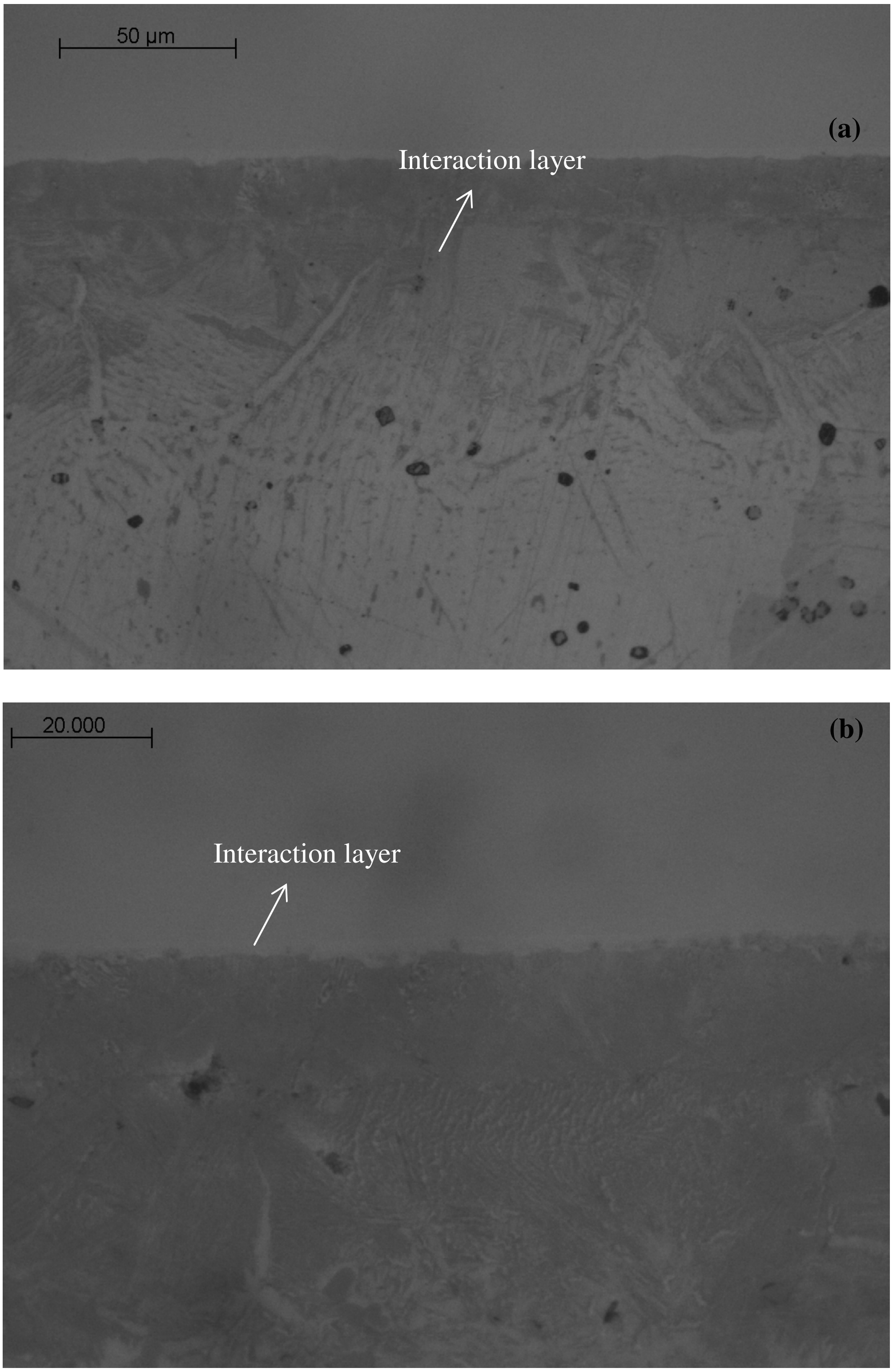

Fig. 4.29 Optical microstructures of hot pressed U-Mo diffusion couple (a) at 500 X and (b) at 1000 X.

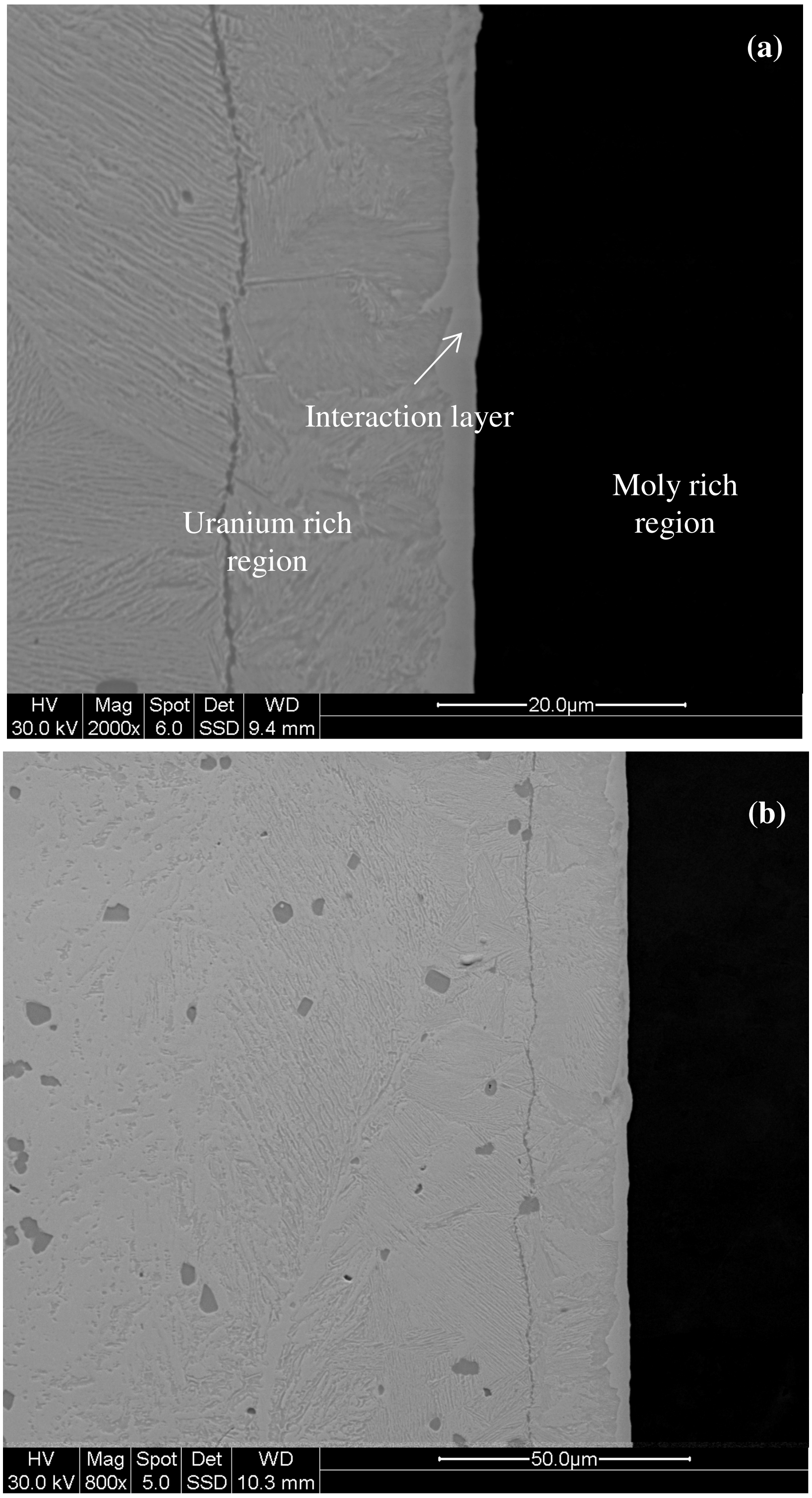

Fig. 4.30 BSE images of hot pressed U-Mo diffusion couple (a) at lower magnification and (b) at higher magnification.

The micro probe analyses result indicates gradual decrease of molybdenum concentration in uranium. However, the same was not observed for uranium, therefore uranium concentration decreased abruptly to zero counts in molybdenum after the interface as shown in *Fig. 4.31(c)*.

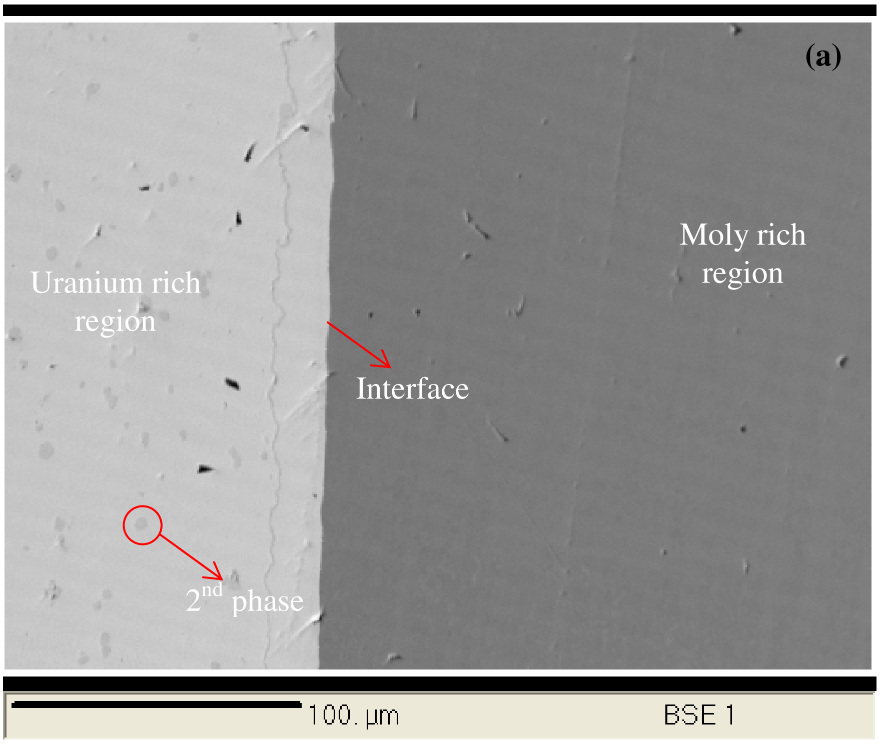

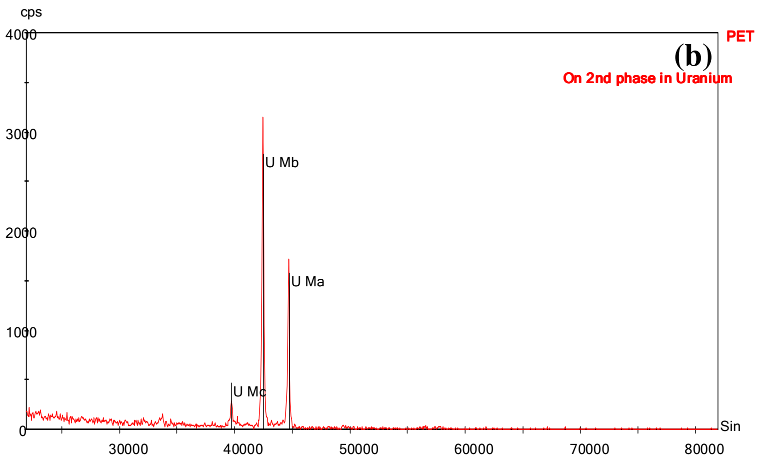

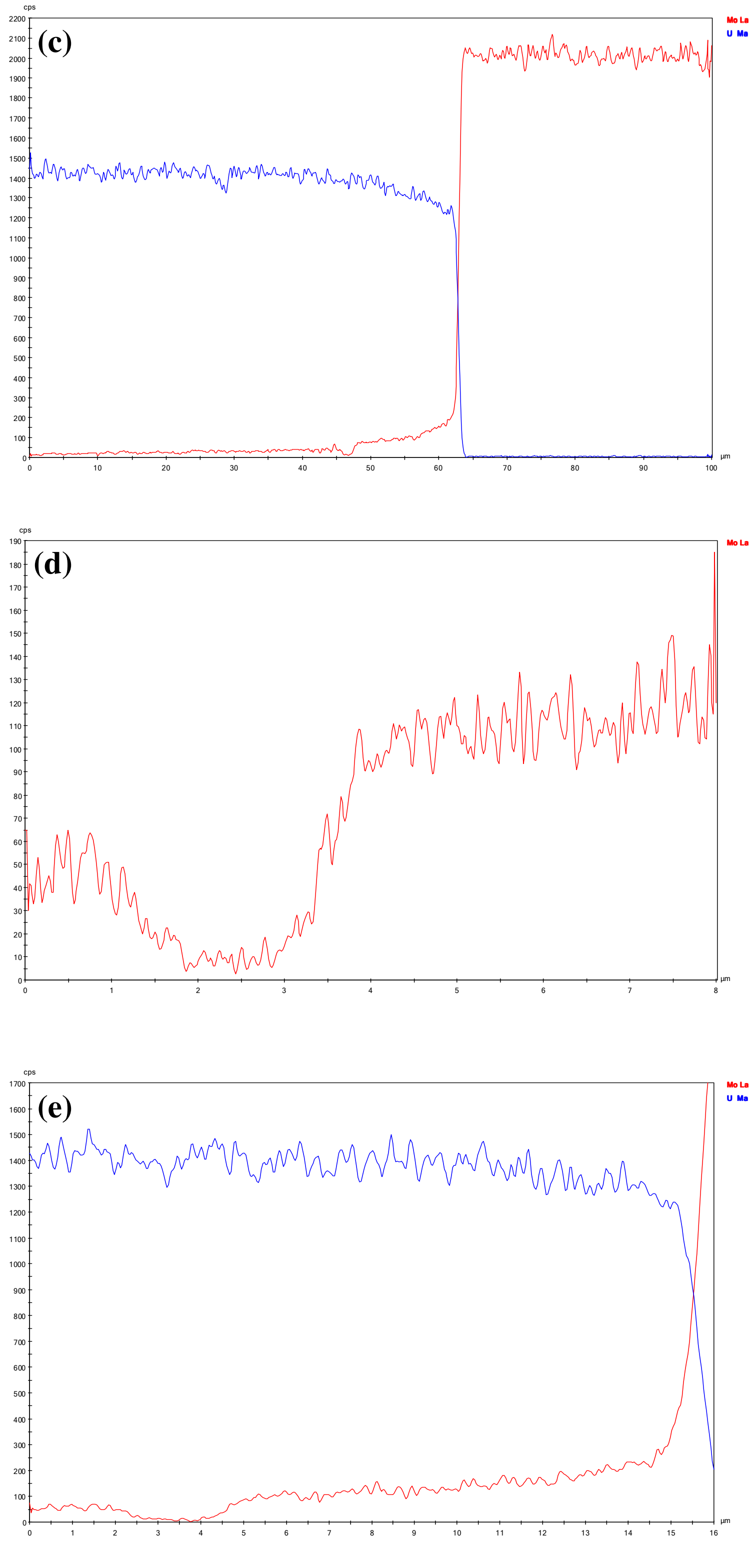

Fig. 4.31 EPMA results (a) BSE image, (b) WDS scan on 2nd phase in uranium, (c) Intensity profile of U & Mo across the interface, (d) Intensity profile of 'Mo' on continuous line phase (e) Intensity profile of U & Mo across the interface with smaller region.

As was discussed earlier, the molybdenum diffusion length in different *U-Mo alloy* compositions viz. 2, 5 and 10wt% Mo for 6 hours of soaking time at 900 °C was calculated as shown in *Appendix-4*. The molybdenum diffusion length calculated for 2, 5 and 10wt% Mo in uranium is 75.07, 38.96 and 39.98 µm respectively. It can be seen from section 3.2.2 that *U-Mo alloys* prepared by powder processing route has 25µm average uranium metal powder size. Therefore, it could be surmised that since the minimum Mo diffusion length in uranium at 900 °C for 6 hours of soaking was 38.96 µm hence, *U-Mo alloys* prepared by processing compact elemental powders of uranium and molybdenum at 1050 °C for 6 hours would result in further increase of Mo diffusion in uranium. This could be attributed from the intrinsic diffusivity coefficient data of Mo in uranium at different temperatures [73]. Therefore, results obtained from the study on *U-Mo* diffusion couple confirm the homogeneous solid solution for 2, 5 and 10wt% Mo by processing the elemental powders at 1050 °C for 6 hours.

5. Conclusions

The present work on *U-Si and U-Mo* alloys involves handling of radioactive and pyrophoric materials. In addition, considerable effort and great care had to be taken, as sample preparation for these materials is highly prone to oxidation and degradation. As a result of this extensive study involving relevant nuclear fuel system with respect to their fabrication behavior and out of pile characterization in detail, the following conclusions were drawn:

5.1 Alloying of U_3Si_2 intermetallic by powder metallurgy route

This study showed alloying of a line compound U_3Si_2 phase by powder processing route with uranium metal powder and silicon powder as the starting materials. The compound U_3Si_2 is considered a potential nuclear fuel material for the upgraded and modified APSARA Research Reactor. In spite of the large density differences between the constituent metal powders, uranium (19.7 g/cc) and silicon (2.33 g/cc), a combination of process parameters such as powder mixing, compaction and homogenization has resulted in the desired single phase compound, as shown by XRD studies.

The processing did not pick up any significant amount of impurity, as evidenced by chemical analysis of starting materials as well as final product. Some small quantity of impurities (mainly oxygen) was present in the starting materials, which resulted in the formation of minor amounts of UO_2 in the final compound. However, from the reactor point of view, these were considered as ‘tolerable impurities’. The U_3Si_2 compound prepared by the powder processing route was found with inherent intragranular porosity. The porosity, as evidenced by SEM pictures is considered beneficial for the performance of nuclear fuel because it is expected it would help in suppressing irradiation induced detrimental effects like swelling.

The starting powders of uranium and silicon were pressed together at high pressures (600 MPa) to induce plastic flow hence ensuring intimate contact between powder particles. A small exothermic reaction ($\Delta H = -39.37$ kJ/mole at 750 °C) coupled with external heating was adequate to synthesize the compound *(as shown in Appendix-2)*. However, the product was deliberately heated in steps *(i.e. 950 °C & 1400 °C)* to accomplish the intended alloying reaction between uranium and silicon and also avoid any unalloyed phases. It was necessary to avoid bulk liquid formation in the process leading to inhomogeneous product. The product was finally heated at 1550 °C for 4 hours to complete the alloying to form the congruent melting compound well below its liquidus point by taking advantage of mushy zone *(liquid plus solid region)*. The sequencing of processes and optimized parameters helped in achieving homogeneous product and imparting porosity with sufficient handling strength. The steps in the experiments are to be scaled to a production level process-flow sheet for large – scale production of nuclear fuel.

5.2 Alloying of U-Mo by powder metallurgy & induction melting routes

This study on *U-Mo alloy* preparation by powder metallurgy route showed that 2, 5 and 10wt% Mo concentration in uranium could be prepared with uranium and molybdenum metal powders as starting materials. The study also showed that proper combination of process parameters viz. mixing, compaction and optimized heating regime, would result in homogenized product though their melting temperatures differ largely *(melting points of uranium and molybdenum are 1132 ℃ and 2623 ℃).* The phase characterization and microscopy results of *U-Mo alloys* prepared by powder processing route were in close agreement with those prepared by induction melting route for similar compositions. The only difference observed with *U-Mo alloys* synthesized by powder processing was the presence of intragranular porosity, which in turn would help in retaining fission products.

The chemical characterization results exhibited the care and precautions employed during alloy preparation and therefore controlling the impurity pick-up. The powder metallurgy processing route also highlighted a homogeneous product surmounting high temperatures and repeat melting. In this context, this study opens up an entirely innovative fabrication possibility where tubes of either zirconium or other structural material for intended nuclear reactor application can be compacted with the mixture of constituent elemental powders *(i.e. uranium and molybdenum)*, in desired proportions, followed by heat treatment to prepare fuel elements directly without employing any melting. However, the feasibility of this innovative fuel fabrication route needs further evaluation and study for metallurgical and process engineering point of view. Nevertheless, the technique would help in reducing the high capital cost and technical complications employed by existing process equipments (viz. atomizer, rotating disk and rotating anode) for preparing *U-Mo granules*.

5.3 Evaluation of cubic γ-phase metastability in U-Mo alloys

The study to evaluate cubic phase metastability in *U-Mo alloys* was carried out to examine the minimum concentration of molybdenum required to metastabilize the high temperature γ-phase under furnace cooling condition. Reducing molybdenum content in uranium alloys to the best possible extent is significant because Mo has higher parasitic neutron capture cross section. Therefore, increased Mo percentage would adversely affect the neutron economy in the reactor. The present study showed that with minimum addition of 8wt% Mo, the cubic γ-phase could be retained at room temperature under furnace cooling condition.

Analyses of the XRD patterns and precise lattice parameter calculations concluded that molybdenum has reacted with uranium to form solid solutions and no free molybdenum was leftover. The lattice parameters of α-phase did not differ much, due to low solubility of Mo in that phase. On the other hand, the lattice parameter of cubic γ-phase was found to decrease monotonically from 3.4683 A° in 2wt%Mo to 3.4213 A° in 10wt%Mo alloys. Although the XRD results of alloys ≥6wt% Mo concentration did not exhibit the equilibrium phase products viz. α and U_2Mo in the cast samples, further investigation by microscopy coupled with image analysis resolved that second phase (i.e. α and U_2Mo) could be removed completely in furnace cooled as cast alloys with minimum 8wt% Mo. The microstructural examinations of alloys samples showed mixture of three phases, i.e. α-phase, U_2Mo and γ-phase, in 2wt%Mo alloy, whereas the quantity of α-phase and U_2Mo decreased with increased Mo-content up to 7wt%. In alloys with ≥8wt%Mo, only γ-phase could be observed.

Therefore it could safely be concluded from the study that use of U-Mo alloys granules or monolithic with 8wt% Mo concentration would improve neutron economy in a reactor when compared with higher Mo concentration alloys, while prevailing the fundamental metallurgical requirement of retaining complete cubic γ-phase to improve irradiation induced detrimental effects.

5.4 Phase transformation in U-Mo alloy

A detailed examination was performed to study the decomposition of retained γ-phase in *U-Mo alloys* into equilibrium phase products of α and U_2Mo. The phase transformation study showed that fraction of equilibrium phase product in heat treated alloys increased with heating duration. The quantitative phase analysis, as calculated from XRD patterns of heat treated U-

Mo alloys at 68 hours and 240 hours suggested that by lowering the exposure time at 500 °C, the retained cubic γ-phase fraction could be increased. In fact the study shows that retained cubic γ-phase volume fraction is 1.75 times more in all three U-Mo alloy compositions *(i.e. 8, 9 and 10wt% Mo)* after 68 hours of heat treatment when compared with 240 hours. It could also be concluded from the present study that by increase in Mo concentration in uranium, the cubic γ-phase exhibits higher resistance for phase transformation resulting in formation of equilibrium phase products viz. α and U_2Mo.

It could also be concluded from the results obtained using *"Kolmogorov-Johnson-Mehl-Avrami equation"* that the data on phase transformation study on 8, 9 and 10wt% Mo alloys may serve as a guideline to predict life-expectancy of dispersions in the form of fuel plates under normal reactor operating conditions. It is important to note that these data are collected at 500°C albeit much higher than the actual temperature encountered during reactor operation. Therefore, this analysis may be employed as an indicator of actual time taken for transformation. Therefore, it may be termed as accelerated test under out-of-pile condition.

It could also be concluded from the present study that volume fraction of U_2Mo intermetallic in the transformed phase does not vary much with either soaking time or Mo concentration in the alloy. However, the change in volume fraction of α and γ phase with soaking time and Mo concentration in the alloy are closely dependent upon each other. Therefore, it could be concluded that diffusion of Mo plays a crucial role in the formation of equilibrium phases and since α-phase has very poor solubility for Mo, its transformation from γ-phase is sluggish because Mo concentration in this case is required to come down from 8, 9 or 10 wt% (depending upon alloy composition) to few atom percent. Therefore, it could also be concluded that lowering of fuel operating temperature in these alloys may result in lower phase transformations thus enhance the fuel performance. However, prediction of life expectancy of *U-Mo* alloys under reactor operation does require its detailed study under neutron fluence *(i.e. in-pile characterization)*, which is beyond the scope of present investigation.

5.5 Experimentation on U-Mo diffusion couple

The study on *U-Mo* diffusion couple was performed to evaluate the desired soaking time for alloying of U-Mo alloys by powder metallurgy route. The results derived from U-Mo diffusion couple shows that minimum diffusion length for molybdenum in uranium at 900 °C for 6 hours of soaking is around 38 μm. Therefore, it may be inferred that molybdenum would diffuse completely in uranium after 6 hours of soaking at 900 °C, under prevailing experimental conditions. In the present study, U-Mo alloys prepared by powder metallurgy route have average uranium particle size of ~25 μm and the processing was carried out at 1050 °C for 6 hours of heating duration. Therefore, under these parameters *U-Mo alloys* by powder metallurgy route is expected to be homogeneous, which is confirmed from the XRD and microscopy results of alloys prepared by powder metallurgy route.

5.6 Scope for future studies

The study performed in the thesis is mainly attributed towards development of line compound phase U_3Si_2 and U-Mo alloys by powder processing route so as to comply our specific requirement where LEU is present in metal powder form as well. The study was accomplished to the desired aim and objective of the thesis and U_3Si_2 & U-Mo alloys were prepared and characterized using standard metallurgical tools. However, like always said, science is a never ending process therefore, based upon the present investigations, experimentation and results, it is suggested that some of the work may be attempted in future for further in-depth understanding of systems investigated and also from technological development points, especially in *INDIAN* context. Therefore the scope of future studies suggested is as follows:

- It may be noted here that most of the work attempted in the present study is intended for dispersion type fuel and either U_3Si_2 or U-Mo alloy granules can be used as dispersoid, depending upon desired in-core reactivity and fabrication convenience. In most cases the fuel elements would be with plate geometry and aluminium as matrix and clad. Therefore, a detailed evaluation on chemical interaction between dispersoid and matrix is always valuable. Hence, study could be planned in future to examine the time and temperature dependence of chemical interaction between dispersoid and matrix. This study would also help in finding the life expectancy of fuel elements.

- As discussed earlier in section 5.2, the scope of future work could be on exploring and developing the technology to fabricate fuel elements, with uranium and molybdenum metal powder as starting materials.
- A detailed metallurgical examination may be planned for future studies on U-Mo alloys, so that effect of cooling rates on cubic phase metastability can be established. In fact, attempts must be made to evaluate the cooling curves with different U-Mo compositions. The study will serve as the basis in designing the process equipment and also the experimental data would result in imparting in-depth and basic understanding for fuel designers.
- A future study can also be planned on predicting transformation kinetics of cubic γ-phase on actual reactor operating temperatures.
- As stated in the literature survey that attempts were carried out in past to prepare ternary uranium alloys. However, presence of many line compounds in ternary uranium alloys inhibits its further development. Therefore, study on the development of ternary uranium alloys can be planned in future so as to offer increased metastability to cubic γ-phase. In addition development of these alloys can also be attempted by powder processing route to check if any advantage can be drawn.
- A future study can also be attempted to evaluate the diffusion kinetics in more detail. In addition in-pile study on U-Mo phase transformation can be evaluated as future work.

Appendix-1

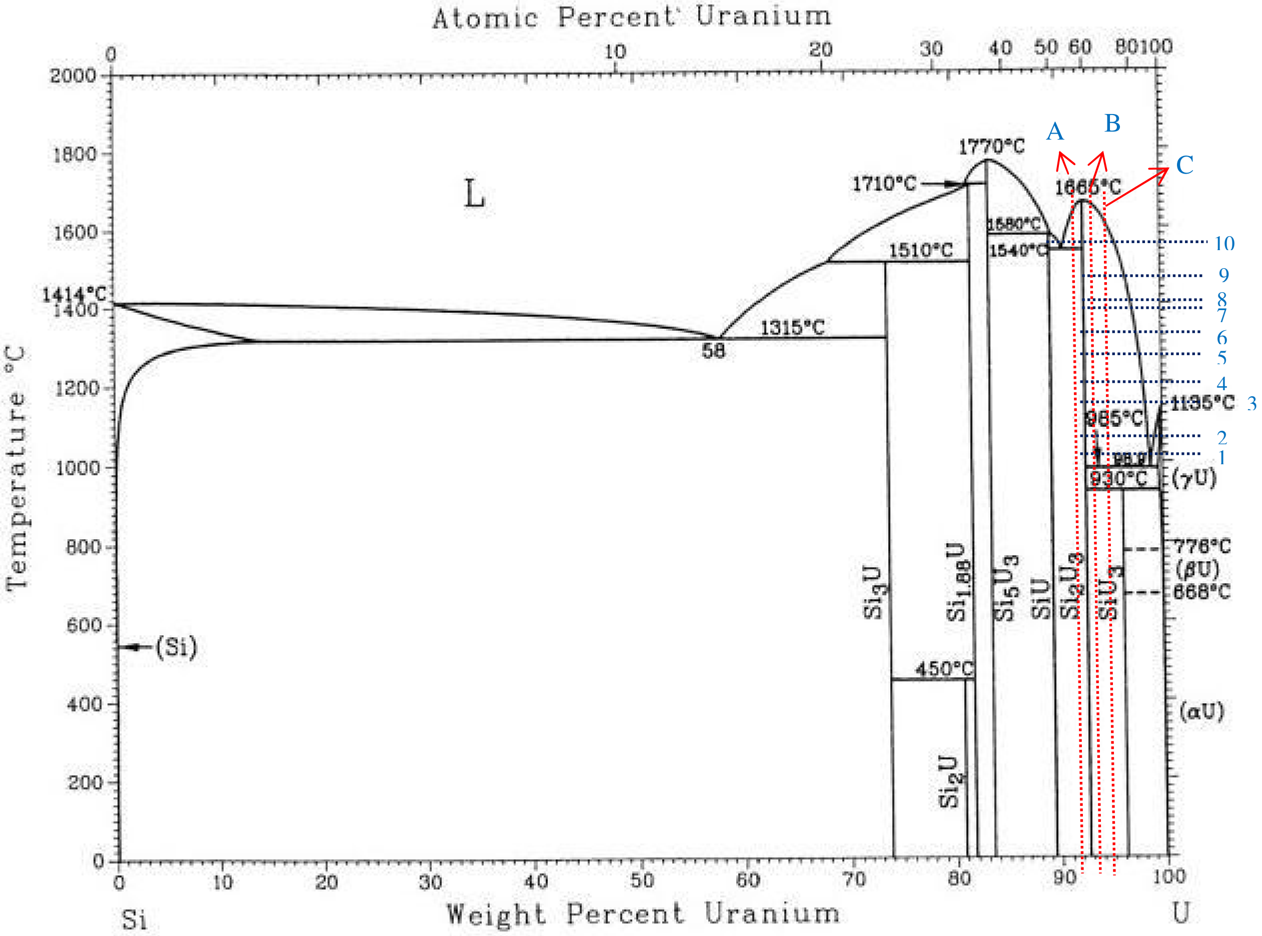

Fig. A-1 Uranium - silicon phase diagram with desired composition and data points to evaluate different phase percentages [113].

The phase diagram (as shown in Fig. A-1) was used to calculate different volume percentage of the liquid and U_3Si_2 phases at various temperatures for both hypo and hyper compositions. Three different alloy compositions, namely A (hypo), B and C (both hyper) were assumed hypothetically for the above mentioned purpose. The alloy compositions were chosen on random basis to facilitate the calculation. The alloy composition with lower uranium percentage (if compared with U_3Si_2 composition) is termed as hypo and with higher uranium percentage is termed as hyper. Similar terminology is used elsewhere in this chapter for convenience. The volume percentage of liquid and U_3Si_2 phases at different temperatures were calculated using Lever Rule and the result is surmised in Table A-1 and Fig. A-2. A schematic of heating profile followed in the alloying of U_3Si_2 is shown in Fig. A-3.

Temperature (°C)	***Stages in alloying***	***Reaction condition***	***Volume percent of liquid phase***		
			A	*B*	*C*
RT-950	Solid state reaction	Slope heating	Nil	Nil	Nil
1030	Peritectic	Slope heating	Nil	15.38	46.15
1080	Peritectic	Slope heating	Nil	16.66	50.00
1160	Peritectic	Slope heating	Nil	17.24	51.72
1210	Peritectic	Slope heating	Nil	17.54	52.63
1280	Peritectic	Slope heating	Nil	18.18	54.54
1340	Peritectic	Slope heating	Nil	20.00	60.00
1400	Peritectic	Step heating	Nil	20.83	62.80
1420	Peritectic	Slope heating	Nil	23.81	71.43
1480	Peritectic	Slope heating	Nil	25.00	75.00
1550	Peritectic	Step heating	75.00	28.57	85.71

Table A-1 Phase volume percentage calculation of liquid phase for off-stoichiometry compositions (e.g. 92.5wt% U & 7.5wt% Si).

The liquid and U_3Si_2 phase volume percentage was calculated at various temperatures for hyper composition, however for hypo composition it was calculated only at 1550 °C because no liquid phase is shown below 1540 °C in U-Si phase diagram.

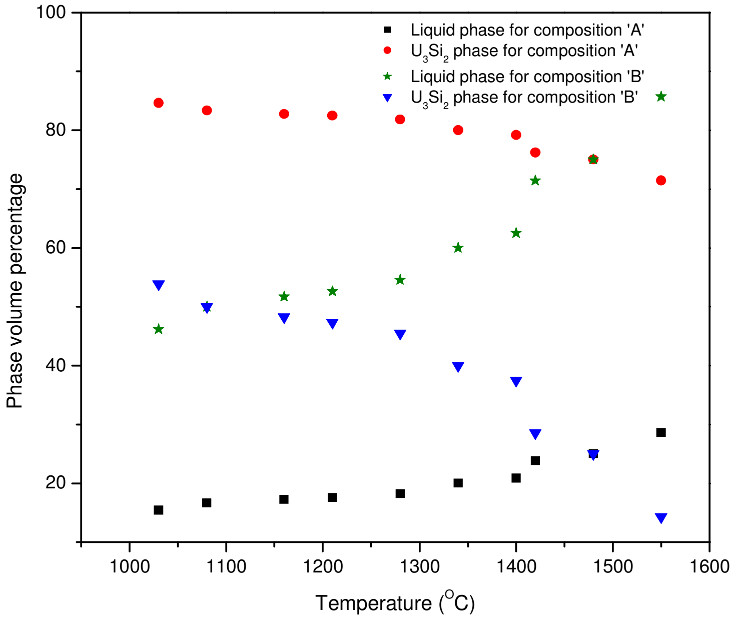

Fig. A-2 Plot between liquid and U_3Si_2 volume percentage for hyper composition and temperature.

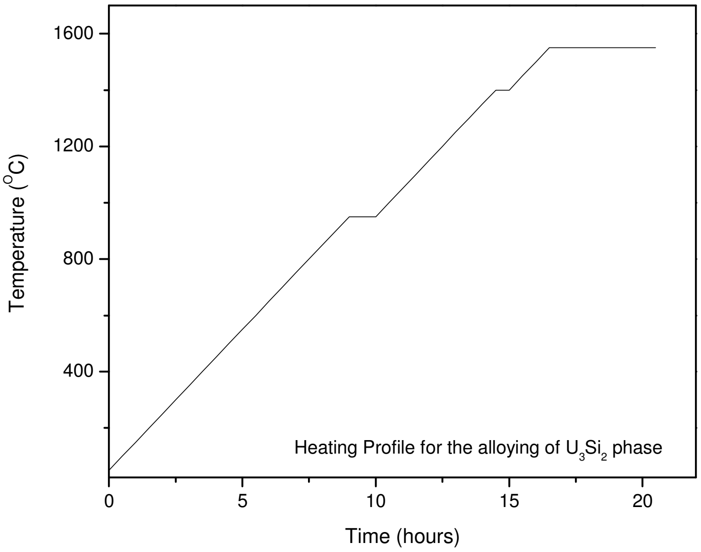

Fig. A-3 Schematic of heating profile followed in the alloying of U_3Si_2.

Appendix-2

The alloying reaction between uranium and silicon to form U_3Si_2 is represented below in equation B-1:

$3U + 2Si \rightarrow U_3Si_2$ B-1

On the basis of equation B-1, the enthalpy for 1 mole of U_3Si_2 at temperature, T is shown in equation B-2,

$$\Delta H_{298}^{T} = \Delta H_{298}^{\circ} + \int_{298}^{T} (c_p, U_3Si_2)dT - 3\int_{298}^{T} (c_p, U)dT - 2\int_{298}^{T} (c_p, Si)dT \qquad \text{B-2}$$

The value of ΔH_{298}° for U_3Si_2 formation is known from the literature as −35.95 kJ/mol [179]

In addition the values of $\int_{298}^{1023}(c_p, U)dT$ & $\int_{298}^{1023}(c_p, Si)dT$ from the computer generated program (ASTD) were calculated as 32.3668 and 20.4567 KJ/mol [180]. It may also be noted that enthalpy of uranium was calculated by taking in account its allotropic transformation at 668 °C.

In addition, the c_p for U_3Si_2 as a function of temperature could also be found as [181]:

$(c_p, U_3Si_2) = (0.199 + 0.000104T)$ J/g-K

Molecular weight of U_3Si_2 is 770, hence the above equation can be re-written as:

$(c_p, U_3Si_2) = \{(0.199 + 0.000104T) \times 770\}$ J/mol-K B-3

Equation A-3 was applied for the calculation of U_3Si_2 heat of formation at 750 °C. Therefore the function shown in equation B-3 is plotted in Fig. B-1 and the area under the curve from 25 °C to 750 °C was calculated.

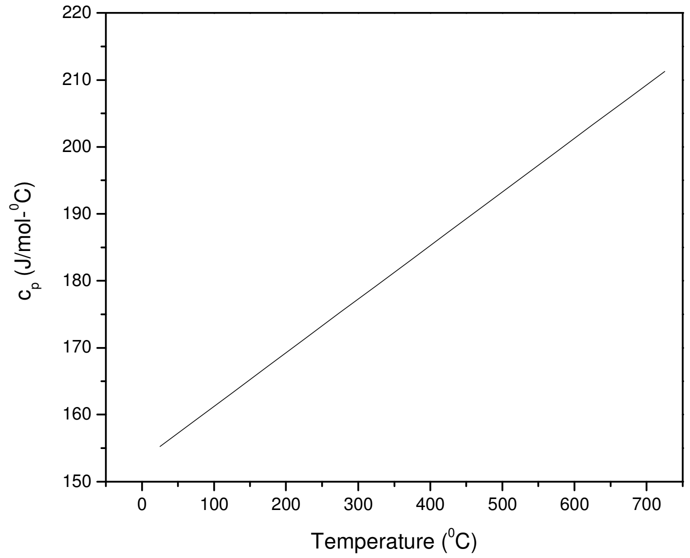

Fig. B-1 Data plot of c_p as a function of temperature in the range 25 °C to 750 °C for U_3Si_2.

Therefore, the value of $\int_{298}^{1023}(c_p, U_3Si_2)dT$ is 133.589 kJ/mol. If the values are now put in equation B-1, then enthalpy of formation of U_3Si_2 will be: $\Delta H_{298}^{1023}(U_3Si_2) = -40.37$ kJ/mol

With the assumption that at 725 °C the reaction between uranium and silicon completes, then the enthalpy of U_3Si_2 from 750 °C to 925 ° C can be calculated using equation B-3, $\Delta H_{1023}^{1198}(U_3Si_2) = 38.55$ kJ/mol.

Similarly, for $\Delta H_{1223}^{1823}(U_3Si_2) = 151.998$ kJ/mol

Appendix-3

Equation 4.3, described in section 4.4.4 can be re-written as:

$$(1-f)=e^{-kt^{n}} \tag{C-1}$$

$$\left[\ln\left(\frac{1}{1-f}\right)\right]=kt^{n} \tag{C-2}$$

$$\left[\ln\left[\ln\left(\frac{1}{1-f}\right)\right]\right]=\ln[k]+n\ln[t] \tag{C-3}$$

The value of *'f'* is taken from *Table 4.5* and the left hand side function viz. $\left[\ln\left[\ln\left(\frac{1}{1-f}\right)\right]\right]$ is calculated. For convenience this function is hence worth termed as *'y'*

Case I: U-8wt% Mo after 68 hours of heat treatment

f = {(24.26+47.13)/100}

= 0.7139

y = 0.2243

Case II: U-8wt% Mo after 240 hours of heat treatment

f = {(33.35+50.17)/100}

= 0.8352

y = 0.5895

Case III: U-9wt% Mo after 68 hours of heat treatment

f = {(16.06+48.65)/100}

= 0.6471

y = 0.0407

Case IV: U-9wt% Mo after 240 hours of heat treatment

$f = \{(24.90+54.74)/100\}$

= 0.7964

y = 0.4647

Case V: U-10wt% Mo after 68 hours of heat treatment

$f = \{(3.72+51.88)/100\}$

= 0.5560

y = -0.2083

Case VI: U-10wt% Mo after 240 hours of heat treatment

$f = \{(15.17+59.72)/100\}$

= 0.7489

y = 0.3235

The value for X-axis i.e. $\ln[t]$ is shown below and for convenience this function is hence worth termed as *'x'*:

For 68 hours

x = 12.4082 seconds

For 240 hours

x = 13.6693 seconds

As described in section 4.4.4, equation 4.3 was used to calculate the function $\left[\ln\left[\ln\left(\frac{1}{1-f}\right)\right]\right]$ for Y-axis and $[\ln(t)]$ for X-axis values respectively and is shown in *Table C-1*. This data is then plotted and shown in *Fig. C-1.*

Alloy Composition & Heat treatment cycle		$y = \left[\ln\left[\ln\left(\frac{1}{1-f}\right)\right]\right]$	$x = \left[\ln(t)\right]$
U-8wt% Mo	**68 h**	0.2243	12.4082
	240 h	0.5895	13.6693
U-9wt% Mo	**68 h**	0.2053	12.4082
	240 h	0.2877	13.6693
U-10wt% Mo	**68 h**	-0.2083	12.4082
	240 h	0.3235	13.6693

Table C-1 Transformation kinetics data.

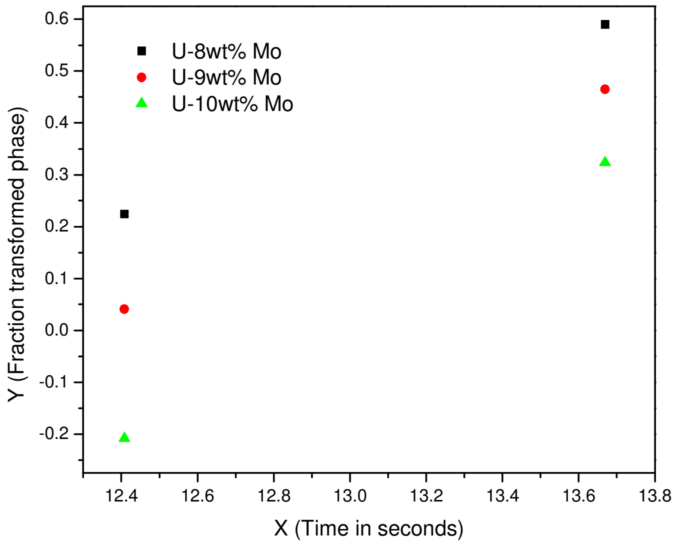

Fig. C-1 Plot between transformed product and time.

Appendix-4

The *U-Mo* diffusion couple discussed in section 4.5 may be considered as the case for *'Thin Film method.* Therefore, the solution could be derived from equation D-1.

$$C(x,t) = \frac{B}{\sqrt{\pi D_{Mo} t}} e^{\left(\frac{-x^2}{4 D_{Mo} t}\right)} \qquad \text{D-1}$$

In equation D-1, *C(x,t)* is the solute concentration at a distance x and time t. B is a constant, D_{Mo} is the intrinsic diffusivity coefficient of Mo, x is distance in millimeter and t is time in seconds. The *Fig. 4.31(c)* was used to determine the values for equation D-1 and is as follows:

The counts observed for pure Mo (i.e. 100 wt%) in *Fig 4.31(c)* is 2050 cps, therefore 103 cps would correspond to 4.976 wt% Mo in uranium.

Hence, $C(x,t) = 0.04976$

$x = 6\mu\text{m} = 6 \times 10^{-6}\ \text{m}$

$t = 3\ \text{hours} = 1.08 \times 10^{4}\ \text{seconds}$

$D_{Mo} = 5.2 \times 10^{-14}\ \text{m}^2/\text{second}$

The above mentioned values are put in equation 4.7 to find the value for B and are as follows:

$$0.04976 = \frac{B}{\sqrt{3.14157 \times 5.2 \times 10^{-14} \times 1.08 \times 10^{4}}} \left(\frac{1}{e^{\left(\frac{\left(6 \times 10^{-6}\right)^2}{4 \times 5.2 \times 10^{-14} \times 1.08 \times 10^{4}} \right)}} \right)$$

$B = 4.164 \times 10^{-6}\ \text{m}$

Equation 4.7 can be re-written as:

$$\ln[C(x,t)] = \ln\left[\frac{B}{\sqrt{\pi D_{Mo} t}}\right] - \frac{x^2}{4D_{Mo}t} \tag{D-2}$$

The value of *B* as derived above is substituted in equation B-2 to determine the Mo diffusion length in *U-Mo alloys.* It is also important to note that calculation is carried out for 6 hours (2.16 x 10^4 seconds) of heat treatment at 900 °C. Mo diffusion length under these conditions for *U-Mo alloys* of 2, 5 and 10wt% compositions are shown below:

Case-I: U-2wt% Mo alloy

$$\ln(0.02) = \ln\left(\frac{4.164\times10^{-6}}{\sqrt{3.14157\times5.2\times10^{-14}\times2.16\times10^{4}}}\right) - \left(\frac{x^2}{4\times5.2\times10^{-14}\times2.16\times10^{4}}\right)$$

$x = 75.07\ \mu\text{m}$

Case-II: U-5wt% Mo alloy

$$\ln(0.05) = \ln\left(\frac{4.164\times10^{-6}}{\sqrt{3.14157\times5.2\times10^{-14}\times2.16\times10^{4}}}\right) - \left(\frac{x^2}{4\times5.2\times10^{-14}\times2.16\times10^{4}}\right)$$

$x = 38.96\ \mu\text{m}$

Case-III: U-10wt% Mo alloy

$$\ln(0.1) = \ln\left(\frac{4.164\times10^{-6}}{\sqrt{3.14157\times5.2\times10^{-14}\times2.16\times10^{4}}}\right) - \left(\frac{x^2}{4\times5.2\times10^{-14}\times2.16\times10^{4}}\right)$$

$x = 39.98\ \mu\text{m}$

6. References

[1] The History of Nuclear Energy, ***U.S. Department of Energy, Washington, D.C. 20585, DOE/NE-0088***.

[2] Edelson Edward, The Journalist Guide to Nuclear Energy, ***Nuclear Energy Institute, 1994***.

[3] Samuel Glasstone, Sourcebook on Atomic Energy, ***Princeton, D. Van Nostrand Company, 3rd Edition, 1979***.

[4] Fuel Cycle and Waste, ***A News Letter of the Division of Nuclear Fuel Cycle and waste Technology, Vol.2, No.1, April 2006***.

[5] The Argonne News, ***Vol. 7, Issue No. 7, Page 2, December 1952***.

[6] Enrico Fermi, The development of first chain reaction pile, ***Proceedings of the American Philosophical Society, Vol. 90, No. 1, Jan 1946***.

[6] International Atomic Energy Agency, Nuclear Research Reactor in the World, ***Reference data series 3, December 1994 Edition***.

[7] P.J. Gilmer and M.Du Bois, Teaching social responsibility: The Manhatten Project, ***Science and Engineering Ethics, No. 2, 8(2002)206***.

[8] P.J. Gilmer, Education and the research environment, Committee on Science, Space and Technology, Subcommittee on Investigations and Oversight, ***US Congressional Record, pp. 76–91, 382–384, (28 June 1989)***.

[9] Prepared by office of the Assistant General Manager for Reactors, Nuclear Reactors built, being built or planned in the United States as of ***June 30, 1970, TID-8200 (22nd Revision)***.

[10] David Duerr, Lift of Shippingport Reactor Pressure Vessel, ***Journal of Construction Engineering and Management, No. 1, 116(1990)188***.

[11] G. Kennedy and J. St. Pierre, LEU Fuelled SLOWPOKE-2 Research Reactor: Operational Experience and Utilization, ***Proceedings of the International Meeting on Reduced Enrichment for Research and Test Reactors, Bariloche (2002)***.

[12] International Atomic Energy Agency, Nuclear Research Reactor in the World, ***Reference data series 3, September 2000 Edition***.

[13] D. Stahl, Fuels for Research and Test Reactors, ***Status Review: July 1982, ANL-83-5, Argonne National Laboratory Report, December 1982***.

[14] Decommissioning Techniques for Research Reactors, ***Technical Series No. 373, IAEA 1994***.

[15] Colin West, Research reactors: on overview, ***ANS Nuclear News, October 1997***.

[16] A book on India's First Research Reactor APSARA, Fifty Years of Operation & Utilization, ***Bhabha Atomic Research Centre, Trombay, December-2006***.

[17] India's First Research Reactor APSARA, Fifty Years of Operation and Utilization, ***Bhabha Atomic Research Centre 2006***.

[18] G. J. Prasad, C. Ganguly and P. R. Roy, Fabrication of Aluminium Clad Al-Pu Fuel Plates, ***Bhabha Atomic Research Centre Report, BARC/I-423 (1976)***.

[19] P. R. Roy, Determination of Alpha Aluminium Solid Solubility Limits in the Aluminium-Uranium and Aluminium-Plutonium System, ***J. Nucl. Mater. 11(1964)59***.

[20] Nuclear Fuel Fabrication (NUFFAB '88'), ***Proceedings of Symposium on Nuclear Fuel Fabrication, held at BARC, Bombay during 12-14, 1986***.

[21] C. Ganguly, G. J. Prasad, K. N. Mahule, K. V. J. Asari, K. N. Chandrashekharan, S. Muralidhar, T. S. Balan and P. R. Roy, ***Fabrication Experience of Al-U^{233} and Al-Pu Plate Fuel for Purnima-III and Kamini Reactors, Nucl. Tech. 96(1991)1***.

[22] G. J. Prasad, K. V. J. Asari and C. Ganguly, Development and Fabrication of Al-U^{233} and Al-Pu Plate Fuel Elements for Purnima-III/ Kamini, ***Materials Science Forum, Vol. 48 & 49 (Nuclear Fuel Fabrication) (1989)315***.

[23] C. Ganguly, P. V. Hegde and G. J. Prasad, ***Proc. of the Int. meeting on RERTR, Jakarta, Indonesia, 4-7 Nov, (1991)***.

[24] P. V. Hegde, G. J. Prasad and C. Ganguly, ***Trans. of Powder Metallurgy Association of India (PMAI), 21(1994)54***.

[25] S. Muralidhar, V. D. Pandey, K. N. Mahule, G. J. Prasad and J. K. Ghosh, Evolution of Bonding in Kamini Plate Fuels Using Ultrasonic Immersion Technique, ***Bhabha Atomic Research Centre Report, BARC/I-1472 (1989)***.

[26] G. J. Prasad, Studies on the Fabrication and Characterization of Plate type Fuel Elements for Nuclear Research Reactors, ***Ph.D. Thesis (1996)***.

[27] P. V. Hegde, G. J. Prasad and C. Ganguly, Powder metallurgy route for fabrication of Al-UAl_3, Al-U_3O_8 and Al-U_3Si_2 dispersion fuel for nuclear

research reactors, ***Trans. of Powder Metallurgy Association of India (PMAI) 20(1993)27***.

[28] K. Conlon and D. Sears, Neutron Powder Diffraction of Irradiated Low Enriched Uranium-Molybdenum Dispersion Fuel, ***10th Topical Meeting on Research Reactor Fuel Management (European Nuclear Society), Sofia, Bulgaria, May 2006***.

[29] G. L. Hofman, A Short note on High Density Dispersion Fuel, ***Argonne National Laboratory, 9700 South Cass Avenue, Argonne, IL 60439 USA, June 1996***.

[30] H.S. Kalish et al., Uranium Alloys in Reactor Handbook, ***Vol. I, Materials, p. 174, C.R. Tipton Ed., Interscience Publishers, Inc., New York (1960)***.

[31] D. Stahl, "Fuels for Research and Test Reactors, ***Status Review, July 1982", ANL-83-5, December 1982***.

[32] A.N. Holden, Physical Metallurgy of uranium, ***Addison-Wesley publishing Co. Inc., USA, (1958)***.

[33] R.W. Knight, Observations in the Manufacture of Aluminum-Based Research Reactor Fuel Elements, ***ORNL/TM-11809, Oak Ridge National Laboratory Report, July 1993***.

[34] A.G. Samoilov, A.I. Kashtanov, and V.S. Volkov, Dispersion-Fuel Nuclear Reactor Elements (1965), ***translated from the Russian by A. Aladjem, Israel Program for Scientific Translations Limited, Jerusalem, pp. 54-57 (1968)***.

[35] J.A. Perrota, P.E.O. Lainetti, Program of Converting IEA-R1 Brazilian Research Reactor from HEU to LEU, ***Proceedings of the International Meeting on Reduced Enrichment for Research and Test Reactors, Seoul, October, 1996***.

[36] M. K. Meyer, C. L. Trybus, G. L. Hofman, S. M. Frank, T. C. Wiencek, Selection and Microstructures of High Density Uranium Alloys, ***Proceedings of the 1997 International Meeting on Reduced Enrichment for Research and Test Reactors, Jackson Hole, WY, October 5-10, 1997, ANL/TD/TM99-06 (1999)***.

[37] C.K. Kim, Y.S. Lee, D.B. Lee, S.J. Oh, K.H. Kim, H.T. Chae, J.M. Park, D.S. Sohn, Status of the Back-end Optional Advanced Research Reactor Fuel Development in Korea, ***Proceedings RERTR-2003 International Meeting Chicago, USA, October 5-10, 2003***.

[38] J.L. Snelgrove, R.F. Domagala, G.L. Hofman, T.C. Wiencek, G.L. Copeland, R.W. Hobbs and R.L. Senn, The Use of U_3Si_2 Dispersed in Aluminum in Plate-Type Fuel Elements for Research and Test Reactors, ***ANL/RERTR/TM-11, Argonne National Laboratory Report, October 1987***.

[39] T.C. Wiencek, Summary Report on Fuel Development and Miniplate Fabrication for the RERTR Program, 1978 to 1990, ***ANL/RERTR/TM-15, Argonne National Laboratory Report, August 1995***.

[40] J.P. Durand, Y. Lavastre, P. Colomb, Silicide Fuel Development at CERCA - Status as of September 1995, ***International Meeting on Reduced Enrichment for Research and Test Reactors, Paris, September 18-22, 1995***.

[41] K.H. Kim, D.B. Lee, C.K. Kim, G.L. Hofman, Development of High Loading U-Mo Alloy Fuel by Centrifugal Atomization, ***Proceedings of the International Meeting on Reduced Enrichment for Research and Test Reactors, Seoul, October, 1996***.

[42] J.M. Chaussy, A. Ballagny, J.P. Beylot, J. Guidez, Review of Research and Development Work into Silicide Fuels, ***Proceedings of the International Meeting on Reduced Enrichment for Research and Test Reactors, Paris l, September 18-22, 1995***.

[43] J.L. Snelgrove, G.L. Hofman, C.L. Trybus, T.C. Wiencek, Development of Very-High-Density Fuels by RERTR Program, ***International Meeting on Reduced Enrichment for Research and Test Reactors, Seoul, October 7-10, 1996***.

[44] A. Travelli, Status and Progress of the RERTR Program, ***Proceedings of the International Meeting on Reduced Enrichment for Research and Test Reactors, Seoul, October, 1996***.

[45] J. Guidez, A. Ballagny, RERTR Programme-French Situation in 1996, ***Proceedings of the International Meeting on Reduced Enrichment for Research and Test Reactors, Seoul, October, 1996***.

[46] Research Reactor Core Conversion Guide Book, ***IAEA-TECDOC 643***.

[47] D. M. Wachs, RERTR Fuel Development and Qualification Plan**,** ***INL/EXT-05-01017 Rev. 3, January 2007***.

[48] S.L. Hayes, C.L. Trybus, M.K. Meyer, Irradiation Testing of High-Density Uranium Alloy Dispersion Fuels, ***Proceedings of the 1997***

International Meeting on Reduced Enrichment for Research and Test Reactors, Jackson Hole, WY, October 5-10, 1997, ANL/TD/TM99-06 (1999).

[49] J. Gomez, R. Morando, E.E. Perez, D.R. Giorsetri, G.L. Copeland, G.L. Hofman, J.L. Snelgrove, Postirradiation Examination of High-U-Loaded, Low-Enriched U_3O_8, UAl_2, and U_3Si Test Fuel Plates, ***Proc. of the 1984 International Meeting on Reduced Enrichment for Research and Test Reactors, Argonne, IL, Oct 15-18 (1984)***.

[50] C.K. Kim, K.H. Kim, J.M. Park, D.B. Lee, S.J. Oh, K.H. Lee, H.T. Chae, and D.S. Sohn, Progress of U-Mo Dispersion Rod Fuel Qualification Program in Korea, ***Proceedings of the 2004 International Meeting on Reduced Enrichment for Research and Test Reactors, San Carlso de Bariloche, Argentina Nov. 3-8(2002), ANL/TD/TM03-04 (2003)***.

[51] J.M. Park, H.J. Ryu, Y.S. Lee, D.B. Lee, S.J. Oh, B.O. Ryu, Y.H. Jung, D.S. Sohn, C.K. Kim, An investigation of the Irradiation Behavior of Atomized U-Mo/Al Dispersion Rod Fuels, ***Proceedings of the 2004 International Meeting on Reduced Enrichment for Research and Test Reactors, Vienna, Austria, Nov. 7-12(2004)***.

[52] R.G. Muranaka, Conversion of research reactors to low-enrichment uranium fuels, ***IAEA Bulletin, Vol. 25, No.1***.

[53] Research reactor core conversion from the use of highly enriched uranium to the use of low-enriched uranium fuels, ***IAEA-TECDOC-233***.

[54] H.B. Peacock, Co-extrusion of 60 to 30 wt% U_3O_8 Nuclear Fuel Elements, ***DPST-80-447, E.I. du Pont de Nemours and Company (1980)***.

[55] G.L. Copeland, Performance of Low Enrichement U_3Si_2-Aluminium Dispersion Fuel Elements in the Oak Ridge Research Reactors, ***Argonne National Laboratory Report, ANL/RERTR/TM-10 (1987)***.

[56] J. P. Durand and Y. Fanjas, LEU Fuel Development at CERCA: Status as of October 1993, Proceedings of the 16th International Meeting on Reduced Enrichment for Research and Test Reactors, ***Japan Atomic Energy Research Institute Report, Oarai, Japan, JAERI-M 94-02, 71-78***.

[57] James A. Lake, Donald K. Parsons, John L. Liebenthal, John M. Ryskamp, Deslonde R. Deboisblanc and Garry N. Fillmore, Ultra High Flux Reactor Design Probing the Limits of Plate Fuel Technology, ***Nuclear Instrumentation and Mehtods in Physics Research A249(1986)41***.

[58] Usha Pal and V. Jagannathan, A Conseptual, High Flux Reactor Design with Scope for use in ADS Applications, ***Indian Academy of Sciences Vol.68, No.2 (2007)151***.

[59] J.P. Durand, P. Laudamy and K. Richter, Preliminary Developments on MTR Plates with Uranium Nitride, Proceedings International Meeting on Reduced Enrichment for Research and Test Reactors, 18-23 September, ***Argonne National Laboratory Report, ANL/RERTR/TM-20, Williamsburg***.

[60] G.I. Snelgrove, The Use of U_3Si_2 Dispersed in Aluminium in Plate-type Fuel Elements for Research and Test Reactors, ***Argonne National Laboratory Report, ANL/RERTR/TM-11 (1987)***.

[61] C.L. Trybus, T.C. Wiencek, M.K. Meyer, D.J. McGann and C.R. Clark, Proceedings of the 20th International Meeting on Reduced Enrichment for

Research and Test Reactors, ***Argonne National Laboratory Report ANL/TD/TM99-06(1999), p.19***.

[62] M.K. Meyer, C.L. Trybus, G.L. Hofman, S. M. Frank and T.C. Wiencek, Proceedings of the 1997 International Meeting on Reduced Enrichment for Research and Test Reactors, ***Argonne National Laboratory Report ANL/TD/TM99-06(1999), p.81***.

[63] T.C. Wiencek, Summary Report on Fuel Development and Miniplate Fabrication for the RERTR Program 1978 to 1990, ***ANL/RERTR/TM-15, Argonne National Laboratory Report, August 1995***.

[64] T.C. Weincek, A Study of the Effect of Fabrication Variables on the Quality of Fuel Plates, ***Proc. 1986 Int. Mtg. on Reduced Enrichment for Research and Test Reactors, Gatlinburg, Tennessee, November 3-6, 1986, Argonne National Laboratory Report ANL/RERTR/TM-9, CONF-861185 (May 1988) p. 54***.

[65] J.L. Snelgrove, R.F. Domagala, G.L. Hofman, T.C. Weincek, G.L. Copeland, R.W. Hobbs, and R.L. Senn, The Use of U_3Si_2 Dispersed in Aluminum in Plate-Type Fuel Elements for Research and Test Reactors, ***ANL/RERTR/TM-11, October 1987***.

[66] U.S. Nuclear Regulatory Commission: "Safety Evaluation Report Related to the Evaluation of Low-Enriched Uranium Silicide-Aluminum Dispersion Fuel for Use in Non-Power Reactors," U.S. Nuclear Regulatory Commission Report NUREG-1313 (July 1988).

[67] M.T. Simnad, Perspective on Research Reactors and Their Fuel Elements, ***J. Nucl. Mater. 100(1981)***.

[68] Standardization of Specifications and Inspection Procedures for LEU Plate-Type Research Reactor Fuels, ***IAEA-TECDOC-467, 1988***.

[69] F. M. Marshall, Advance Test Reactor Capabilities and Future Irradiation Plans, ***Idaho National Laboratory DE-AC07-051D14517***.

[70] R.F. Domagala, T.C. Wiencek and H.R. Tresh, U-Si and U-Al-Si Dispersion Fuel Alloy Development for Research and Test Reactors, ***Nucl. Tech. 62(1983)353***.

[71] R.W. Cahn, P.Haasen and E.J. Kramer, ***Materials Science and Technology, Vol. 10A, Nuclear Materials Part I, p.12-105***.

[72] Peng Hong Lien and Hiroshi Sekimoto, Core safety characteristics of High Flux Safe Reactor (HFSR), ***Journal of Nuclear Science, 30(7)(1993)648***.

[73] N.L. Peterson, Diffusion in refractory metals, ***Wright air development division, United States air force, Wright-Patterson air force base, Ohio, 29-1102, May 1961***.

[74] C.W. Jacob and B.E. Warren, The Crystalline Structure of Uranium, ***J. Am. Chem. Soc, 59(1937)2588***.

[75] C.W. Tucker, An approximate crystal structure for the beta phase of uranium, ***Science, 112(1950)448***.

[76] A.S. Wilson and R.E. Rundle, The Structures of Uranium Metal, ***Acta Cryst., A24(1968)282***.

[77] P. Duwez, The Effect of the Rate of Cooling on the Allotropic Transformation Temperatures of Uranium, ***J. Appl. Phys., 24(1953)152.***

[78] H.H. Klepfer and P. Chiotti, Characteristics of the Solid State Transformations in Uranium, ***USAEC Report ISC-893, Iowa State College, 1957***.

[79] A.N. Holden, The isothermal transformation of metastable beta-uranium single crystals, ***Acta Met., 1(1953)617***.

[80] Y. Takahashi, K. Yamamoto, T. Ohsato, H. Shimada, Takayuki Terai and M. Yamawaki, Heat capacities of uranium-zirconium alloys from 300 to 1100 K, ***J. Nucl. Mater. 167(1989)147***.

[81] W.J. Kitchingman, The atomic mechanism of the body-centred cubic to σ-phase transformation, ***Acta Cryst., A24(1968)282.***

[82] G. Laberberg, Phase transformations in a uranium-zirconium alloy containing 2 weight per cent zirconium, ***J. Nucl. Mater. 9(1963)261***.

[83] M. Akabori, A. Itoh, T. Ogawa, F. Kobayashi and Y. Suzuki, Stability and structure of the δ phase of the U-Zr alloys, ***J. Nucl. Mater. 188(1992)249***.

[84] A.A. Bauer, ***Report No. BMI-1350, UC-25 Metallurgy and Ceramics (TID-4500, 15th Edition)1959***.

[85] S.T. Zegler, ***Report No. ANL-6055, Metal, Ceramic and Materials, (TID-4500, 15th Edition) 1962***.

[86] J.M. Beeston, R.R. Hobbins, G.W. Gibson, and W.C. Francis, Development and Irradiation Performance of Uranium Aluminide Fuels in Test Reactors, ***Nuclear Tech. 49(1980)136***.

[87] D.B. Lee, K.H. Kim and C.K. Kim, Thermal Compatibility Studies of Unirradiated U-Mo Alloys Dispersed in Aluminum, ***J. Nucl. Mater. 250(1997)79***.

[88] ASM International, Properties and Selection: ***Non ferrous alloys and special-purpose materials, Vol. 2, 1965-1994***.

[89] K. Tangri and G.I. Williams, Metastable Phases in the Uranium-Molybdenum System and their Origin, ***J. Nucl. Mater. 4(1961)226***.

[90] H.M. Volz, R.E. Hackenberg, A.M. Kelly, W.L. Hults, A.C. Lawson, R.D. Field, D.F. Teter and D.J. Thoma, X-ray Diffraction Analysis of Aged U-Nb alloys, ***J. Alloys. Comp. 444(2007)217***.

[91] A.G. Harding and M.B. Waldron, ***UKAEA (Harwell Report, AERE M/R-2673), part1 (1958)***.

[92] M.K. Meyer, T.C. Wiencek, S.L. Hayes and G. L. Hofman, Irradiation Behavior of U_6Mn-Al Dispersion Fuel Elements, ***J. Nucl. Mater. 278(2000)358***.

[93] G.L. Hofman, R F. Domagala and G.L. Copel, Irradiation behavior of Low-Enriched U_6Fe-Al Dispersion Fuel Elements, ***J. Nucl. Mater. 150(1987)238***.

[94] Baek-Seok Seong, Chang-Hee Lee, Jeong-Soo Lee, Hae-Seop Shim, Jin-Ho Lee, Ki Hwan Kim, Chang Kyu Kim and Vyacheslav Em, Neutron Diffraction Study of U-10wt%Mo alloy, ***J. Nucl. Mater. 277(2000)274***.

[95] G. Ostberg, M. Moller and B. SChonning-Christiansson, Metallographic Study of the Transformation of γ-phase into (α+γ’) phases in a U-1.6wt%Mo Alloy, ***J. Nucl. Mater. 4(1963)329***.

[96] J.M. Park, H.J. Ryu, Y.S. Lee, D.B. Lee, S.J. Oh, B.O. Ryu, Y.H. Jung, D.S. Sohn, and C.K. Kim, An Investigation on the Irradiation Behavior of

Atomized U-Mo/Al Dispersion Rod Fuels, ***Proceedings RERTR-2004 International Meeting, Vienna, Austria, Nov. 7-12, 2004***.

[97] G.L. Hofman, Crystal Structure Stability and Fission Gas Swelling in Intermetallic Uranium Compound, ***J. Nucl. Mater. 140(1986)256***.

[98] G.L. Hofman and Y.S.Kim, A Classification of Uniquely Different Types of Nuclear Fission Gas Behavior, ***Nucl. Eng. Technol., 37(2005)299***.

[99] J. Rest and G.L. Hofman, Dynamics of Irradiation Induced Grain Subdiviaion and Swelling, ***J. Nucl. Mater 210(1994)187***.

[100] M.K. Meyer, G.L. Hofman, S.L. Hayes, C.R. Clark, T.C. Wiencek, J.L. Snelgrove, R.V. Strain and K.H. Kim, Low Temperature Irradiation Behaviour of Uranium-Molybdenum Alloy Dispersion Fuel, ***J. Nucl. Mater. 304(2002)221***.

[101] M.R. Finlay, G.L. Hofman and J.L. Snelgrove, Irradiation Behaviour of Uranium Silicide Compounds, ***J. Nucl. Mater. 325(2004)118***.

[102] H.E. Fairman and A. Kelly, ASM Handbook, ***Vol. 9, (2004) p. 918***.

[103] John Peterson, Margaret MacDonell, Lynne Haroun, Fred Monette, R. Douglas Hildebrand and Anibal Taboas, Radiological and Chemical Fact Sheets to Support Health Risk Analyses for Contaminated Areas, ***March 2007, Argonne National Laboratory, EVS***.

[104] Weston Stacey, Nuclear Reactor Physics (First Edition), ***January 16, 2001***.

[105] AERB Safety Code, Radiation Protection for Nuclear Fuel Cycle Facilities, ***AERB SAFETY CODE NO. AERB/NF/SC/RP***.

[106] J.P. Durand, Y. Lavastre and M. Grasse, Proceedings of the 20th International Meeting on Reduced Enrichment for Research and Test Reactors, ***Argonne National Laboratory Report ANL/TD/TM99-06(1999)28***.

[107] Steven L. Hayes, Basics of Nuclear Fuels, ***Idaho National Laboratory, ATR-NSUF Users Week, June 8, 2010***.

[108] S. Nazaré, Low Enrichment Dispersion Fuel for Research and Test Reactors, ***J. Nucl. Mater. 124(1984)14***.

[109] J. Marín, J. Lisboa, J. Ureta, L. Olivares, H. Contreras and J.C. Cha′vez, Synthesis and Clad Interaction Study of U_3Si_2 Powder Dispersed in an Aluminium Matrix, ***J. Nucl. Mater. 228(1996)61***.

[110] Chang-Kye Rhee, Su-II Pyun and II-Hiun Kuk, Phase formation and Growth at Interface between U_3Si and Aluminium, ***J. Nucl. Mater. 184(1991)161***.

[111] Dennis D. Keiser Jr., Jan-Fong Jue, Nicolas E. Woolstenhulme, Ashley Ewh, Potential annealing treatments for tailoring the starting microstructure of low-enriched U–Mo dispersion fuels to optimize performance during irradiation, ***J. Nucl. Mater, Issue 1-3, 419(2011)226***.

[112] J. Lehmann, ***Comptes Rend. Acad. Sci. (Paris). 248(1959)2098***.

[113] ASM Handbook, ***Alloy Phase Diagram, Vol. 3, 2004***.

[114] P. Chiotti and J.A. Kateley, Thermodynamic Properties of Uranium-Aluminum Alloys, ***J. Nucl. Mater. 32(1969)135***.

[115] J.M. Chaussy, A. Ballagny, J.P. Beylot, J. Guidez, Review of Research and Development Work into Silicide Fuels, ***Proceedings of the International***

Meeting on Reduced Enrichment for Research and Test Reactors, Paris l, September 18-22, 1995.

[116] R.W. Knight, Observations in the Manufacture of Aluminum-Based Research Reactor Fuel Elements, ***ORNL/TM-11809, Oak Ridge National Laboratory Report, July 1993***.

[117] J.L. Snelgrove, G.L. Hofman, M.K. Meyer, C. L. Trybus and T. C. Wiencek, Development of Very-high-density Low-enriched-uranium Fuels, ***Nucl. Eng. Des., 178(1997)119***.

[118] R.L. Craik, D. Birch, C. Fizzotti and F. Saraceno, Phase Equilibria in Uranium-rich Binary Alloys Containing Molybdenum and Zirconium and the Effect of Ternary Additions of Carbon, ***J. Nucl. Mater. 6(1962)13***.

[119] M. Ugajin, A. Itoh, M. Akabori, N. Ooka and Y. Nakakura, Irradiation Behavior of High Uranium-Density Alloys in the Plate Fuels, ***J. Nucl. Mater. 254(1998)78***.

[120] S. Nicholson, D. G. Harris and J. J. Stobo, The Effect of Ternary Additions on the Microstructures of Dilute U-Mo alloys, ***J. Nucl. Mater. 12(1964)173***.

[121] B.W. Howlett, A Study of the Shear Transformations from the Gamma-phase in Uranium-Molybdenum alloys containing 6.0 - 12.5 at% molybdenum, ***J. Nucl. Mater. 35(1970)278***.

[122] K. Tangri, D.K. Chawdhuri and C.N. Rao, Metastable Phases in Uranium Alloy with High Solute Solubility in the BCC Gamma Phase. Part – II. The system U-Ru, ***J. Nucl. Mater. 4(1965)288***.

[123] G.L. Hofman, M.K. Meyer and A.E. Ray, Design of High Density gamma-phase Uranium alloys for LEU Dispersion Fuel applications, ***Reduced Enrichment for Test Reactor Conference, Sao Paulo, Brazil, October 18-23, 1998***.

[124] Jong-Man Park, Ki-Hwan Kim, Dong-Seong Sohn, Chang-Kyu Kim, Gerard L. Hofman, Characterization of U–Nb–Zr dispersion fuel prepared by centrifugal atomization process, ***J. Nucl. Mater, Issue 1-2, 265(1999)38***.

[125] ***Personal meeting with ANL and ORNL scientist at Karlsruhe in 2010***.

[126] E. Perez, B. Yao, D.D. Keiser Jr., Y.H. Sohn, Microstructural analysis of as-processed U–10 wt.%Mo monolithic fuel plate in AA6061 matrix with Zr diffusion barrier, ***J. Nucl. Mater, Issue 1, 402(2008)8***.

[127] A.A. Bochvar, V.G. Kuznetsova and V.S. Sergeev, ***Transactions of the second International Conference on the peaceful use of Atomic Energy, Geneva 1958, Vol 3, 1959, pp. 1970***.

[128] H. Shimizu, The Properties and Irradiation Behavior of U_3Si_2, ***Atomics International Report NAA-SR-10621, p.14 (July 25, 1965)***.

[129] T.C. Weincek, R.F. Domagala, and H.R. Thresh, Thermal compatibility Studies of Unirradiated Uranium Silicide Dispersed in Aluminum, ***Proc. 1984 Int. Mtg. on Reduced Enrichment for Research and Test Reactors, Argonne, Illinois, October 15-18, 1984, Argonne National Laboratory Report ANL/RERTR/TM-6, CONF-8410173 (July 1985) p. 61***.

[130] R.F. Domagala, T.C. Weincek, and H.R. Thresh, Some Properties of U-Si Alloys in the Composition Range from U_3Si to U_3Si_2, ***Proc. 1984 Int. Mtg. on Reduced Enrichment for Research and Test Reactors, Argonne, Illinois,***

October 15-18, 1984, Argonne National Laboratory Report ANL/RERTR/TM-6, CONF-8410173 (July 1985) p. 47.

[131] J.L. Snelgrove, R.F. Domagala, G.L. Hofman, T.C. Weincek, G.L. Copeland, R.W. Hobbs, and R.L. Senn The Use of U_3Si_2 Dispersed in Aluminum in Plate-Type Fuel Elements for Research and Test Reactors, ***ANL/RERTR/TM-11, October 1987***.

[132] R.K. Williams, R.S. Graves, R.F. Domagala, and T.C. Weincek, Thermal Conductivities of U_3Si and U_3Si_2-Al Dispersion Fuels, ***Proc. 19th Int. Conf. on Thermal Conductivity, Cookville, Tennessee, October 21-23, 1985***.

[133] R.F. Domagala, Phases in U-Si Alloys, ***Proc. 1986 Int. Mtg. on Reduced Enrichment for Research and Test Reactors, Gatlinburg, Tennessee, November 3-6, 1986, Argonne National Laboratory Report ANL/RERTR/TM-9, CONF-861185 (May 1988) p. 45***.

[134] Jeong-Soo Lee, Chang-Hee Lee, Ki Hwan Kim, Vyacheslav Em, Neutron Diffraction Study of U-5.4wt% Mo Alloy, ***J. Nucl. Mater. 280(2000)116***.

[135] Dennis D. Keiser Jr., Adam B. Robinson, Jan-Fong Jue, Pavel Medvedev, Daniel M. Wachs and M. Ross Finlay, Microstructural Development in Irradiated U-7Mo/6061 Al Alloy Matrix Dispersion Fuel, ***J. Nucl. Mater. 393(2009)311***.

[136] H. Vacelet, P. Sacristan, A. Langwille, Y. Lavastre, M. Grasse, Irradiation of Full Size UMo plates, ***22nd RERTR in Budapest(1999)47***.

[137] Y.S. Kim, G.L. Hofman, H.J. Ryu and S.L. Hayes, Irradiation-enhanced Interdiffusion in the Diffusion Zone of U-Mo Dispersion Fuel in Al, ***J. Phase Equil. Diff., 27(2006)614***.

[138] D.B. Lee, K.H. Kim and C.K. Kim, Thermal Compatibility Studies of Unirradiated U-Mo Alloys Dispersed in Aluminum, ***J. Nucl. Mater. 250(1997)79***.

[139] A. Leenaers, S. Van den Berghe, E. Koonen, C. Jarousse, F. Huet, M. Trotabas, M. Boyard, S. Guillot, L. Sannen and M. Verwerft, Post-irradiation Examination of Uranium–7 wt% Molybdenum Atomized Dispersion Fuel, ***J. Nucl. Mater. 335(2004)39***.

[140] A. Leenaers, S. Van den Berghe, W. Van Renterghem, F. Charollais, P. Lemoine, C. Jarousse, A. Röhrmoser, W. Petry, Irradiation behavior of ground U(Mo) fuel with and without Si added to the matrix, ***J. Nucl. Mater, Issue 1, 412(2011)41***.

[141] Ho Jin Ryu, Yeon Soo Kim, G.L. Hofman, Amorphization of the interaction products in U–Mo/Al dispersion fuel during irradiation, ***J. Nucl. Mater, Issue 3, 385(2009)623***.

[142] Dennis D. Keiser Jr., J. Gan, J.F. Jue, B.D. Miller, C.R. Clark, Electron microscopy characterization of an as-fabricated research reactor fuel plate comprised of U–7Mo particles dispersed in an Al–2Si alloy matrix, ***Materials Characterization, Issue 11, 61(2010)1157***.

[143] Dennis D. Keiser Jr., Jan-Fong Jue, Adam B. Robinson, Pavel Medvedev, Jian Gan, Brandon D. Miller, Daniel M. Wachs, Glenn A. Moore, Curtis R. Clark, Mitchell K. Meyer, M. Ross Finlay, Effects of irradiation on

the microstructure of U–7Mo dispersion fuel with Al–2Si matrix, ***J. Nucl. Mater, Issue 1-3, 425(2012)156***.

[144] Yeon Soo Kim, Jong Man Park, Ho Jin Ryu, Yang Hong Jung, G.L. Hofman, Reduced interaction layer growth of U–Mo dispersion in Al–Si, ***J. Nucl. Mater, Issue 1-3, 430(2012)50***.

[145] L.R. Aronin and J.L. Klein, Use of a density method as a sensitive absolute measure of alloy compositions and its applications to the Aluminium-Uranium system, ***Cambridge, Nuclear Metals. Inc. (NMI-1118), 1954***.

[146] W. Dienst, S. Nazaré, F. Thümmler, Irradiation behaviour of UAl_x-Al dispersion fuels for thermal high flux reactors, ***J. Nucl. Mater, Issue 1-2, 64(1977)1***.

[147] S. Nazaré, G. Ondracek, F. Thümmler, Investigations on UAlx-Al dispersion fuels for high-flux reactors, ***J. Nucl. Mater, Issue 3, 56(1975)251***.

[148] L. Kniznik, P.R. Alonso, P.H. Gargano, G.H. Rubiolo, Simulation of UAl_4 growth in an UAl_3/Al diffusion couple, ***J. Nucl. Mater, Issue 2, 414(2011)309***.

[149] Yeon Soo Kim, Uranium Intermetallic Fuels (U–Al, U–Si, U–Mo), *Comprehensive Nuclear Materials*, *3(2012)391.*

[150] P. Chiotti, J.A. Kateley, Thermodynamic properties of uranium-aluminum alloys, ***J. Nucl. Mater, Issue 1, 32(1969)135***.

[151] W.C. Thurber, R.J. Beaver, Dispersions of uranium carbides in aluminum for plate-type fuel elements requiring high-uranium concentrations, ***J. Nucl. Mater, Issue 3, 1(1959)226***.

[152] A.F. Lillie, Zirconium Hydride fuel element performance characteristics, ***Canoga Park, CA: Atomics International (AI-AEC-13084), 1973***.

[153] J. Gan, D.D. Keiser Jr., B.D. Miller, J.-F. Jue, A.B. Robinson, J.W. Madden, P.G. Medvedev, D.M. Wachs, Microstructure of the irradiated U_3Si_2/Al silicide dispersion fuel, ***J. Nucl. Mater, Issue 1-3, 419(2011)97***.

[154] Xi-Shu Wang, Yong Xu, Experiments, characterizations and analysis of a U_3Si_2–Al dispersion fuel plate with sandwich structure, ***J. Nucl. Mater, Issue 2-3, 328(2004)243***.

[155] Xi-Shu Wang, Shuang-Shou Li, Qing-Yuan Wang, Yong Xu, Effect of the fabrication process on fatigue performance of U_3Si_2 fuel plate with sandwich structure, ***J. Nucl. Mater, Issue 1-3, 342(2005)42***.

[156] K. Böning, W. Petry, Test irradiations of full-sized U_3Si_2–Al fuel plates up to very high fission densities, ***J. Nucl. Mater, Issue 3, 383(2009)254***.

[157] Yeon Soo Kim, G.L. Hofman, J. Rest, A.B. Robinson, Temperature and dose dependence of fission-gas-bubble swelling in U_3Si_2, ***J. Nucl. Mater, Issue 3, 389(2009)443***.

[158] Bo Yao, Emmanuel Perez, Dennis D. Keiser Jr., Jan-Fong Jue, Curtis R. Clark, Nicolas Woolstenhulme, Yongho Sohn, Microstructure characterization of as-fabricated and 475 °C annealed U–7 wt.% Mo dispersion fuel in Al–Si alloy matrix, ***J. Alloys Comp., Issue 39, 509(2011)9487***.

[159] S. Van den Berghe, Y. Parthoens, F. Charollais, Y.S. Kim, A. Leenaers, E. Koonen, V. Kuzminov, P. Lemoine, C. Jarousse, H. Guyon, D. Wachs, D. Keiser Jr, A. Robinson, J. Stevens, G. Hofman, Swelling of U(Mo)–Al(Si)

dispersion fuel under irradiation – Non-destructive analyses of the LEONIDAS E-FUTURE plates, ***J. Nucl. Mater, Issue 1-3, 430(2012)246***.

[160] S. Van den Berghe, W. Van Renterghem, A. Leenaers, Transmission electron microscopy investigation of irradiated U–7 wt%Mo dispersion fuel, ***J. Nucl. Mater, Issue 3, 375(2008)340***.

[161] ASM Handbook, **Vol. 9,** ***Metallography and Microstructures 2004***.

[162] R.T. De Hoff and F.N. Rhines, Quantitative Microscopy, **McGraw-Hill, 1968**.

[163] W.R. Cribb, Quantitative Metallography of Poly-Phase Microstructures, ***Scr. Metall.,*** **Vol 12 (No. 10), 1978, p 893–898**.

[164] Test Methods for Characterizing Duplex Grain Sizes, ***E 1181-87, Annual Book of ASTM Standards, Section 3: Metals Test Methods and Analytical Procedures, ASTM International, 1999, p 741–755***.

[165] Test Methods for Estimating the Largest Grain Observed in a Metallographic Section (ALA Grain Size), ***E 930-92, Annual Book of ASTM Standards, Section 3: Metals Test Methods and Analytical Procedures, ASTM International, 1999, p 683–687***.

[166] Test Methods for Determining Average Grain Size Using Semiautomatic and Automatic Image Analysis, ***E 1382-97, Annual Book of ASTM Standards, Section 3: Metals Test Methods and Analytical Procedures, ASTM International, 1999, p 867–890***.

[167] Leica Metallurgy Application Briefing, Application Solutions for Metallurgy, ***Leica Microsystems Imaging Solutions Ltd, Clifton Road Cambridge, CB1 3QH, p 1-127***.

[168] Don W. Green and Robert H. Perry, Perry's chemical engineer, Handbook, ***8^{th} Edition, The McGraw-Hill publication house, Section 21, Page 23, 2008***.

[169] A. Berche, C. Rado, O. Rapaud, C. Guéneau, J. Rogez, Thermodynamic study of the U–Si system, ***J. Nucl. Mater. 389(2009101***.

[170] C. Ganguly, Nuclear Reactor Fuel Fabrication (Including Quality Control), Encyclopedia of Materials, ***Science and Technology (Second Edition), 2001, Page 1-15***.

[171] V.P. Sinha, G.P. Mishra, S. Pal, K.B. Khan, P.V. Hegde, G.J. Prasad, Development of powder metallurgy technique for synthesis of U_3Si_2 dispersoid, ***J. Nucl. Mater. 383(2008)196***.

[172] V.P. Sinha, G.J. Prasad, P.V. Hegde, R. Keswani, C.B. Basak, S. Pal, G.P. Mishra, Development, Preparation and Characterization of uranium molybdenum alloys for dispersion fuel application, ***J. Alloys and Comp. 473(2009)238***.

[173] R. Balasubramaniam, Calister's Materials Science and Engineering, ***Wiley-India Edition, 2007***.

[174] B.D. Cullity, Elements of X-ray diffraction, ***Addison-Wesley publishing Co. Inc., USA(1989), 360-363***.

[175] J.C.Slater, Atomic radii in crystals, ***J. Chem. Phys., 41 (10), 3199-3205 (1964)***.

[176] V.P. Sinha, G.J. Prasad, G.K. Dey and P.V. Hegde, Effect of molybdenum addition on metastability of cubic γ-uranium, ***J. Alloys and Comp. 491(2010)753***.

[177] Yanzhi Zhang, Weijun Guan, Qinguo Wang, Xiaolin Wang, Xinchun Lai, Maobing Shuai, Study the Oxidation Kinetics of Uranium Using XRD and Rietveld Method, ***IOP Conf. Series: Materials Science and Engineering 9 (2010) page 1***.

[178] V.P. Sinha, G.J. Prasad, G.K. Dey and P.V. Hegde, Phase transformation of metastable cubic γ-phase in U-Mo alloys, ***J. Alloys and Comp. 506(2010)253***.

[179] A. Berche, C. Rado. O. Rapaud, C. Guéneau, J. Rogez, Thermodynamic study of the U–Si system, ***J. Nucl. Mater. 389(2009)101***.

[180] G.V. Belov, B.G. Trusov, ASTD, Computer-aided Reference Book in Thermodynamical, Thermochemical and Thermophysical Properties of species, ***Version 2.0 (C), 1983-1985, Moscow***.

[181] J. L. Snelgrove, R. F. Doraagala, G. L. Hofraan, T. C. Wiencek, G. L. Copeland, R. W. Hobbs, R. L. Senn, The use of U_3Si_2 dispersed in aluminium in Plate-Type fuel elements for research and test reactors, ***ANL/RERTR/TM-11, Page 6***.